BUCKLING, POSTBUCKLING AND NON-SELF-SIMILAR DECOHESION ALONG A FINITE INTERFACE OF UNILATERALLY CONSTRAINED DELAMINATIONS IN COMPOSITES

by

Khaled W. Shahwan

A dissertation submitted in partial fulfillment
of the requirements for the degree of
Doctor of Philosophy
(Aerospace Engineering)
in The University of Michigan
1995

Doctoral Committee:

Associate Professor Anthony M. Waas, Chairman
Professor William J. Anderson
Associate Professor Nicolas Triantafyllidis
Professor Alan S. Wineman
Professor Wei-Hsuin Yang

To Eva and William for *all* what they have done

ACKNOWLEDGEMENTS

First and foremost, and at a loss of words, I would like to thank the Creator, the Maker, and the Divine Scientist for granting me the power, the well, and the ability to contribute, though an infinitesimal contribution, to the great *toy* of science. Thank you GOD.

I would like to thank Professor Anthony M. Waas for giving me the opportunity to work under his supervision which has been, and will always be, an educational experience. Tony has been an educator, a teacher, an advisor as well as a friend. With his knowledge and ambitions, he motivated, inspired, and encouraged me to undertake many issues and considerations, technical and otherwise, for which I will always be in debt. His endless help and generosity were always appreciated and will never be forgotten.

I would like to thank Professor William J. Anderson, Professor Nicolas Triantafyllidis, Professor Alan Wineman (Mechanical Engineering and Applied Mechanics) and Professor Wei-Hsuin Yang (ME&AM) for their constructive comments, advice and for willing to serve on my dissertation committee.

Special thanks should go to my greatest inspiration and love, my parents, Eva and William, without whom I would never have reached this stage. They gave me the honor of having them as the first "members" to serve on my "dissertation" committee. My father William, for his endless teachings and "lectures" from the very basic to the most important. His endless support and encouragements have always left their

marks, and always will. My mother Eva, for her unbelievable endurance and capacity, and for being my first teacher and advisor. Her love, care and support cannot be measured. Their contributions, direct and indirect, can never be matched. I would like to thank my dear sister Khawla for being my first "research collaborator" and a very dear one. Her life has changed mine in many different ways, for which I will always be in debt. My dear brother Tareq, for exhibiting the rare qualities of being nice and honest, not to mention the rarest, a true and a knowledgable scientist. And, my dear brother Ghassan, for being a loving and caring person and for exhibiting the ever-evolving qualities of wisdom and sincerity. Khawla, Tareq and Ghassan have been inspiring figures in my life.

I would like to thank my dearest *friend* Dr. Nahed M. Mohsen, for her greatest enlightenment, and for the endless support, encouragements, motivations and inspirations. Our intellectual discussions were extremely interesting and will always be cherished.

I would like to thank my dear friend and "brother" Dr. Sami A. Bayyuk for his honesty and sincerity, and for the endless but very interesting technical and philosophical discussions we always engaged in during late night hours.

Special thanks should go to Dr. Lei Fu and Dr. Amadi Nwankpa for their kindness, patience and for being there whenever I needed help with softwares, networking and computer resources; Professor Peter Washabaugh and Professor Kenneth Powell for their kindness in providing their computational resources. And, to Mr. John M. Comiez for the experimental work on delamination buckling that was carried out at the Composite Structures Laboratory.

I would like to thank (in alphabetical order) Professor Bijan Aalami of San Francisco State University (SFSU), Professor Timothy D'Orazio (SFSU), Professor

Antonie E. Naaman of The University of Michigan and Professor Wolfram Stadler (SFSU), for motivating, inspiring and helping me in their own ways to excel, pursue and continue my graduate studies.

I would like to thank my following colleagues (in alphabetical order): Mr. Michael R. Dungan, Dr. Amir R. Khamseh, Ms. Laura S. Kistler, Dr. Erol Şenocak and Dr. Seung J. Song who contributed, in their own ways, to my stay in the department.

Finally, I am greatly appreciative of the financial support received from the Department of Aerospace Engineering through Teaching Assistance, Research Assistance and other numerous Fellowships. Such support, which I received throughout my stay, gave me the opportunity to pursue my doctoral studies and research for which I will always be appreciative. Also, I wish to acknowledge the financial support received through Air Force Office of Scientific Research (AFOSR) Initiation Grant RI-B-91-06 awarded through the Engineering Foundation during the early stages of this work.

TABLE OF CONTENTS

LIST OF FIGURES

Figure

LIST OF TABLES

LIST OF APPENDICES

Appendix

CHAPTER I

INTRODUCTION AND LITERATURE REVIEW

1.1 General Perspective

It is customary to start a discussion on *composites* by stating that they offer significant weight savings and have attractive mechanical properties. These properties have been realized by many civilizations few thousands of years ago but quantified only in the past few decades.

By definition, a composite implies the existence of two or more constituents. From this implication it can be inferred that composites, or more specifically, composite materials, exhibit more complex properties and behavior than their counterparts, "traditional materials", of which metals are a prime example. Although these complexities bring more advantages, they come with a "price" that manifests itself in new phenomena. Phenomena such as delamination, fiber microbuckling and fiber-matrix debonding, to mention a few, were not present in traditional (homogeneous) materials. In most situations, the price is justified when quantified rationally and correctly, i.e., such phenomena can be tolerated if accounted for properly.

Delamination, as the name implies, is the process of separating two or more bonded layers (plies) from one another (Figure 1.1). Hence, one can deduce that the

delamination process is unique to laminated materials (or structures) rather than to composites in the general sense. Laminated composites are a special type of composites in which each lamina can be isotropic or otherwise.

Consider, for example, a laminated plate that is made up of identical thin aluminum plies, perfectly jointed. Such a plate is isotropic, and can be analyzed accordingly. The only complication to the analysis that must be considered is the fact that such thin layers can start to debond (delaminate) along an interface altering the behavior significantly. Such a behavior is usually not accounted for nor predicted by classical analysis unless special considerations are incorporated into the formulation governing the mechanics of the problem. These special considerations are predominantly nonlinear, making the task of solving the governing equations a formidable one. Such considerations range from large deformation effects to contact due to unilateral constraints.

The main reason for studying delamination can be simply stated as follows: *delamination damage in composites is a notorious problem which might seriously affect the integrity of structures.* Delamination damage can be caused during manufacturing or during service life of the structure [38]. The manufacturing process can cause imperfections such as inclusions, wrinkles, gas bubbles and/or voids. Further, the damage may be introduced by machining the components for fastener holes or cutouts. The service life damage can be due to a variety of reasons. In aircraft structures for example, damage may result from impact by runway debris, bird strike, ground service vehicles, hailstones, ballistics, ...etc. Dropping tools accidentally is another cause of damage that can take place during manufacturing as well as during the service life of the structure.

In many instances, delamination damage may not be visible or barely visible on

the structure but may significantly reduce the strength (and stiffness) of the structural component. Rhodes and Williams [82] investigated the effect of impact damage on the compressive strength of a T300/5208 Graphite/Epoxy $(\pm 45/0_2/\pm 45/0_2/\pm 45/0/90)_{2S}$ laminated panel when impacted by an aluminum projectile (12.5 mm diameter ball). They showed that the damage may be visible on the contact surface only at impact velocities higher than 80-100m/s, but the compressive strength of the panel is significantly reduced by the invisible damage. Since normal inspection practice relies primarily on visual inspections, it is therefore possible that the internal damage, which is mainly delaminations, caused by the low level impact may not be detected for the lifetime of the structure. Therefore, damage-tolerant design criteria are established for composite structures to ensure that growth from non-visible damage will not degrade the strength to less than the design ultimate strength during the life of the structure. This requirement for current Graphite/Epoxy composites is ensured by limiting the design strain to about 0.4% [32, 46] even though the fibers have a failure strain of over 1.3%. Such a restriction leads to an increase in structural weight and limits the exploitation of the full potential that composites have to offer. James and Williams [46] showed that the weight saving can be up to 10-12% if the design strain can be increased from 0.4% to 0.6% for a wing structure.

Amongst the three principal damage mechanisms in laminated composites, namely, intra-ply cracking, interlaminar matrix delamination and fiber failure, the interlaminar matrix delamination mechanism is of major importance. The delamination in a structure subjected to inplane loads is a subcritical failure mode [67, 77] whose effect may be stiffness loss, local stress concentration, and a local instability causing further deformations leading to compressive failure. Therefore, Wilkins *et al.* [110] described delaminations as the most prevalent life limiting damage growth mode in

laminated composite structures. (The word *delamination* sometimes refers to the delaminated region itself rather than to the delamination process.)

1.2 Problem Statement

Generally speaking, there are three main issues pertaining to the analysis of delamination behavior. These issues have been the subject of intense studies and investigations for the past 15-20 years and no study thus far has "closed the chapter" on any of these issues. Although this study is *not* an exception, it will attempt to treat these three main issues as one. Such an attempt is the main contribution of this dissertation. These three issues are:

1. *Determining the delamination behavior when contact is involved. In other words, how would the presence of a unilateral constraint influence the buckling and postbuckling behavior, growth criteria, and the shape of the delamination front? (Figure 1.2)*

2. *Determining the decohesion and growth criteria. In other words, at what point in the loading (deformation) history would the delamination front move? (Figure 1.3)*

3. *Determining the delamination front contour. In other words, after the decohesion criteria have been met, how would the new delamination zone look? (Figure 1.3)*

Having stated the main issues, it is warranted to state the problem statement on which this work will focus on:

When a thin layer, fully or partially bonded to a much thicker and stiffer solid, is subjected to a loading and/or deformation field(s), what are the

phenomena involved in the response, and how would the layer respond? Further, if the layer is partially bonded, how would the pre-existing delaminated (debonded) region change its size and location?

The format of the following discussion is to take on each issue and explain it, present how other researchers addressed it and their contributions, and finally present the contributions of this dissertation regarding these issues. Due to the fact that issues 2 and 3 are intertwined, they will be presented and discussed together, in the same section.

1.3 Buckling and Postbuckling of Unilaterally Constrained Plates

Consider the situation where an arbitrarily-shaped surface delamination in a laminated structure can be thought of as a plate with arbitrary boundary contour. The fact that the plate is located near the surface implies that the substrate is a much thicker structure that can deform only in its plane, and that its deformations do not obstruct those of the surface plate, only its presence (Figure 1.2). In other words, the substrate imposes a unilateral constraint on the surface delamination. This plate which is part of a larger body can buckle when subjected to a compressive stress field. The buckling mode (eigenmode) is, as always, a function of the plate parameters, e.g., boundary conditions and aspect ratio. For a certain combination of these parameters, and contrary to the common intuitive belief, such a buckling mode can be of one sign (i.e., positive or negative) *or* multi-sign having several waves. For the former buckling mode, the situation can be easily predicted and the unilateral constraint can be accounted for by proper scaling of the eigenmode. For the latter, the situation is entirely different, and the unilateral constraint imposed on the buckling

mode must be accounted for in the formulation and the solution process resulting in a nonlinear eigenvalue problem whose solution is a formidable task.

It is well known that the buckling mode of an elastic rectangular plate is significantly dependent on its aspect ratio [39, 40, 99]. For example, an elastic, simply-supported rectangular plate having an aspect ratio of 1 (square plate) that is subjected to a uniaxial stress field buckles in such a way that the out-of-plane deformations are of one sign. On the other hand, the same plate with an aspect ratio $\geq \sqrt{2}$ (the loaded edges being the shorter ones) buckles in a sinusoidal fashion. Classically, such a unilaterally unconstrained plate-buckling problem was formulated and solved as a linear eigenvalue problem yielding the lowest eigenvalue as the buckling load, and the first eigenmode as the corresponding buckling mode. However, what is not well known, is how the presence of a unilateral constraint affects the buckling characteristics of such plates.

The presence of a unilateral constraint is sometimes referred to in the literature as the *Signorini* problem [35]. In 1933, Signorini was the first to consider a unilateral problem in elasticity. His problem corresponds to the equilibrium problem of an elastic body, which in its natural configuration is supported by a rigid frictionless surface. A general theoretical treatment on the subject can be found in [35]. But such a treatment with its theoretical generality offers little practical use especially when eigenvalue analysis is involved. The eigenvalue analysis of this type of unilaterally constrained boundary value problems is one of the least investigated problems in mathematical physics. In order to confine the subject, and to cover a wide range of problems in which the buckling behavior of unilaterally constrained plates is sought after, the overall strategy of the following discussion will be to investigate two categories of rectangular plates: *infinite and finite*. The advantage of doing so manifests

it self in the fact that the results of the former become a special limiting case for the latter, which facilitates verification of the results.

1.3.1 Infinite Plates

One common simplification when addressing buckling of unilaterally constrained structures is the assumption that the structure, being a beam or a plate, is infinite. Several issues pertaining to this subject have been studied in different contexts. The buckling of a unilaterally constrained infinite beam (thin strip) was addressed by many investigators [1, 4, 44, 73, 83, 105, 115], to mention a few, and it was shown that such a system is completely imperfection-sensitive, with theoretically infinite buckling load in the absence of imperfections or weightlessness.

Weitsman [107] presented an approximate solution for the problem of contact between an elastic plate and a semi-infinite elastic half space[1]. In [108, 109], the same author presented several examples of beam and plate type structures resting on an elastic half space and subjected to transverse distributed and concentrated loads. In these investigations the extent of the contact area that develops between the beam/plate and the half space was determined by an approximate technique. The case of a beam that is subjected to a single concentrated transverse force and resting on a rigid foundation was addressed by Civelek and Erdogan [25]. Gladwell [41] considered a variety of plane, frictionless, unbonded contact problems and provided approximate solutions in terms of Chebyshev polynomials. Some corrections to the earlier work by Weitsman [109] were provided in this article. The problem of transversely loaded circular plates resting on bimodulus and tensionless foundation was addressed by Kamiya [49]. A geometrically nonlinear formulation was adopted

[1] Although buckling is of our main concern, it is important to review part of literature related to the problem of constrained plate deformations in the general sense.

and Berger's [7] simplification to the von Kármán large deflection equations were used in analyzing axisymmetric plate deformations. More recently, Celep [18], addressed the behavior of transversely loaded rectangular elastic plates resting on a tensionless Winkler foundation. In this investigation Galerkin's method was used to obtain results for the areas of contact and plate displacement distributions.

Roorda [83] presented many aspects of unilateral buckling problems in one-dimensional settings, and Seide [85] presented some work on the buckling behavior of an infinitely long, simply supported isotropic plate. Attaching the plate to a tensionless elastic foundation and subjecting it to a far field uniaxial compressive load, the latter author presented results for the buckling load as well as the buckling wave length. Assuming a periodic response and using a limiting process, the solution for a unilaterally constrained simply supported infinite plate was recovered from the exact solutions of the governing differential equations. Such an exact solution showed that the unilateral constraint increases the buckling load by 33%. Using a similar formulation, more general results were obtained by Shahwan and Waas [86]. The formulation as well as the results pertaining to the latter are presented in Chapter II.

1.3.2 Finite Plates

The situation here is not only quite different, it is also mathematically more involved. Unlike the previously presented situation where it was possible to make some assumptions regarding the buckling response (e.g., periodic), this situation offers no such possibility and similar assumptions cannot be employed.

Buckling of unilaterally constrained finite plates has been investigated in different contexts. The physical problems where such a situation occurs are of varying nature.

Of our concern, and to keep a focus on the overall goal of the dissertation, one such problem is the determination of the critical loading conditions of a finite, rectangular, and linear elastic plate that is unilaterally constrained by the presence of a rigid surface parallel to its undeformed middle plane. The distance between the rigid surface and the plate's middle plane is taken to be half the plate's thickness, implying that a gap does not exist.

In the vast literature on the subject of buckling of unilaterally constrained delaminations (which are essentially plates), the unilateral constraint is usually avoided indirectly by either modeling the delamination as a narrow plate (wide column) or as an axisymmetric circular plate or annulus [5, 10, 15, 22, 84], which are essentially one-dimensional models[2]. By resorting to one-dimensional models, the governing partial differential equations are reduced to ordinary differential equations. This implies that for such boundary value problems, the eigenmode corresponding to the lowest eigenvalue is of one sign, hence, no contact occurs (within the boundaries) between the plate and the constraining rigid surface.

Issues pertaining to the equilibrium and stability of discrete one-way structural systems were dealt with in a general manner by Burgess [16]. This author also presented an analysis that showed that the discrete method converges to the continuum solution by studying a radially constrained imperfect ring [17]. In these works the notion of a critical state is classified and the evaluation of the buckling load was carried out in the context of a postbuckling analysis.

An analysis to extend the classic variational theory for eigenvalue problems so as to define the Euler critical load of a unilaterally constrained finite beam is presented in [101]. The variational formulation also provided a method of bounding the buck-

[2]However, it is to be noted that except for certain inner/outer radii ratio, annuli can exhibit a non-axisymmetric behavior [36, 57].

ling load by comparison, and a few important theorems and remarks were stated. Using an elastica approach, Soong and Choi [90] derived equations for continuous contact between a beam and its boundary, as well as multiple discrete point contacts. They presented examples in which the elastica curvature assumes values which are less than the curvature of the restraining boundary, thus resulting in line contact. A finite element solution was presented in [91] with an updated-Lagrangian formulation to investigate the stability of rods with unilateral constraints. These authors showed good agreement in comparing their solutions to those available in the literature. The axisymmetric upheaval buckling of a heavy plate in unilateral contact with a rigid subgrade was presented in [43].

Similar issues relating to the behavior of unilaterally constrained plates have been considered by other researchers in different contexts. Motivated by a problem that arises in magnetic tape recording, Benson [6] used classical plate theory to study plate tenting with one-sided constraint using an energy minimization formulation. A more indepth study on unilateral boundary value problems as related to the nonlinear theory of plates was reported in [60, 61]. This author presented a variational formulation along with an existence theorem and a uniqueness result for a variational solution for thin plates under normal load. The existence of equilibrium states of such plates is also studied.

The buckling of thin plates using von Kármán plate theory in a variational inequality formulation was presented in [29, 30, 52]. Do [30] distinguished three problems in his discussion on the bifurcation of non-zero solutions from the trivial one, the latter being the inplane response. One of the problems was the buckling of a clamped, perfectly flat plate placed directly against a rigid flat surface (no gap). It was concluded that there is no solution which bifurcates from the trivial solution,

more exactly, an infinite load is the only bifurcation value. Such a conclusion shows that there is no quasi-static process which allows one to go from the flat equilibrium state to another equilibrium state in which the plate is buckled.

Using a variational principle with penalty in a finite element formulation, Ohtake *et al.* [69, 70] provided a more convenient basis for computational methods by introducing a penalty term and adding it to the potential energy. In effect, this term is identically zero whenever the plate's out-of-plane deformation is not in contact with the rigid constraint, and greater than zero otherwise. It was possible in this work to linearize the nonlinear equilibrium equations about the unconstrained state (penalty term = 0) due to the presence of an initial gap. The authors stated that bifurcation occurs at the simple eigenvalue of the linearized problem but did not state that this is true only for the case where a gap is initially present between the bottom surface of the plate and the rigid constraining surface.

In the context of delaminations, an analysis of the one-dimensional situation where the sublaminate has some finite bending rigidity, revealed that certain buckling configurations exist in which contact conditions occur [22]. One of the earliest work that addressed the issue of unilateral constraints as related to the problem of two-dimensional delamination buckling was reported by Chai and Babcock [23]. Modeling the delamination as a thin elliptic plate, and based on rather limited number of assumed admissible Rayleigh-Ritz displacement terms, they studied the dependence of overlap conditions on ellipse aspect ratio and load level. More recently, the buckling and post-buckling of elliptical delaminations was investigated by Chai [20, 21] who carried out a simplified contact analysis by limiting the contact regions to isolated points. Although such an assumption resulted in an accuracy within $\pm 30\%$, it would not hold in cases were the geometry, boundary conditions and loading are of

a more complicated nature so that surface rather than point contact would dominate the response. The same author presented a simplified mixed-mode fracture analysis combining nonlinear thin-plate stress solutions with crack-tip elasticity results in thin-film debond problems associated with large film deformations [19]. He showed that film-substrate overlap (unilateral contact) may occur under compression loading. Further, overlap prevention by substrate (unilateral constraint) may drastically increase the energy available for crack propagation, particularly for narrow debonds loaded along their long axis.

Jensen and Thouless [47] analyzed, theoretically and experimentally, the buckling instability of a system where a straight crack lies at the interface between a thin elastic film and a substrate and showed that buckling of the unilaterally constrained system can cause the crack to propagate in a non-straight manner. In their study, the unilateral constraint condition was accounted for using a tensionless foundation model. In a similar and more recent study Suemasu *et al.* [96] presented an experimental as well as an analytical study on the buckling of edge delaminations and showed that the global buckling load reduction is significant and almost proportional to the delamination width. Further, they accounted for the unilateral constraint by introducing an imaginary displacement spring along with two rotational springs at each of the constraint points.

1.4 Delamination Growth

Although it has been the tradition to label the delamination problem as "Delamination Buckling, Postbuckling and Growth" it was often argued that the ordering of the words implies that the three events, namely, buckling, postbuckling and growth, are chronological. In the majority of the literature on the subject it has been assumed

that this is the case and the analysis presented are based on such an assumption. Further, most of the reported delamination growth analyses are self-similar owing to the fact that the cases investigated were either one-dimensional or axi-symmertic. Such an implication and assumptions will be discussed and commented on subsequently. The issues of delamination onset and growth will be explained along with some of the contributions reported in the literature.

Classically, the problem of delamination buckling and growth has been treated by analyzing the growth subsequent to buckling of a finite one-dimensional or axi-symmetric delamination embedded in an infinite medium. While being a valid treatment on the subject resulting in a variety of useful and practical results, this approach significantly hampers the ability to obtain results for 2-dimensional non-self-similar growth. In addition, these studies were based on formulations that circumvent the ability to study the interaction between the "local" and the "global" problem. The local being the delamination and the global being the structure[3] containing the delamination. These deficiencies can be overcome by treating the two problems (i.e., local and global) as one and allowing the distinction to evolve as part of the solution.

1.4.1 Onset of Delamination

Garg [38] presented a condensed overview on this issue. Basically there are two methods to approach the issue of delamination onset: one based on fracture mechanics and the other on strength. The fracture mechanics method, which appears to be more accurate, employs the assumption that the delamination front is an edge of a crack at the interface. This leads to the determination of the stress intensity factor, K or the strain energy release-rate[4], G (after A. A. Griffith who, in 1920, introduced

[3]Throughout this study, the global structure is always a plate.

[4]The strain energy release-rate is the incremental strain energy release per unit gain of delamination area.

the concept of surface energy of a solid). Depending on the values of K or G relative to their critical values, the prediction of the delamination onset or propagation is made. The strength method involves the detailed stress analysis near the free edge used in conjunction with a failure criteria such as the point stress and average stress criteria. However, these criteria are suitable only when the delamination onset is governed by σ_z (out-of-plane) stress component. Other criteria have been proposed when shear stresses are involved. The fracture mechanics approach is the most commonly used due to its simplicity as compared to the other approach where the 3-dimensional stress field needs to be known in order to be compared against the onset criteria, a requirement not easily achievable by employing plate- or shell-type theories[5].

1.4.2 Fracture Mechanics Concepts

Generally speaking, delamination onset and growth criteria were, and still are, fracture mechanics-based. This is predominantly due to the simplicity of implementing fracture mechanics concepts as opposed to others. In the analysis of fracture in elastic bodies it is convenient to consider the energy change in the system due to the fracture growth arising from the changes in external work and internal energy. But it must be remembered that although an overall energy balance must be maintained, there is not, as in normal deformation processes, a simple balance of external work and internal energy. This is because the usual compatibility condition for deformation is violated by fracture and results in an energy change. This occurrence of an energy release-rate is not unique to fracture and can arise in any

[5]Some plate and shell theories include, to the first order (and sometimes higher), σ_z stress in them. Such theories involve computational drawbacks that offset their contributions, and in many situations lead to a system of governing equations that has a degree of complexity similar to that of 3-dimensional elasticity.

system involving discontinuous changes of boundary conditions [111]. The two main fracture mechanics concepts pertaining to delamination growth are:

- The stress intensity factors K_I, K_{II} and K_{III} or the strain energy release-rates G_I, G_{II} and G_{III} which are used in the analysis of elastic systems.
- The J-integral which is used in the analysis of inelastic (dissipative) systems.

K_I, K_{II} and K_{III} refer to stress intensities in crack opening modes I, II and III[111], and likewise for G_I, G_{II} and G_{III}. For the fracture analysis of elastic systems, the concepts of the stress intensity factors and strain energy release rates are related. For example, for a linear isotropic material, the plane strain values for G_I, G_{II} and G_{III} are $G_I = (1-\nu^2)\frac{K_I^2}{E}$, $G_{II} = (1-\nu^2)\frac{K_{II}^2}{E}$ and $G_{III} = (1+\nu)\frac{K_{III}^2}{E}$, and combined modes are simply described by superposition. Thus, at the crack tip in an elastic material, the local stress field can be characterized by the values of K_I, K_{II} and K_{III}, and that critical values would be expected to form a fracture criteria. If we confine our attention to mode I, for example, then we can postulate that fracture will occur when $K_I = K_{Ic}$, where K_{Ic} is a critical value. While K_I is a loading parameter, K_{Ic} is a material parameter that is determined experimentally. Hence, for a particular material one can define K_{Ic}, K_{IIc} and K_{IIIc} as well as G_{Ic}, G_{IIc} and G_{IIIc}, and when used as fracture criteria, both concepts K_c and G_c are entirely equivalent[6].

In other situations where crack tip plasticity is present, employing K_c or G_c as fracture criteria leads to erroneous results. In such situations, and within certain limitations, the J-integral, or simply J, provides a means to determine an energy release rate for cases where plasticity effects are not negligible. J has been proposed as a more universal fracture criteria than G, because it is claimed to be applicable

[6] K_c and G_c are used in general to designate critical stress intensity factor(s) and critical strain energy release rate(s).

to cases where crack growth and fracture are associated with appreciable plastic deformation [12]. Note that for an elastic system, $J = G$, which is a precise statement since the deformations are history-independent. For dissipative systems, this is not necessarily so since the deformations may be history-dependent but, if the loading is monotonic and increasing, then path dependence will not occur and J will be an accurate representation. Under such circumstances, the use of a critical value of J, J_c, to characterize crack initiation is sensible.

For most of the graphite/epoxy laminated composites, delaminations occurs in a brittle fashion with no significant plasticity near the delamination front (crack tip). Hence, and in general, delamination growth has been categorized as a brittle fracture allowing for the employment of K and G concepts.

1.4.3 Delamination Growth using Fracture Mechanics Concepts

One of the earliest introductory treatments on the subject was given by Kachanov [48] who presented, in a simplified fashion, different aspects of one-dimensional delamination buckling and growth based on the strain energy release-rate concept. While in a one-dimensional (or axisymmetric) setting the crack (or delamination front) will propagate in a self-similar manner from the original shape so that the change in fractured area could be defined in terms of a single parameter, in a general two-dimensional (asymmetric) setting this is not the case. In the latter, the growth occurs in a non-self-similar manner which makes the determination of the new crack front profile a free boundary problem whose solution is considerably difficult. The latter situation is still one of the most fundamental yet not fully solved problems in fracture mechanics, especially for composite materials.

By employing fracture mechanics concepts, delamination growth is assumed to

depend upon the stress state of the crack tip which is governed by the mixed mode stress intensity factors K_I, K_{II} and K_{III} or the strain energy release-rates G_I, G_{II} and G_{III}. It is not necessary that all three modes exist together. Only one or two modes may dominate the fracture propagation. This does not simplify the analysis nor the prediction of the fracture propagation direction.

The growth of edge delamination is a stable fracture process in laminates subjected to tensile loading [66, 106]. O'Brien [66] considered that the onset of delamination criteria G_c is a material property independent of ply orientation which contradicts other studies that reported G_c to be strongly dependent on the ratio $\frac{K_{III}}{K_I}$ for angle ply laminates and obtained a relationship in the form

$$G_c \propto \sqrt{1 + \left(\frac{K_{III}}{K_I}\right)^2} \tag{1.1}$$

Further, the mixed mode delamination growth is not observed to follow a single propagation law [38]. Various laws have been used by different investigators and the simplest mixed mode delamination propagation law was defined based on the *total* strain energy release-rate G_T. G_T was defined as

$$G_T = G_I + G_{II} \tag{1.2}$$

and when it reaches G_c, propagation takes place. However, the relationship (1.2) may describe the mixed mode delamination growth only for materials that have $G_{Ic} = G_{IIc}$. But for most of the graphite/epoxy composites, $G_{Ic} \ll G_{IIc}$ and thus equation (1.2) may not adequately describe the delamination growth. A more appropriate interaction relation to describe the growth was assumed to have the following form:

$$\left(\frac{G_I}{G_{Ic}}\right)^m + \left(\frac{G_{II}}{G_{IIc}}\right)^n = 1 \tag{1.3}$$

where the exponents m and n have been found to have different values for different cases. Different investigators have used values like $\frac{1}{2}$, 1 and 2 for m and/or n to fit their experimental data yielding, in many cases, good agreements. Other models for mixed mode fracture criteria have been suggested, such models are [31, 38]:

For graphite/epoxy composites,

$$G_c = c_1 - e^{-c_2\sqrt{1+\left(\frac{K_{III}}{K_I}\right)^2} - c_3} \tag{1.4}$$

where c_1, c_2 and c_3 are experimentally determined curve-fit parameters. Using G instead of K, equation (1.4) was also given in the following form:

$$G_c = 503.3 - e^{-0.25\sqrt{1+\left(\frac{G_{II}}{G_I}\right)\sqrt{\frac{E_L}{E_T}}} - 6.31} \tag{1.5}$$

where E_L and E_T are the longitudinal and transverse moduli of the laminate. For graphite/PEEK composites,

$$\frac{G_I}{G_{Ic}} + \left(\frac{G_{II}}{G_{IIc}}\right)^{\frac{3}{2}} = 1 \tag{1.6}$$

Another and a more general criterion was proposed by Hahn [42]

$$\left(1 - \frac{G_{Ic}}{G_{IIc}}\right)\left(\frac{G_I}{G_{Ic}}\right)^{\frac{1}{2}} + \left(\frac{G_{Ic}}{G_{IIc}}\right)\left(\frac{G_I}{G_{Ic}}\right) + \left(\frac{G_{II}}{G_{IIc}}\right) = 1 \tag{1.7}$$

Although it has been demonstrated that the above delamination growth criteria fit some experimental data fairly well, such criteria lack generality and physical/mathematical basis. Despite all of their deficiencies, such criteria are the main driving force behind most of the progress achieved in the field to date. Hutchinson and Suo [45] presented a comprehensive study on mixed mode cracking in layered materials. Their work included very important and useful results pertaining to fracture and growth criteria.

Yin [112] analyzed the axisymmetric buckling and growth of a circular delamination in a compressed laminate and reported that under a specified fixed boundary compression load, the energy release-rate in the laminate was found to increase monotonically with the growth of a circular thin-film delamination. Further, and in contrast to the reported growth behavior of one-dimensional delaminations reported in [22], the uniform-expansion growth of a circular thin-film delamination, once started, is always catastrophic.

In another study, Yin and Jane [113, 114] investigated the buckling and post-buckling behavior of two-dimensional elliptical delaminations using the Rayleigh-Ritz method. Although their main work concentrated on self-similar growth using energy-release rate, they stated correctly that the actual growth mode is generally *not* a combination of growth along two *fixed* principal directions and, strictly speaking, it can only be determined by evaluating the pointwise values of the energy release-rate along the delamination boundary. In their study of the same problem but in an anisotropic setting, the same authors came across a common analysis difficulty that arises when studying crack/delamination fronts. This difficulty is caused by the fact that the maximum and minimum values of the boundary forces (stresses), moments and energy release-rates generally do *not* occur at the apices. Consequently, growth

of an initially elliptical delamination generally proceeds in the such a manner that the shape of the delamination becomes non-elliptical.

Nairn and Hu [59] proposed a quasi-three dimensional model using lumped springs for the prediction of the propagation of arbitrarily shaped delamination fronts due to tensile stress field. In their study they investigated the delamination behavior using the energy release-rate concept adopted from fracture mechanics. They showed that although the quasi-three dimensional model cannot account for free-edge interlaminar stresses, the predicted crack (delamination front) growth is in qualitative agreement with experimental observations once the delamination growth has proceeded a few ply depths [28]. Experimental observations of microcrack-induced delaminations suggest that delamination growth is not necessarily self-similar and through-the-width [28].

Storåkers and Andersson [93] derived a general expression for the energy released at progressing delamination in plates consisting of an arbitrary distribution of layers of different material properties. The derived expression introduced a quantity that may be interpreted as a plate analogue of Eshelby's energy momentum tensor. Although the expression is quite general its applicability was not demonstrated for two-dimensional non-self-similar delamination growth since the authors investigated only two axisymmetric cases that are, mathematically, one-dimensional (growth is always self-similar).

Employing a Griffith type criterion, Bottega [9] derived a growth law which governs the propagation of a delamination embedded in a layered plate, with the shape of the delamination area and of the plate assumed to be arbitrary. The derivation is based on a point wise growth criterion. In this study, the author did not demonstrate the applicabilities of the derived growth law.

In most of the studies on delamination, the problem of delamination buckling

and growth has been approached by employing structural mechanics theories such as those for beams and plates. Such theories entail approximations which lead to certain constraints on the solution process. Such constraints are the assumption that the edges of the delamination be either free, simply-supported or clamped, and that the delamination cannot grow unless the delaminated layer buckles. As a result, delamination growth has been determined either by enforcing a global energy-balance of the system or by incorporating the concept of energy release-rate after the buckling point is reached. Madenci [56] studied the problem of delamination buckling and growth by employing the stability equations of elasticity theory which overcome these limitations. The author's analysis focused on assessment of the delamination growth parameter K_I (the stress intensity factor) due to the slight opening of the delamination surface. As expected, the value of K_I was shown to be bounded by the results from the simplified model of a clamped and a simply-supported thin plate analysis. Further, the study showed that, should K_I be greater than or equal to the interfacial fracture toughness of the laminate, unstable delamination growth can take place even *before* the buckling load (stress) is reached. The latter result was obtained earlier by Pavier and Chester [72] who, experimentally, found that delaminations in carbon fiber-reinforced epoxy tend to grow in size prior to failure due to buckling.

Another related subject that has received some attention is the folding patterns of buckling-driven thin-film blisters [45, 71]. In [71] the authors showed that thin films and coatings in a state of residual compression can, under appropriate conditions, decohere and buckle away from the substrate to form blisters. They studied the morphology and complex folding patterns of buckling-driven thin-film blisters by formulating the problem in terms of the total energy of the film, which is the sum of the membrane and bending energies, the latter being a singular perturbation of

the former, and constructed solutions by a matched asymptotic expansion. The obtained film deflections were found to match, in surprising detail, the observed complex folding patterns adopted by delaminated films.

1.4.4 Contact and Frictional Effects

Storåkers and Nilsson [94] studied imperfection sensitivity at delamination buckling and growth using a methodology that is based on the affinity between initial and postbuckling transverse deflections. Modeling the delamination as a plate and the delamination front as a crack they investigated three cases, a wide column, a circular plate subjected to an axisymmetric compression and a circular plate subjected to a uniaxial compression. They showed that while the first two cases yielded the expected self-similar growth, the last case resulted in a non-self-similar growth due to the loss of full symmetry of the problem. For the latter, they observed that at the pre-bifurcation load the stress intensity factor is negative (implying contact) although only in the vicinity where stress intensity factors are small. In a recent combined theoretical and experimental study of delamination growth by Nilsson *et al.* [64] it was found that the shape of the delamination was not much affected by the contact provided that the crack growth is expected remote from a contact region. The magnitude of crack parameters was affected, although only slightly. Although the latter study's account for contact was, in some sense, general, its generality was not clearly demonstrated when global contact dominates the response-a situation of prime importance.

Jensen and Thouless [47] analyzed, theoretically and experimentally, the buckling instability of a system where a straight crack lies at the interface between a thin elastic film and a substrate and showed that buckling of the system can cause the

crack to propagate in a non-straight manner. In their study, the unilateral constraint condition was accounted for using a tensionless foundation model.

Thouless *et al.* [97] studied buckling-driven delaminations of thin films in plane-strain setting and showed that, when the effects of contact regions in which frictional effects shield the crack tip, the Coulomb frictional stress required to explain the apparent toughness observed in this regime is larger than the shear yield strength of the interface. Hence, they inferred that for this to be the case then large-scale plasticity may have a significant effect on the obtained results.

In another study that considered frictional effects, Stringfellow and Freund [95] analyzed the process of frictional interaction during the delamination of a compressed thin film from a substrate in order to assess the effect of Coulomb friction, arising from compressive contact, on the energy release-rate, G, driving the delamination. Modeling the system as a two-dimensional elastic half-space containing a thin layer of material adjacent to the free surface (the film) they found that G decreases by about 35% when the coefficient of interfacial friction is equal to one. Using finite elements methods they further found that when the film is more compliant than the substrate, frictional interaction is enhanced and the calculated energy release rate decreases substantially. Further, when bending forces are taken into account, G is significantly affected only when the ratio of the length of the delamination to the thickness of the film is relatively small. Their main conclusion was that frictional effects can be significant in reducing the delamination driving force, and that they can play an important role in the observed arrest of spreading delaminations.

1.4.5 Delamination Buckling and Growth as a Dynamic Problem

Physically, the buckling problem is a dynamic one, and delamination buckling and growth are no exception. Although few studies have investigated this problem in a dynamic setting, this physical situation is still primarily modeled as a quasi-static one. Bottega and Maewal [11] studied the dynamics of delamination buckling for a uniform triangular transverse tension pulse with constant radial compressive load and for three types of radial loading functions with vanishing transverse load. They have reported that for a linearly increasing radial loading function the dynamic growth in circular plates with circular delaminations differs from that predicted by quasi-static analysis and that this behavior is dependent upon the loading rate. Further, the static analysis predicts more extensive delamination growth for the cases considered. Finally, the authors stated that a large magnitude short duration radial pulse loading was seen to exhibit a simple vibratory motion of the delamination with no growth.

The current research will focus on analyzing delamination buckling and growth as a quasi-static problem. The structure containing the delamination(s) will be subjected to either an inplane load-controlled or an inplane displacement-controlled environments. These controlled environments will be assumed to be quasi-static uninfluenced by any inertia effects.

1.5 Delamination as an Interphase Problem

To overcome some of the limitations and deficiencies introduced by employing fracture mechanics concepts, there has been increasing interest in developing theories where fracture emerges as a natural outcome of the deformation history. Such theories utilize what is referred to in the literature as the interface models. Such models replace the interface which has zero thickness and no constitutive proper-

ties with a layer (an interphase) that has a finite thickness along with constitutive properties.

Although these models have been used by different investigators and in a variety of different contexts, they share common drawbacks. One of the major drawbacks for the use of interface models in the analysis of decohesion, especially for composite delaminations, is the difficulty in identifying model parameters. Such a difficulty is attributed to the fact that experiments cannot be directly done on the interface. Hence, indirect information must be derived from tests.

Assuming a homogeneous and linear elastic interphase, Waas [102] studied the effect of the interphase on compressive strength of a unidirectional monofilament composite. The study concentrated on investigating the effect of interphase properties on the composite buckling strain. Although no decohesion was considered in the analysis, the study showed that for such a configuration a "soft" interphase, whose thickness is approximately $\frac{1}{10}$ of the fiber thickness or greater, will have a detrimental effect on the compressive stability of unidirectional composites.

1.5.1 Decohesion of an Interphase

Corigliano [27] generalized the formulation of the already existing interface models which relate tractions to displacement jumps and which can be used to simulate fracture processes. Further, he included in his formulation the issue of softening interfaces and concluded that the proposed interface models and formulation are suitable for mixed mode propagation, for the cases studied. Although the models were referred to as "interface models" they are actually interphase models describing the kinematics and constitutive properties of certain interphases.

A general class of interface models, which generalize the models proposed for

delamination by many investigators and summarized in [27], is expressed by the following relationship:

$$E = \frac{1}{2}(1-d_1)k_1[u_1]^{e^2} + \frac{1}{2}(1-d_2)k_2[u_2]^{e^2} + \frac{1}{2}(1-d_3)k_3^{+} < [u_3]^e >_{+}^{2} + \frac{1}{2}k_3^{-} < [u_3]^e >_{-}^{2} + \Psi \tag{1.8}$$

where the indices 1, 2 and 3 refer to the local principal directions of the interface, and

$$[\mathbf{u}] = [\mathbf{u}]^e + [\mathbf{u}]^p \tag{1.9}$$

are the displacement discontinuities which are the sum of an elastic (reversible) part and a plastic (irreversible) one. E is the free energy per unit surface, d_i are damage variables for the three directions, k_i are interface elastic stiffnesses with the dimension of force per length cube. The unilateral effects are accounted for via $< >_-$ and $< >_+$ symbols which denote the negative and positive parts of the quantity inside. Ψ is a function that represents an energy per unit surface which depends on micromechanical rearrangements. In [27] it was stated that the choice of interface elastic stiffnesses k_i does not appear to be crucial for delamination analysis and that these stiffness parameters can be given by:

$$k_1 \cong \frac{2G_{13}}{e},\ k_2 \cong \frac{2G_{23}}{e},\ k_3^{+} \cong \frac{E_3}{e} \tag{1.10}$$

where e is a fictitious thickness attributed to the interface, and G_{13}, G_{23} and E_3 are the shear and Young's moduli which can be chosen equal to those of the homogenized

composite laminate. In some of the cases investigated in the latter study, e was given a value approximately equal $\frac{1}{5}$ of a single ply thickness.

Needleman [62] addressed the problem of tensile decohesion along an interface in his investigation of the decohesion of a viscoplastic block from a rigid substrate. Although normal as well as shearing effects were considered in his finite element analysis, the problem was in a 1-dimensional setting giving a priori knowledge on the decohesion direction. In a more recent study [63] the same author presented an analysis of fracture where the initial-boundary value problem formulation allows for the possibility of a complete loss of stress carrying capacity, with the associated creation of a new free surface, and without employing any fracture criterion. He mentioned that in grid-based numerical methods, such as the finite element or finite difference methods, a length scale is introduced by the discretization. Further, when numerical analyses of localization or toughness are carried out without some length scale in the initial-boundary value problem formulation, the length scale introduced by the discretization can determine key features of the computed behavior.

1.5.2 Multiple Delaminations

In most of all of the analyses presented on delamination buckling, postbuckling and growth the finite delamination was assumed to be embedded in an *infinite* medium (1- or 2-dimensional) [5, 10, 22, 23, 93, 112, 113, 114], to mention a few. Such an assumption leads to two distinct features of such analyses:

- Only the behavior of the delamination is captured. The behavior of the medium containing the delamination as well as the interaction between the medium and the delamination is rarely part of the analyses. Hence, such analyses are generally local.

- Only a single delaminated region is analyzed. The presence of multiple, unconnected and co-planner delaminated regions is never considered.

In the above discussion, the term "local" implies a region of the size of the delamination (including its boundary). On the other hand, the term "global" implies the entire domain containing all delaminated regions. The above two features are limitations that are implicit in the formulation leading to the commonly reported results. Based on physical grounds it is believed that these limitations can be overcome by treating the two problems (i.e., local and global) as one and allowing the distinction to evolve as part of the solution. This facilitates the ability to study multiple (unconnected) delaminated regions as well as their interactions. For this part of the study no literature was found on the subject. It is believed that the mathematical complexity of such a physical situation is the sole reason for this lack in the technical literature[7].

1.6 Overview of the Dissertation's Contribution

This dissertation will treat the issue of unilateral constraint in the context of buckling of plates. One of the ways to incorporate the unilateral constraint condition in the formulation of solid mechanics problems is to introduce a fictitious elastic layer as a substitute for the rigid constraint. The elastic layer can then be modeled as an elastic foundation composed of a bed of nonlinear axial springs. Although, the nonlinearity can manifest itself in the geometry of springs' deformation and/or the force-displacement constitutive relationship, it is the latter that is of interest to us at this stage. One type of constitutive nonlinearity is a deformation-sign dependency which is believed to be well suited for capturing the physics of unilaterally

[7]This does not imply that this situation was never investigated. The main implication is that pertaining literature was not available.

constrained problems. Hence, the problem of unilateral constraint is modeled by introducing a nonlinear elastic foundation exhibiting such nonlinearity. It is important to remember that this is a feature of the modeling that is introduced and not necessarily of the problem at hand. Further, two types of situations will be considered: *infinite* and *finite* plates. The first will be solved exactly and approximately for simply-supported and clamped-free specially orthotropic plates, respectively. For the first situation, the plates are infinite in the loaded direction and the foundation model used is perfectly tensionless. For the second situation, a different mechanical model will be employed and an appropriate solution method for the critical loading conditions of a rectangular, linear elastic plate will be considered. In both situations the plates are modeled along the lines of classical plate theory employing Kirchhoff-Love hypothesis. The analysis will involve the determination of the buckling loads and modes only, postbuckling of such plates will not be considered in this context but will be dealt with subsequently.

With regards to decohesion and growth it was apparent from the presented literature on the subject that this issue has been analyzed in many different contexts and situations using very similar methods and growth criteria. By employing the strain energy release-rates concept along with other fracture criteria many different problems have been solved, and many limits of the fracture criteria have been reached[8]. Hence, using fracture criteria for delamination growth will not be included in this work. This implies that this dissertation will not contribute directly to delamination growth in the classical (fracture mechanics) sense. Rather an attempt will be made to present a simplified as well as unified treatment on the subject where the three aspects, namely, unilaterally constrained buckling, postbuckling and non-self-similar

[8]This is mainly in mixed mode fracture criteria, especially for composite materials.

growth are accounted for simultaneously. Replacing the interface by a nonlinear elastic interphase only the mechanical properties (stiffness, thickness, ...etc.) will be required to fully characterize the decohesion process without resorting to any fracture mechanics concepts. Further, during the formulation no distinction will be made between the phenomena of buckling (and postbuckling) and non-self-similar growth. In other words, the same equations govern the entire behavior from beginning (starting to load/displace the structure) to end (complete delamination and/or loss of stiffness) without specification to certain regimes of validity. The entire decohesion process will be assumed to be elastic and conservative and all the energy released by will be redistributed back to the structure with no net dissipated elastic energy.

1.7 Organization of the Dissertation

The dissertation is divided into six chapters, and the following is a brief description of each:

Chapter I

This chapter introduces the general problem along with a literature review pertaining to all of its aspects. No literature review will be given in subsequent chapters.

Chapter II

This chapter deals with the problem of buckling of unilaterally constrained *infinite* plates. The problem, which is infinite in one direction, will be formulated and solved for different boundary conditions and material properties. The results of this chapter will be used to verify the results of Chapter III, the former being a limiting case for the latter.

Chapter III

This chapter deals with the problem of buckling of unilaterally constrained *finite* plates. The problem, which is in a rectangular domain, will be formulated and solved for different boundary conditions and material properties. The results of this chapter will be used to demonstrate that using nonlinear foundation models to model unilateral constraints is viable, paving the way for implementing such models into delamination growth models, the latter being the subject of Chapters IV and V.

Chapter IV

This chapter deals with the formulation of the interphase problem as a modeling technique to overcome the limitations of fracture mechanics approaches in predicting delamination growth. Using a virtual work formulation, the plate-interphase-substrate system is modeled as one, resulting in a system of integral equations that will be solved using an approximate method.

Chapter V

This chapter presents few case studies along with the results and analysis of the results. The cases presented are few and their choice was based solely on the fact that they demonstrate the validity, applicability and generality of the interphase model as well as the modeling presented in Chapter IV.

Chapter VI

This chapter presents a summary of the dissertation along with its main conclusions.

The tables and figures of each chapter are located at the end of the chapter and not at the end of the thesis. On the other hand, the bibliography and references are

located at the end of the thesis. Similarly, appendices are located at the end of the thesis.

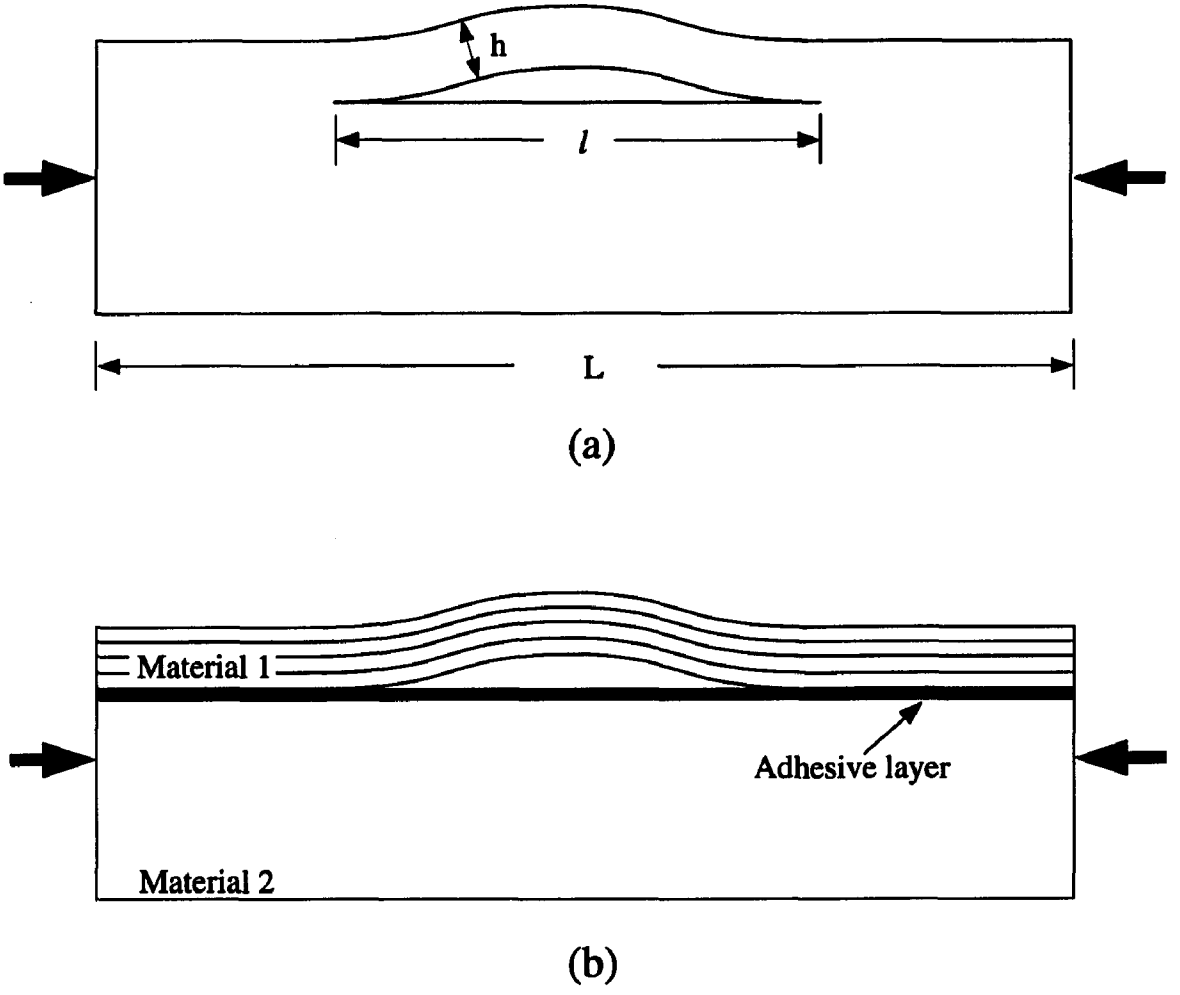

Figure 1.1: A schematic showing a delamination process. (a) Although there is only one homogeneous material without an apparent interface, the separation process is called delamination. This is the most investigated delamination situation. (b) In laminated composites, the delaminated layer(s) can have different material properties (material 1) than the supporting substrate (material 2). At their interface, there exists an adhesive layer whose thickness is usually taken to be equal to zero in order to simplify the formulation of the problem. In the analysis of both situations, it is common to take $l \ll L$ as well as $h \ll l$ (i.e., thin film in an infinite medium).

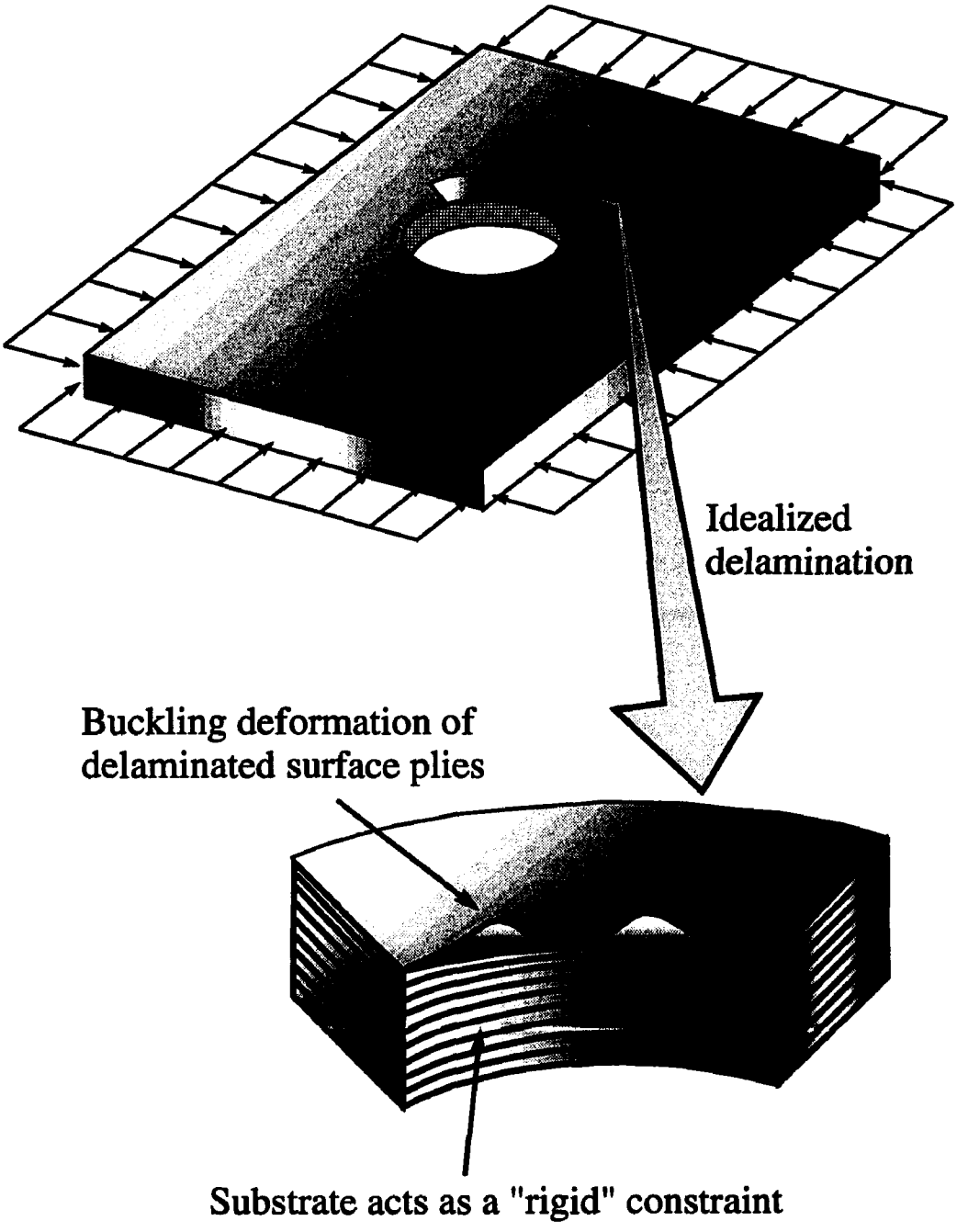

Figure 1.2: A schematic showing an idealized delamination at the edge of a circular hole. When surface plies of a laminated structure delaminate, a compressive stress field can cause these delaminated plies to buckle. The buckling mode is significantly influenced by the presence of the thick and, relatively speaking, "rigid" substrate.

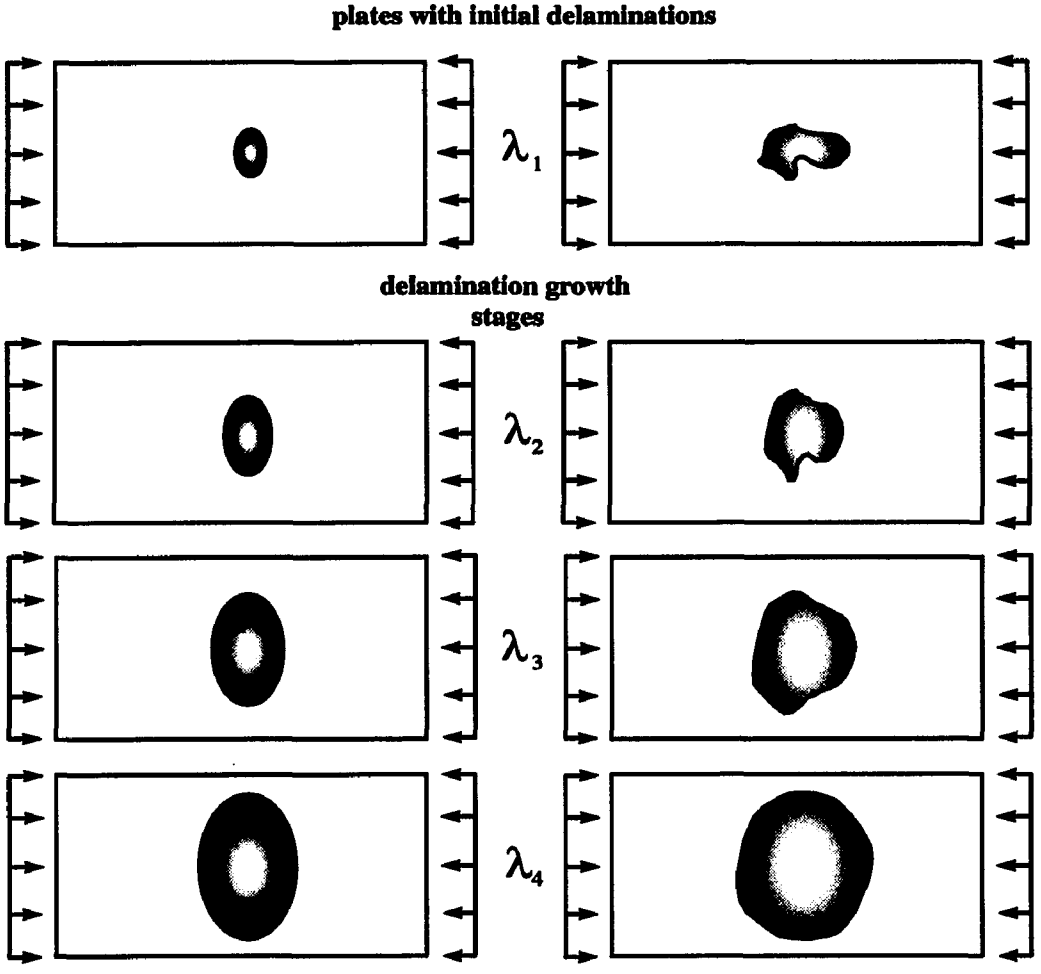

• Elliptical and self-similar delamination growth • Classical fracture mechanics can be used for growth criteria	• Arbitrary and non-self-similar delamination growth • Classical fracture mechanics leads to impractical growth criteria

λ is a load/displacement control parameter

Figure 1.3: Comparison between a self-similar and a non-self-similar delamination growth in a plate subjected to edge loads/displacements.

CHAPTER II

BUCKLING OF UNILATERALLY CONSTRAINED INFINITE PLATES

2.1 Introduction

Although the problem of unilateral buckling is not the main focus of the overall study, it is of particular importance since it plays a vital role in the prediction of delaminations' response. While this role will be assessed in subsequent chapters, this chapter focuses on modeling unilaterally constrained infinite plates so that it can be incorporated in the buckling and postbuckling analysis of delaminations.

The unilateral constraint condition is a physical situation which implies that a plate, when subjected to some loads, will only deform in the direction of the constraint's outward normal and any other direction perpendicular to it. In the forthcoming discussion attention will be focused on obtaining buckling loads that conform to this physical situation.

The buckling behavior of an infinitely long, simply supported isotropic plate (Figure 2.1) was presented by Seide [85]. Attaching the plate to a tensionless elastic foundation and subjecting it to a far field uniaxial compressive load, he presented results for the buckling load as well as the buckling wave length. Using a limiting process, the solution for a unilaterally constrained simply supported infinite plate

was recovered from the exact solutions of the governing differential equations. Such an exact solution showed that the unilateral constraint increases the buckling load by 33%.

Similar attention has not been given to the buckling behavior of infinitely long anisotropic plates with boundary conditions other than simple. To analyze such plates one needs to formulate the problem in such a way so that boundary conditions other than simple can be easily incorporated. Although general anisotropy introduces coupling between the inplane and the out-of-plane behavior, which in turn increases the number of governing differential equations, such a complication can be simplified by considering symmetric orthotropic plates.

Due to the linearity of the elastic plates being considered as well as the symmetry and invariance of all the parameters involved, the latter two being in the infinite direction, the buckling of linear elastic infinite plates resting on tensionless elastic foundations will be categorized as periodic in nature (Figure 2.1). Such parameters are the distribution of the applied axial load, distribution of the tensionless elastic foundation and the boundary conditions.

2.2 Problem Formulation

Although the following formulation is similar in spirit to the approach adopted by Seide [85] it was extended in order to examine a variety of material orthotropies as well as different boundary conditions on the unloaded edges of the plate. Throughout this work, the starting point for any derivation will be energy-based where either total potential energy formulation or virtual work formulation will be employed. Here, we start by using the total potential energy formulation. Consider a rectangular specially orthotropic plate under the action of an inplane compressive uniaxial load

N_{11} and attached to an elastic foundation as shown in Figure 2.2. Modeling the plate along the lines of classical plate theory employing Kirchhoff-Love hypothesis, and realizing the fact that we are investigating the bifurcation from the principal (inplane) solution, the total potential energy $\hat{\Pi}$ is given by,

$$\hat{\Pi} = \frac{1}{2}\int_{\hat{y}_1}^{\hat{y}_2}\int_{\hat{x}_1}^{\hat{x}_2}\left[\ \hat{D}_{11}\hat{w}_{,\hat{x}\hat{x}}^2 + 2\ \hat{D}_{12}\hat{w}_{,\hat{x}\hat{x}}\hat{w}_{,\hat{y}\hat{y}} + \hat{D}_{22}\hat{w}_{,\hat{y}\hat{y}}^2 + 4\ \hat{D}_{66}\hat{w}_{,\hat{x}\hat{y}}^2\ \right] d\hat{x}d\hat{y}$$
$$+ \int_{\hat{y}_1}^{\hat{y}_2}\int_{\hat{x}_1}^{\hat{x}_2}\mathbf{W}_f\ d\hat{x}d\hat{y} - \frac{1}{2}\int_{\hat{y}_1}^{\hat{y}_2}\int_{\hat{x}_1}^{\hat{x}_2} N_{11}\hat{w}_{,\hat{x}}^2\ d\hat{x}d\hat{y} \tag{2.1}$$

where $\hat{x}_1, \hat{x}_2, \hat{y}_1$ and $\hat{y}_2$ are integration limits that depend on the choice of the coordinate system, $\hat{w}$ is the plate's out-of-plane deflection, $\hat{D}_{ij}$ are the bending stiffnesses defined by Classical Lamination Theory (CLT), and $\mathbf{W}_f$ is the elastic foundation's strain energy density functional. Since N_{11} is a constant, that is independent of the deformation $\hat{w}$, the above formulation is linearized about the buckling (bifurcation) point. Throughout this work the following notation is employed:

$$(\ )_{,x} = \frac{\partial(\ )}{\partial x}$$
$$(\ )_{,xx} = \frac{\partial^2(\ )}{\partial x^2}$$

and likewise for cross and higher order derivatives.

The elastic foundation's strain energy density functional, $\mathbf{W}_f$, is defined as,

$$\mathbf{W}_f = \int k\ \hat{w}\ \Psi(\hat{w})\ d\hat{w} \tag{2.2}$$

where k is a stiffness coefficient that is usually taken to be a constant and Ψ is a general nondimensional functional that depends on the type of foundation present. In the case of a linear elastic foundation (Winkler Foundation), $\Psi(\hat{w}) = 1$, and hence $\mathbf{W}_f = \frac{1}{2}k\hat{w}^2$, where k is the linear foundation stiffness. The constant of integration

(not shown) in (2.2) is always taken to be = 0 based on an energy conservation argument. Calculating the first variation of $\hat{\Pi}$ yields;

$$\begin{aligned}\delta\hat{\Pi} = \int_{\hat{y}_1}^{\hat{y}_2}\int_{\hat{x}_1}^{\hat{x}_2} [&\hat{D}_{11}\hat{w}_{,\hat{x}\hat{x}}\delta\hat{w}_{,\hat{x}\hat{x}} + \hat{D}_{12}(\hat{w}_{,\hat{y}\hat{y}}\delta\hat{w}_{,\hat{x}\hat{x}} + \hat{w}_{,\hat{x}\hat{x}}\delta\hat{w}_{,\hat{y}\hat{y}}) \\ &+\hat{D}_{22}\hat{w}_{,\hat{y}\hat{y}}\delta\hat{w}_{,\hat{y}\hat{y}} + 4\ \hat{D}_{66}\hat{w}_{,\hat{x}\hat{y}}\delta\hat{w}_{,\hat{x}\hat{y}} + k\ \hat{w}\ \Psi(\hat{w})\delta\hat{w} \\ &-N_{11}\hat{w}_{,\hat{x}}\delta\hat{w}_{,\hat{x}}]\ d\hat{x}d\hat{y}\end{aligned} \tag{2.3}$$

where δ is the variational operator and the variation of $\mathbf{W}_f$ is as follows:

$$\begin{aligned}\delta\int_{\hat{y}_1}^{\hat{y}_2}\int_{\hat{x}_1}^{\hat{x}_2}\mathbf{W}_f\ d\hat{x}d\hat{y} &= \delta\int_{\hat{y}_1}^{\hat{y}_2}\int_{\hat{x}_1}^{\hat{x}_2}\int k\ \hat{w}\ \Psi(\hat{w})\ d\hat{w}d\hat{x}d\hat{y} \\ &= \int_{\hat{y}_1}^{\hat{y}_2}\int_{\hat{x}_1}^{\hat{x}_2}\delta\int k\ \hat{w}\ \Psi(\hat{w})\ d\hat{w}d\hat{x}d\hat{y} \\ &= \int_{\hat{y}_1}^{\hat{y}_2}\int_{\hat{x}_1}^{\hat{x}_2} k\ \hat{w}\ \Psi(\hat{w})\delta\hat{w}\ d\hat{x}d\hat{y}\end{aligned} \tag{2.4}$$

Note that the variational operators δ and the partial derivative operators $()_{,x}$, $()_{,y}$, $()_{,xx}$, etc., are commutative. Equation (2.3) represent the first variation of the total potential energy for a specially orthotropic plate that is subjected to an inplane compressive load in the $\hat{x}$-direction and attached to an elastic foundation. Integrating (2.3) by parts and applying the divergence theorem one arrives at the following form of the first variation:

$$\begin{aligned}\delta\hat{\Pi} = \int_{\hat{y}_1}^{\hat{y}_2}\int_{\hat{x}_1}^{\hat{x}_2} [&\hat{D}_{11}\hat{w}_{,\hat{x}\hat{x}\hat{x}\hat{x}} + 2\hat{D}_s\hat{w}_{,\hat{x}\hat{x}\hat{y}\hat{y}} + \hat{D}_{22}\hat{w}_{,\hat{y}\hat{y}\hat{y}\hat{y}} \\ &+N_{11}\hat{w}_{,\hat{x}\hat{x}} + k\hat{w}\Psi(\hat{w})]\ \delta\hat{w}\ d\hat{x}d\hat{y} \\ &-\int_{\hat{y}_1}^{\hat{y}_2}\left(M_{\hat{x}\hat{x}}\delta\hat{w}_{,\hat{x}} - V_{\hat{x}}\delta\hat{w}\right)_{\hat{x}=\hat{x}_1}^{\hat{x}=\hat{x}_2}\ d\hat{y} \\ &-\int_{\hat{x}_1}^{\hat{x}_2}\left(M_{\hat{y}\hat{y}}\delta\hat{w}_{,\hat{y}} - V_{\hat{y}}\delta\hat{w}\right)_{\hat{y}=\hat{y}_1}^{\hat{y}=\hat{y}_2}\ d\hat{x} + R_c\end{aligned} \tag{2.5}$$

where $M_{\hat{x}\hat{x}}$, $M_{\hat{y}\hat{y}}$, $V_{\hat{x}}$, $V_{\hat{y}}$ and R_c are the boundary moments, boundary shear forces, and the sum of corner forces, respectively, and in terms of $\hat{w}(\hat{x},\hat{y})$ are given in the

following equations:

$$
\begin{aligned}
M_{\hat{x}\hat{x}} &= -\Big(\hat{D}_{11}\hat{w}_{,\hat{x}\hat{x}} + \hat{D}_{12}\hat{w}_{,\hat{y}\hat{y}}\Big) \\
M_{\hat{y}\hat{y}} &= -\Big(\hat{D}_{12}\hat{w}_{,\hat{x}\hat{x}} + \hat{D}_{22}\hat{w}_{,\hat{y}\hat{y}}\Big) \\
M_{\hat{x}\hat{y}} &= -2\hat{D}_{66}\hat{w}_{,\hat{x}\hat{y}} \\
V_{\hat{x}} &= -\Big[\hat{D}_{11}\hat{w}_{,xxx} + (2\hat{D}_s - \hat{D}_{12})\hat{w}_{,\hat{x}\hat{y}\hat{y}} + N_{11}\hat{w}_{,\hat{x}}\Big] \\
V_{\hat{y}} &= -\Big[\hat{D}_{22}\hat{w}_{,yyy} + (2\hat{D}_s - \hat{D}_{12})\hat{w}_{,\hat{x}\hat{x}\hat{y}}\Big] \\
R_c &= \Big((2M_{\hat{x}\hat{y}}\delta\hat{w})_{\hat{x}=\hat{x}_1}^{\hat{x}=\hat{x}_2}\Big)_{\hat{y}=\hat{y}_1}^{\hat{y}=\hat{y}_2}
\end{aligned}
\tag{2.6}
$$

For convenience, the two bending stiffnesses $\hat{D}_{12}$ and $\hat{D}_{66}$ have been lumped into one quantity, $\hat{D}_s$, where "s" stands for shear.

$$
\hat{D}_s = \hat{D}_{12} + 2\hat{D}_{66} \tag{2.7}
$$

It is implicit in (2.5) and (2.6) that $\hat{D}_{ij}$ are independent of $\hat{x}$ and $\hat{y}$. This implies that the plate is homogeneous and has a constant thickness.

The integral equation (2.5) represents the weak form of the equilibrium equation. To solve the equilibrium equation for the lowest eigenvalue (buckling load) and the corresponding eigenmode (buckling mode) one needs to find a $\hat{w}$ (other than the trivial solution) such that (2.5) is satisfied. This can be done by operating on either the weak form (i.e., (2.5)) or on the strong form that can be extracted from (2.5). Here, a combined approach will be followed. In the forthcoming analysis, the out-of-plane displacement $\hat{w}(\hat{x},\hat{y})$ was assumed to have the following form:

$$
\hat{w}(\hat{x},\hat{y}) \;=\; A\;\Phi(\hat{x},\hat{y}), \tag{2.8}
$$

where $\Phi(\hat{x},\hat{y})$ is a spatial function that has the following separable form:

$$
\Phi(\hat{x},\hat{y}) \;=\; \phi(\hat{x})\;\varphi(\hat{y}) \tag{2.9}
$$

and A is a displacement amplitude coefficient. The first variation of $\hat{w}$, $\hat{w}_{,\hat{x}}$ and $\hat{w}_{,\hat{y}}$ are,

$$\begin{aligned}
\delta\hat{w} &= \delta A\ \phi(\hat{x})\ \varphi(\hat{y}) \\
\delta\hat{w}_{,\hat{x}} &= \delta A\ \phi_{,\hat{x}}(\hat{x})\ \varphi(\hat{y}) \\
\delta\hat{w}_{,\hat{y}} &= \delta A\ \phi(\hat{x})\ \varphi_{,\hat{y}}(\hat{y})
\end{aligned} \tag{2.10}$$

Investigation of equilibrium states requires the necessary and sufficient condition that the total potential energy $\hat{\Pi}$ be stationary, hence, the vanishing of its first variation,

$$\delta\hat{\Pi} \ = \ 0 \tag{2.11}$$

Substituting (2.8) and (2.9) into (2.5) and in conjunction with (2.11) results in the following integral equation:

$$\begin{aligned}
&\int_{\hat{y}_1}^{\hat{y}_2}\int_{\hat{x}_1}^{\hat{x}_2} \phi\left(\varphi^2\phi_{,\hat{x}\hat{x}\hat{x}\hat{x}} + 2D_s\varphi\varphi_{,\hat{y}\hat{y}}\phi_{,\hat{x}\hat{x}} + D_{22}\varphi\varphi_{,\hat{y}\hat{y}\hat{y}\hat{y}}\phi + \right. \\
&\qquad \left. \frac{N_{11}}{\hat{D}_{11}}\varphi^2\phi_{,\hat{x}\hat{x}} + \frac{k}{\hat{D}_{11}}\varphi^2\phi\right)\ A\ \delta A\ d\hat{x}d\hat{y} + \\
&\int_{\hat{x}_1}^{\hat{x}_2}\left\{\phi\Big[D_{12}\varphi\varphi_{,\hat{y}}\phi_{,\hat{x}\hat{x}} + D_{22}\varphi_{,\hat{y}}\varphi_{,\hat{y}\hat{y}}\phi - D_{22}\varphi\varphi_{,\hat{y}\hat{y}\hat{y}}\phi - \right. \\
&\qquad \left.\Big(2D_s - D_{12}\Big)\varphi\varphi_{,\hat{y}}\phi_{,\hat{x}\hat{x}}\Big]\right\}_{\hat{y}_1}^{\hat{y}_2}\ A\ \delta A\ d\hat{x} + \\
&\int_{\hat{y}_1}^{\hat{y}_2}\left\{\varphi\Big[D_{12}\varphi_{,\hat{y}\hat{y}}\phi\phi_{,\hat{x}} + \varphi\phi_{,\hat{x}}\phi_{,\hat{x}\hat{x}} - \varphi\phi\phi_{,\hat{x}\hat{x}\hat{x}} - \right. \\
&\qquad \left.\Big(2D_s - D_{12}\Big)\varphi_{,\hat{y}\hat{y}}\phi\phi_{,\hat{x}} - \frac{N_{11}}{\hat{D}_{11}}\varphi\phi\phi_{,\hat{x}}\Big]\right\}_{\hat{x}_1}^{\hat{x}_2}\ A\ \delta A\ d\hat{y} - \\
&\Big((4D_{66}\varphi\varphi_{,\hat{y}}\phi\phi_{,\hat{x}})_{\hat{x}=\hat{x}_1}^{\hat{x}=\hat{x}_2}\Big)_{\hat{y}=\hat{y}_1}^{\hat{y}=\hat{y}_2}\ A\ \delta A\ = \ 0
\end{aligned} \tag{2.12}$$

where

$$\begin{aligned}
D_s &= \frac{\hat{D}_s}{\hat{D}_{11}} \\
D_{ij} &= \frac{\hat{D}_{ij}}{\hat{D}_{11}}
\end{aligned} \tag{2.13}$$

In (2.12) it was assumed that the foundation is linear (i.e., $\Psi(\hat{w}) = 1$). Such an assumption is valid because, as we will see later on, the contact condition which is inherently nonlinear was handled in such a way as to render the problem linear by splitting it into two problems, one where the foundation is active and another where it is inactive. Collecting terms in (2.12) and rearranging leads to the following form:

$$\begin{aligned}
&\int_{\hat{x}_1}^{\hat{x}_2}\Bigg\{\phi_{,\hat{x}\hat{x}\hat{x}\hat{x}}\left(\int_{\hat{y}_1}^{\hat{y}_2}\varphi^2 d\hat{y}\right)+\phi\frac{k}{\hat{D}_{11}}\left(\int_{\hat{y}_1}^{\hat{y}_2}\varphi^2 d\hat{y}\right)+\\
&\quad\phi_{,\hat{x}\hat{x}}\left(2D_s\int_{\hat{y}_1}^{\hat{y}_2}\varphi\varphi_{,\hat{y}\hat{y}}d\hat{y}+2\left(D_{12}-D_s\right)\left(\varphi\varphi_{,\hat{y}}\right)_{\hat{y}=\hat{y}_1}^{\hat{y}=\hat{y}_2}+\frac{N_{11}}{\hat{D}_{11}}\int_{\hat{y}_1}^{\hat{y}_2}\varphi^2 d\hat{y}\right)+\\
&\quad\phi\left[D_{22}\int_{\hat{y}_1}^{\hat{y}_2}\varphi\varphi_{,\hat{y}\hat{y}\hat{y}\hat{y}}d\hat{y}+D_{22}\left(\varphi_{,\hat{y}}\varphi_{,\hat{y}\hat{y}}-\varphi\varphi_{,\hat{y}\hat{y}\hat{y}}\right)_{\hat{y}=\hat{y}_1}^{\hat{y}=\hat{y}_2}\right]\Bigg\}\phi\ A\ \delta A\ d\hat{x}-\\
&\left[4D_{66}\int_{\hat{y}_1}^{\hat{y}_2}\varphi\varphi_{,\hat{y}\hat{y}}\ d\hat{y}+\frac{N_{11}}{\hat{D}_{11}}\int_{\hat{y}_1}^{\hat{y}_2}\varphi^2\ d\hat{y}\right]\left(\phi\phi_{,\hat{x}}\right)_{\hat{x}=\hat{x}_1}^{\hat{x}=\hat{x}_2}\phi\ A\ \delta A+\\
&\left[\int_{\hat{y}_1}^{\hat{y}_2}\varphi^2\ d\hat{y}\right]\left(\phi_{,\hat{x}}\phi_{,\hat{x}\hat{x}}-\phi\phi_{,\hat{x}\hat{x}\hat{x}}\right)_{\hat{x}=\hat{x}_1}^{\hat{x}=\hat{x}_2}\phi\ A\ \delta A-\\
&\left(\left(4D_{66}\varphi\varphi_{,\hat{y}}\phi\phi_{,\hat{x}}\right)_{\hat{x}=\hat{x}_1}^{\hat{x}=\hat{x}_2}\right)_{\hat{y}=\hat{y}_1}^{\hat{y}=\hat{y}_2}\ A\ \delta A\ =\ 0
\end{aligned}\tag{2.14}$$

The integral equation in (2.14) must be valid for all admissible ϕ's as well as any arbitrary A. Extracting the differential equation and boundary terms from (2.14) lead to the following results:

Differential equation:

$$\phi_{,\hat{x}\hat{x}\hat{x}\hat{x}}+\Gamma_2\ \phi_{,\hat{x}\hat{x}}+\Gamma_1\ \phi=0 \tag{2.15}$$

and

Boundary terms:

$$-\left[4D_{66}\int_{\hat{y}_1}^{\hat{y}_2}\varphi\varphi_{,\hat{y}\hat{y}}\ d\hat{y}+\frac{N_{11}}{\hat{D}_{11}}\int_{\hat{y}_1}^{\hat{y}_2}\varphi^2\ d\hat{y}\right]\left(\phi\phi_{,\hat{x}}\right)_{\hat{x}=\hat{x}_1}^{\hat{x}=\hat{x}_2}$$

$$+\left[\int_{\hat{y}_1}^{\hat{y}_2}\varphi^2\,d\hat{y}\right]\left(\phi_{,\hat{x}}\phi_{,\hat{x}\hat{x}}-\phi\phi_{,\hat{x}\hat{x}\hat{x}}\right)_{\hat{x}=\hat{x}_1}^{\hat{x}=\hat{x}_2} \tag{2.16}$$
$$-\left(\left(4D_{66}\varphi\varphi_{,\hat{y}}\phi\phi_{,\hat{x}}\right)_{\hat{x}=\hat{x}_1}^{\hat{x}=\hat{x}_2}\right)_{\hat{y}=\hat{y}_1}^{\hat{y}=\hat{y}_2}=0$$

where

$$\Gamma_1=\left(\frac{\pi}{\hat{y}_2-\hat{y}_1}\right)^4\left\{\frac{\int_{\hat{y}_1}^{\hat{y}_2}\left[\alpha\varphi^2+D_{22}\left(\frac{\hat{y}_2-\hat{y}_1}{\pi}\right)^4\varphi_{,\hat{y}\hat{y}}^2\right]d\hat{y}}{\int_{\hat{y}_1}^{\hat{y}_2}\varphi^2\,d\hat{y}}\right\} \tag{2.17}$$

$$\Gamma_2=\left(\frac{\pi}{\hat{y}_2-\hat{y}_1}\right)^2\left\{\lambda+\frac{\left[2\gamma D_s\left(\frac{\hat{y}_2-\hat{y}_1}{\pi}\right)^2\varphi\varphi_{,\hat{y}}\right]_{\hat{y}_1}^{\hat{y}_2}-2\int_{\hat{y}_1}^{\hat{y}_2}D_s\left(\frac{\hat{y}_2-\hat{y}_1}{\pi}\right)^2\varphi_{,\hat{y}}^2\,d\hat{y}}{\int_{\hat{y}_1}^{\hat{y}_2}\varphi^2\,d\hat{y}}\right\} \tag{2.18}$$

and

$$\alpha=\frac{k(\hat{y}_2-\hat{y}_1)^4}{\pi^4\hat{D}_{11}} \tag{2.19}$$

$$\gamma=\frac{\hat{D}_{12}}{\hat{D}_s} \tag{2.20}$$

$$\lambda=\frac{N_{11}(\hat{y}_2-\hat{y}_1)^2}{\pi^2\hat{D}_{11}} \tag{2.21}$$

The nondimensional parameters α, γ and λ are the foundation stiffness parameter, the normalized shear coefficient and inplane load coefficient, respectively. The differential equation (2.15) is ordinary, fourth order, linear and can be solved using standard methods of solution. The boundary conditions can be extracted from the boundary terms given in (2.16) by enforcing the strong conditions that

$$\left(\phi\ \phi_{,\hat{x}}\right)_{\hat{x}=\hat{x}_1}^{\hat{x}=\hat{x}_2}=0 \tag{2.22}$$

$$(\phi_{,\hat{x}}\ \phi_{,\hat{x}\hat{x}})_{\hat{x}=\hat{x}_1}^{\hat{x}=\hat{x}_2} = 0 \tag{2.23}$$

and

$$(\phi\ \phi_{,\hat{x}\hat{x}\hat{x}})_{\hat{x}=\hat{x}_1}^{\hat{x}=\hat{x}_2} = 0 \tag{2.24}$$

Without loss of generality, the last term in (2.16) was set equal to zero, i.e.,

$$\left((4D_{66}\varphi\varphi_{,\hat{y}}\phi\phi_{,\hat{x}})_{\hat{x}=\hat{x}_1}^{\hat{x}=\hat{x}_2}\right)_{\hat{y}=\hat{y}_1}^{\hat{y}=\hat{y}_2} = 0 \tag{2.25}$$

This will be justified when the ϕ boundary conditions are discussed. For homogeneous boundary conditions on ϕ, the resulting problem is an eigenvalue problem where the lowest eigenvalue is identified with the buckling load and the corresponding eigenvector with the buckling mode.

In most of the literature dealing with the analysis of plates on elastic foundations it is assumed that when the plate deforms it will not separate from the foundation. In other words, there will be no regions where there is no contact between the plate and the foundation. In such an analysis, one only requires a single differential equation to describe the response of the plate. In the case where the plate is not attached to the foundation (i.e., no bond exists) there will be some regions where contact is not present. In such a case, the problem is conveniently addressed by considering the contacted and uncontacted regions separately and using appropriate matching conditions at the common boundary between these two regions (Figure 2.3(a)).

Due to the fact that we have two regions of interest in every one period (recall that the response was assumed to be periodic), one needs to show that the governing differential equations can be derived separately from the Principle of Minimum Potential Energy. Consider the periodic response of a "very long" (almost infinite)

plate with N_p periods (waves). Because, by definition, all periods are identical, the total potential energy of the plate is

$$\hat{\Pi} = N_p \hat{\Pi}_p \tag{2.26}$$

where $\hat{\Pi}_p$ is the potential energy of one period. For the problem at hand, in every period there are two regions, a region of contact and a region of separation between the plate and the foundation. Designating the potential energy of one period's contacted region by $\hat{\Pi}_{pc}$ and of the separated region by $\hat{\Pi}_{ps}$, one can express $\hat{\Pi}_p$ as the sum of both, i.e.,

$$\hat{\Pi}_p = \hat{\Pi}_{pc} + \hat{\Pi}_{ps} \tag{2.27}$$

Substituting (2.26) into the statement of the principle of minimum total potential energy (2.11), yields;

$$\delta(N_p \hat{\Pi}_p) = 0 \tag{2.28}$$

which can be written as,

$$N_p(\delta \hat{\Pi}_p) = 0 \tag{2.29}$$

Since the value of $N_p \neq 0$, one arrives at the principle of minimum potential energy for one period, i.e.,

$$\delta \hat{\Pi}_p = 0 \tag{2.30}$$

Substituting (2.27) into (2.30) yields;

$$\delta(\hat{\Pi}_{pc} + \hat{\Pi}_{ps}) = 0 \tag{2.31}$$

and due to the linearity of the variational operator δ, (2.31) can be expressed as the sum of the variations, i.e.,

$$\delta\hat{\Pi}_{pc} + \delta\hat{\Pi}_{ps} = 0 \tag{2.32}$$

Based on the fact that there exists two regions of interest, it is assumed that

$$\hat{w}_1(\hat{x}_1, \hat{y}) = A_1\phi_1(\hat{x}_1)\varphi(\hat{y}) \tag{2.33}$$

is the out-of-plane deformation function in the contacted region and

$$\hat{w}_2(\hat{x}_2, \hat{y}) = A_2\phi_2(\hat{x}_2)\varphi(\hat{y}) \tag{2.34}$$

is the out-of-plane deformation function in the uncontacted (separated) region as shown in Figure 2.3(b). Without loss of generality, one can set $A_1 = A_2$. The functionals $\hat{\Pi}_{pc}$ and $\hat{\Pi}_{ps}$ are functions of $\hat{w}_1$ and $\hat{w}_2$, respectively, hence, (2.32) can be written as

$$\delta f(\hat{w}_1) + \delta g(\hat{w}_2) = 0 \tag{2.35}$$

where f and g are two independent functions. For (2.35) to be valid for all variations of f and g the following must hold:

$$\delta f(\hat{w}_1) = 0$$

$$\delta g(\hat{w}_2) = 0$$

The above result is equivalent to

$$\delta\hat{\Pi}_{pc} = 0 \tag{2.36}$$

$$\delta\hat{\Pi}_{ps} = 0 \tag{2.37}$$

Equations (2.36) and (2.37) are necessary and sufficient conditions which, when integrated as previously done, will result in the two governing differential equations:

$$\phi_{1,\hat{x}_1\hat{x}_1\hat{x}_1\hat{x}_1} + \Gamma_2\ \phi_{1,\hat{x}_1\hat{x}_1} + \Gamma_1\ \phi_1 = 0 \tag{2.38}$$

(holds in the contacted region)

$$\phi_{2,\hat{x}_2\hat{x}_2\hat{x}_2\hat{x}_2} + \Gamma_2\ \phi_{2,\hat{x}_2\hat{x}_2} + \bar{\Gamma}_1\ \phi_2 = 0 \tag{2.39}$$

(holds in the uncontacted region)

where

$$\hat{x}_1 \in [-c\Omega, c\Omega]$$

$$\hat{x}_2 \in [-(1-c)\Omega, (1-c)\Omega]$$

It is important to point out that the notation $\hat{x}_1$ and $\hat{x}_2$ in (2.38) and (2.39) implies two different spatial variables and not the two limits of integration defined in equation (2.1). Since the $\hat{y}$-spatial dimension is common to both $\hat{x}_1$ and $\hat{x}_2$, and since $\hat{y} \in [\hat{y}_1, \hat{y}_2]$, it follows that one can specialize the definitions of Γ_1 and Γ_2 as well as $\bar{\Gamma}_1$ as follows:

$$\Gamma_1 = \left(\frac{\pi}{b}\right)^4 \left\{ \frac{\int_0^b \left[\alpha\varphi^2 + D_{22}\left(\frac{b}{\pi}\right)^4 \varphi_{,\hat{y}\hat{y}}^2\right]\, d\hat{y}}{\int_0^b \varphi^2\, d\hat{y}} \right\} \tag{2.40}$$

$$\bar{\Gamma}_1 = \left(\frac{\pi}{b}\right)^4 \left\{ \frac{\int_0^b D_{22} \left(\frac{b}{\pi}\right)^4 \varphi_{,\hat{y}\hat{y}}^2 \, d\hat{y}}{\int_0^b \varphi^2 \, d\hat{y}} \right\} \tag{2.41}$$

$$\Gamma_2 = \left(\frac{\pi}{b}\right)^2 \left\{ \lambda + \frac{\left[2\gamma D_s \left(\frac{b}{\pi}\right)^2 \varphi\varphi_{,\hat{y}}\right]_0^b - 2\int_0^b D_s \left(\frac{b}{\pi}\right)^2 \varphi_{,\hat{y}}^2 \, d\hat{y}}{\int_0^b \varphi^2 \, d\hat{y}} \right\} \tag{2.42}$$

where we have assigned $\hat{y}_1 = 0$ and $\hat{y}_2 = b$ (plate's finite width). λ and α can be expressed as follows:

$$\alpha = \frac{kb^4}{\pi^4 \hat{D}_{11}} \tag{2.43}$$

$$\lambda = \frac{N_{11} b^2}{\pi^2 \hat{D}_{11}} \tag{2.44}$$

$\bar{\Gamma}_1 = \Gamma_1(\alpha = 0)$. Γ_1, $\bar{\Gamma}_1$ and Γ_2 are functions of several variables including the displacement function in the $\hat{y}$-direction, φ. However, they are not functions of ϕ, implying that equations (2.38) and (2.39) are linear differential equations. By assuming the plate's response is periodic, and by further assuming that every period contains two regions, it was possible to formulate the problem so that two linear differential equations govern the behavior of the entire period, and hence, the entire plate. Formulating the problem differently, e.g., by considering the entire period as one region, would have resulted in a nonlinear differential equation whose solution is considerably more difficult. It will be demonstrated in Chapter III that the latter approach will be adopted when considering the unilateral buckling behavior of finite plates.

In order to solve (2.38) and (2.39) it is necessary that some boundary and matching conditions be imposed. Such conditions can be arrived at from equations (2.22)-(2.24). By considering these conditions for both regions the following conditions will be arrived at:

- Boundary conditions:

$$\phi_1\ (\hat{x}_1 = c\Omega) = 0 \tag{2.45}$$

$$\phi_2\ (\hat{x}_2 = -(1-c)\Omega) = 0 \tag{2.46}$$

- Matching conditions:

$$\phi_{1,\hat{x}_1}\ (\hat{x}_1 = c\Omega) = \phi_{2,\hat{x}_2}\ (\hat{x}_2 = -(1-c)\Omega) \tag{2.47}$$

$$\phi_{1,\hat{x}_1\hat{x}_1}\ (\hat{x}_1 = c\Omega) = \phi_{2,\hat{x}_2\hat{x}_2}\ (\hat{x}_2 = -(1-c)\Omega) \tag{2.48}$$

$$\phi_{1,\hat{x}_1\hat{x}_1\hat{x}_1}\ (\hat{x}_1 = c\Omega) = \phi_{2,\hat{x}_2\hat{x}_2\hat{x}_2}\ (\hat{x}_2 = -(1-c)\Omega) \tag{2.49}$$

c and Ω are unknowns that need to be determined, where $c \in [0,1]$ and Ω is the half-wave length of the buckling mode (Figure 2.3(b)). The boundary conditions at $\hat{x}_1 = -c\Omega$ and at $\hat{x}_2 = (1-c)\Omega$ were not considered in favor of the assumed periodicity of ϕ. Going back to (2.25), one can justify the equality based on the following conditions:

1. *Boundary conditions*

   - $\phi_1\ (\hat{x}_1 = c\Omega) = 0$
   - $\phi_2\ (\hat{x}_2 = -(1-c)\Omega) = 0$

2. *Periodicity conditions*

   - $\phi_1\ (\hat{x}_1 = -c\Omega) = 0$

- $\phi_2\ (\hat{x}_2 = (1-c)\Omega) = 0$

To show that, we substitute the above conditions into (2.25) and the results are as follows:

In the contacted region, $\hat{x}_1 \in [-c\Omega, c\Omega]$:

$$\left((4D_{66}\varphi\varphi_{,\hat{y}}\phi_1\phi_{1,\hat{x}_1})_{\hat{x}_1=-c\Omega}^{\hat{x}_1=c\Omega}\right)_{\hat{y}=0}^{\hat{y}=b} =$$

$$4D_{66}\left((\varphi\varphi_{,\hat{y}}\phi_1\phi_{1,\hat{x}_1})_{\hat{x}_1=c\Omega} - (\varphi\varphi_{,\hat{y}}\phi_1\phi_{1,\hat{x}_1})_{\hat{x}_1=-c\Omega}\right)_{\hat{y}=0}^{\hat{y}=b} = 0$$

and

In the uncontacted region, $\hat{x}_2 \in [-(1-c)\Omega, (1-c)\Omega]$:

$$\left((4D_{66}\varphi\varphi_{,\hat{y}}\phi_2\phi_{2,\hat{x}_2})_{\hat{x}_2=-(1-c)\Omega}^{\hat{x}_2=(1-c)\Omega}\right)_{\hat{y}=0}^{\hat{y}=b} =$$

$$4D_{66}\left((\varphi\varphi_{,\hat{y}}\phi_2\phi_{2,\hat{x}_2})_{\hat{x}_2=(1-c)\Omega} - (\varphi\varphi_{,\hat{y}}\phi_2\phi_{2,\hat{x}_2})_{\hat{x}_2=-(1-c)\Omega}\right)_{\hat{y}=0}^{\hat{y}=b} = 0$$

Expressing (2.40), (2.41) and (2.42) in a more compact form yields;

$$\Gamma_1 = \left(\frac{\pi}{b}\right)^4 (\alpha + \mu D_{22}) \tag{2.50}$$

$$\bar{\Gamma}_1 = \left(\frac{\pi}{b}\right)^4 (\mu D_{22}) \tag{2.51}$$

$$\Gamma_2 = \left(\frac{\pi}{b}\right)^2 (\lambda - 2\eta D_s) \tag{2.52}$$

where we have introduced the *stiffness coefficients* μ and η which are defined as follows:

$$\mu = \left(\frac{b}{\pi}\right)^4 \frac{\int_0^b \varphi_{,\hat{y}\hat{y}}^2 \, d\hat{y}}{\int_0^b \varphi^2 \, d\hat{y}} \tag{2.53}$$

$$\eta = \left(\frac{b}{\pi}\right)^2 \frac{\int_0^b \varphi_{,\hat{y}}^2 \, d\hat{y} - \gamma \left(\varphi\varphi_{,\hat{y}}\right)_0^b}{\int_0^b \varphi^2 \, d\hat{y}} \tag{2.54}$$

μ and η depend on the assumed form of φ as well as D_s. It is important to note that μ and η apply to any problem of this type and through the coefficients Γ_1, $\bar{\Gamma}_1$ and Γ_2 they characterize the effect of the plate's boundary conditions in the $\hat{y}$-direction.

It is implicit in this formulation that in order to obtain valid results, φ must be admissible satisfying the boundary conditions at $\hat{y} = 0$ and $\hat{y} = b$. The general solutions for the governing differential equations (2.38) and (2.39) are:

$$\begin{aligned}\phi_1(\hat{x}_1) = {} & B_1 \cosh(\rho_1 \frac{\hat{x}_1}{b}) \cos(\rho_2 \frac{\hat{x}_1}{b}) + B_2 \cosh(\rho_1 \frac{\hat{x}_1}{b}) \sin(\rho_2 \frac{\hat{x}_1}{b}) + \\ & B_3 \sinh(\rho_1 \frac{\hat{x}_1}{b}) \sin(\rho_2 \frac{\hat{x}_1}{b}) + B_4 \sinh(\rho_1 \frac{\hat{x}_1}{b}) \cos(\rho_2 \frac{\hat{x}_1}{b})\end{aligned} \tag{2.55}$$

and

$$\begin{aligned}\phi_2(\hat{x}_2) = {} & B_5 \cos(\varrho_1 \frac{\hat{x}_2}{b}) + B_6 \sin(\varrho_1 \frac{\hat{x}_2}{b}) + B_7 \cos(\varrho_2 \frac{\hat{x}_2}{b}) + \\ & B_8 \sin(\varrho_2 \frac{\hat{x}_2}{b})\end{aligned} \tag{2.56}$$

where $B_1 - B_8$ are coefficients to be determined and ρ_1, ρ_2, ϱ_1 and ϱ_2 are the roots of the characteristic polynomial equations of (2.38) and (2.39), and are defined as follows:

$$\rho_1 = \left(\frac{\pi}{2}\right) \sqrt{2\left(\sqrt{\alpha + \mu D_{22}}\right) - (\lambda - 2\eta D_s)} \tag{2.57}$$

$$\rho_2 = \left(\frac{\pi}{2}\right)\sqrt{2\left(\sqrt{\alpha+\mu D_{22}}\right)+(\lambda-2\eta D_s)} \tag{2.58}$$

$$\varrho_1 = \left(\frac{\pi}{2}\right)\sqrt{2(\lambda-2\eta D_s)-\sqrt{4(\lambda-2\eta D_s)^2-16\mu D_{22}}} \tag{2.59}$$

$$\varrho_2 = \left(\frac{\pi}{2}\right)\sqrt{2(\lambda-2\eta D_s)+\sqrt{4(\lambda-2\eta D_s)^2-16\mu D_{22}}} \tag{2.60}$$

It is to be pointed out that the posed problem has an inherent symmetry, i.e., $\phi_1(\hat{x}_1)$ and $\phi_2(\hat{x}_2)$ are symmetric functions in their perspective domains of definition (Figure 2.3(b)). As such, the coefficients multiplying unsymmetric terms in $\phi_1(\hat{x}_1)$ and $\phi_2(\hat{x}_2)$ must vanish and all other symmetric terms must be retained. Such a simplification reduces (2.55) and (2.56) to the following:

$$\phi_1(\hat{x}_1) = B_1\cosh(\rho_1\frac{\hat{x}_1}{b})\cos(\rho_2\frac{\hat{x}_1}{b}) + B_3\sinh(\rho_1\frac{\hat{x}_1}{b})\sin(\rho_2\frac{\hat{x}_1}{b}) \tag{2.61}$$

and

$$\phi_2(\hat{x}_2) = B_5\cos(\varrho_1\frac{\hat{x}_2}{b}) + B_7\cos(\varrho_2\frac{\hat{x}_2}{b}) \tag{2.62}$$

It is important to note that, in order to obtain physically admissible solutions in both regions, some bounds must exist on the coefficients of both differential equations (2.38) and (2.39), namely, Γ_1, $\bar{\Gamma}_1$ and Γ_2. Such bounds are,

$$\begin{aligned} \Gamma_2 &> 0 \\ \Gamma_2^2 - 4\Gamma_1 &\leq 0 \\ \Gamma_2^2 - 4\bar{\Gamma}_1 &\geq 0 \end{aligned} \tag{2.63}$$

The solution for B_1, B_3, B_5 and B_7 constitutes solving an eigenvalue problem where the ratios of these coefficients can be solved for. Since there are five boundary and matching conditions, four constants, and being an eigenvalue problem, such a combination implies that solving for the constant coefficients would result in a total

of three independent equations. Indeed, when the boundary and matching conditions are employed, two equations relating B_1, B_3, B_5 and B_7, and three equations relating only B_3 and B_7 were obtained. The latter three equations were identical, as expected. Hence, the net number of equations is three. Rearranging these three equations and casting them in a form that is a function of λ as well as the wave-length parameters c and Ω yields the following two final equations[1]:

$$(1-c)\frac{\Omega}{b} = \frac{1}{\varrho_1}\arctan\left(\frac{\frac{T_3}{2\rho_1}\sinh(2\rho_1\frac{c\Omega}{b}) + \frac{T_4}{2\rho_2}\sin(2\rho_2\frac{c\Omega}{b})}{\varrho_1\left[\cosh(2\rho_1\frac{c\Omega}{b}) + \cos(2\rho_2\frac{c\Omega}{b})\right]}\right) \tag{2.64}$$

and

$$\left(\frac{\frac{T_1}{2\rho_1}\sinh(2\rho_1\frac{c\Omega}{b}) + \frac{T_2}{2\rho_2}\sin(2\rho_2\frac{c\Omega}{b})}{\varrho_2\left[\cosh(2\rho_1\frac{c\Omega}{b}) + \cos(2\rho_2\frac{c\Omega}{b})\right]}\right) =$$

$$\tan\left\{\frac{\varrho_2}{\varrho_1}\left[\arctan\left(\frac{\frac{T_3}{2\rho_1}\sinh(2\rho_1\frac{c\Omega}{b}) + \frac{T_4}{2\rho_2}\sin(2\rho_2\frac{c\Omega}{b})}{\varrho_1\left[\cosh(2\rho_1\frac{c\Omega}{b}) + \cos(2\rho_2\frac{c\Omega}{b})\right]}\right)\right]\right\} \tag{2.65}$$

where

$$T_1 = \varrho_1^2 - \rho_2^2 + 3\rho_1^2 \tag{2.66}$$

$$T_2 = \varrho_1^2 + \rho_2^2 - 3\rho_1^2 \tag{2.67}$$

$$T_3 = \varrho_2^2 - \rho_2^2 + 3\rho_1^2 \tag{2.68}$$

$$T_4 = \varrho_2^2 + \rho_2^2 - 3\rho_1^2 \tag{2.69}$$

2.3 Methods of Solution

Equations (2.64) and (2.65) constitute an indeterminant coupled system of two nonlinear equations with three unknowns, λ, c and Ω, where the latter two enter the

[1]Detailed algebraic steps are not presented for the sake of brevity.

equations as $c\frac{\Omega}{b}$ and $(1-c)\frac{\Omega}{b}$. Hence, given a value of the foundation stiffness α, one can find unique values (if they exist) for λ and $(1-c)\frac{\Omega}{b}$ for a particular value of $c\frac{\Omega}{b}$. In other words, treating $c\frac{\Omega}{b}$ as a constant with a preassigned value, the two equations are uncoupled, and one can solve for the two unknowns λ and $(1-c)\frac{\Omega}{b}$. Note that the condition of existence of a solution depends on the assumed value of $c\frac{\Omega}{b}$, which in turns depends on α. For a given α, the minimum eigenvalue, λ_{cr} (i.e., buckling load), corresponds to a unique value of $c\frac{\Omega}{b}$. Further, for a particular $c\frac{\Omega}{b}$ a unique value for λ is guaranteed provided the search for λ is in the range given below,

$$2\left(\eta D_s + \sqrt{\mu D_{22}}\right) \leq \lambda \leq 2\left(\eta D_s + \sqrt{\alpha + \mu D_{22}}\right) \tag{2.70}$$

The above bounds on λ are a direct consequence of the bounds on Γ_1, $\bar{\Gamma}_1$ and Γ_2 given in (2.63) and can be realized based on physical grounds. While the lower bound corresponds to λ_{cr} for a vanishing foundation stiffness ($\alpha = 0$), the upper bound corresponds to λ_{cr} for a plate that is completely attached to a Winkler Foundation of nondimensional stiffness α. λ_{cr} for a plate resting (unattached) on a rigid surface falls between the two bounds. For the latter situation a closed-form expression can be obtained by taking the limit in (2.65) as $\alpha \to \infty$. For the sake of brevity, the details of such a limiting process can be found in Appendix A.

2.4 Results

In this study five different materials were used. While the first was isotropic the remaining four were of the specially orthotropic type having the properties presented in Table 2.10. The results will focus on two cases. The first is the buckling of a simply-supported plate, and the second is the buckling of a clamped-free plate. It is to be noted that these boundary conditions are specified at the $\hat{y} = 0$ and $\hat{y} = b$

edges and are for the entire[2] infinite plate. By definition, no boundary conditions exist at the $\hat{x} = \pm\infty$ edges.

2.4.1 Case 1: Simply-Supported Plate

An exact solution can be obtained for the buckling loads as well as the buckling wave length if the following form for the function φ is assumed:

$$\varphi = \sin\left(\pi\frac{\hat{y}}{b}\right) \tag{2.71}$$

Calculating the values of the factors η and μ for this function yields $\eta = \mu = 1$. This problem was analyzed for the five materials as well as for different values of the parameters α, and the results of such a parametric analysis are tabulated in Tables 2.4, 2.5 and 2.6 and are presented graphically in Figures 2.5-2.13.

2.4.2 Case 2: Clamped-Free Plate

This case is solved by using approximate methods due to the fact that an exact close-form solution cannot be obtained. Here, it was decided to calculate the buckling load coefficient λ_{cr} as well as the buckled wave length $2\frac{\Omega}{b}$ for the two limiting cases of $\alpha = 0$ and $\alpha = \infty$ (i.e., without a foundation and with a rigid tensionless foundation, respectively). Two different methods of solution will be utilized the first being the Rayleigh method, and the second the being the stiffness coefficients using μ and η as defined earlier.

Rayleigh Method

The reason for choosing the Rayleigh method over the Rayleigh-Ritz (sometimes referred to as the Ritz method) will be made clear subsequently. It is worth while

[2]The word 'entire' is used to distinguish between one wave length and the global infinite structure.

noting that the only formal difference between the Rayleigh and the Rayleigh-Ritz method is in the number of degrees of freedom (number of trial functions and hence, the number of unknown coefficients). Formally, the Rayleigh-Ritz method is nothing more than a generalization of the method of Rayleigh to include many degrees of freedom, which usually (not always) results in a far more accurate solution[3].

By assuming the following deformation shape functions,

$$\phi(\hat{x}) = \cos^2\left(\frac{\pi\hat{x}}{2\Omega}\right) \tag{2.72}$$

$$\varphi(\hat{y}) = 1 - \cos\left(\frac{\pi\hat{y}}{2b}\right) \tag{2.73}$$

an approximate expression for λ_{cr} and $2\frac{\Omega}{b}$ that correspond to such an assumed buckling mode can be arrived at. Note that this mode shape ensures that the buckling displacements are of one sign as shown in Figure 2.4. For the sake of brevity, the Rayleigh method will be applied only to the case where the foundation is rigid. Substituting (2.72) and (2.73) into (2.8) and (2.9), then substituting the result into the expression for the total potential energy (2.1) yields;

$$\begin{aligned}\hat{\Pi} = \frac{1}{2}A^2\Bigg[&\hat{D}_{11}\left(\frac{\Omega b}{4}\right)\left(\frac{\pi}{\Omega}\right)^4\left(\frac{3}{2}-\frac{4}{\pi}\right) + 2\hat{D}_{12}\left(\frac{\Omega b}{4}\right)\left(\frac{\pi}{\Omega}\right)^2\left(\frac{\pi}{2b}\right)^2\left(\frac{2}{\pi}-\frac{1}{2}\right) + \\ &\hat{D}_{22}\left(\frac{3\Omega b}{8}\right)\left(\frac{\pi}{2b}\right)^4 + 4\hat{D}_{66}\left(\frac{\Omega b}{8}\right)\left(\frac{\pi}{\Omega}\right)^2\left(\frac{\pi}{2b}\right)^2 - \\ &N_{11}\left(\frac{\pi}{2}\right)^2\left(\frac{b}{\Omega}\right)\left(\frac{3}{2}-\frac{4}{\pi}\right)\Bigg]\end{aligned} \tag{2.74}$$

Implicit in (2.74) is the fact that the foundation is tensionless and rigid, implying the vanishing of its contribution to the energy of the system. For such a physical situation

[3]However, there is no guarantee that by including more terms in the trial function and increasing the degrees of freedom, the Rayleigh-Ritz method will converge to the exact result unless the sequence functions form a *complete set*.

one can always assure such a contribution by considering a one-term approximation, e.g., Rayleigh method. For higher order approximations (two terms or more), e.g., Rayleigh-Ritz method, one needs to formulate and solve the problem differently simply because of the following reason: Assuming the deformation function $\hat{w}_2(\hat{x}_2, \hat{y})$ to have the following form:

$$\hat{w}_2(\hat{x}_2, \hat{y}) = \sum_{i=1}^{M} \sum_{j=1}^{N} A_{ij} \Phi_{ij}(\hat{x}_2, \hat{y}) \tag{2.75}$$

one can simply deduce that *although each term (admissible function) can be of one sign, say positive, the sum (i.e., $\hat{w}_2$) of the product of the coefficients (the A's) and these functions (the Φ's) cannot be guaranteed to have a positive value, implying a nonvanishing foundation-contribution to the total potential energy.* This reason is the justification for choosing the Rayleigh over the Rayleigh-Ritz method.

Minimizing $\hat{\Pi}$ with respect to the amplitude A and recalling the definition of λ from equation (2.44) yields

$$\lambda = 4\left(\frac{b}{2\Omega}\right)^2 + 0.301 D_{12} + 2.205 D_{66} + 0.103 D_{22}\left(\frac{2\Omega}{b}\right)^2 \tag{2.76}$$

The lowest value of λ (i.e., λ_{cr}) corresponds to a wave length to width ratio $(2\frac{\Omega}{b})$ of

$$\frac{2\Omega}{b} = 2.495\,(D_{22})^{-\frac{1}{4}} \tag{2.77}$$

and hence the value of λ_{cr} is

$$\lambda_{cr} = 1.286\sqrt{D_{22}} + 2.205 D_{66} + 0.301 D_{12} \tag{2.78}$$

Stiffness Coefficients Method

This method was applied for two different values of α; $\alpha = 0$ and $\alpha = \infty$. For each value of α two different forms of the deformation shape function, φ, were investigated. The φ functions that were used in this method are:

$$\varphi(\hat{y}) = \left(\frac{\hat{y}}{b}\right)^2 \tag{2.79}$$

$$\varphi(\hat{y}) = 1 - \cos\left(\frac{\pi\hat{y}}{2b}\right) \tag{2.80}$$

This method when compared to the the Rayleigh method is "semi-approximate" in that only one part of the spatial variation is assumed. Thus, by assuming one of the deformation shape functions one can solve for the other. To perform the required analysis for this case, the two equations (2.79) and (2.80) were substituted in (2.53) and (2.54) and the stiffness coefficients, μ and η, were calculated for each function. The remaining part of the analysis follows the same procedure used to analyze simply supported plates, which, as mentioned previously, can be solved exactly. The results of the analysis of cases 1 and 2 are tabulated in Tables 2.4-2.9 and are presented graphically for case 1 only. A discussion of these results will follow.

For the limiting case of an infinitely rigid foundation a closed-form expression for λ_{cr} was obtained (see Appendix A) and is given below:

$$\lambda_{cr} = 2\left(\eta D_s + \sqrt{\vartheta\mu D_{22}}\right) \tag{2.81}$$

where

$$\vartheta = \frac{1}{1 - \left[\dfrac{1 - \left(\dfrac{2m-1}{2n-1}\right)^2}{1 + \left(\dfrac{2m-1}{2n-1}\right)^2}\right]^2}, \tag{2.82}$$

$m = 1, 2, 3, \ldots, \infty$, and $n = 1, 2, 3, \ldots, \infty$. m and n are integers that have no physical meaning. Further, the buckling half-wave length, $(1-c)\frac{\Omega}{b}$, was also obtained in Appendix A and is given below,

$$(1-c)\frac{\Omega}{b} = \frac{1}{2}\frac{(2n-1)}{\sqrt{\sqrt{\vartheta} - \sqrt{\vartheta - 1}}}(\mu D_{22})^{-\frac{1}{4}} \tag{2.83}$$

The total wave length $2\frac{\Omega}{b}$ can be calculated for this limiting case by using the following general relationship (Figure 2.3):

$$2\frac{\Omega}{b} = 2\left[(1-c)\frac{\Omega}{b} + c\frac{\Omega}{b}\right] \tag{2.84}$$

Based on physical considerations, the value of $c\frac{\Omega}{b}$ at buckling is 0 (Appendix A). Substituting $c\frac{\Omega}{b}$ into (2.84) yields the following value for $2\frac{\Omega}{b}$:

$$2\frac{\Omega}{b} = \frac{(2n-1)}{\sqrt{\sqrt{\vartheta} - \sqrt{\vartheta - 1}}}(\mu D_{22})^{-\frac{1}{4}} \tag{2.85}$$

The most interesting feature of the integers m and n in (2.82) is their symmetry. Interchanging them would not change the value of ϑ (Table 2.1). Further, setting $m = n$ leads to $\vartheta = 1$ (the case of a plate without foundation). Hence, for $m = n$, the value of λ_{cr} coincides with the lower bound given in (2.70) (Table 2.2). Table 2.3 shows values of $(1-c)\frac{\Omega}{b}$ for different values of m and n. In Table 2.2 the boxed value (i.e., $\boxed{5.333}$) is the lowest λ_{cr} value (lowest eigenvalue) for a rigidly constrained

plate. Values for λ_{cr} between 4.000 and 5.333 correspond to discontinuities in the characteristic equation rather than to eigenvalues. Such discontinuities arise during root searching. Further, in Table 2.3, the boxed value (i.e., $\boxed{0.866}$) is the half-wave length ($(1-c)\frac{\Omega}{b}$) for a rigidly constrained plate at buckling, which corresponds to $\lambda_{cr} = 5.333$. Note that $4.000 < \lambda_{cr} < 5.333$ yield values for $(1-c)\frac{\Omega}{b} > 3$, while $\lambda_{cr} = 5.333$ yields $(1-c)\frac{\Omega}{b} = 0.866$, a much smaller half-wave length. This clearly indicates that at buckling the buckling mode attains the lowest wave length possible. I.e., buckling corresponds to the shortest wave length.

Equation (2.81) gives the value of the buckling load coefficient λ_{cr} for an infinite specially orthotropic plate resting on a rigid surface. Recall that λ_{cr} for an unconstrained plate ($\alpha = 0$) is given by

$$\lambda_{cr} = 2\left(\eta D_s + \sqrt{\mu D_{22}}\right) \tag{2.86}$$

If we designate λ_{cr} given in (2.81) for the rigidly *constrained* plate by λ^c_{cr}, and λ_{cr} given in (2.86) for the *unconstrained* plate by λ^u_{cr}, then one realizes that $\lambda^u_{cr} = \lambda^c_{cr}(\vartheta = 1)$. This indicates that λ^u_{cr} is a special case of λ^c_{cr}, which can be obtained by setting $\vartheta = 1$. In turn, $\vartheta = 1$ can be obtained if and only if $m = n$ (see Tables 2.1 and 2.2).

As previously indicated, equations (2.81) and (2.83) were derived for the limiting case where the foundation stiffness $\alpha \to \infty$. For the case of a finite α, more laborious steps need to be followed in order to arrive at values for λ and $(1-c)\frac{\Omega}{b}$ satisfying (2.64) and (2.65). In this case, the solution process commenced by assigning a value to α. Then, a value for $c\frac{\Omega}{b}$ was selected rendering (2.65) determinant with only one unknown, λ. In (2.65) the value of λ was varied with small increments[4] (typically, increments of 0.001 were used). The process was terminated when (2.65)

[4]The increment size depends on the behavior of (2.65) at this selected $c\frac{\Omega}{b}$.

was satisfied within an allowable tolerance. Then the process was repeated for other values of $c\frac{\Omega}{b}$ and new values for λ were obtained. Of these λ values, the lowest value obtained was designated λ_{cr} since it will be the first value of λ at which the plate will buckle[5] (solution bifurcates). This entire process was repeated for different values of α. During the search, the value of λ was always kept between its upper and lower bounds given in (2.70).

2.5 Discussion

The following section is devoted to the analysis of the results obtained earlier. The discussion focuses on the two cases considered, namely, the simply-supported case and the clamped-free case of infinitely long specially orthotropic plate on tensionless foundations.

2.5.1 Case 1: Simply-Supported Plate

This is the case where the plate is simply supported at $\hat{y} = 0$ and $\hat{y} = b$. An exact solution to this case can be obtained by solving the field equations in each of the contacted and uncontacted regions and applying the matching conditions at the boundary between the two regions. In this case the solution is separable and the exact deformation shape functions are

$$\hat{w}_1(\hat{x}_1, \hat{y}) = A\phi_1(\hat{x}_1)\sin\left(\pi\frac{\hat{y}}{b}\right)$$
$$\hat{w}_2(\hat{x}_2, \hat{y}) = A\phi_2(\hat{x}_2)\sin\left(\pi\frac{\hat{y}}{b}\right)$$

where ϕ_1 and ϕ_2 are obtained by the solution of the field equations. Details of this calculation are not presented but follow closely the method outlined in [85]. If the

[5]This value of λ_{cr} is for a particular α.

same "y" shape function as given above is used in the proposed approximate method then the same exact result will be arrived at. The results of the variation of the buckling load coefficient λ_{cr} as a function of the foundation stiffness α are shown in Figure 2.5. The results obtained via the stiffness coefficients method reduce to those for isotropic materials reported in [85], when the appropriate simplifications to the bending stiffnesses D_{ij} are made. Relevant results for the isotropic case are also included in Figure 2.5. From this figure, it is seen that for a given material there exists a value of α, beyond which the buckling load remains unchanged. For these large α values, the buckling mode shape is as shown in Figure 2.4, with the displacements being of one sign. Further, in the limit as $\alpha \rightarrow \infty$ (rigid foundation), the obtained buckling loads are seen to be higher than the case of no foundation ($\alpha = 0$). These results are summarized in Table 2.4 including some results for the intermediate value of $\alpha = 1$. The percent increase in the buckling load between the two extreme cases is tabulated in Table 2.5. Except for the C-IM7 material, the % increase is close to the 30% range.

In Figure 2.6 the variation of λ with $c\frac{\Omega}{b}$ for $\alpha = 1$ is shown. The parameter $c\frac{\Omega}{b}$ is a measure of (fraction of) the plate's wave length that remains in contact with the foundation. Some values of $c\frac{\Omega}{b}$ are tabulated in Table 2.4 for different values of α at buckling. Notice that as α increases the contact length diminishes to zero corresponding to point contact. The manner in which this decrease occurs is shown in Figure 2.7 for three different materials. This figure clearly indicates that $c\frac{\Omega}{b}$ is insensitive to the type of material studied, but is seen to diminish rapidly with α showing a tendency to level off beyond $\alpha \approx 70$.

Figures 2.8, 2.9, 2.10 and 2.11 show typical relationships between λ and the wave-length parameters $c\frac{\Omega}{b}$ and $(1-c)\frac{\Omega}{b}$ for two different types of materials. These

plots were determined for an intermediate value of α ($\alpha = 1$). Figure 2.12 shows a 3-dimensional plot of the above three parameters in the λ-$(1-c)\frac{\Omega}{b}$-$c\frac{\Omega}{b}$ space. Such a plot is analogous (in character) to the phase-time trajectories for a stable focus of a linear damped oscillator. For such an oscillating system, plotting displacement vs. velocity vs. time results in a 3-dimensional plot analogous to the one shown in Figure 2.12. Two interesting features to be pointed out are the the limiting cases of no foundation ($\alpha = 0$) and an infinitely-rigid tensionless foundation ($\alpha = \infty$). The former corresponds to $c\frac{\Omega}{b} = (1-c)\frac{\Omega}{b} = 0.5$, hence, a straight vertical line in the λ-$(1-c)\frac{\Omega}{b}$-$c\frac{\Omega}{b}$ space. The latter corresponds to $c\frac{\Omega}{b} = 0$, hence, the λ-$(1-c)\frac{\Omega}{b}$-$c\frac{\Omega}{b}$ space is compressed into the λ-$(1-c)\frac{\Omega}{b}$ plane. Note that λ_{cr} is always the point on the curve closest to the $c\frac{\Omega}{b}$-$(1-c)\frac{\Omega}{b}$ plane.

Figure 2.13 shows a typical relationship between λ and the total wave length $2\frac{\Omega}{b}$ for two different materials. In this figure as well as all previous ones where λ (not λ_{cr}) is plotted against another parameter, the value of λ_{cr} corresponds to the lowest point on the curve (whether being a function or not, e.g., λ-$(1-c)\frac{\Omega}{b}$ curve).

Table 2.6 shows the results of the comparison between the attached and unattached foundations for the case of $\alpha = 1$. As expected, the buckling load is substantially higher for the case with attachment. It is to be noted that for the cases where $\alpha = 0$ and $\alpha = \infty$ the values of λ can be determined from the lower and upper limits, respectively, of (2.70) after substituting $\eta = \mu = 1$.

2.5.2 Case 2: Clamped-Free Plate

This case corresponds to the clamped-free boundary conditions at $\hat{y} = 0$ and $\hat{y} = b$, respectively, for which an exact solution is not available. Results obtained from the Rayleigh method and the stiffness coefficients method are presented. The

results shown in Table 2.7 were obtained by assuming the mode shapes (2.72) and (2.73) in conjunction with the Rayleigh method for the case of a rigid foundation ($\alpha = \infty$). The results tabulated in Table (2.8) were obtained by assuming the same mode shape in the $\hat{y}$-direction in conjunction with the stiffness coefficients method for the case of a rigid foundation. The values obtained via the Rayleigh method are seen to be higher than those obtained by the other method. Thus, the stiffness coefficients method is seen to furnish a better approximation to the buckling load than the Rayleigh method. Finally, the percent increases in the buckling loads due to the constraint of a one-sided buckling mode are presented in Table 2.9. Here, it is seen that for all materials studied and similar to case 1, the increase in the buckling load falls close to the 30% range.

2.6 Concluding Remarks

This chapter focused on finding the buckling loads for isotropic and specially orthotropic infinite plates when the buckling mode is constrained to be of one sign. The plates were modeled along the lines of classical plate theory employing Kirchhoff-Love hypothesis. The condition of contact at buckling which renders the problem to be of the nonlinear eigenvalue type was bypassed by modeling the plate as having two distinct regions, a contacted and an uncontacted regions, which resulted in a problem of the linear eigenvalue type. Considering, as case studies, plates with simply-supported (case 1) and clamped-free (case 2) boundary conditions that are made up of isotropic as well as different orthotropic materials, the resulting system of equations was solved exactly and approximately, for cases 1 and 2, respectively. Due to the constraint on the deformation being one-sided, an increase in the buckling load of (i) $22 - 33\%$ for the case of simple supports and (ii) $24 - 36\%$ for the case

of clamped-free supports, over the unconstrained situation, was obtained for such cases. Hence, one notices that by having a unilateral constraint, the increase in the buckling load falls approximately near the +30% range. One ought to keep in mind that such conclusions are valid only for infinite plates. Since the main goal in this study is to investigate the behavior of delaminations, which can be thought of as "finite plates", similar results are needed in order to characterize the buckling and postbuckling behavior of such plates. By having an infinite plate, it was possible to simplify the physical situation, arising from the unilateral constraint, by assuming a periodic response. For finite plates such as assumption is clearly invalid and one has to solve the nonlinear problem. The latter will be the focus of the next chapter which will present a treatment on the subject by modeling the unilateral constraint as a nonlinear elastic foundation and allowing the plate's deformed shape to evolve as part of the solution rather than as part of the formulation as in the situation presented thus far.

	n = 1	2	3	4
m = 1	1.000	2.778	6.760	12.755
2	2.778	1.000	1.284	1.907
3	6.760	1.284	1.000	1.118
4	12.755	1.907	1.118	1.000

Table 2.1: Values of ϑ for different values of m and n.

	n = 1	2	3	4
m = 1	4.000	$\boxed{5.333}$	7.200	9.143
2	$\boxed{5.333}$	4.000	4.267[a]	4.762
3	7.200	4.267	4.000	4.114
4	9.143	4.762	4.114	4.000

[a] $\lambda_{cr} \in (4.000, 5.333)$ correspond to a discontinuity in the characteristic equation rather than an eigenvalue. Hence, the lowest eigenvalue for the rigidly constrained case is $\boxed{5.333}$.

Table 2.2: Values of λ_{cr} for different values of m and n. The material is isotropic ($D_s = D_{22} = 1.0$) and the boundary conditions are simple ($\mu = \eta = 1.0$).

	n = 1	2	3	4
m = 1	0.500	2.598	5.590	9.260
2	$\boxed{0.866}$	1.500	3.227	5.346
3	1.118	1.936	2.500	4.141
4	1.323	2.291	2.958	3.500

Table 2.3: Values of $(1-c)\frac{\Omega}{b}$ for different values of m and n. The material is isotropic ($D_s = D_{22} = 1.0$) and the boundary conditions are simple ($\mu = \eta = 1.0$).

Material	$\alpha = 0.0^a$		$\alpha = 1.0$			$\alpha = \infty^b$	
	λ_{cr}	$(1-c)\frac{\Omega}{b}$	λ_{cr}	$c\frac{\Omega}{b}$	$(1-c)\frac{\Omega}{b}$	λ_{cr}	$(1-c)\frac{\Omega}{b}$
Isotropic	4.000	0.500	4.330	0.414	0.562	5.333	0.866
A-IM7/8551-7	2.826	0.500	3.198	0.400	0.652	3.650	1.100
A-T300/BP907	2.992	0.500	3.350	0.425	0.658	3.902	1.047
B-IM7/8551-7	7.375	0.500	7.633	0.355	0.396	9.530	0.681
C-IM7-8551-7	5.382	0.500	5.730	0.400	0.548	6.540	0.927

[a] $c\frac{\Omega}{b} = 0.500$ for any material.
[b] $c\frac{\Omega}{b} = 0.000$ for any material.

Table 2.4: Results of parametric analysis for three values of the foundation stiffness parameter α (case 1).

Material	λ_{cr}		
	No foundation	Rigid foundation	% Change
Isotropic	4.000	5.333	+33
A-IM7/8551-7	2.826	3.650	+29
A-T300/BP907	2.992	3.902	+30
B-IM7/8551-7	7.375	9.530	+29
C-IM7-8551-7	5.382	6.540	+22

Table 2.5: Influence of the type of foundation (rigid or not present) on λ_{cr} (case 1).

Material	λ_{cr} for ($\alpha = 1.0$)		
	Attached foundation	Unattached foundation	% Change
Isotropic	4.828	4.330	-12
A-IM7/8551-7	3.940	3.198	-23
A-T300/BP907	4.048	3.350	-21
B-IM7/8551-7	7.944	7.633	-4
C-IM7-8551-7	6.293	5.730	-10

Table 2.6: Influence of the type of foundation (attached or unattached) on λ_{cr}, for $\alpha = 1.0$ (case 1).

Material	λ_{cr}	$2\frac{\Omega}{b}$
Isotropic	2.124	2.495
A-IM7/8551-7	1.465	3.171
A-T300/BP907	1.567	3.020
B-IM7/8551-7	3.822	1.963
C-IM7-8551-7	2.647	2.674

Table 2.7: Approximate values for the buckling load coefficient λ_{cr} and the buckled wave length to width ratio $2\frac{\Omega}{b}$ using Rayleigh method. The foundation is considered rigid (case 2).

Material	$\varphi = 1 - \cos\left(\frac{\pi\hat{y}}{2b}\right)$				$\varphi = \left(\frac{\hat{y}}{b}\right)^2$			
	λ_{cr}	$2\frac{\Omega}{b}$	η	μ	λ_{cr}	$2\frac{\Omega}{b}$	η	μ
Isotropic	1.876	2.833	0.320	0.138	2.193	2.488	0.341	0.205
A-IM7/8551-7	1.281	3.520	0.325	0.138	1.488	3.260	0.348	0.205
A-T300/BP907	1.380	3.424	0.329	0.138	1.608	3.100	0.355	0.205
B-IM7/8551-7	3.343	2.227	0.325	0.138	3.883	2.015	0.348	0.205
C-IM7-8551-7	2.246	3.038	0.321	0.138	2.565	2.748	0.343	0.205

Table 2.8: Values of λ_{cr}, $2\frac{\Omega}{b}$ and the modified stiffness coefficients μ and η, for the case of a rigid foundation (case 2).

Material	λ_{cr}		
	No foundation	Rigid foundation	% Change
Isotropic	1.381	1.876	+36
A-IM7/8551-7	0.975	1.281	+31
A-T300/BP907	1.042	1.380	+32
B-IM7/8551-7	2.544	3.343	+31
C-IM7-8551-7	1.815	2.246	+24

Table 2.9: Influence of the type of foundation (rigid or not present) on λ_{cr} (case 2).

Material	$\hat{D}_{11}$[a]	$\hat{D}_{22}$	$\hat{D}_s$	$\hat{D}_{12}$	$\hat{D}_{66}$	D_{22}	D_s	$\frac{\hat{D}_{12}}{\hat{D}_s} = \gamma$
Isotropic[b]	.....	.....	.....	.....	.....	1.000	1.000	0.333
A-IM7/8551-7	250.0	95.8	198.5	64.1	67.2	0.383	0.794	0.323
A-T300/BP907	236.0	110.0	191.9	60.7	65.6	0.466	0.813	0.316
B-IM7/8551-7	95.8	250.0	198.5	64.1	67.2	2.610	2.072	0.323
C-IM7-8551-7	161.0	122.0	293.1	96.1	98.5	0.758	1.821	0.328

[a]Values are in (x 10 N-m).

[b]Since results are functions of D_{22} and D_s, the explicit values of $\hat{D}_{11}$, $\hat{D}_{22}$ and $\hat{D}_s$ are irrelevant in this case.

Table 2.10: Laminate bending stiffnesses of the five types of materials used in this study.

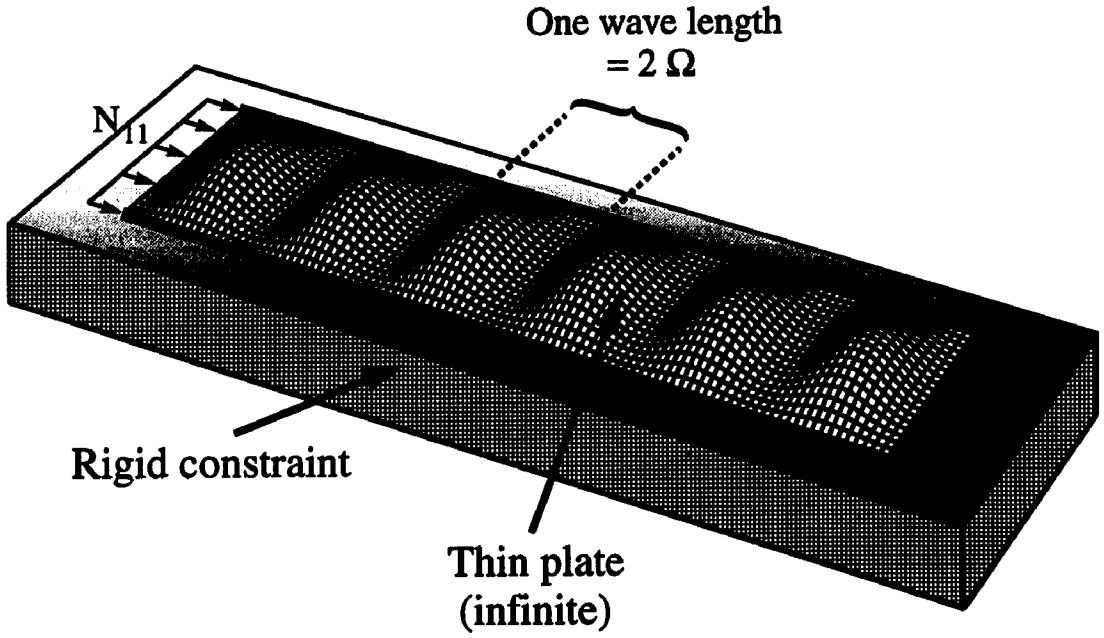

Figure 2.1: Buckling of a unilaterally constrained infinite plate. Note the periodic nature of the response. The loads N_{11} are applied at $x = \pm\infty$. Although the figure shows 6 waves, the infinite plate has infinite number of waves.

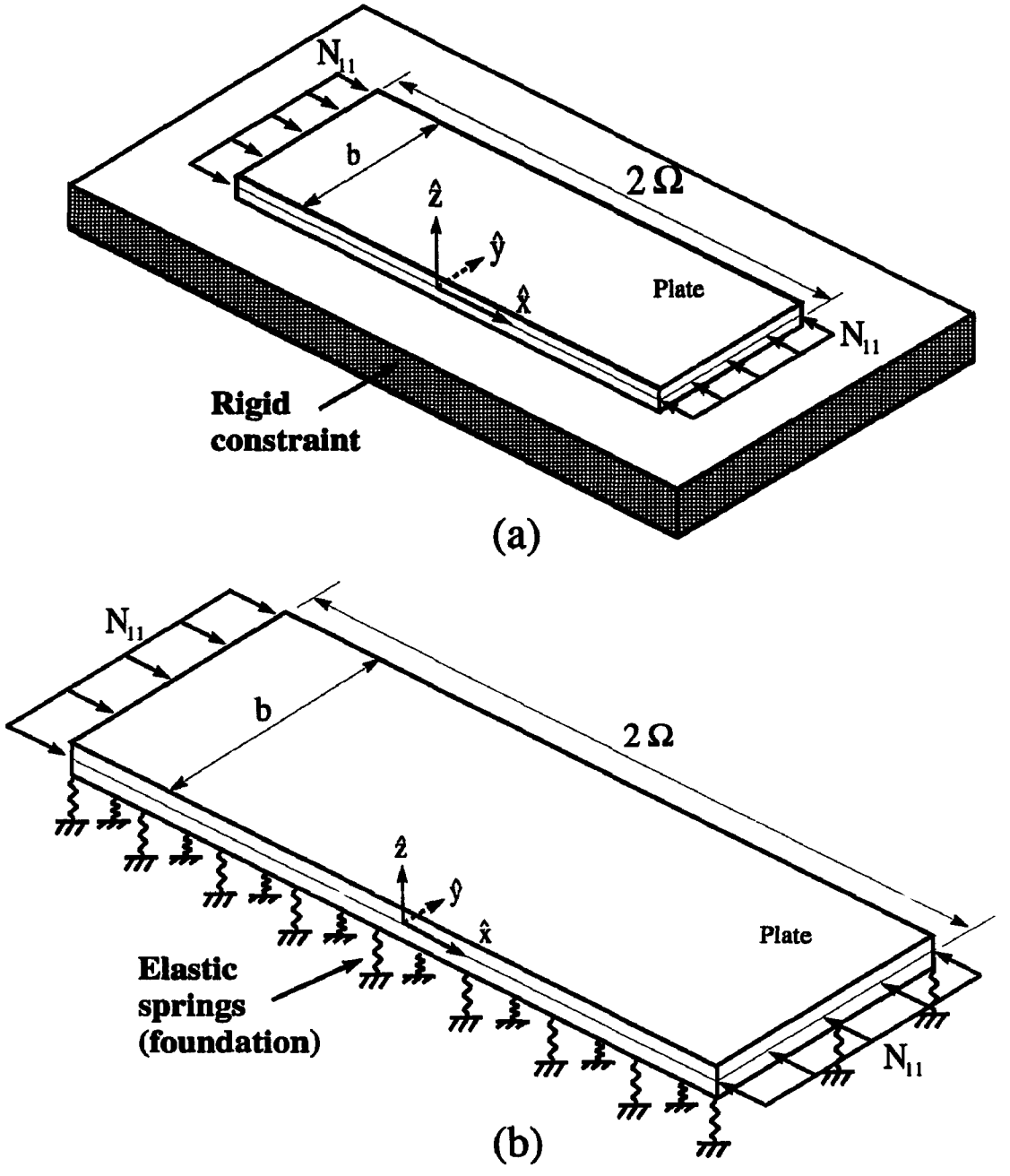

Figure 2.2: One period of a thin elastic infinite plate constrained by a rigid surface and under the action of an applied inplane uniform load. (a) The physical problem, (b) the mathematical model. 2Ω represents the wave length of one period.

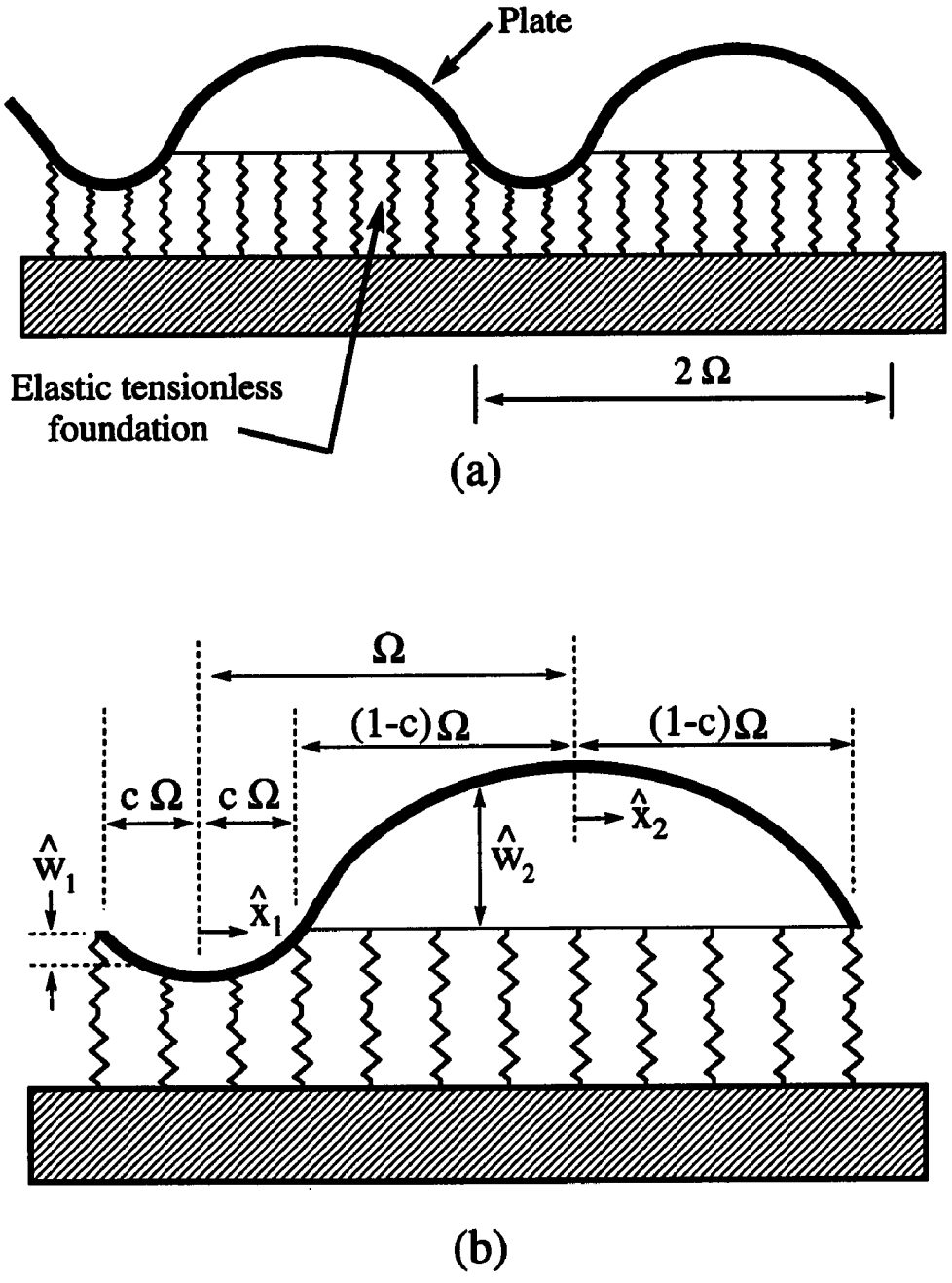

Figure 2.3: Mathematical model. (a) Two waves showing the plate and the contacting and non-contacting regions, (b) one wave showing the physical meaning of the deformation variables, c, Ω, $\hat{w}_1$ and $\hat{w}_2$.

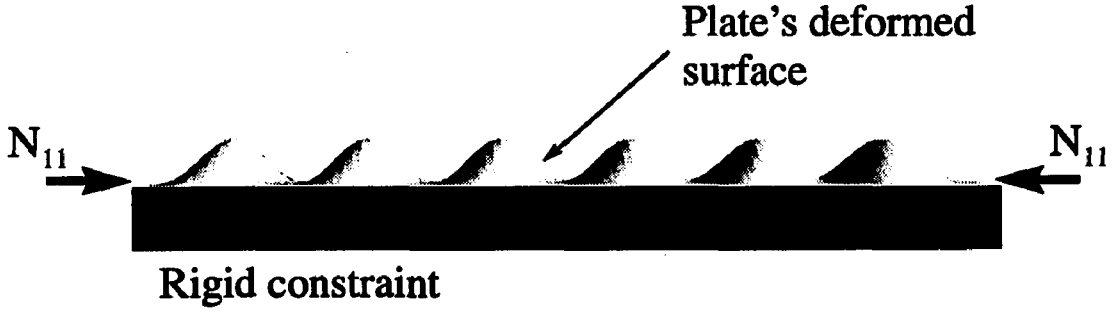

Figure 2.4: Limiting buckled shape for a plate resting on a rigid tensionless foundation ($\alpha = \infty$). The deformations are exaggerated for clarity.

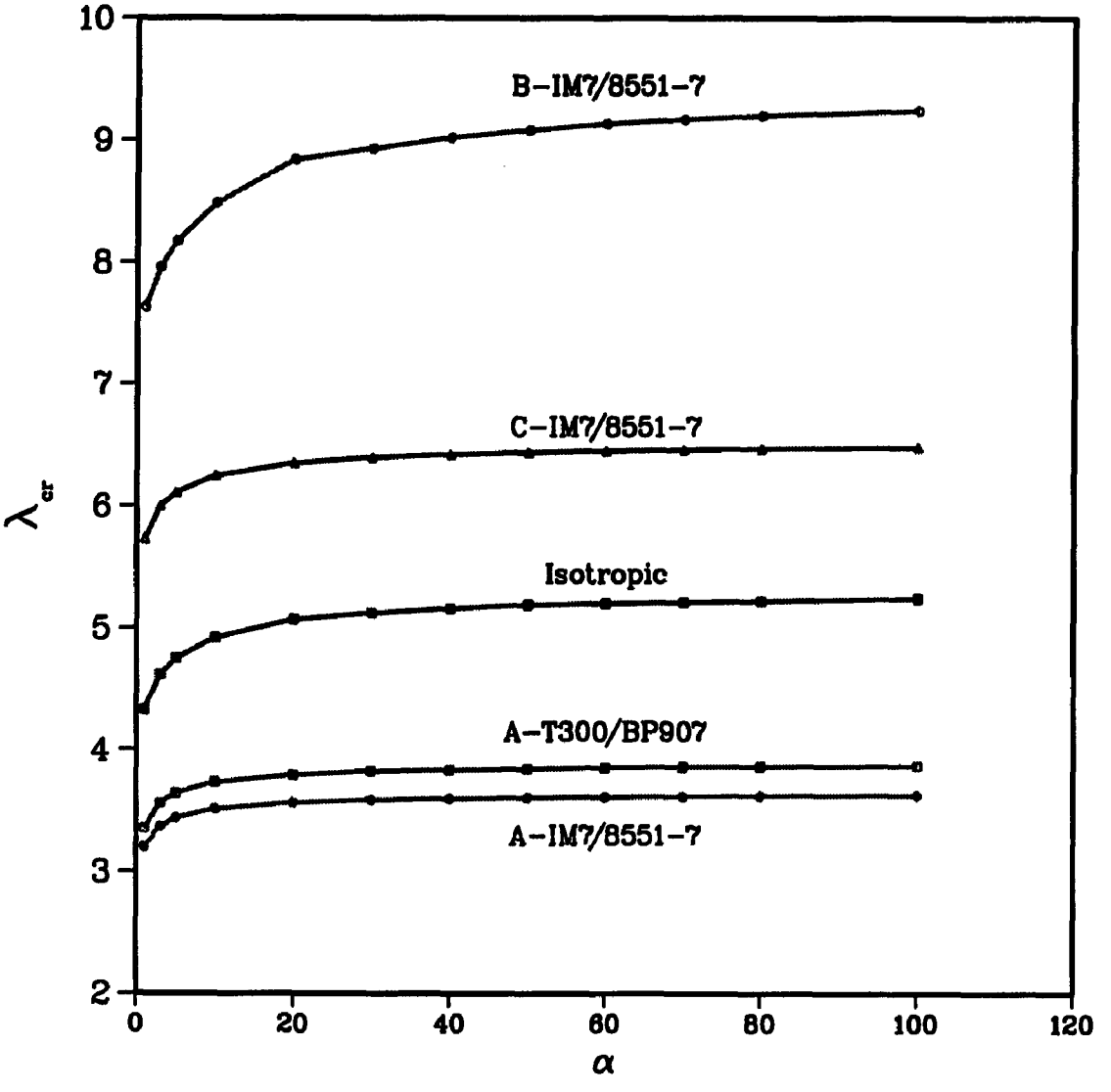

Figure 2.5: Buckling load λ_{cr} vs. foundation stiffness α for all materials used in this study (case 1).

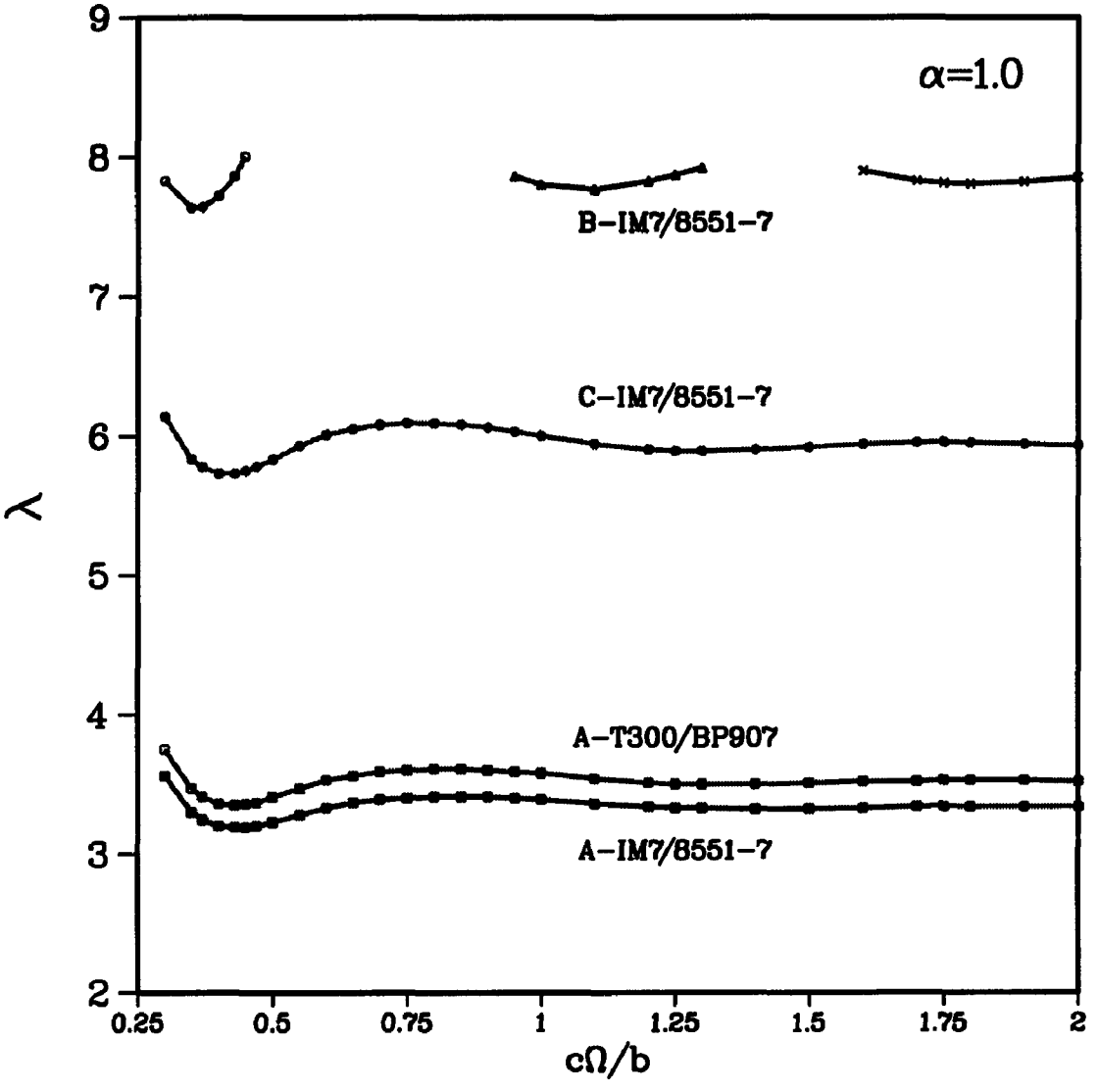

Figure 2.6: Inplane load λ vs. $c\frac{\Omega}{b}$ for four types of laminates used in this study at $\alpha = 1.0$ (case 1).

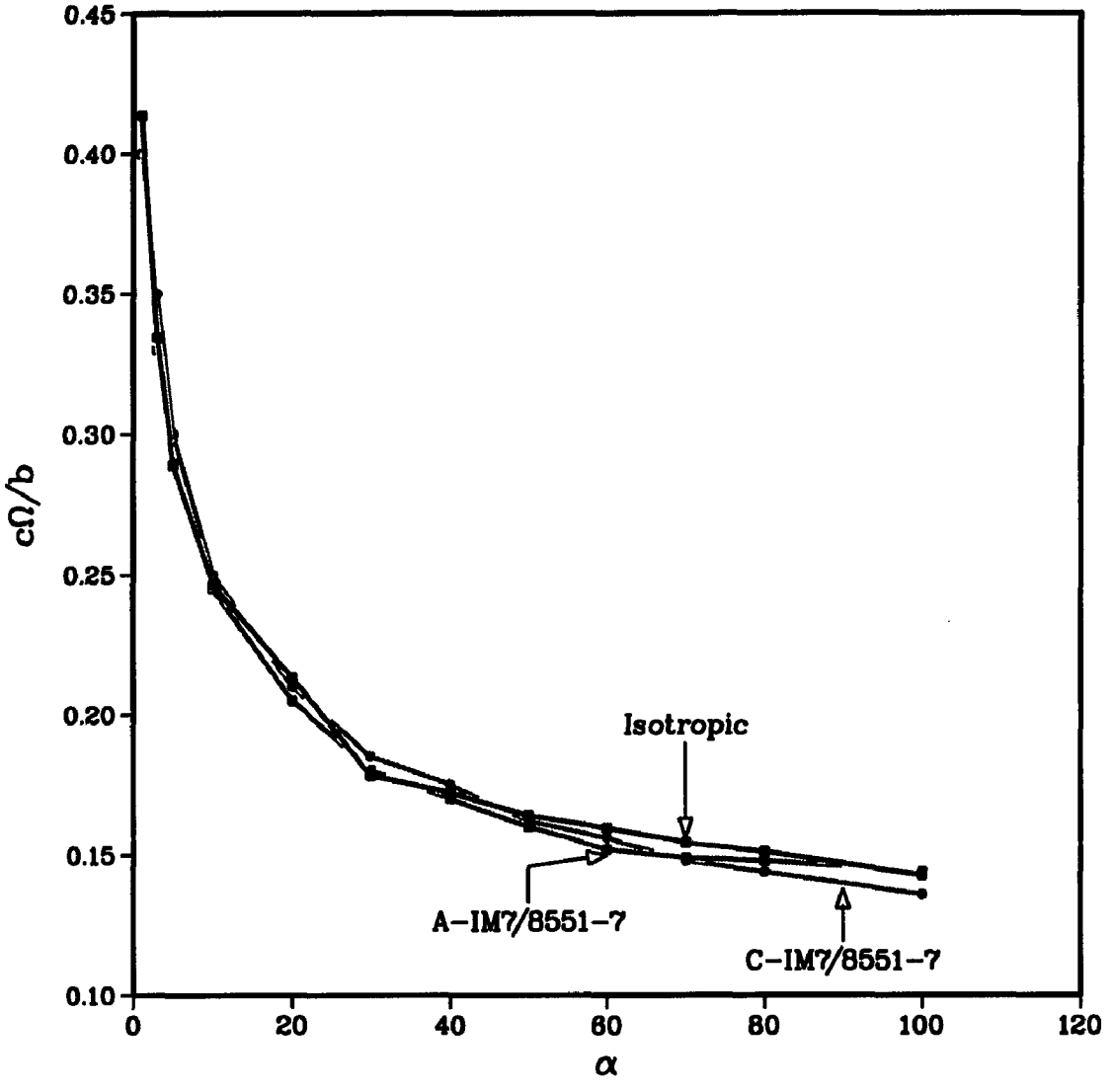

Figure 2.7: $c\frac{\Omega}{b}$ vs. the foundation stiffness α at buckling for Isotropic, A-IM7 and C-IM7 laminates (case 1).

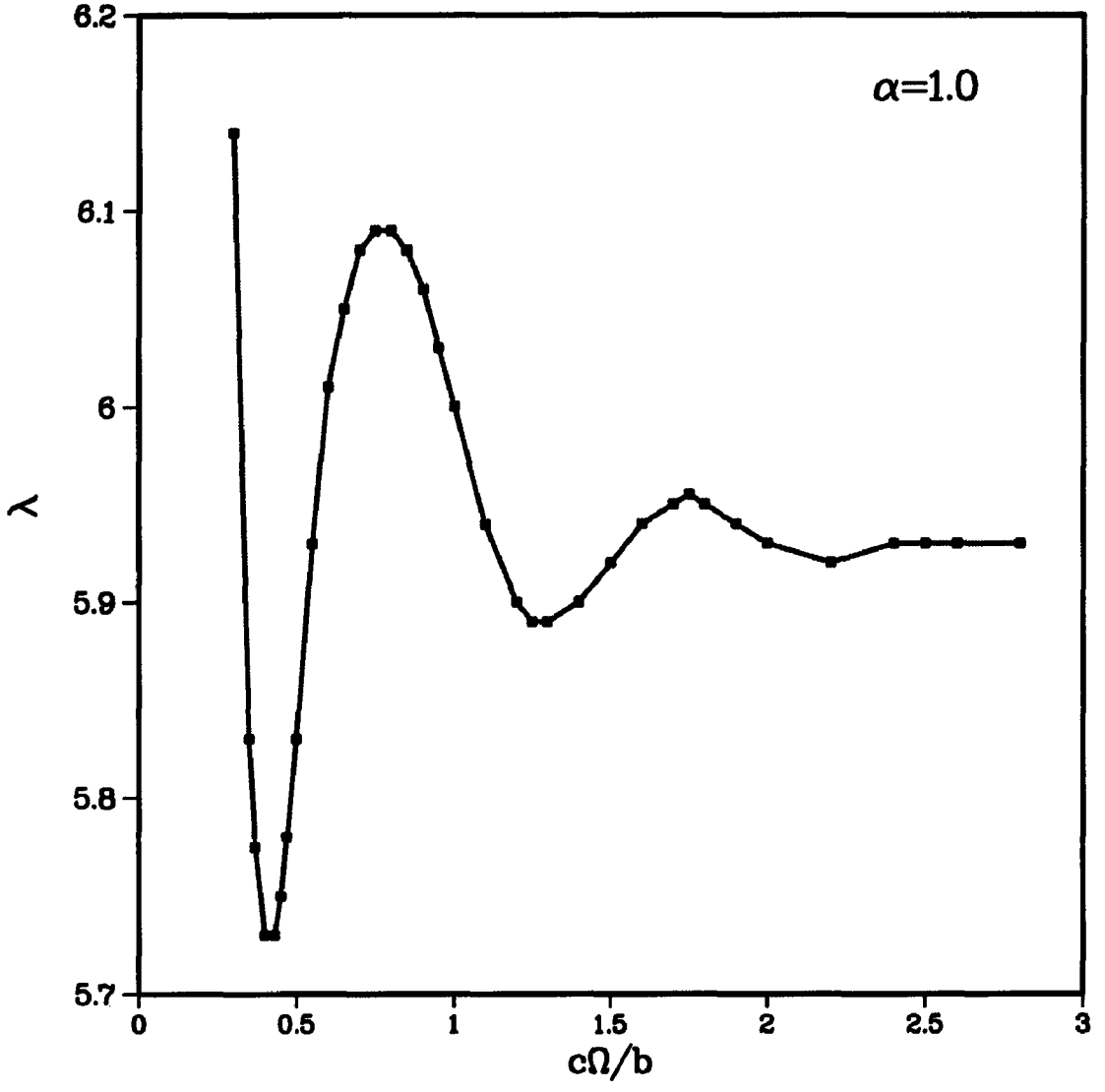

Figure 2.8: Inplane load λ vs. $c\frac{\Omega}{b}$ at $\alpha = 1.0$ for C-IM7-8551-7 laminate (case 1).

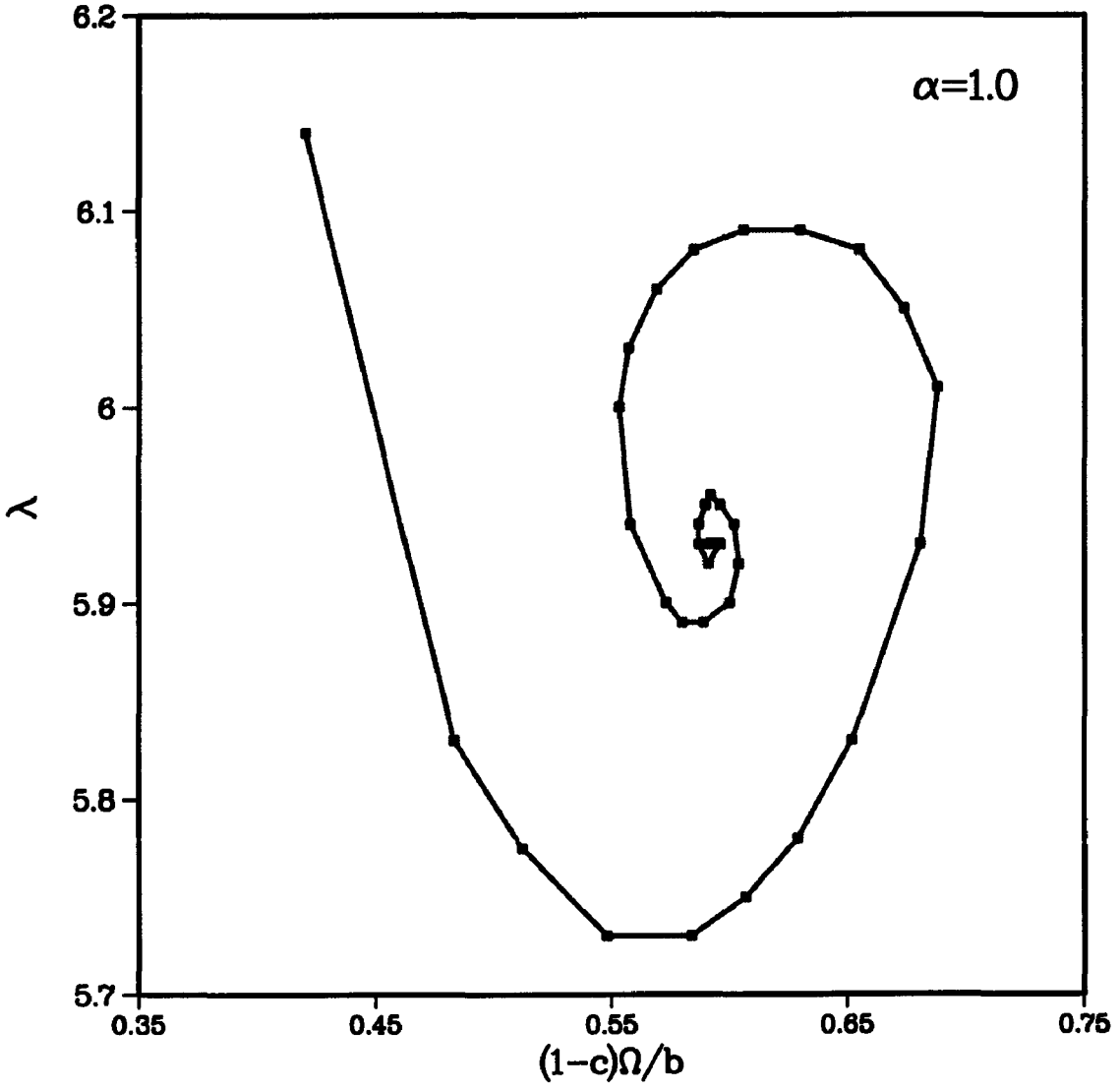

Figure 2.9: Inplane load λ vs. $(1-c)\frac{\Omega}{b}$ at $\alpha = 1.0$ for C-IM7-8551-7 laminate (case 1).

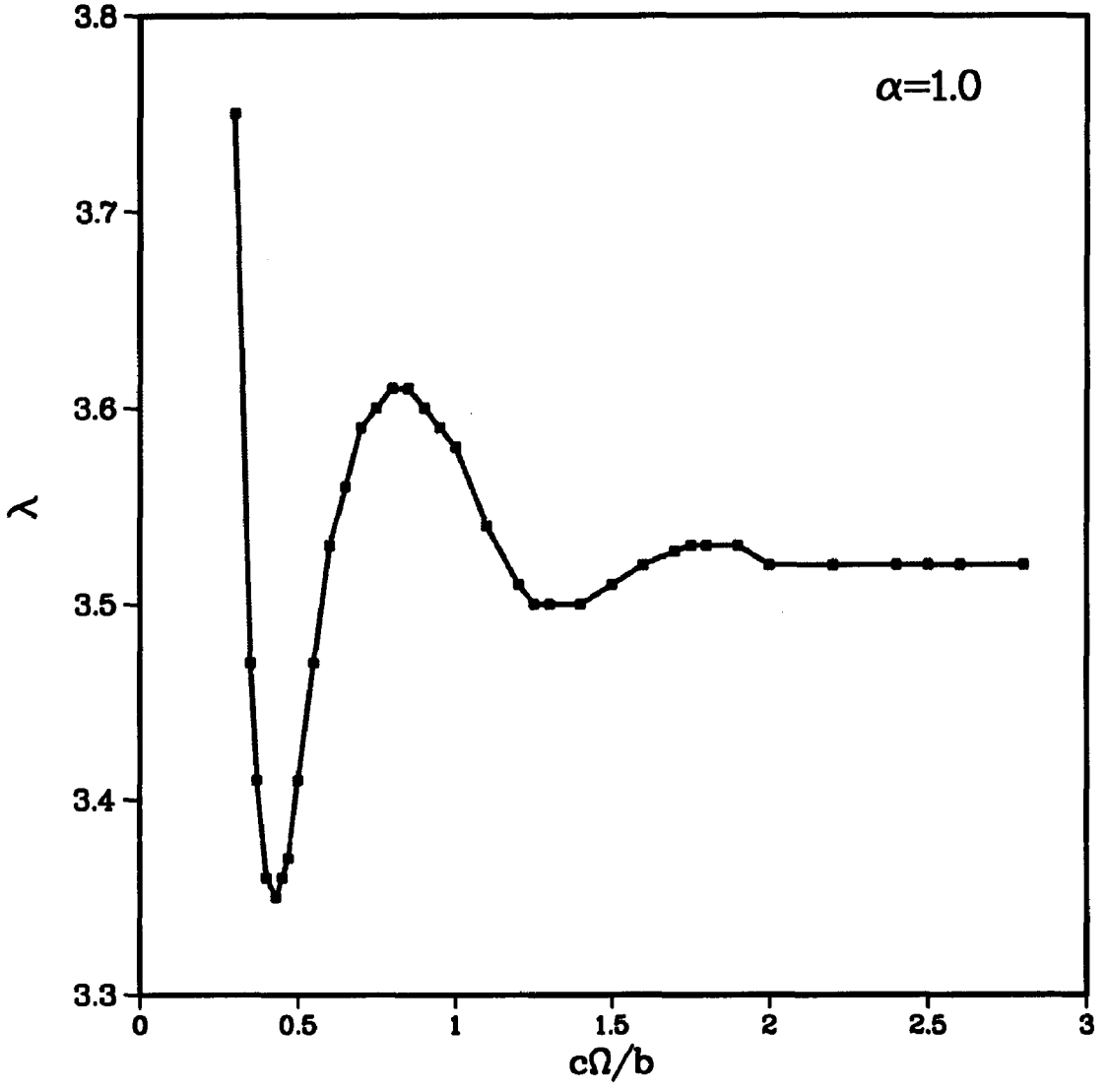

Figure 2.10: Inplane load λ vs. $c\frac{\Omega}{b}$ at $\alpha = 1.0$ for A-T300/BP907 laminate (case 1).

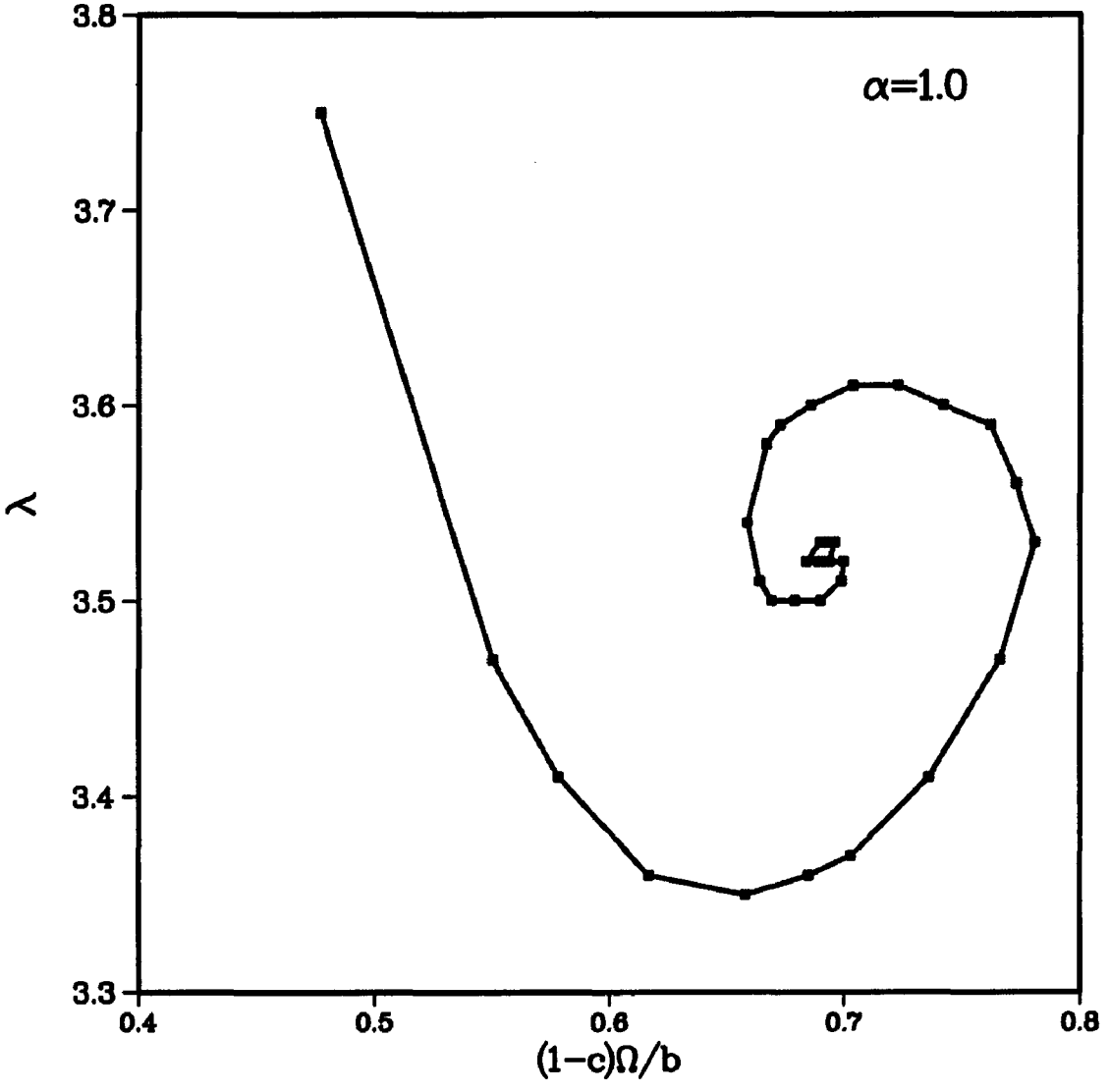

Figure 2.11: Inplane load λ vs. $(1-c)\frac{\Omega}{b}$ at $\alpha = 1.0$ for A-T300/BP907 laminate (case 1).

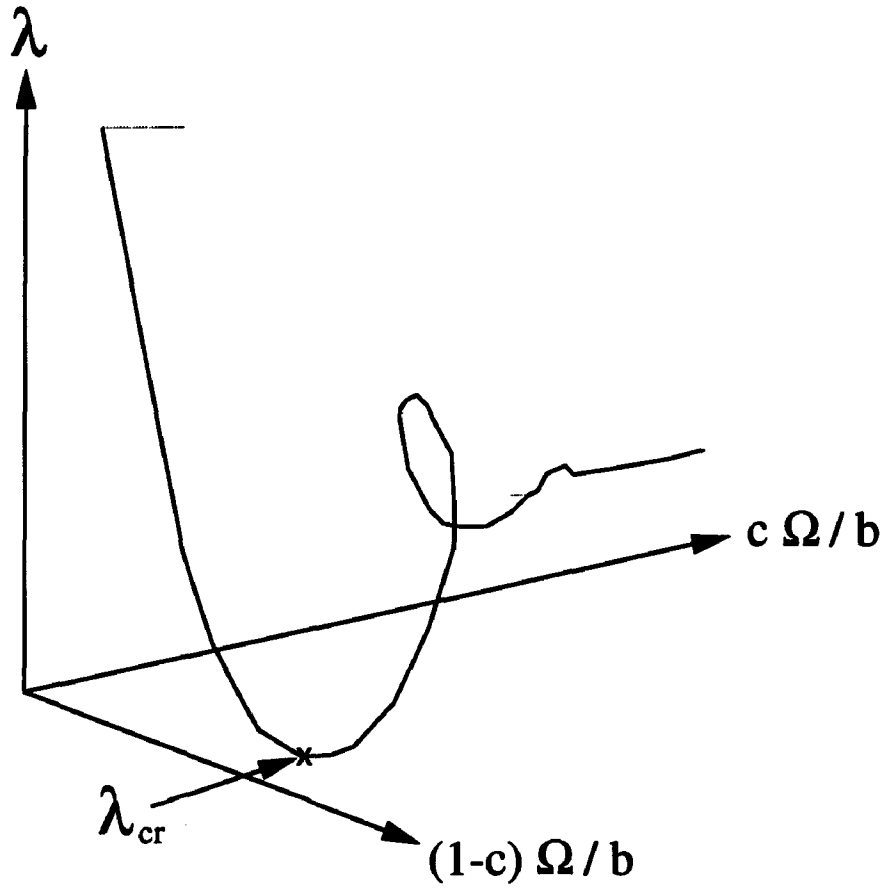

Figure 2.12: The λ-$(1-c)\frac{\Omega}{b}$ -$c\frac{\Omega}{b}$ space for finite α. As $\alpha \to \infty$, $c\frac{\Omega}{b} \to 0$ and the 3-D space is compressed into the λ-$(1-c)\frac{\Omega}{b}$ plane.

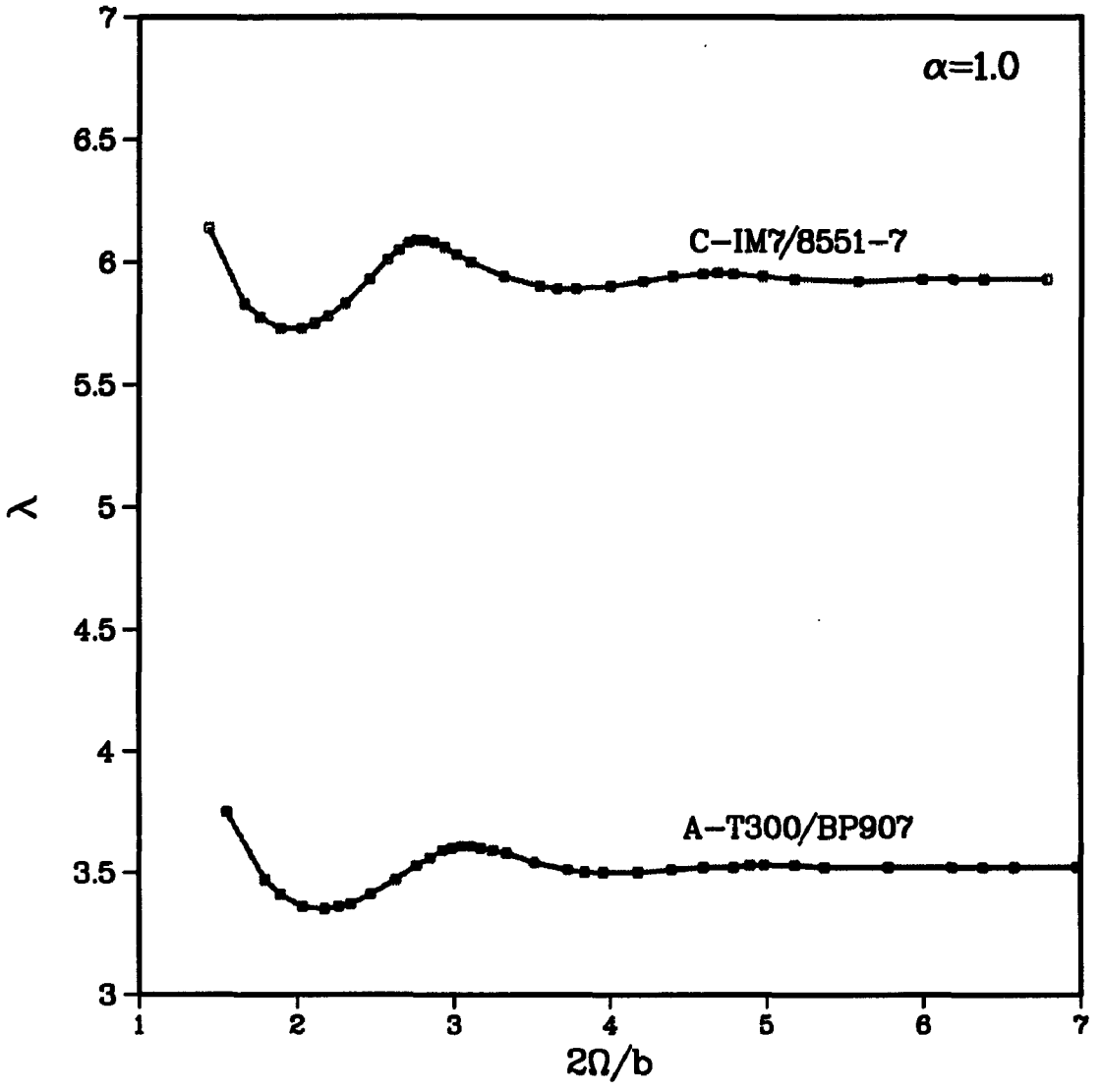

Figure 2.13: Inplane load λ vs. $2\frac{\Omega}{b}$ at $\alpha = 1.0$ for A-T300/BP907 and C-IM7-8551-7 laminate (case 1).

CHAPTER III

BUCKLING OF UNILATERALLY CONSTRAINED FINITE PLATES

3.1 Introduction

In contrast to the earlier discussion on *infinite* plates, this discussion will focus on the somewhat more difficult problem of buckling of unilaterally constrained *finite* plates. Due to the nature of the imposed constraint on the plate's lateral deflection as well as the way this physical situation was modeled, solving for the buckling load requires the solution of a *nonlinear* partial differential equation that governs the equilibrium of the plate.

In this chapter we will consider a mechanical model and an appropriate solution method for the critical loading conditions of a finite, rectangular, and linear elastic plate that is unilaterally constrained by the presence of a rigid surface parallel to the plate's undeformed middle plane as shown in Figure 3.1. The distance between the rigid surface and the plate's middle plane is taken to be half the plate's thickness, implying that a gap does not exist. The plate is subjected to transverse distributed loading as well as a uniform inplane stress field. While the plate is modeled along the lines of classical plate theory employing Kirchhoff-Love hypothesis, the nonlinearity arose from the fact that the plates were attached to nonlinear elastic foundations ex-

hibiting a deformation sign dependent force-displacement relationship. This feature was introduced to model the unilateral constraint.

For the classical situation of a bilaterally unconstrained rectangular plate, solving for the nondimensional buckling load parameter λ_{cr} requires the solution of a *linear* differential equation. Further, depending on the boundary conditions, exact solutions relating λ_{cr} to various other parameters can be obtained. One such typical relationship is the equation relating λ_{cr} to the plate's aspect ratio ξ for a plate attached to a Winkler Foundation with stiffness α. For a simply-supported linear elastic isotropic plate the exact relationship for the uniaxial loading case is a follows:

$$\lambda_{cr} = \min_i \left[2 + \left(\frac{i}{\xi}\right)^2 + (1+\alpha)\left(\frac{\xi}{i}\right)^2 \right], \qquad i = 1, 2, 3, \ldots \tag{3.1}$$

where the parameters λ and α are as defined earlier (equations (2.43) and (2.44)) and

$$\xi = \frac{a}{b} \tag{3.2}$$

i represents the number of half-waves in the loaded direction, a and b are the length and the width of the plate, respectively, and are shown in Figure 3.1. A plot of equation (3.1) is given in Figure 3.2. It is apparent in (3.1) that the absolute minimum for λ_{cr} is 4. Further, it is implicit in (3.1) that the number of half-waves in the direction perpendicular to the loading direction is always 1. The physical meaning of this is that uniaxially loaded plates buckles in such a way that there can be several half-waves in the direction of compression but only one half-wave in the perpendicular direction [99].

In this chapter, similar plots will be obtained for unilaterally constrained plates. As it will become apparent subsequently in this chapter, there is a fundamental difference in the $\lambda_{cr} - \xi$ curves between bilaterally unconstrained and unilaterally constrained plates. While the former exhibit a pattern similar to that shown in Figure 3.2, the latter exhibit a pattern similar to that shown in Figure 3.3. While at "low" aspect ratios the behavior of the two problems is indistinguishable, the constrained plate displays a clear increase in λ_{cr} which plateaus to a constant value.

Also in this chapter, the influence of different boundary conditions, material orthotropy, and transverse load distributions on plates' response will also be investigated. For each case to be considered, the weak form of the governing differential equation will be solved via the Galerkin's method.

3.2 Problem Formulation

In order to account for the physical constraint imposed on the plate's buckling displacements, a nonlinear elastic foundation model that exhibits a deformation sign dependent force-displacement relationship was implemented. Such types of nonlinearities present analytical difficulties in that an exact close-form solution cannot be easily obtained, if not impossible. As such, an approximate method of solution must be followed to formulate the equations governing the plate's response. From the expression of the total potential energy $\hat{\Pi}$ (3.3), one can operate either on its functional form directly (e.g., Rayleigh-Ritz method), or on its first variation form (e.g., Galerkin's method).

$$\hat{\Pi} = \frac{1}{2}\int_0^b\int_0^a \Big[\, \hat{D}_{11}\hat{w}^2_{,\hat{x}\hat{x}} + 2\,\hat{D}_{12}\hat{w}_{,\hat{x}\hat{x}}\hat{w}_{,\hat{y}\hat{y}} + \hat{D}_{22}\hat{w}^2_{,\hat{y}\hat{y}} + 4\,\left(\hat{D}_{16}\hat{w}_{,\hat{x}\hat{x}} + \hat{D}_{26}\hat{w}_{,\hat{y}\hat{y}}\right)\hat{w}_{,\hat{x}\hat{y}} + 4\,\hat{D}_{66}\hat{w}^2_{,\hat{x}\hat{y}} \,\Big]\, d\hat{x}d\hat{y} + \tag{3.3}$$

$$\int_0^b\int_0^a \mathbf{W}_f \, d\hat{x}d\hat{y} - \frac{1}{2}\int_0^b\int_0^a \left(N_{11}\hat{w}_{,\hat{x}}^2 + 2N_{12}\hat{w}_{,\hat{x}}\hat{w}_{,\hat{y}} + N_{22}\hat{w}_{,\hat{y}}^2\right) d\hat{x}d\hat{y} - \int_0^b\int_0^a q(\hat{x},\hat{y})\, d\hat{x}d\hat{y}$$

where N_{ij} are the applied inplane loads and $q(\hat{x},\hat{y})$ is the applied transverse distributed load. It is implicit in (2.1) that, by assuming N_{ij} to be constants independent of the deformation $\hat{w}$, the above formulation is linearized about the "buckling point" of the eigenvalue problem where N_{ij} are the prebuckling inplane loads.

The elastic foundation's strain energy density functional, $\mathbf{W}_f$, was defined in (2.2) and is restated below for convenience,

$$\mathbf{W}_f = \int k\ \hat{w}\ \Psi(\hat{w})\ d\hat{w} \tag{3.4}$$

where Ψ is a general nondimensional functional that depends on the type of foundation present. In the case of a linear elastic foundation, $\Psi(\hat{w}) = 1$, and hence $\mathbf{W}_f = \frac{1}{2}k\hat{w}^2$, where k is the linear foundation stiffness. Nondimensionalizing (3.3) and using equations (2.13), (2.43) and (2.44) will result in the following expression for the total potential energy:

$$\begin{aligned}\Pi = \frac{1}{2}\int_0^1\int_0^\xi &\left[w_{,xx}^2 + 2D_{12}w_{,xx}w_{,yy} + D_{22}w_{,yy}^2 + \right.\\ &\left. 4(D_{16}w_{,xx} + D_{26}w_{,yy})w_{,xy} + 4D_{66}w_{,xy}^2\right] dxdy - \\ \frac{1}{2}\int_0^1\int_0^\xi &\lambda\pi^2\left[w_{,x}^2 + 2\eta_{12}w_{,x}w_{,y} + \eta_{22}w_{,y}^2\right] dxdy - \\ \int_0^1\int_0^\xi &Q(x,y)\ w\ dxdy + \int_0^1\int_0^\xi \alpha\pi^4\left(\int w\Psi(w)dw\right) dxdy\end{aligned} \tag{3.5}$$

where

$$Q(x,y) = \frac{q(\hat{x},\hat{y})\ b^4}{\hat{D}_{11}\ h}$$

$$
\begin{aligned}
h &= \text{plate's thickness} \\
x &= \frac{\hat{x}}{b} \in [0, \xi] \\
y &= \frac{\hat{y}}{b} \in [0, 1] \\
w &= \frac{\hat{w}}{h} \\
\Pi &= \frac{\hat{\Pi}\, b^2}{\hat{D}_{11}\, h^2} \\
\eta_{12} &= \frac{N_{12}}{N_{11}} \\
\eta_{22} &= \frac{N_{22}}{N_{11}}
\end{aligned}
$$

Calculating the first variation of Π and applying the divergence theorem along with equation (2.4) yields the following variational equation:

$$
\begin{aligned}
\delta\Pi = \int_0^1 \int_0^\xi [\; & w_{,xxxx} + 2\ (D_{12}\ +\ 2\ D_{66}\ )\ w_{,xxyy} + D_{22} w_{,yyyy} + \\
& 4\ (D_{16} w_{,xxxy}\ +\ D_{26} w_{,xyyy}\ ) + \lambda\pi^2\, (w_{,xx} + 2\eta_{12} w_{,xy}\ + \\
& \eta_{22} w_{,yy}) + \pi^4\ \alpha\ w\ \Psi(w) - Q(x,y)\ ]\ \delta w\ dxdy \qquad (3.6) \\
& - \int_0^1 (M_{xx}\ \delta w_{,x} + M_{xy}\ \delta w_{,y} - V_x\ \delta w)_{x=0}^{x=\xi}\ dy \\
& - \int_0^\xi (M_{xy}\ \delta w_{,x} + M_{yy}\ \delta w_{,y} - V_y\ \delta w)_{y=0}^{y=1}\ dx
\end{aligned}
$$

where M_{xx}, M_{yy}, M_{xy}, V_x, and V_y are the nondimensional moments and shear forces at the plate's boundary and in terms of $w(x,y)$ are given in the following equations:

$$
\begin{aligned}
M_{xx} &= -\Big(w_{,xx} + D_{12} w_{,yy} + 2D_{16} w_{,xy}) \\
M_{yy} &= -\Big(D_{12} w_{,xx} + D_{22} w_{,yy} + 2D_{26} w_{,xy}) \\
M_{xy} &= -\Big(D_{16} w_{,xx} + D_{26} w_{,yy} + 2D_{66} w_{,xy})
\end{aligned}
$$

$$
\begin{aligned}
V_x = -[&w_{,xxx} + 3D_{16}w_{,xxy} + \Big(D_{12} + 2D_{66}\Big)w_{,xyy} \\
&+D_{26}w_{,yyy} + \lambda\pi^2\Big(w_{,x} + \eta_{12}w_{,y}\Big)] \\
V_y = -[&D_{16}w_{,xxx} + \Big(D_{12} + 2D_{66}\Big)w_{,xxy} \\
&+3D_{26}w_{,xyy} + D_{22}w_{,yyy} + \lambda\pi^2\Big(\eta_{12}w_{,x} + \eta_{22}w_{,y}\Big)]
\end{aligned}
\tag{3.7}
$$

Investigation of equilibrium states requires the necessary and sufficient condition that the total potential energy Π be stationary, hence, the vanishing of its first variation,

$$\delta\Pi = 0. \tag{3.8}$$

From (3.6), (3.7) and (3.8) the governing differential equation can be extracted along with the boundary conditions. A close-form solution of the differential equation is highly dependent on the form of $\Psi(w)$. While for nonlinear $\Psi(w)$ such a solution is near impossible, it is easily obtainable if $\Psi(w)$ is linear in w and if the boundary conditions are of certain type and combination. Hence, for nonlinear $\Psi(w)$, one has to resort to approximate methods such as the Finite Element Method, Rayleigh-Ritz method, or Galerkin's method, to mention a few. In this study it was decided to employ the Galerkin's method, and in order to carry out the solution procedure, kinematically admissible global displacement functions must be assumed. It is important to note that although the plate is unilaterally constrained, such a constraint does not play any role in choosing these functions and as mentioned earlier, this constraint condition will be accounted for indirectly via the nonlinearity of the elastic foundation model. Further, the out-of-plane displacement field w can be assumed to be of a separable form where shape functions in x are multiplied by those in y. These functions can be chosen to be the buckling and/or free vibration eigenmodes of beams and/or plates having the same kinematic boundary conditions. Throughout

this study, beam-vibration eigenmodes were employed and can be found in Appendix B. In the forthcoming analysis, the out-of-plane displacement functions $w(x,y)$ were chosen to have the following form:

$$w(x,y) \;=\; \sum_{i=1}^{M}\sum_{j=1}^{N} A_{ij}\Phi_{ij}(x,y), \tag{3.9}$$

where A_{ij} are unknown generalized displacement coefficients and $\Phi_{ij}(x,y)$ are spatial functions that have the following separable form:

$$\Phi_{ij}(x,y) \;=\; \phi_i(x)\,\varphi_j(y) \tag{3.10}$$

$\phi_i(x)$ and $\varphi_j(y)$ must satisfy their corresponding plate's kinematic boundary conditions as well as be continuously differentiable up to the highest corresponding derivative in the governing differential equation. The spatial functions used throughout this study are continuously differentiable (see Appendix B). The first variation of $w(x,y)$ with respect to the generalized displacement coefficients A_{ij} is,

$$\delta w(x,y) \;=\; \sum_{i=1}^{M}\sum_{j=1}^{N} \delta A_{ij}\;\Phi_{ij}(x,y). \tag{3.11}$$

Substituting (3.11) in (3.6) and in conjunction with the statement of stationary total potential energy (3.8) one arrives at the following set of MxN equations in the MxN unknowns A_{ij};

$$\begin{aligned}\int_0^1\int_0^{\xi} \quad & \Big[w_{,xxxx} + 2\Big(D_{12}+2D_{66}\Big)w_{,xxyy} + D_{22}w_{,yyyy} \\ & + 4\Big(D_{16}w_{,xxxy} + D_{26}w_{,xyyy}\Big) + \lambda\pi^2\Big(w_{,xx} + 2\eta_{12}w_{,xy} \\ & + \eta_{22}w_{,yy}\Big) + \alpha\pi^4\Psi(w) - Q(x,y)\Big]\,\Phi_{ij}(x,y)\,dxdy - \\ \int_0^1 \quad & \Big(M_{xx}\,\Phi_{ij,x} + M_{xy}\,\Phi_{ij,y} - V_x\,\Phi_{ij}\Big)_{x=0}^{x=\xi}\,dy -\end{aligned} \tag{3.12}$$

$$\int_0^{\xi} \left(M_{xy}\, \Phi_{ij,x} + M_{yy}\, \Phi_{ij,y} - V_y\, \Phi_{ij} \right)_{y=0}^{y=1} dx \;=\; 0.$$

where we have used the fact that (3.6) must be valid for all δA_{ij}. Equation (3.12) can be expressed in a more standard form upon the substitution of (3.9) yielding,

$$[\mathbf{K} \;+\; \lambda\, \mathbf{K}_\lambda]\; \mathbf{A} \;+\; \mathbf{F}_f(\mathbf{A}) \;=\; \mathbf{P}_Q \tag{3.13}$$

where $\mathbf{K}$ is the linear stiffness matrix (not including elastic foundation's contribution), $\mathbf{K}_\lambda$ is the geometric stiffness matrix due to the inplane load λ, $\mathbf{F}_f$ is the force vector generated by the presence of the foundation (note that for a nonlinear foundation $\mathbf{F}_f$ is a function of $\mathbf{A}$ for the general Ψ case) and $\mathbf{P}_Q$ is load vector due to the applied transverse load Q.

3.3 Foundation Model

One of the ways to incorporate a unilateral constraint condition in the formulation of solid mechanics problems is to introduce a fictitious elastic layer as a substitute for the rigid constraint. The elastic layer can then be modeled as an elastic foundation composed of a bed of nonlinear axial springs. Although, the nonlinearity can manifest itself in the geometry of springs' deformation and/or the force-displacement constitutive relationship, it is the latter that is of interest to us at this stage.

Although there are variety of constitutive models reported in the literature, a common feature that is shared by all is the fact that springs must exhibit a force-displacement relationship that is deformation-sign dependent. Such a feature was found by many investigators to be the type of constitutive nonlinearity that best captures the physics of unilaterally constrained problems. Hence, the foundation was modeled as extensional springs[1] having such a relationship. Such models have

[1]The terms "spring(s)" and "foundation" are used interchangeably to mean the same thing.

been considered by many investigators in the treatment of beams and plates resting on nonlinear foundations [18, 34, 100]. In these studies, the *sgn*, Dirac delta as well as Heaviside step functions were used to describe the bimodulus nature of the elastic foundation (bimodulus in the sense that compression stiffness is different than that for tension). In this study, a model that utilizes the switching property of the *tanh* function was implemented (Figure 3.4).

The force-displacement relationship for this model is given below as,

$$F = \alpha\, w\, \Psi(w) \tag{3.14}$$

where

$$\Psi(w) = \frac{1}{2}\left[1 - \tanh\left(\beta w\right)\right] \tag{3.15}$$

α is a nondimensional stiffness parameter, w is the normalized deformation, β is a spring (foundation) attachment coefficient that is > 0. A plot of (3.15) is shown in Figure 3.5. The foundation attachment can be controlled by changing the value of the parameter β. Large values of β implies less attachment as shown in Figure 3.6. Theoretically, $\beta = \infty$ implies that the foundation is fully unattached (tensionless), while $\beta = 0$ implies the foundation is fully attached (note that if $\beta = 0$ the $\frac{1}{2}$ factor in (3.15) should be replaced by 1 in order to recover the linear Winkler Foundation case where $\Psi = 1$). Furthermore, while foundation stiffness can be increased to larger values by increasing α, increasing β will result in a decrease in the ratio of the tension/compression stiffnesses.

It is worthwhile noting that although the nonlinearity in the physical problem is geometrical, arising from the constraints imposed on the plate's kinematics, the nonlinearity in the governing equations arises from the elastic foundation's constitutive

model. Notice that this is a feature of the mechanical model that is employed in the present work.

The type of nonlinearity in the physical problem invalidates any linearization procedure of the governing equations about any particular state. As such, the fully nonlinear equations must be solved which introduces complications that are associated with the foundation's force-displacement relationships (3.14) and (3.15) where linearization of $\tanh(\beta w)$ for large β does not reflect the intended physical situation. The inability to linearize the governing equations without substantially changing the physics of the problem is a distinguishing feature of this class of problems.

3.4 Method of Solution

In problems of the type presented here, it is often easier to obtain the buckling loads by treating a response problem[2] and determining the value of the inplane load parameter (λ) corresponding to a rapid growth in the response. More specifically, the notion of a rapid growth in the context of the numerical solution that we have obtained is clearly discussed next. Thus, values of buckling load presented here were obtained, and the term buckling load is used, in this context.

The buckling load parameter λ_{cr} as well as A_{ij} were determined using an incremental load approach. The solution algorithm, which is based on a load-controlled criterion (for this part of the study), increments the value of λ and monitors the determinant of the incremental stiffness matrix (Figure 3.7). λ_{cr} was obtained when the incremental stiffness matrix became singular (or near singular). Such an approach is used frequently in the analysis of nonlinear problems and will be elaborated on subsequently. Figure 3.7 shows a sketch of such operations. At increment j, the

[2]Response problems differ from eigenvalue problem due to the presence of a right-hand-side term ("forcing" term) in the governing equation(s).

value of λ increment ($\Delta\lambda_j$) is proportional to the previous increment value, i.e., $\Delta\lambda_{j-1}$, through the coefficient σ_j. For uniform increments the value of σ was set to unity ($\sigma = 1$). Although having uniform small increments (i.e., $\Delta\lambda$ of the order of $0.001\lambda_{cr}$) simplifies the algorithm significantly, the number of increments increases significantly and so does the total computations' time. In general, at the beginning (approximately $\lambda < 0.5\lambda_{cr}$), having small uniform increments ($\sigma = 1$) is clearly not an "optimum" choice because in that regime of the response curve the relationship is almost linear and much larger increment size can be used (i.e., $\Delta\lambda = 0.2\lambda_{cr}$, or even larger).

Although for many problems the value of λ_{cr} is not known a priori, one can estimate it based on the fact that for a wide range of problems (see Chapter II) the value of λ_{cr} for a unilaterally constrained rectangular plate is about 30% larger than the corresponding value for the bilaterally unconstrained case. Further, in this study it was observed[3] that for $\lambda < 0.5\lambda_{cr}$ a reasonable value for the load-parameter increment is $\Delta\lambda = 0.2$.

It is warranted at this stage to make a clear distinction between what has been described above and what is commonly referred to in the computational mechanics literature as the *method of incremental loading*[4][68]. While in the latter the load increments ($\Delta\lambda$) are sufficiently small that during each step the response of the body (structure) is rendered linear and the governing equations are solved as such, in the former the load increments are arbitrary and the original governing equations are solved as (fully) nonlinear and no linearization (other than that inherent in the derivation of the governing equations) was performed at any stage in the computa-

[3]Although not reported for the sake of brevity, few hundred case studies were carried out for verification.

[4]A variety of terms are used in the literature to describe methods of incremental loading: *imbedding methods*, *continuation methods* or *methods of variation of parameters*.

tional process.

In carrying out the solution process, the value of β in (3.15) posed a computational drawback. Although large values for α as well as β are required in simulating the presence of the rigid surface, they cannot be chosen arbitrarily large. It was observed that while, $\alpha = 100$ ("high stiffness" foundation) yields adequate and physically admissible results independent of w, the value of β was dependent on w so as to maintain the product βw as large as possible for all values of w. Further, assigning a large constant value for β, led, in some cases, to numerical difficulties that were encountered in the numerical solver (to be described). In these cases, a physically inadmissible result such as plate penetration into the "rigid" foundation was found to exist. An improvement on this foundation model (3.15) that eliminates such dependency can be achieved by casting (3.15) in the following form:

$$\Psi(w) = \frac{1}{2}\left[1 - \tanh\left(\beta\frac{w}{|w|}\right)\right], \tag{3.16}$$

where the notation $|\ |$ implies *absolute value.* Using the above form of $\Psi(w)$, and after investigating a wide range of problems, it was found that $\beta = 10$ is an adequate value for an attachment coefficient representing the unattached situation. Figure 3.8 demonstrates the dependence of λ_{cr} on β as a function of ξ for plates having clamped and simply supported boundary conditions along their loaded and unloaded edges, respectively. Curves for $\beta > 10$ are indistinguishable from the $\beta = 10$ curve.

Unlike the form of Ψ given in (3.15), this form (3.16) has a structure that seems to be unsuited for numerical computations (especially near the point $w = 0$). As such, various case studies along with those to be reported subsequently have been investigated using this form (3.16). Such investigations revealed that, with special considerations at the point $w = 0$, the numerical scheme (to be discussed) has

converged to the "physically" correct results (and in some cases, the expected known results). One of the main reasons for such a convergence is the fact that, except at the constrained boundaries where there are no springs, it is nearly impossible to have, numerically, an "exact zero" displacement. To have an "exact zero" w displacement requires that all the Φ_{ij} functions (or all the A_{ij} coefficients) in (3.9) be exactly zero, which is a highly improbable situation.

A simplification to the solution algorithm rests in the fact that, λ_{cr} is bounded from above and below. The lower bound corresponds to λ_{cr} when $\alpha = 0$, while the upper bound corresponds to λ_{cr} when $\beta = 0$. Such bounds were used as guides in the incremental method and it was noticed that, in general, for unilaterally constrained plates, λ_{cr} is closer to its lower bound than its upper indicating that the rigid surface constraint does not increase the buckling load significantly confirming what has been reported earlier in [85] and Chapter II (also [86]). For example, for an isotropic, simply-supported (along the unloaded edges) infinite plate, such an increase was found to be 33%.

3.4.1 Galerkin's Method

Equation (3.12) is the mathematical statement of Galerkin's Method which is a "direct method" in the calculus of variations. The form of Galerkin's method to be described is sometimes referred to as Bubnov-Galerkin Method [75]. In general, for a problem having non-quadratic energy functional (nonlinear problem), *true solution* ("exact solution") rarely exists, and as introduced by Ritz[5], the solution of the problem will be assumed to admit a series expansion in terms of coordinate functions satisfying certain appropriate conditions. This expansion is used "directly" in the

[5]The Ritz method, which is sometimes referred to as the Rayleigh-Ritz method, is just a generalization of the Rayleigh method. See footnote 3 in Chapter II.

variational functional relationship, which becomes a condition for the evaluation of the series coefficients. Such condition appears in the form of set of equations, usually known as equations of Rayleigh-Ritz or Galerkin. By means of the direct method, an approximate solution or only an approximation to the solution (a weak solution) may be obtained.

Although a common starting point for the derivation of Galerkin's method is the governing differential equation(s), the derivation presented thus far represent an alternative way to derive the method based on a variational principle. The form (3.12) is sometimes referred to as the *Extended* Galerkin's Method due to its inclusion of the boundary terms [53]. Strictly speaking, the form of Galerkin's method that is widely reported in the applied mathematics literature includes only the integral of the governing differential equation without boundary terms [2, 3], and it is a valid representation of the method. Galerkin's method is an averaging method and it is perhaps one of the most powerful techniques for solving nonlinear elasticity problems as well as generating acceptable finite-element models of nonlinear equations. Though the method amounts to a special case of the methods of weighted-residuals (and a generalization of the Ritz method), it involves a rational choice of the weight functions (Φ_{ij}) so as to be consistent with the form of the analytic approximation involved.

It is known that the methods of Rayleigh-Ritz and Galerkin are equivalent, if the underlying mechanical problem is conservative, and if the coordinate functions being used satisfy *all* conditions of constraint. Moreover, it is generally assumed that the equations of Rayleigh-Ritz are advantageous, since for this method, the assumed coordinate functions must only satisfy the kinematic constraints. Yet, it has to be admitted that the Rayleigh-Ritz method in its classical form does not hold for

nonconservative problems because it requires the existence of an energy functional. Hence this method is restricted in its applicability. On the other hand, the method of Galerkin is applicable without restriction, also to nonconservative problems. That is the great advantage of Galerkin's method. However, the assumed coordinate functions must satisfy *all* conditions of constraint, kinematic and dynamic[6] ones. Such requirement can hamper the choice of coordinate functions, thus making Galerkin's method sometimes impractical. Hence, to relax such a constraint (satisfying all conditions) the extended form of Galerkin's method is employed. It is important to note that the problem being modeled is conservative and the choice of using Galerkin's method was based solely on the method's generality and versatility.

3.5 Numerical Scheme

By using Galerkin's method the governing nonlinear differential equation was reduced to a system of MxN nonlinear equations (3.12). Although systems of nonlinear equations have been encountered in problems of applied mechanics for centuries, no general method for obtaining exact solutions exists. Thus, we take for granted that numerical methods must be used and that, in general, it will be possible to obtain solutions only to within a preassigned degree of accuracy. As was described earlier, the method adopted in solving for the generalized displacement coefficients' vector $\mathbf{A}$ and the normalized buckling load (λ_{cr}) was an incremental one.

Most numerical schemes used to solve equations begin with an initial estimate $\mathbf{A}^0$ of the solution, called *initial guess point* or *test point.* In general, some process is then used to compute a sequence of such points which, hopefully, converges to the solution of the system of equations. The process used falls into one of two categories:

[6]Dynamic constraints are sometimes referred to as *force* or *natural* [37].

sequential methods or *nonsequential methods.* The numerical scheme used in this study falls into the former category and is based on a direct attack of the nonlinear system of equations.

In this study, the solution of the resulting system of nonlinear equations was carried out iteratively using the Levenberg-Marquardt method [13]. For a general system of nonlinear equations

$$\mathbf{f}(\mathbf{A}) = 0 \tag{3.17}$$

where $\mathbf{A}$ is the vector of unknowns and $\mathbf{f}$ is the vector of equations, the Levenberg-Marquardt algorithm is given as

$$\mathbf{A}^{k+1} = \mathbf{A}^k - \left[\rho^k \mathbf{I} + \mathbf{J}^{k^T} \mathbf{J}^k\right]^{-1} \mathbf{J}^{k^T} \mathbf{f}(\mathbf{A}^k) \tag{3.18}$$

where $\mathbf{J}^k$ is the Jacobian at the k^{th} iteration given by

$$\mathbf{J}^k = \frac{\partial \mathbf{f}}{\partial \mathbf{A}}(\mathbf{A}^k) \tag{3.19}$$

and $\mathbf{J}^{k^T}$ is the transpose of $\mathbf{J}^k$. $\mathbf{A}^k$ is the current, known, approximate value of the vector of unknowns $\mathbf{A}$, $\mathbf{I}$ is the Identity matrix and ρ^k is a scalar that is selected based on a methodology given in [74]. Equation (3.18) can be written in a more standard form as follows:

$$\mathbf{A}^{k+1} = \mathbf{A}^k - \mathbf{H}^k \mathbf{f}(\mathbf{A}^k) \tag{3.20}$$

where

$$\mathbf{H}^k = \left[\rho^k \mathbf{I} + \mathbf{J}^{k^T} \mathbf{J}^k\right]^{-1} \mathbf{J}^{k^T} \tag{3.21}$$

It is to be noted that as ρ^k increases, the step size decreases and the step vector tends towards the pure Steepest Descent vector ($\mathbf{H}^k = \mathbf{J}^{k^T}$). It was shown by Marquardt that for ρ^k sufficiently large the following relationship is satisfied

$$\|\mathbf{f}(\mathbf{A}^{k+1})\| < \|\mathbf{f}(\mathbf{A}^k)\| \tag{3.22}$$

and Marquardt advocates choosing ρ^k this way. In (3.22) the notation $\| \ \|$ implies the sum of the squares. If, on the other hand, $\rho^k = 0$ the method reduces to Newton's ($\mathbf{H}^k = \mathbf{J}^{k^{-1}}$) so that equation (3.21) combines certain features of both this and the method of Steepest Descent. By reducing ρ^k systematically as the solution is approached it is hoped to combine the better features of each method. A further point is that if $\rho^k > 0$ the inverse matrix appearing in (3.21) always exists so that a positive value of ρ^k ensures that the correction is always defined. The only feature that can cause the algorithm to be disrupted is convergence to a local nonzero minimum of $\|\mathbf{f}(\mathbf{A}^k)\|$, a disadvantage shared by the method of Steepest Descent.

The Levenberg-Marquardt algorithm as was proposed by the developers requires an explicit expressions for the Jacobian (3.19). Powell [74] presented a modification to the Levenberg-Marquardt algorithm by which the requirement that the explicit expressions for the Jacobian be available was relaxed. Such a method, which was designated *hybrid*, uses successive values of $\mathbf{f}(\mathbf{A}^k)$ to build up a numerical approximation to the Jacobian matrix, by the technique used in [74]. For convenience, the combined hybrid method as proposed by Levenberg and Marquardt and modified by Powell will be designated LMP.

Although the LMP method was the main algorithm used in obtaining solutions for $\mathbf{A}$, for some cases and for λ near λ_{cr}, the algorithm didn't converge and Newton-Raphson method ($\rho^k = 0$) was temporarily employed. Such a situation did not occur

frequently. In those few instances, we traced the reason for this lack of convergence to be associated with the evaluation of the Jacobian. In the Newton's method, the Jacobian at the k^{th} iteration ($\mathbf{J}^k$) is evaluated with a pre-assigned step size, while, in the LMP method, the $\mathbf{J}^k$ is updated automatically with step size that depends on $\mathbf{A}^k$ as well as the change in the Jacobian from the previous two iterations.

As related to the problem being considered, the Jacobian is a measure of the current stiffness evaluated at the k^{th} iteration using the current value of $\mathbf{A}^k$. From (3.13), we have

$$\mathbf{f}(\mathbf{A}^k) = [\mathbf{K} + \lambda \mathbf{K}_\lambda]\ \mathbf{A}^k + \mathbf{F}_f(\mathbf{A}^k) - \mathbf{P}_Q \tag{3.23}$$

and using the definition of $\mathbf{J}$ from (3.19) we arrive at

$$\mathbf{J}^k = \mathbf{K} + \lambda \mathbf{K}_\lambda + \frac{\partial \mathbf{F}_f}{\partial \mathbf{A}}(\mathbf{A}^k) \tag{3.24}$$

where we have used the fact that $\mathbf{P}_Q$ is independent of $\mathbf{A}$. Note that at the k^{th} iteration the sum $\mathbf{K} + \lambda \mathbf{K}_\lambda$ is a constant independent of $\mathbf{A}$.

3.6 Results and Discussion

While generic buckling curves for bilaterally unconstrained rectangular plates are available in the literature [14, 40] such results are nonexistent for unilaterally constrained plates. Hence, in this study the effort was concentrated on trying to generate such curves for plates having different boundary conditions and subjected to a uniaxial stress field. For uniaxial loading, $\eta_{12} = \eta_{22} = 0$.

3.6.1 Dependency of λ_{cr} on the transverse load $Q(x,y)$

In the absence of $Q(x,y)$ and since the trivial solution ($w = 0$) is an admissible solution for all values of λ, the solution of the governing equations constitutes the determination of the eigenvalues λ_{cr} and their corresponding eigenmodes. But due to the nonlinearity of these equations, such a system falls in the category of a nonlinear eigenvalue problem. As a simplification to the solution process a transverse load $Q(x,y)$ was added which converts the problem from being a nonlinear eigenvalue problem to a nonlinear response problem. In order to establish that the results for λ_{cr} are not significantly influenced by the magnitude and distribution of $Q(x,y)$, different cases were investigated where the sign, magnitude as well as the functional distribution throughout the plate were varied. For presentation purposes as well as convenience it was decided to normalize the $\mathbf{A}$ vector by $\mathbf{A_0}$ where $\mathbf{A_0}$ is the generalized displacement coefficients' vector $\mathbf{A}$ at $\lambda = 0$ and $Q(x,y) \neq 0$ (i.e., $\mathbf{A_0} = \mathbf{A}(\lambda = 0, Q \neq 0)$. This nondimensionalization implies that at $\lambda = 0$, $\frac{\|\mathbf{A}\|}{\|\mathbf{A_0}\|} = 1.0$, always. Although the "response curves" (curves representing λ vs. normalized magnitude of the generalized displacements vector $\frac{\|\mathbf{A}\|}{\|\mathbf{A_0}\|}$) were not significantly influenced by the magnitude of $Q(x,y)$, they were dependent on its sign distribution. However, the value of λ at which the plate response appeared to increase without bound (approaching buckling) was independent of $Q(x,y)$ as expected. If $Q(x,y) = c$, where c is a constant that is < 0 (i.e., Q is pushing the plate against the foundation), the value of λ_{cr} was equal to ∞. If, on the other hand, $c > 0$ (i.e., Q is pulling the plate away from the foundation) the value of λ_{cr} was finite yielding valid results. However, the latter situation has an interesting feature that can be seen in Figure 3.9. In this figure, the response curves for a plate that is clamped along the

loaded edges and simply supported otherwise and under the action of two types of transverse loads are shown. One curve represents the case where $c > 0$ while the other represents the case where $Q(x,y)$ is linear and has a symmetric distribution (symmetry with respect to the center line $x = \frac{\xi}{2}$). In the former, a decrease and then a sudden increase in the slope at some value of $\lambda < \lambda_{cr}$ is observed (actually, this occurs near $\lambda_{cr} \approx 4.4$ which is the value of the buckling load of the unilaterally *unconstrained* plate having identical properties). This behavior is analogous to what was reported in [91]. This can be attributed to the plate "touching" the foundation near the eigenvalue (buckling load) of the linearized unconstrained problem) and immediately experiencing additional stiffness due to the foundation (Figure 3.10). On the other hand, in the latter case where the transverse load has negative as well as positive distributions, "touching" is already present, prior to the application of the axial load. Hence, this sudden slope increase is not strongly present. Further, although such difference between these two curves is strongly present for intermediate values of λ, it vanishes at the early stages of loading (λ) increments as well as when λ approaches the eigenvalue (λ_{cr}). Figure 3.10 also shows that as the magnitude of the normalized generalized displacement vector $\frac{\|\mathbf{A}\|}{\|\mathbf{A_0}\|}$ tends to large values (exceeding 10), the slope of the response curves tend to zero. Note that since $\frac{\|\mathbf{A}\|}{\|\mathbf{A_0}\|}$ is a scalar quantity, the slope of the $\lambda - \frac{\|\mathbf{A}\|}{\|\mathbf{A_0}\|}$ curve is a measure of the determinant of the incremental stiffness matrix and is calculated as follows:

$$|\mathcal{K}| = a \frac{\partial \lambda}{\partial \frac{\|\mathbf{A}\|}{\|\mathbf{A_0}\|}} \tag{3.25}$$

where $|\mathcal{K}|$ is the determinant of the incremental stiffness matrix and a is a constant ≥ 0. In order to determine λ_{cr}, several response curves were plotted for each case,

and in every case we found all the response curves to be within 1% of each other when the maximum value of $\frac{\|\mathbf{A}\|}{\|\mathbf{A_0}\|}$ was approximately 20. The load corresponding to this limit was chosen as λ_{cr}. Clearly, for some plates this limit was reached much earlier ($\frac{\|\mathbf{A}\|}{\|\mathbf{A_0}\|}$ approximately 10).

It is worthwhile pointing out that in the presence of $Q(x,y)$, the obtained λ_{cr} will always be an underestimate of the exact λ_{cr} value (eigenvalue) that would have been obtained by setting $Q(x,y) = 0$, provided a sufficient number of Galerkin terms are used. Although this difference should approach 0 as $Q(x,y)$ approaches 0, its value was kept to a minimum (i.e., $Q(x,y)$ was never set to 0). In order to minimize the effect of the presence of Q on the overall process of determining λ_{cr}, Q's largest magnitude was kept close to 1, i.e., $|Q| \leq 1$. Such a value was found to give satisfactory results simulating the no-load case (eigenvalue problem). Unless noted otherwise, throughout this study $|Q|$ will always be set equal to 1, which is, relatively speaking and from the definition of Q, a small quantity [24].

3.6.2 Dependency of λ_{cr} on the plate's aspect ratio ξ

Figures 3.11 and 3.12 show the dependency of λ_{cr} on the plate's aspect ratio ξ for different types of boundary conditions on the loaded and unloaded edges as well as for different types of materials. As expected, the dependence of λ_{cr} on ξ diminished for large values of ξ and beyond a certain value of ξ, the value of λ_{cr} becomes independent of the boundary conditions on the loaded edges and depends only on the boundary conditions on the unloaded edges. The prediction of this independence of λ_{cr} at large ξ added confidence to the numerical procedures adopted in the present work. Table 3.1 summarizes the limiting values of λ_{cr} as the plate's aspect ratio $\xi \rightarrow \infty$ for the case of an isotropic material. For the "cccc" case (Figure 3.11), the curve

exhibits discontinuities. These discontinuities can be attributed to the fact that in the neighborhood of the particular ξ value corresponding to the discontinuity, topological changes in the buckle patterns occur. Such changes were drastic in the neighborhood of $\xi = 2.5$.

Since the formulation covers material models other than isotropic, example problems for two types of specially orthotropic materials (designated A and B) were also studied. The properties of these materials are tabulated in Table 3.2. The results obtained via the present formulation for unilateral buckling of plates made of these materials are summarized in Figure 3.12. For large aspect ratios the results for buckling loads are seen to converge to certain fixed values and when compared to previous results reported in Chapter II and [86], are found to be in very good agreement.

Table 3.3 compares the results obtained from the solution of the infinite plate problem (Chapter II) to those obtained from finite plate problem (this chapter). In both situations the plates were subjected to uniaxial loading. Two types of boundary conditions along the unloaded edges were compared, namely, simply-supported (ss) and clamped-free (cf). As can be seen, the results compare favorably with a maximum difference of -3.5% in the simply-supported case and -8.7% in the clamped-free case. Note that for all cases the finite plate results are lower than their counterparts in the infinite plate case. This can be attributed to the presence of a transverse load in the finite plate case, which causes a slight drop in λ_{cr} as explained earlier.

An interesting feature of the buckling behavior of this problem is its symmetry. Within the context of linearized analysis of plates (isotropic or orthotropic) the response is invariant with respect to the loaded edge(s) due to the decoupling between the inplane and out-of-plane behaviors. On the other hand, in the analysis were

such coupling is present, the response will be otherwise and the final deformed shape will not be symmetric if the plate being considered is loaded only on one side in the uniaxial case. For a unilaterally constrained plate having homogeneous boundary conditions, the out-of-plane buckling deformation field $w(x,y)$ is a symmetric function with respect to the center line $x = \frac{\xi}{2}$. This feature aids in the selection of the admissible displacement functions in (3.10) such that only the symmetric ones are retained and all others discarded due to their vanishing contribution to the governing equations.

Another interesting feature of the results is the fact that for all values of ξ a plate with symmetric boundary conditions at the $y = 0$ and $y = 1$ edges (i.e., simple-simple or clamped-clamped) buckles in such a way that the number of half-waves in the direction perpendicular to the loading direction is always 1. The physical meaning of this is that a unilaterally constrained plate with symmetric y-boundary conditions buckles in such a way that there can be several half-waves in the direction of compression but only one half-wave in the perpendicular direction. In other words, for a uniaxially loaded plate, the unilateral constraint does not influence the deformation shape in the direction perpendicular to the loading direction, and the plate's response in that direction is identical to the corresponding bilaterally unconstrained case [99].

Unlike Figure 3.3 which shows only a sketch of the qualitative difference in the $\lambda_{cr} - \xi$ curves for the unilaterally constrained and bilaterally unconstrained plates, Figure 3.13 shows actual curves for the case of uniaxially simply-supported isotropic plates. While the λ_{cr} values for the bilaterally unconstrained case were obtained from an exact solution, those for the unilaterally constrained case were obtained using the methodology presented above. As mentioned previously, note the shift between the

two curves for $\xi < \sqrt{2}$ which is the value at which a simply-supported unconstrained plate switches modes (shown in the figure). Contrary to the common "intuitive" belief held by some researchers, a unilaterally constrained simply-supported plate with an aspect ratio $\xi = \sqrt{2} + \epsilon$, where ϵ is a small positive number, will not buckle into a shape that resembles that of the bilaterally unconstrained plate with an aspect ratio $\xi = \sqrt{2} - \epsilon$ (i.e., unimodal).

Figure 3.14 shows typical plots for the evolution of the buckle displacements as a function of applied load for an isotropic plate of aspect ratio three. In this case, the plate was subjected to a uniformly distributed positive transverse pressure loading. Thus, at zero axial load, the plate deformation is the linear response to the pressure load.

3.7 Experimental Investigation

This section is devoted to the experimental investigation conducted by Comiez, Waas and the author at the Composite Structures Laboratory. Most of the details that are pertinent to this investigation, e.g., specimen preparation and test procedure, are omitted and reference must be made to [26] for completeness. In this investigation, model delaminations (plates) with rectangular planforms of different aspect ratios, that are placed in a compressive load environment were considered as suitable candidates resembling those modeled mathematically. This part of the overall study was motivated by the interferometric measurements reported in [103], that describes a study on the failure mechanisms of laminates containing cutouts. In brief, it was found that, subsequent to initial damage formation, the damage propagated away from the hole edge by a combination of delamination buckling and growth. Further, the delaminated portions which approximately resembled areas of

a part of a sector plate, was found to buckle into a mode shape that at any instant of time during the growth was found to contact with the sublaminate beneath it.

A model experiment that determines the buckling characteristics (buckling load and response shapes) of a delaminated plate while allowing out-of-plane deflections to occur in one direction only (unilateral) was chosen. The experiment uses an extruded polystyrene (substrate) as a foundation for a Vinyl plate. The shadow Moiré method is used to visualize the response of the Vinyl plate.

3.7.1 Specimen Design

The specimen design entailed three layers. The bottom layer (the substrate), acts as a 'rigid' foundation and prevents the top layer (Vinyl plate) from having any deflection in the negative transverse direction (into the foundation). The top layer is the plate of interest whose buckling characteristics will be determined. The middle layer is a thin Epoxy layer. The Epoxy bonds the top layer to the bottom layer everywhere except inside the perimeter of the initial delamination planform under consideration, leaving an unbonded region in the middle of the specimen. A summary of the sandwich specimen is given in Figure 3.15 and the mechanical properties of each layer are given in Table 3.4. Given an external compressive load, this unbonded (delaminated) region will buckle. The substrate and Epoxy around the edges of the unbonded region are expected to exert forces and moments which at the first instance may be thought of as being similar in origin to generalized forces exerted by translational and rotational springs.

In selecting a substrate material, the following considerations were employed: The substrate should be made of an isotropic and homogeneous material, and it should have a high bending stiffness as it was desired that the substrate compress in

the axial direction only, thus minimizing any out-of-plane deflections. An additional constraint was the maximum available load of the compression device, at 10,000 lbf. Of a few qualified candidate materials, a 1.0 in thick extruded foamy Polystyrene was chosen for its abilities to satisfy all of the conditions and for being readily available.

Likewise, the following considerations were used in selecting a top layer material: The top layer should be made of an isotropic and homogeneous material, and the combination of bending stiffness, thickness, and unbonded region dimensions should not result in a buckling strain that is too small to be accurately measured. A 0.04 in thick solid Vinyl was chosen for the top layer material, since it satisfied the above requirements.

The only consideration for the middle Epoxy layer is that it should have sufficient strength to allow the top layer (Vinyl plate) to enter the postbuckling region of the test, while allowing no growth of the disbond, prior to buckling. Sample tests showed that Ciba-Geigy 106/953 Araldite fulfilled this consideration. The Araldite was chosen for this experiment.

3.7.2 Specimen Preparation

The substrate was cut into pieces that measured 11.5 in x 4.5 in x 1.0 in. Care was taken to ensure that the specimens have the same dimensions as well as perfectly square and parallel edges.

An adhesive reservoir (Figure 3.16(a)) was cut from the substrate at the intended boundary between the bonded and unbonded regions. The purpose of this reservoir is to collect the excess Epoxy that is forced into the unbonded region during the bonding process (Figure 3.16(b)). It is possible that some Epoxy may protrude into the unbonded region. If a reservoir is not present, the boundary between the bonded

and unbonded region will be erratic. In addition, the unbonded region will become smaller than what was intended. In actuality, the adhesive reservoir does not collect the Epoxy. The Epoxy clings to the Vinyl plate when it is forced into the unbonded region (Figure 3.16(b)). With the presence of the reservoir, the Epoxy adheres to the Vinyl alone, preventing a bond to form between the Vinyl plate and the substrate.

In a similar manner as before, 0.04 in thick Vinyl was cut into 11.5 in x 4.5 in sections. The cut Vinyl plates were spray-painted in preparation for use with the shadow Moiré method. It is desired that the Vinyl plate be as flat as possible, i.e. having an initial imperfection as small as possible. The actual initial imperfection of the Vinyl plate was found to be negligible with respect to its thickness.

After bonding the Vinyl plate to the substrate and curing, the specimen was removed from its compression. Two strain gages were bonded to the specimen. The first strain gage is located in the unbonded region and the second located in the bonded region (Figure 3.16(c)).

3.7.3 Test Procedure and Results

Figure 3.17 shows a sketch of the specimen in place under the applied load. Throughout this work it was emphasized that the situation being modeled is a quasi-static one. Hence, at the commencement of the test, the loading device was programmed to compress the specimen at a crosshead speed of 0.0075 in/min, simulating static conditions. The shadow Moiré method was used to visualize the response of the unbonded region. In addition, the full field displacement contours obtained from this method will visually verify the point of buckling during the test.

Early tests of the three layered specimen showed an unacceptable amount of specimen bending during the tests. Thus, a specimen support system was manufactured

that physically held the four edges of the specimen (Figure 3.17). Six different unbonded region's aspect ratios (ξ) were considered. These ξ values are: 1.00, 1.75, 2.50, 3.25, 4.00 and 5.00.

As expected, just like mode shapes in bilaterally unconstrained plate buckling problems, the mode shapes in unilaterally constrained plate buckling problems are also dependent on the aspect ratio of the plate in question. An aspect ratio of 2.5 has been shown to result in a two hump response and an aspect ratio of 4.0 has been shown to result in a three hump response [26]. A typical Moiré fringe pattern extracted from the results in [26] is shown in Figure 3.18.

The experimental results for the buckling load λ_{cr} are plotted in Figure 3.19 against those predicted by the analytical model. The results obtained by the latter appear to bounds those of the former. While the upper theoretical bound corresponds to the case where the unloaded disbond edges are clamped, the lower bound corresponds to the case where it is "assumed" that these edges are simply supported. For the case where the unloaded edges are clamped (marked in figure as $k_\theta = \infty \Rightarrow$ cccc), the solution exhibits discontinuities as a function of plate aspect ratio (ξ). These discontinuities can be attributed to the fact that in the neighborhood of $\xi = 2.5$, topological changes in the buckle patterns occur. Being bounded from above and below, the experimental results fall closer to the lower bound. This is as expected, since at the disbond/bonded boundary, the delamination is neither clamped nor simply supported but is very likely to be best modeled as being supported by rotational and translational springs. It must be noted that in the experiment, the response of the disbond formed gradually, except in some cases where the disbond 'snapped' from a perfectly flat state to one that is buckled, characteristic of a true bifurcation. This happened only to plates with small aspect ratio. To some extent, this is not

surprising, since the corresponding bilaterally unconstrained buckling problem for plates of small aspect ratio yields buckling modes that are of one sign, whereas for larger aspect ratio plates, the buckle mode contains more than one-half wave along the length (loaded direction).

As suggested earlier, one way to enhance the modeling of the physical problem is to consider elastic nonhomogeneous boundary conditions such as rotational and/or translational linear springs. Since λ_{cr} is more sensitive to the boundary conditions on the unloaded (long) edges, it was decided (for the sake of better understanding and modeling the physical problem) to investigate the situation where rotational elastic linear springs were present at these long edges. No translational springs were considered for the sake of simplifying the modeling and hence the computational effort. It should be mentioned that by adding translational springs the degree of complexity of selecting "proper" values for their stiffnesses increases the computational task significantly. Further, and as it will be shown subsequently, variable rather than constant values for spring stiffnesses will yield results closer to those obtained experimentally. Hence, in addition to trying to approximate stiffness values, their functional variation must also be determined.

Following the analytical formulation presented earlier with the modification of having linear rotational springs at the long unloaded edges, $\hat{y} = 0$ ($y = 0$) and $\hat{y} = b$ ($y = 1$), included in the Galerkin equations (3.12)[7], the equations were solved using the same solution process outlined above. Figure 3.19 shows clearly that in order to best approximate the experimental results, the value of the rotational stiffness k_θ must be chosen such that it is inversely proportional to the plate's aspect ratio ξ. Note that $k_\theta = f(\xi)$ still implies a linear stiffness in the classical sense. Selecting a

[7]The analytical inclusion of the springs into the governing equations follows the classical approach found in many standard textbooks on the subject.

constant k_θ independent of ξ was found (not shown) to fit the experimental data at one end, say ξ close to 1, but not at the other, say ξ close to 5. Further, other efforts were made to investigate the case where the rotational springs are nonlinear having a load dependency, i.e., $k_\theta = f(\lambda)$ as well as $k_\theta = f(\lambda, \xi)$. Such efforts resulted in less satisfactory approximations to the experimental results. At this point, it was decided to pursue further the case where $k_\theta = f(\xi)$. In choosing an appropriate form for the functional dependency several forms like $k_\theta = \frac{c}{\xi}$, $k_\theta = \frac{c}{d+\xi^n}$ and $k_\theta = \frac{\xi}{d+\xi}$, to mention a few, were considered for different value of the constants c, d and n. After investigating a wide variety of such functions, the one that best approximated the experimental results was found to be the following (Figure 3.20):

$$k_\theta = \frac{3}{1+\xi^2} \tag{3.26}$$

The k_θ form in (3.26) is not unique. It was not derived from any principle nor law in mechanics, and by no means implies so. It is a form that was arrived at by trial and error. Careful analysis of the form (3.26) reveals the fact that using such a model for k_θ implies a certain interaction between the rotational stiffness of the boundary and the slenderness of the plate (aspect ratio ξ). The longer the plate the less the boundary's rotational stiffness and visa versa. But such a conclusion is counter intuitive since it suggests that a knowledge of boundary's rotational stiffness alone is not sufficient to use in a classical solution approach without knowing the dimensions (lengths) of the boundary. The later argument suggests a counter argument that, in turns, suggests that classical Winkler-type elastic foundations may not be the proper approach to simulate the experimentally obtained results. To verify such an implication a 3-Dimensional elasticity (or Finite Element) solution of the problem is

warranted. Such verifications are beyond the scope of this work.

3.8 Concluding Remarks

The problem of buckling of unilaterally constrained, finite, rectangular plates was investigated. The plates were modeled along the lines of classical plate theory employing Kirchhoff-Love hypothesis. The presence of a unilateral constraint was accounted for through the use of a nonlinear elastic foundation model that exhibits a deformation sign dependent force-displacement relation. Using Galerkin's method, the resulting system of governing nonlinear equations was solved iteratively. Different boundary conditions were considered and the results for some boundary conditions were compared and shown to be in good agreement with "exact" results reported earlier in Chapter II as well as those available in the literature . The effect of the presence of a transverse load Q was investigated and it was found that the plate's load-displacement (λ-$\frac{\|\mathbf{A}\|}{\|\mathbf{A_0}\|}$) curve can depend on the sign and distribution of Q, while the buckling load parameter (λ_{cr}) was found to be independent of Q. Different material orthotropies were also investigated and results for the buckling load were presented and were found to compare favorably with results reported previously.

Experimental investigation has further revealed that the buckling mode of the delamination (plate) may involve regions or points of contact with the undelaminated portion of the substrate. The effect of this physical constraint was shown to cause the response of the plate to occur in a progressive fashion. The shadow Moiré technique that was employed was able to clearly show that the mode shape was periodic and contained points and/or regions of contact. The results obtained from the theoretical investigation were found to bound the experimental values. It is clear that the stiffness of a postbuckled delaminated plate is highly influenced by

whether the buckled portion involves points (or regions) of contact or not. Thus, in analytical model development, the possibility of the delaminated portion contacting the plate cannot be excluded. Instead, the corresponding buckling problem must be addressed within this wider setting that incorporates the possibility of contact. The resulting boundary value problem solution should then deliver the result whether contact occurs or not.

This part of the study has demonstrated the validity of using nonlinear foundation models in the buckling analysis of unilaterally constrained rectangular plates. Since the formulation is quite general, extensions to study the unilaterally constrained buckling problem of thin film delaminations of arbitrary planform shape, in compressively loaded laminates will be considered in the following chapters. Obtaining a solution to this latter problem was the initial motivation for developing the methodology presented here. While the analysis presented thus far accounted for the presence of a unilateral constraint via the use of a nonlinear constitutive model, the governing equations were derived based on linearization about the buckling load. As a result, moderately large deformations were not accounted for, and the postbuckling regime could not be captured. Such an approximation is valid if the delamination's growth behavior is not sought after. On the other hand, if the growth behavior is of interest, which is the case in this study, the fully nonlinear plate equations (in the von Kármán sense) must be resorted to. As such, this will be the focus of the forthcoming chapter which will deal with the general formulation of the equations governing the large deformations of plates on general elastic foundation.

Loaded Edges[b]	Boundary Conditions[a] cc or ss			
Unloaded Edges[c]	cc	cs	ss	cf
λ_{cr}	9.30	7.22	5.25[d]	1.75

[a]c = clamped, f = free, s = simple.
[b]Loaded edges are in the short (y) direction.
[c]Unloaded edges are in the long (x) direction.
[d]Exact value = 5.33.

Table 3.1: Limiting values of the buckling load parameter (λ_{cr}) as $\xi \rightarrow \infty$ for uniaxially loaded isotropic plates.

Material	D_{12}	D_{16}	D_{22}	D_{26}	D_{66}
Isotropic	0.33	0.00	1.00	0.00	0.33
Orthotropic (A)	0.26	0.00	0.38	0.00	0.27
Orthotropic (B)	0.67	0.00	2.61	0.00	0.70

Table 3.2: Normalized bending properties for the three types of materials used in the theoretical investigation.

Material[b]	Infinite plate solution		Finite plate solution ($\xi = 5$)[a]	
	ss	cf [c]	ss	cf
Isotropic	5.333	1.876	5.250	1.750
Orthotropic (A)	3.650	1.281	3.565	1.180
Orthotropic (B)	9.530	3.343	9.200	3.050

[a] At this aspect ratio the values for λ_{cr} are independent of the boundary conditions on the loaded edges.

[b] Materials of the orthotropic types A and B correspond to material types A-IM7/8551-7 and B-IM7/8551-7, respectively, used in Chapter II.

[c] See Table 2.8.

Table 3.3: Values of λ_{cr} for "long" plates obtained using two solution approaches: Infinite plate solution and Finite plate solution ($\xi = 5$). Boundary conditions are along the two unloaded edges.

Material	Thickness (in)	E (psi)	ν	D (lbs-in)
Rigid Vinyl	0.04	400,000	0.31	2.36
Araldite	≈ 0.02	NA	NA	NA
Extruded Polystyrene	1.0	2300	≈ 0.30	210.62

Table 3.4: Properties of the three types of materials (layers) used in the experimental investigation.

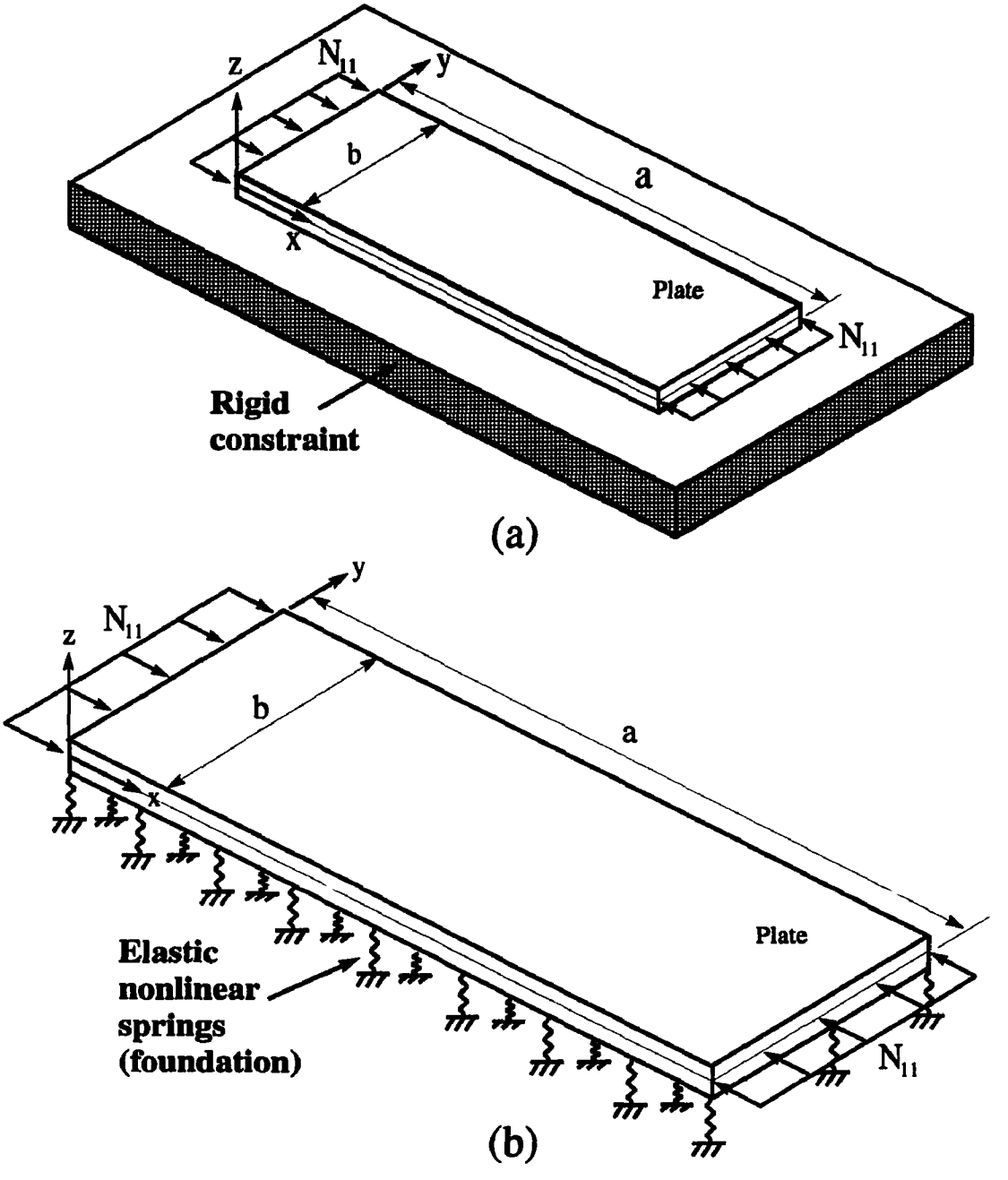

Figure 3.1: Thin elastic plate constrained by a rigid surface and under the action of an applied inplane uniform load. (a) The physical problem, (b) the mathematical model. a represents the total length of the plate. The loads N_{11} are applied at $x = 0$ and $x = a$.

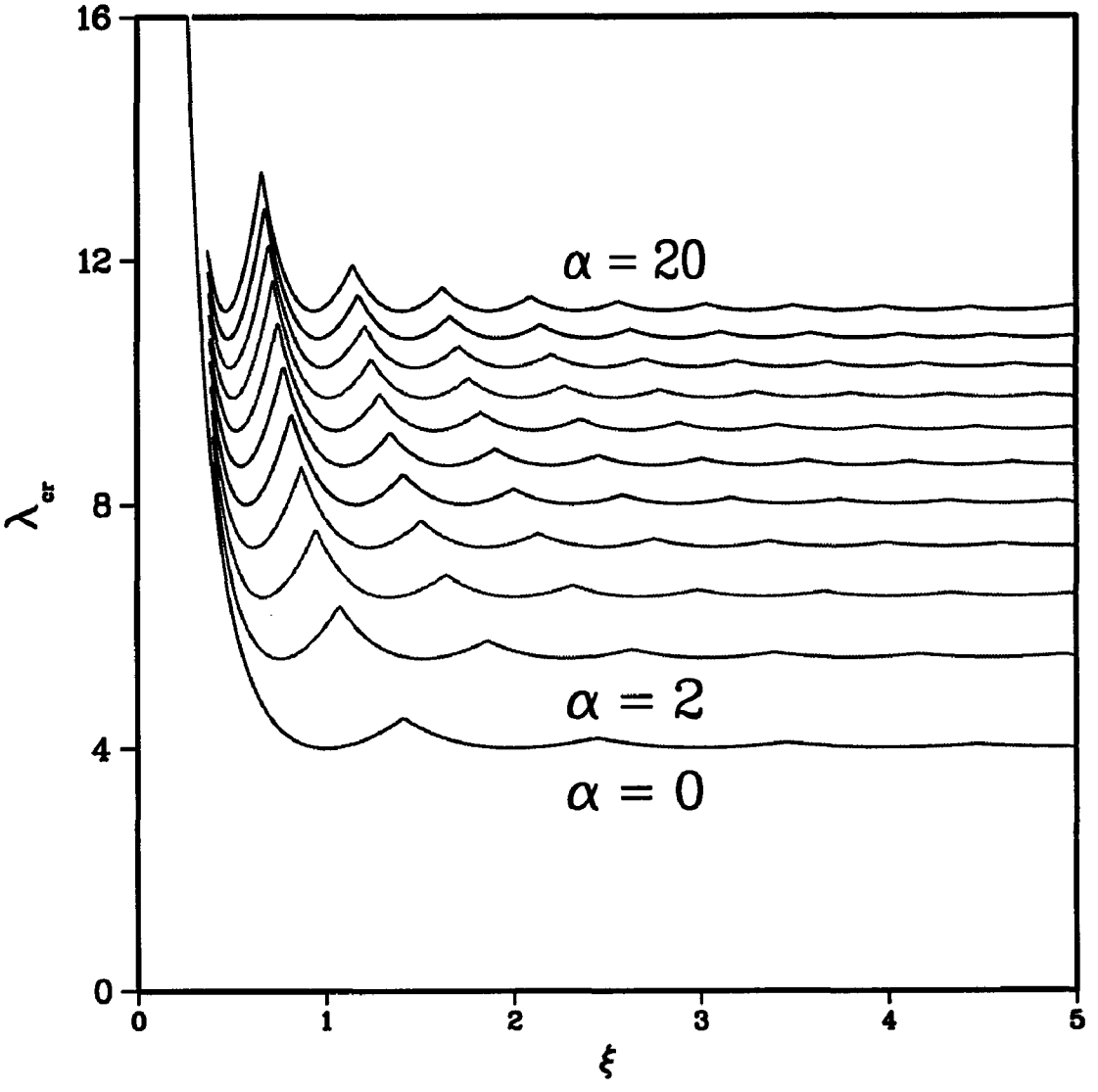

Figure 3.2: Exact values for the buckling load parameter λ_{cr} vs. plate's aspect ratio ξ for isotropic simply-supported ("ssss") plates. The plate is attached to a Winkler Foundation with stiffness α.

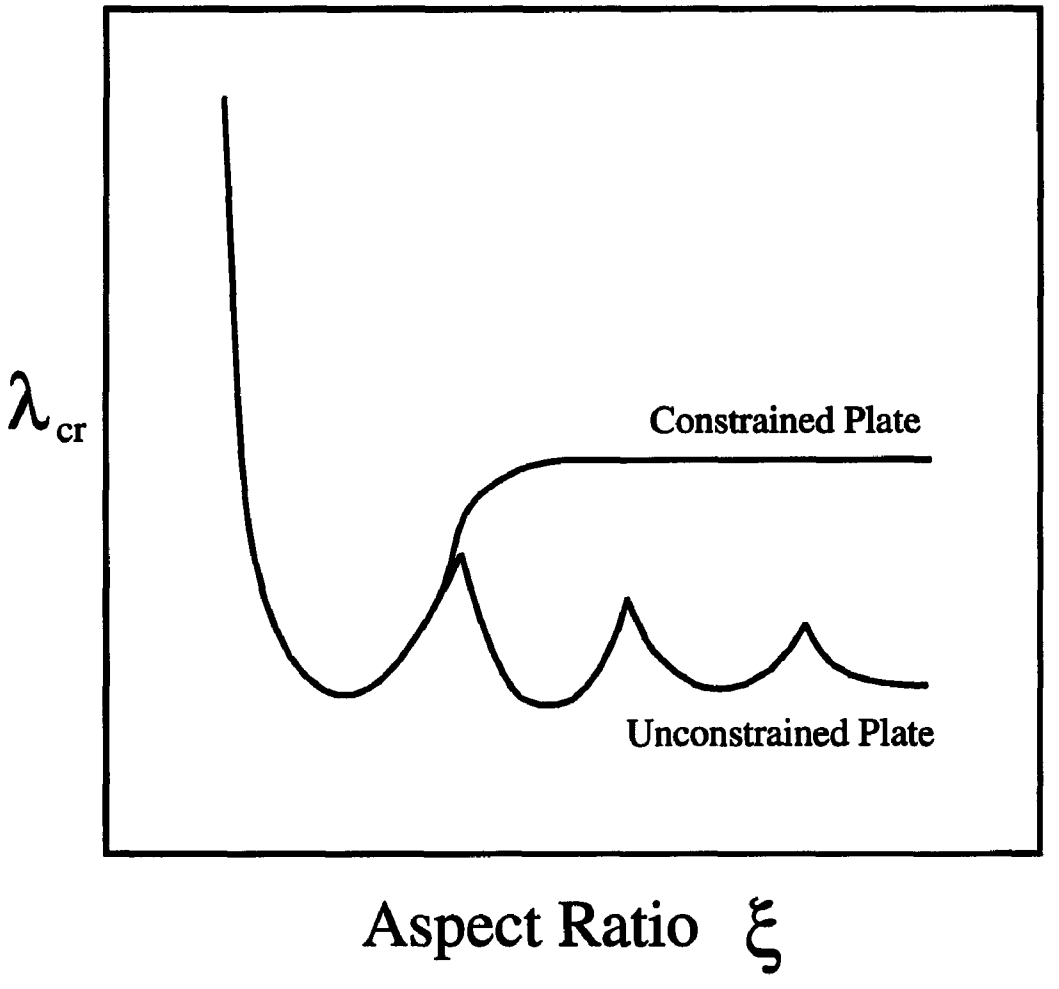

Figure 3.3: A sketch showing the difference in the λ_{cr}-ξ curve between unilaterally constrained and bilaterally unconstrained plates. Note that at lower values of ξ the two curves are indistinguishable.

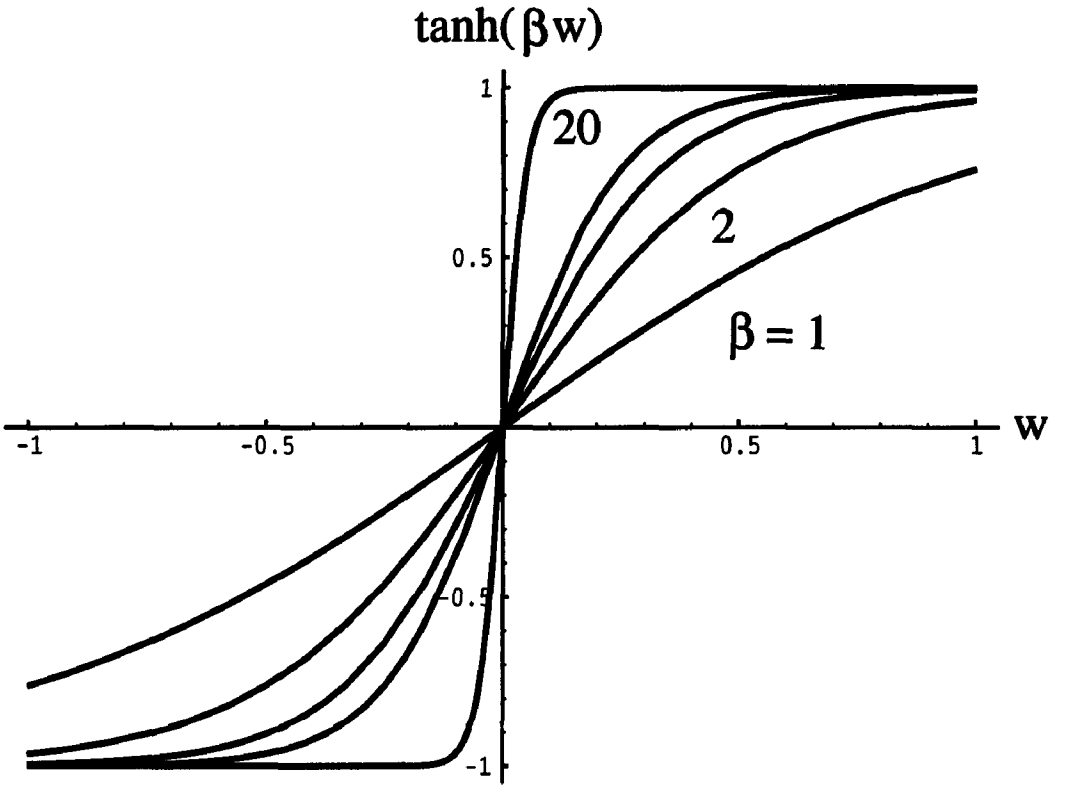

Figure 3.4: $\tanh(\beta w)$ vs. w for different values of β. For large β, the tanh function approaches a step function.

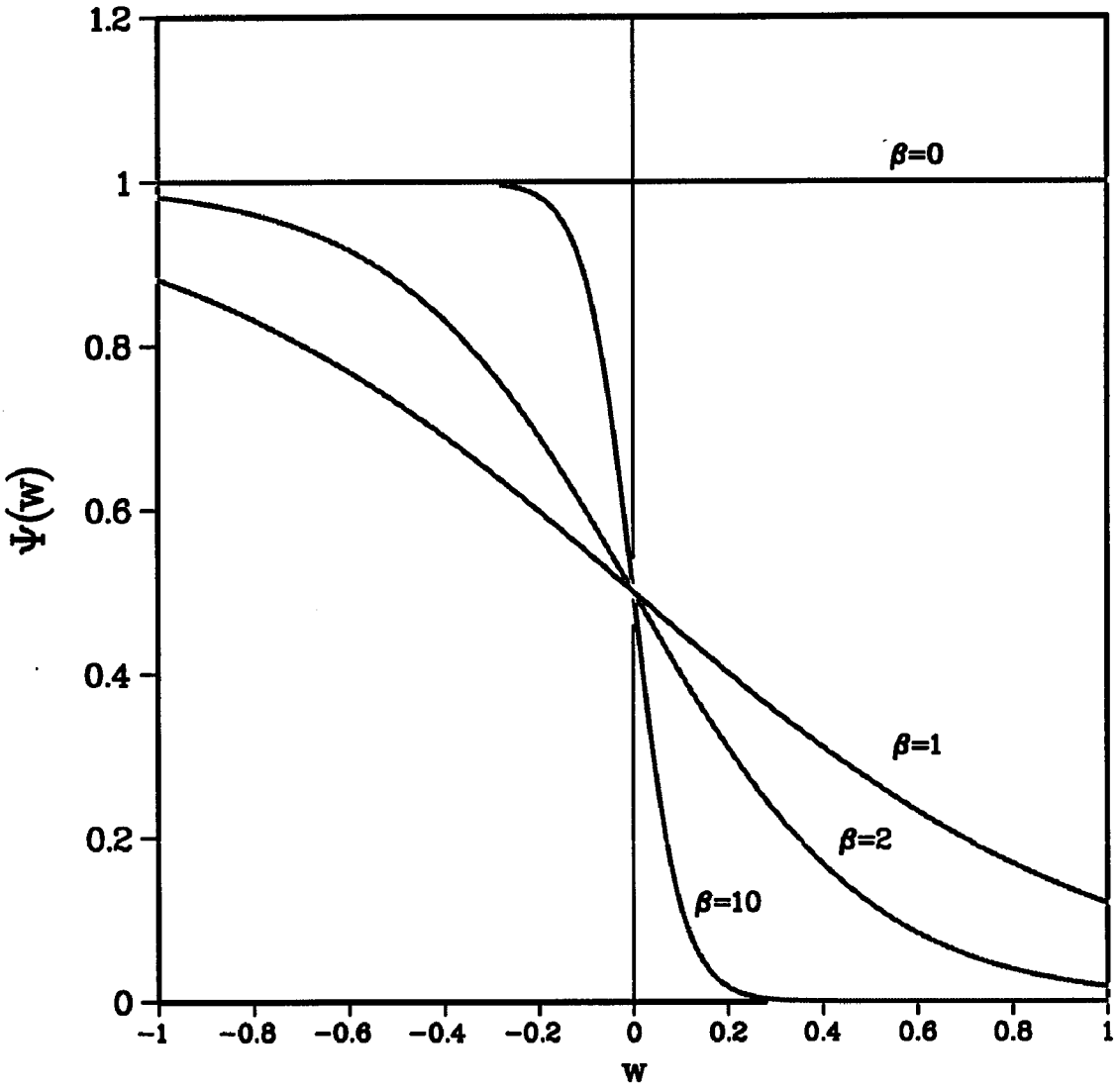

Figure 3.5: Foundation's $\Psi(w)$ function used to model the unilateral constraint.

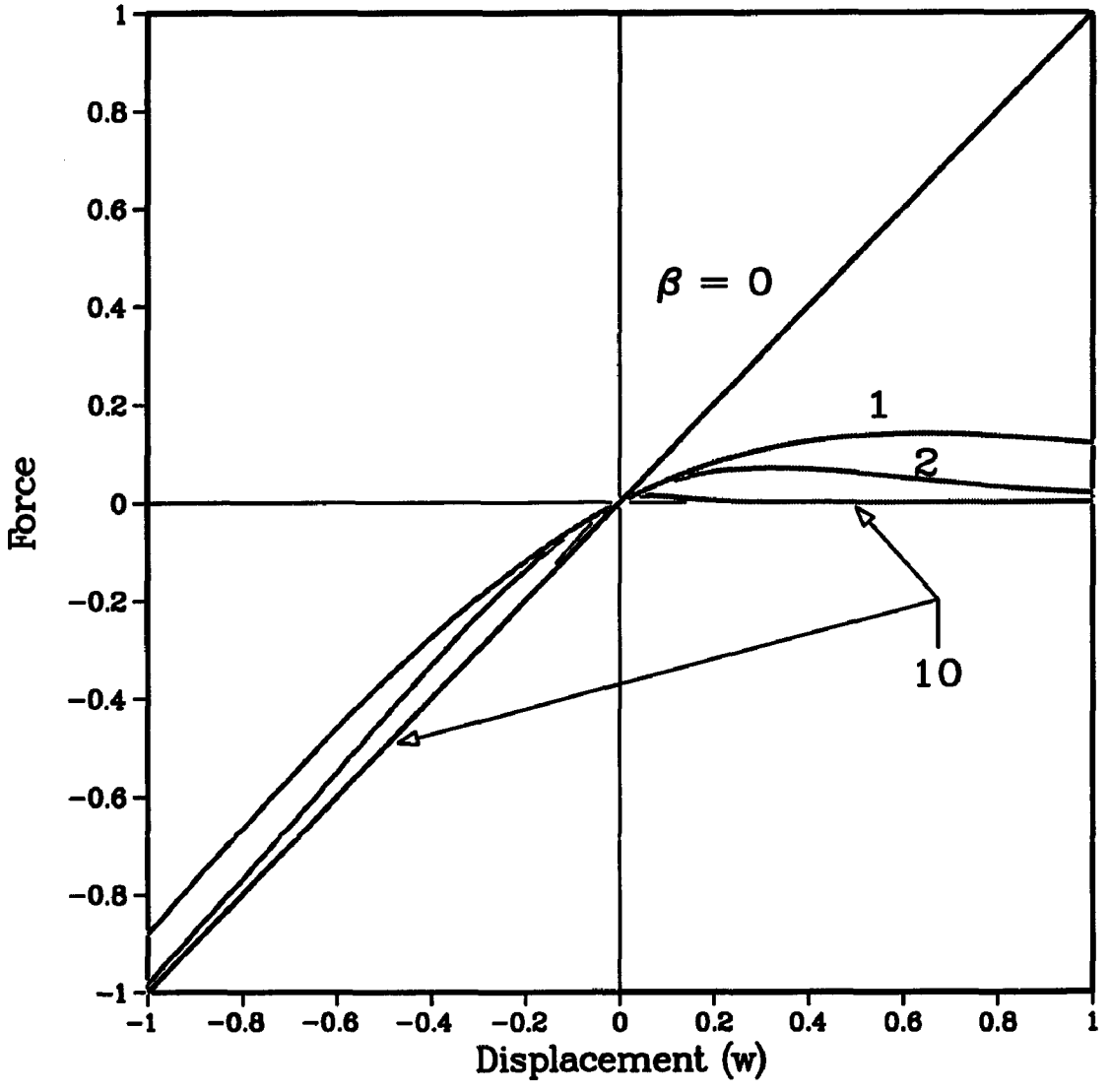

Figure 3.6: Foundation's constitutive Force-Displacement (F-w) relationship used to model the unilateral constraint. $F = \alpha$ w Ψ(w), ($\alpha = 1.0$ in this case).

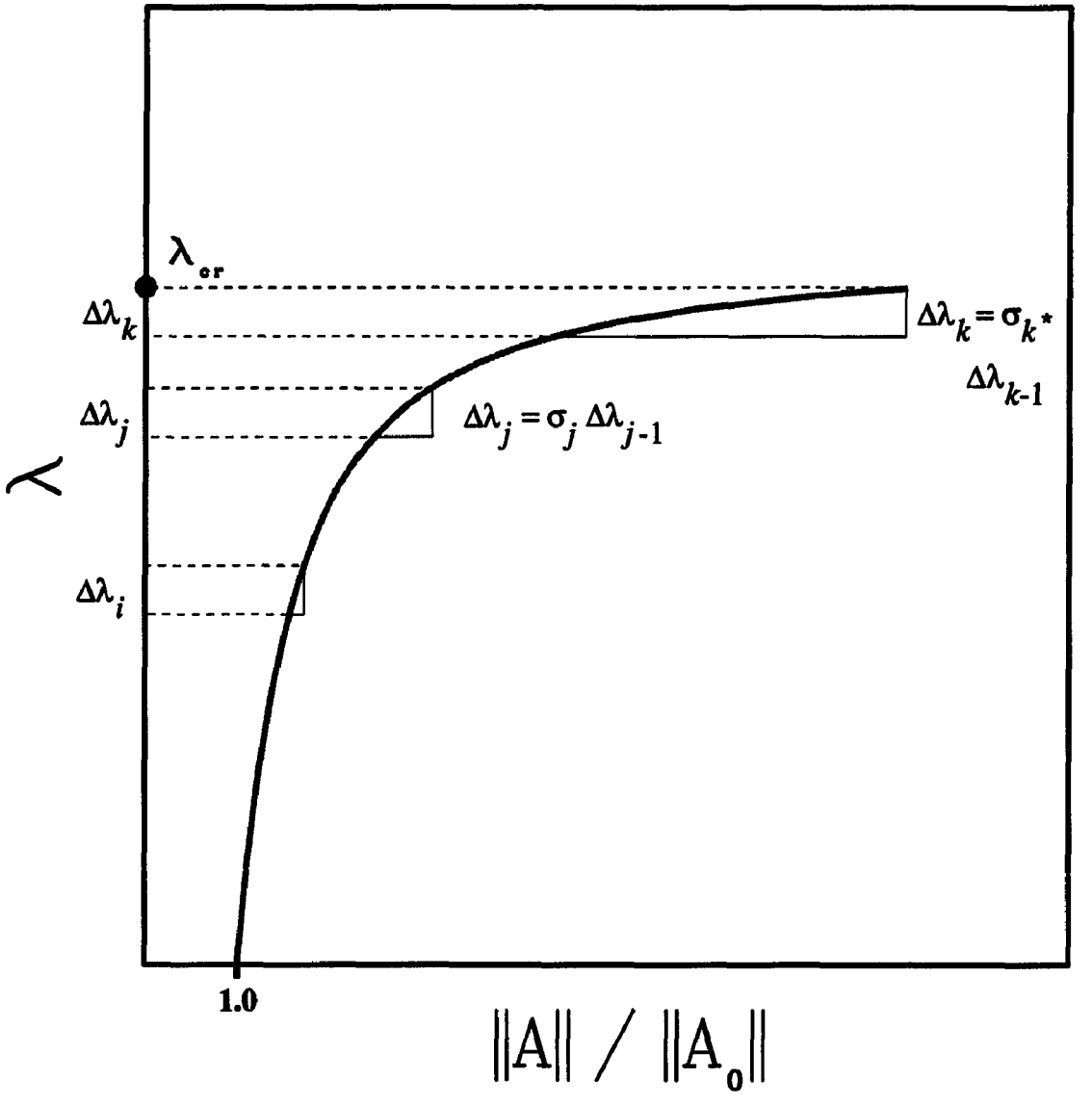

Figure 3.7: Response curve showing a standard incremental scheme. Uniform λ increments implies $\sigma = 1.0$ for all steps.

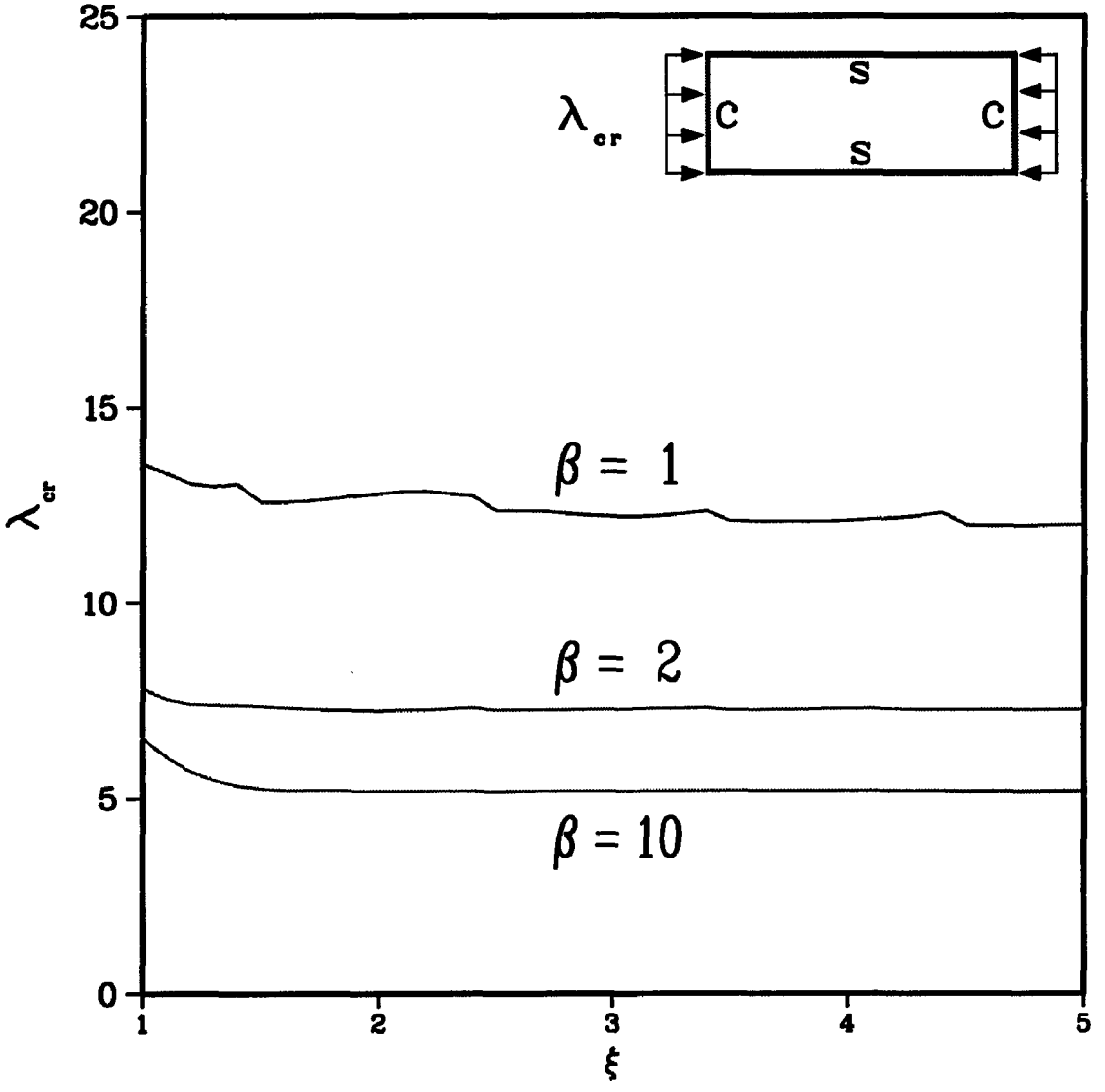

Figure 3.8: The influence of the foundation (springs) attachment coefficient β on the value of the buckling load parameter λ_{cr} for isotropic plates with "ccss" boundary conditions.

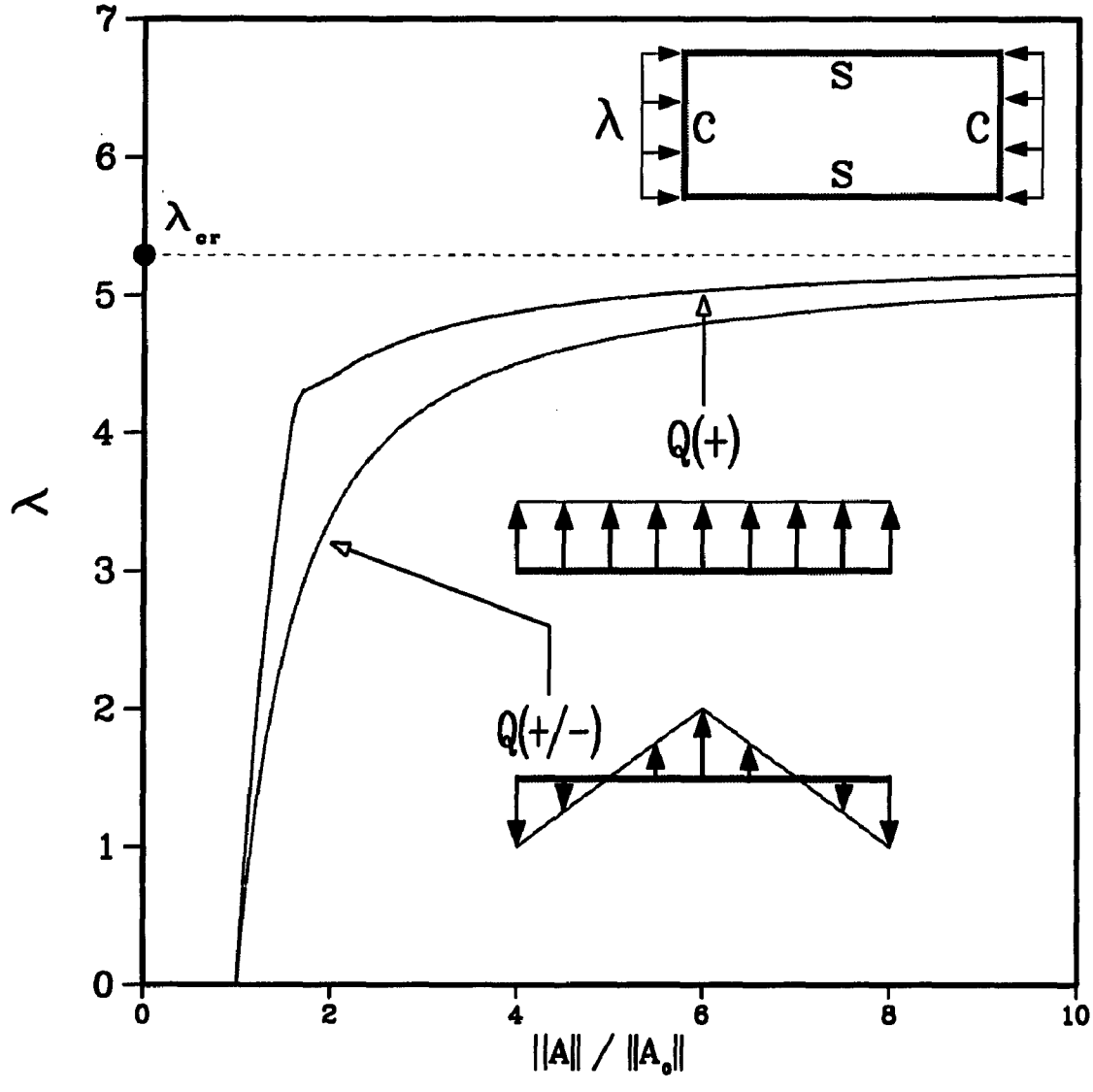

Figure 3.9: Response curves for two different transverse loading $Q(x, y)$ distributions, for an isotropic "ccss" plate of aspect ratio ξ=3. Note that for the same but unilaterally unconstrained plate, $\lambda_{cr} \approx 4.4$.

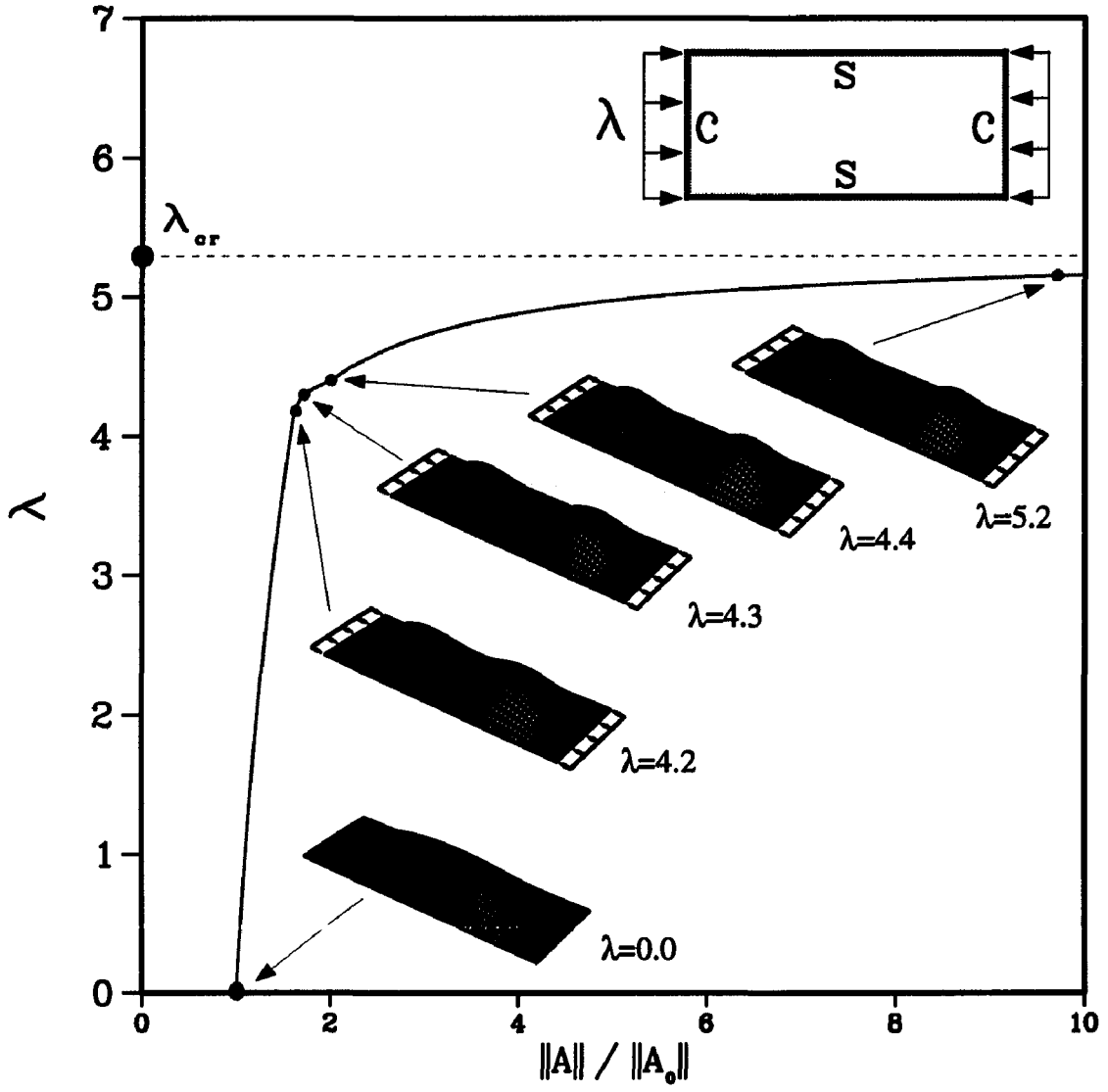

Figure 3.10: Response curves for a uniform transverse loading $Q(x, y)$ distributions, for an isotropic "ccss" plate of aspect ratio ξ=3. A sequence of events shows clearly the reason for the sudden change (increase) in slope (stiffness). Note that for the same but unilaterally unconstrained plate, $\lambda_{cr} \approx 4.4$.

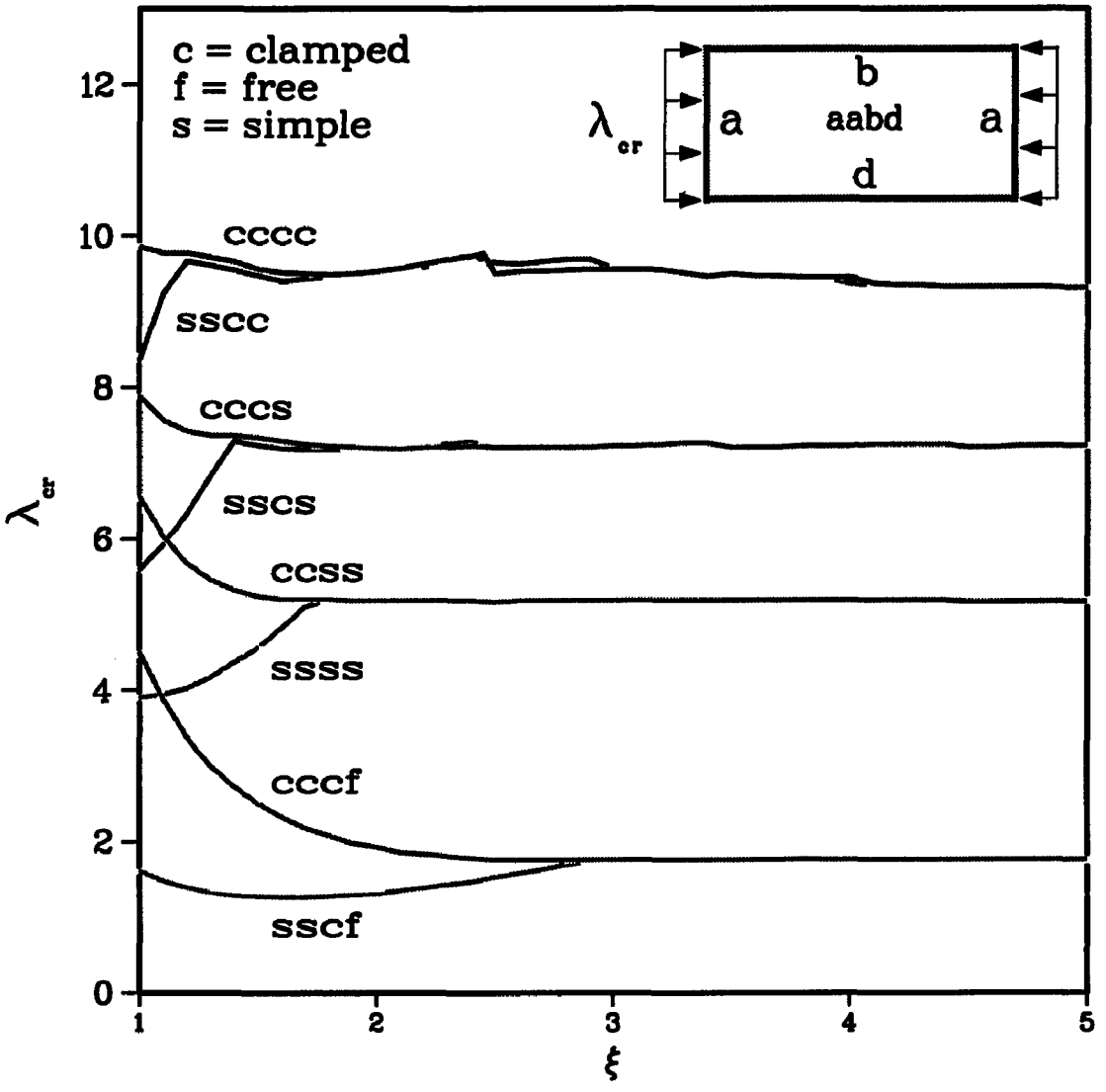

Figure 3.11: Buckling load parameter λ_{cr} as a function of the plate's aspect ratio ξ for unilaterally constrained isotropic plates with different boundary conditions on their loaded and unloaded edges.

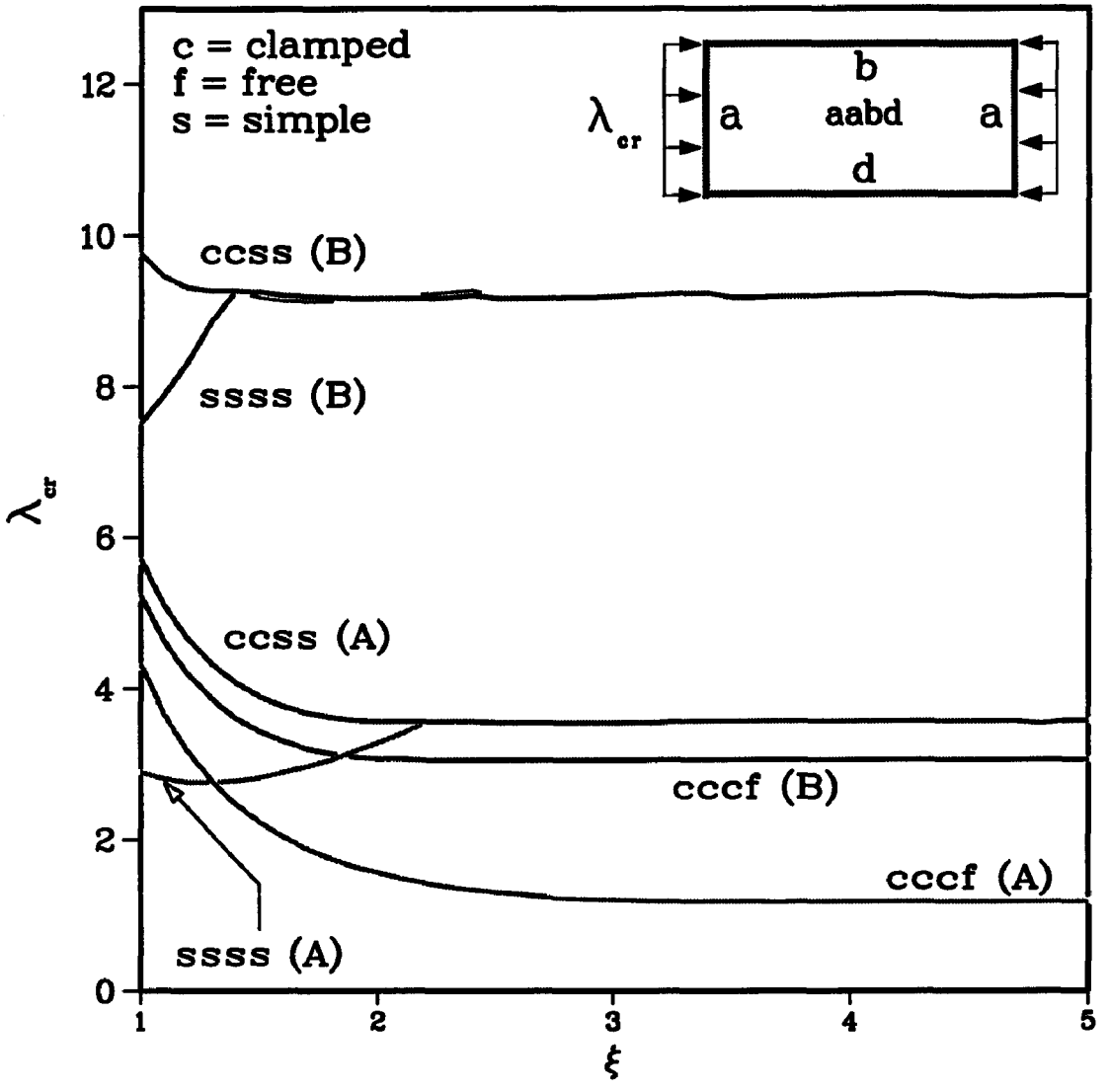

Figure 3.12: Buckling load parameter λ_{cr} as a function of the plate's aspect ratio ξ for two types of unilaterally constrained orthotropic plates (A, and B) with different boundary conditions on their loaded and unloaded edges.

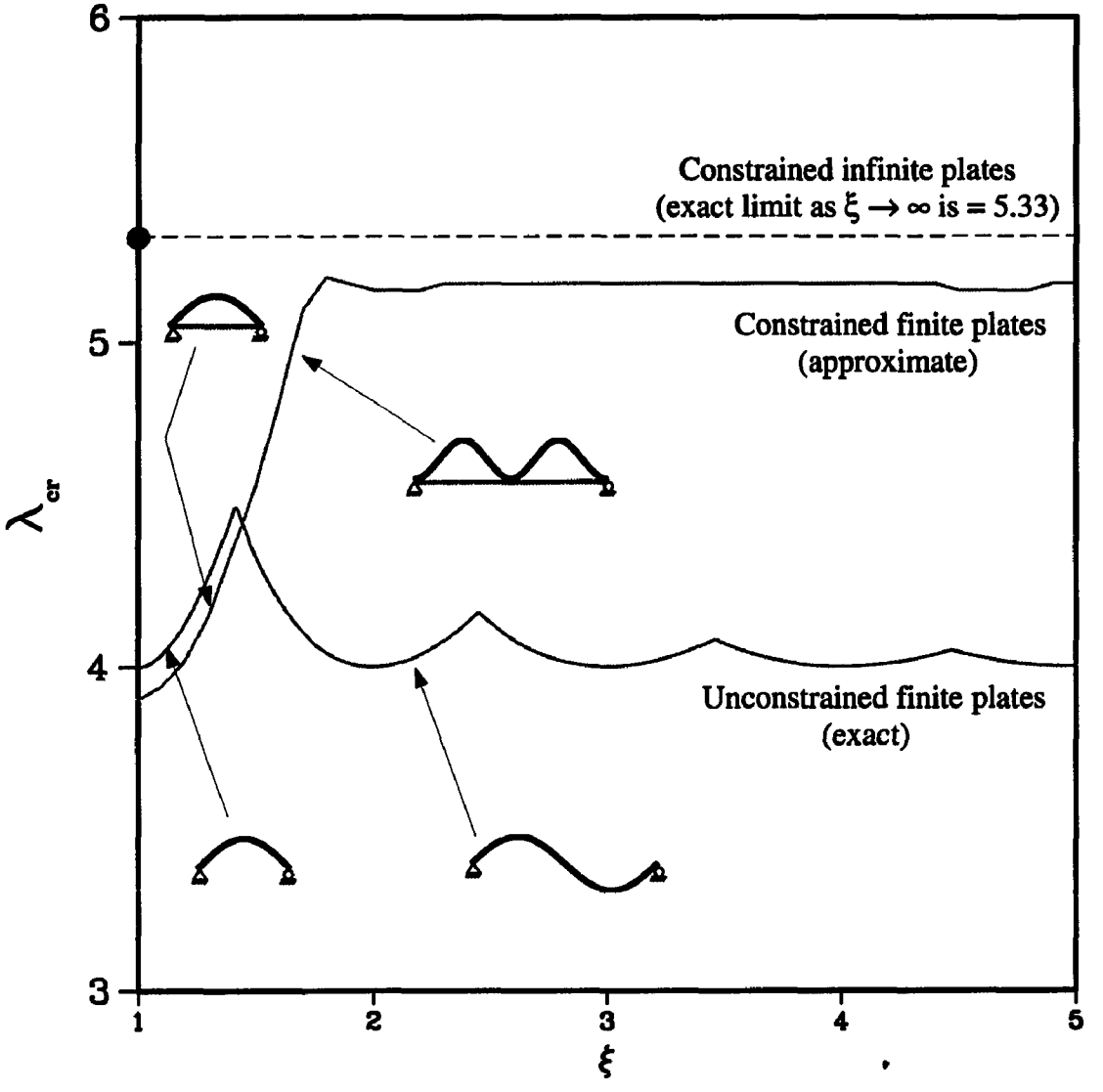

Figure 3.13: Buckling load parameter λ_{cr} as a function of the plate's aspect ratio ξ for isotropic, simply-supported "ssss", unilaterally constrained and bilaterally unconstrained plates.

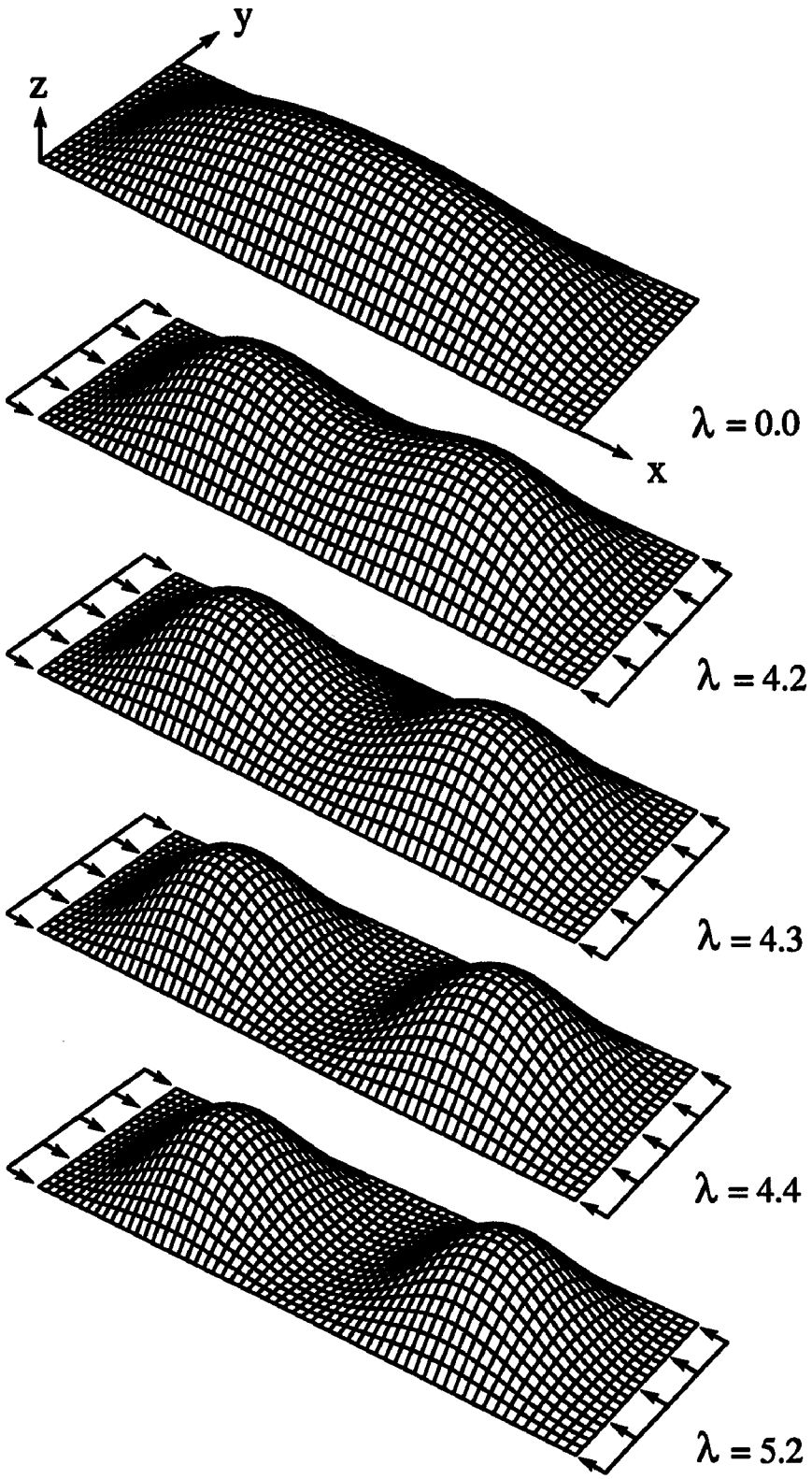

Figure 3.14: Deformation of a "ccss" isotropic plate of aspect ratio $\xi = 3$, under a transverse loading and at different levels of inplane loading. The deformations are exaggerated for clarity.

Layer	Properties	Visual Example
Top	**Material:** Transparent Vinyl **Dimensions:** a = 11.50 in b = 4.50 in t = 0.04 in	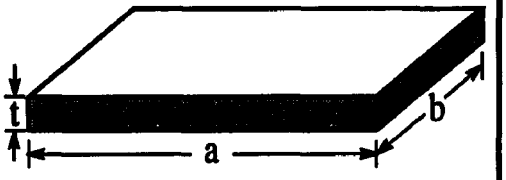
Middle	**Material:** Araldite (Epoxy Structural Adhesive) **Dimensions:** a = 11.50 in b = 4.50 in t = 0.01 in (approx.)	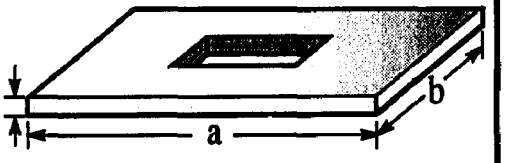
Bottom	**Material:** Extruded Polystyrene (foam) **Dimensions:** a = 11.50 in b = 4.50 in t = 1.00 in	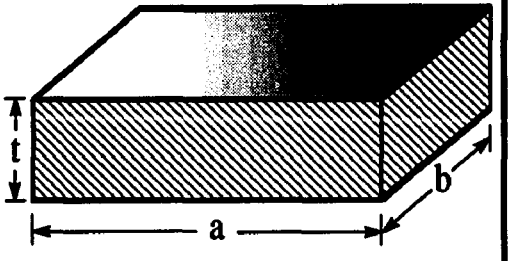

Figure 3.15: Summary of the model specimen used in the experimental investigation.

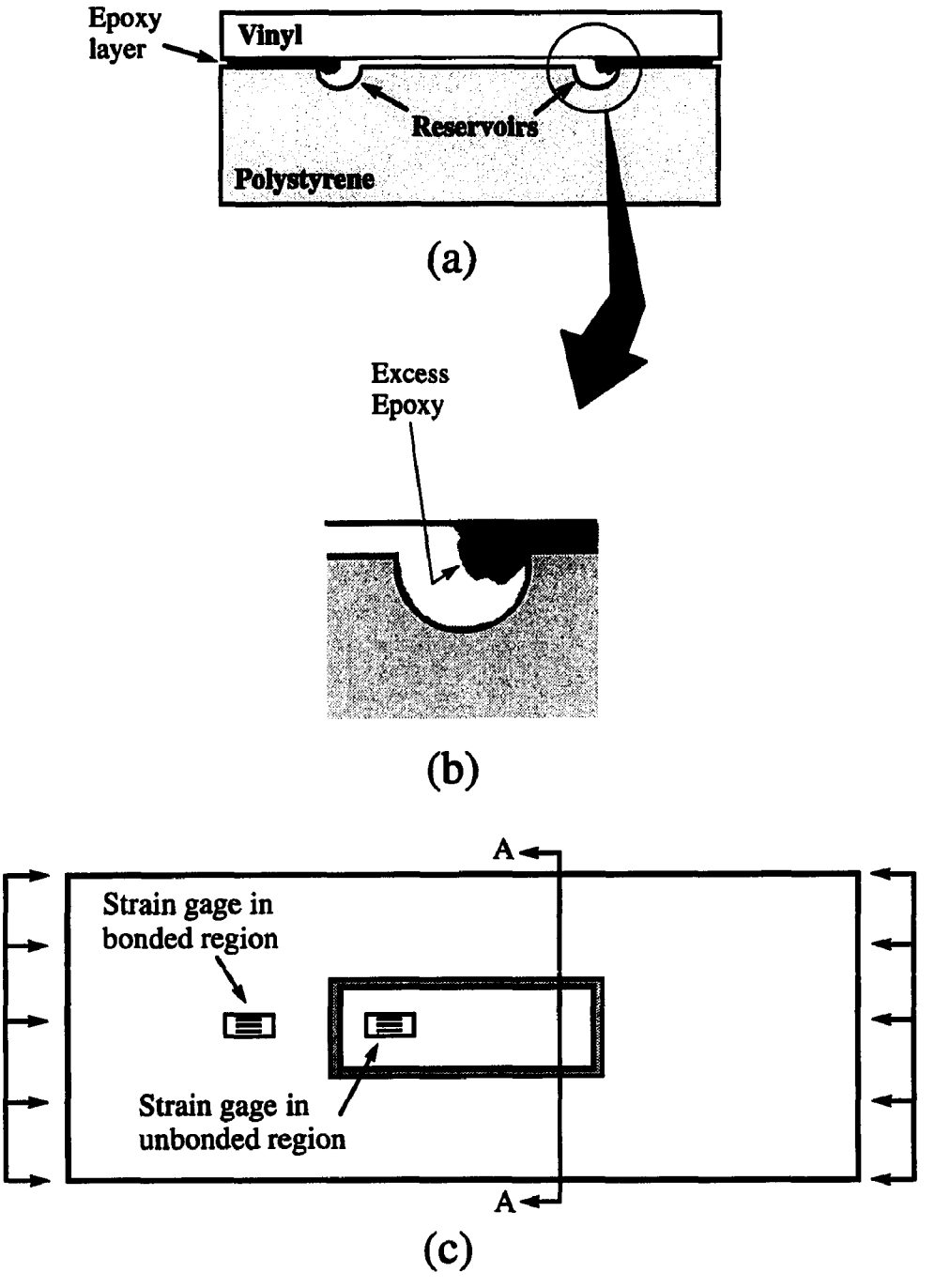

Figure 3.16: Specimen details. (a) Cross-section @ A-A showing the three layers and the reservoir details, (b) a blowup of a reservoir showing the excess Epoxy, and (c) top view showing the location of strain gages.

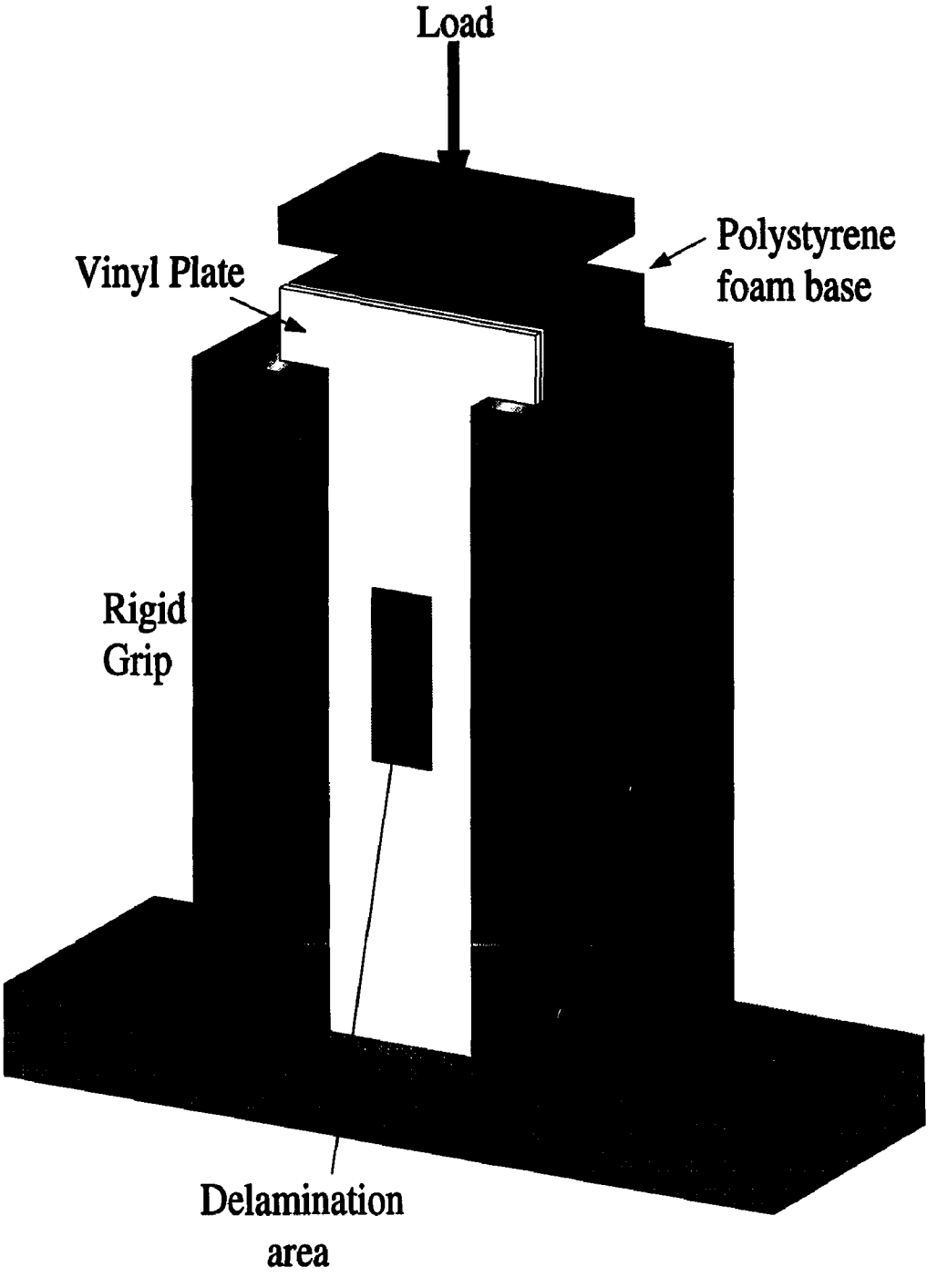

Figure 3.17: Experimental setup showing specimen, rigid grips, delamination area and loading.

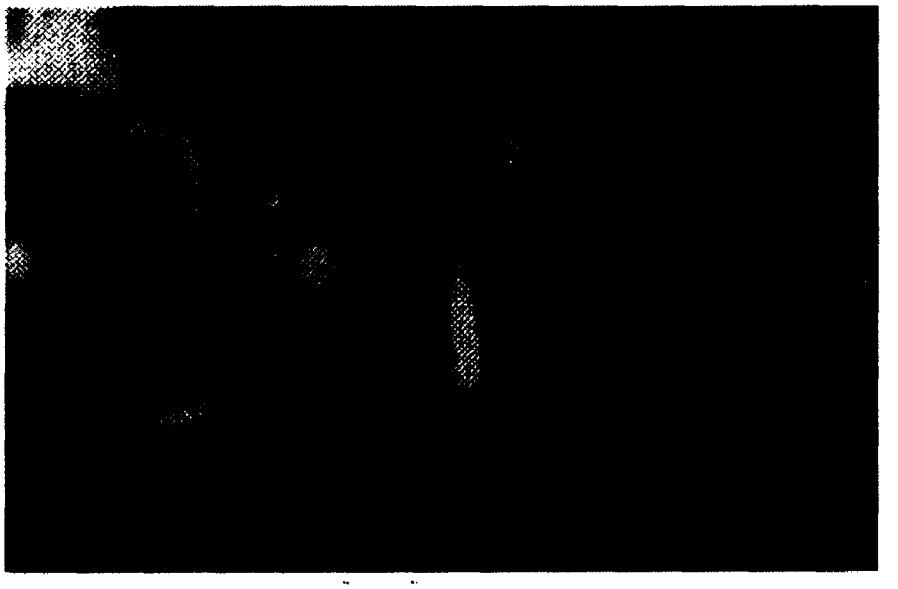

Figure 3.18: A typical Moiré fringe pattern of a buckled unilaterally constrained delamination (after Comiez *et al.* [26]). The actual pattern extends (horizontally) beyond what is shown and was truncated for picture development purposes. This specimen had an aspect ratio $\xi = 5$. Note the relatively flat regions between the humps.

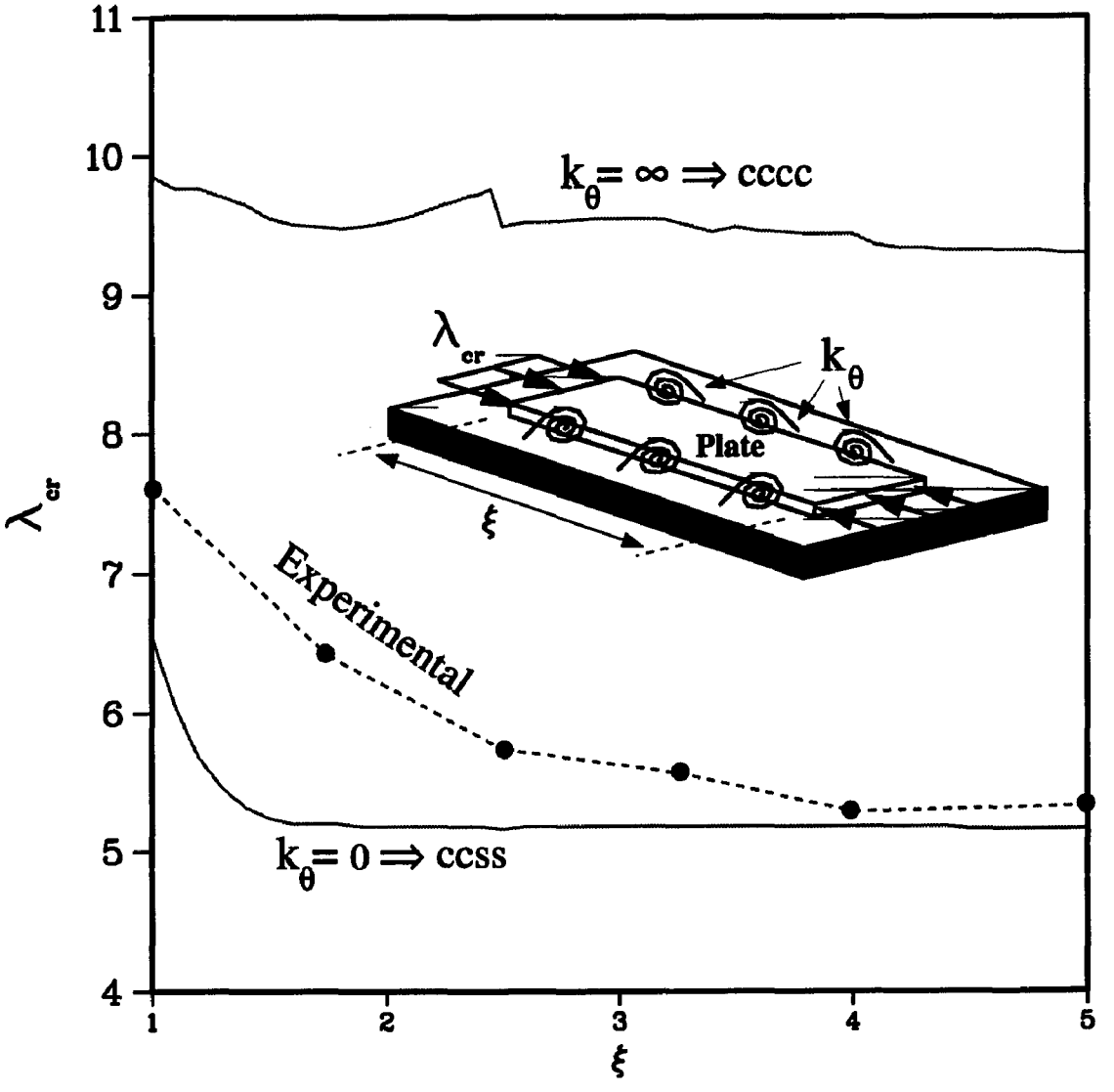

Figure 3.19: Comparison of experimentally determined values of λ_{cr} with those predicted by the approximate method discussed in Chapter III.

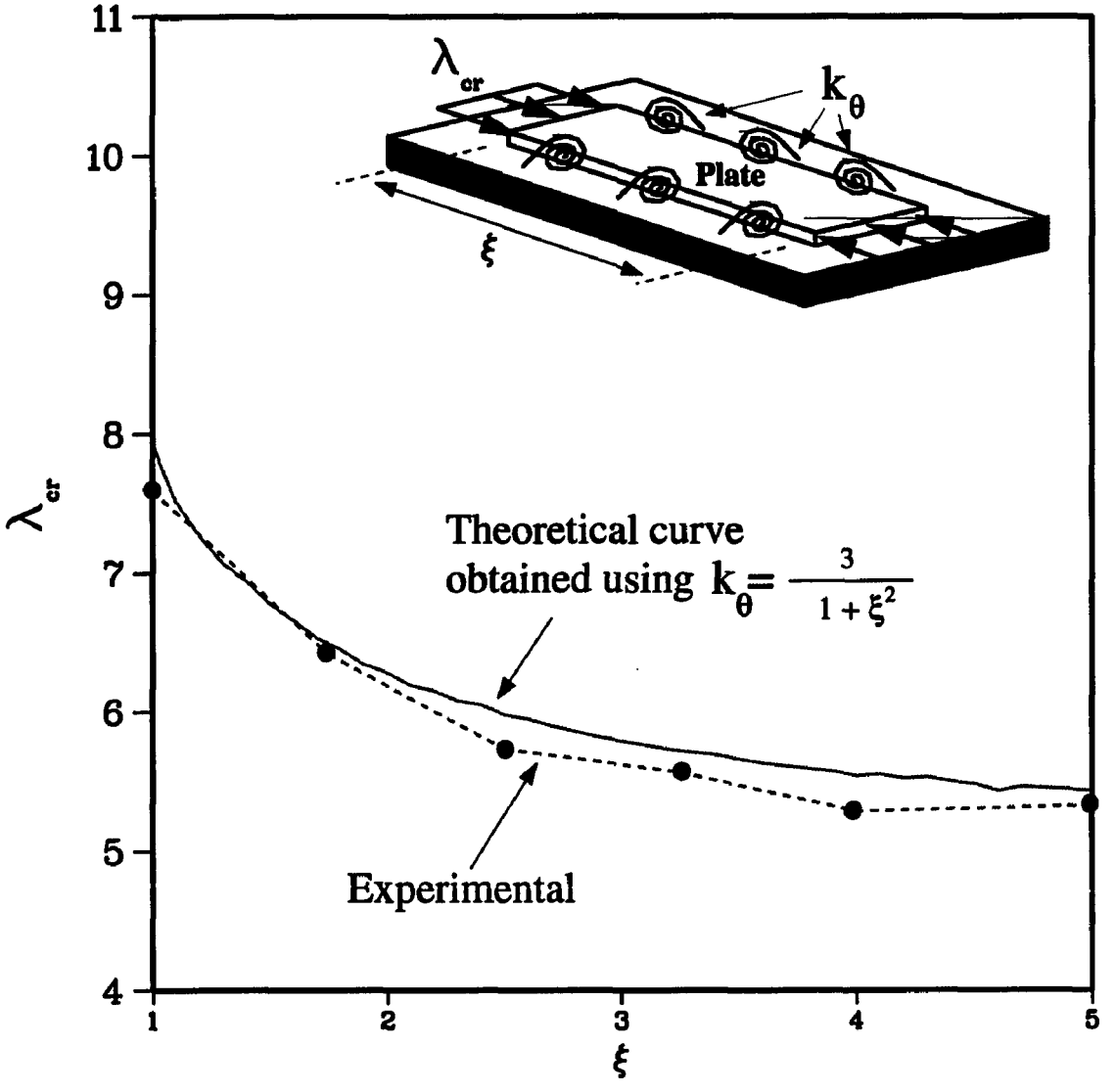

Figure 3.20: A k_θ model that, when incorporated in the analytical model, results in values for λ_{cr} that best approximate the experimentally determined ones.

CHAPTER IV

DECOHESION OF DELAMINATIONS: FORMULATION OF THE INTERPHASE PROBLEM

4.1 Introduction

In the introductory chapter (Chapter I) the main problem was presented and described as the buckling, postbuckling and non-self-similar decohesion along a finite interface of unilaterally constrained delaminations. In subsequent chapters (Chapters II & III), only the unilateral constraint condition was considered along with its influence on the buckling behavior of infinite and finite rectangular plates. Up to this point, the postbuckling and growth behavior of arbitrarily-shaped delaminations has not been considered nor even accounted for in any of the formulation presented thus far. Hence, the goal of this chapter is to present a unified treatment on the subject where the three aspects, namely, postbuckling, non-self-similar decohesion, and being arbitrarily-shaped are accounted for simultaneously. Further, during the formulation no distinction will be made between the phenomena of buckling (and postbuckling) and non-self-similar growth[1]. In other words, the same equations govern the entire behavior from beginning (starting to load/displace the structure) to

[1]We believe that the separation into different regimes is artificial and in fact it will be shown that the decohesion resistance has a significant influence on the response of the delamination prior to the onset of growth

end (complete delamination and/or loss of stiffness) without specification to certain regimes of validity.

Classically, the problem of delamination buckling and growth has been treated by analyzing the growth subsequent to buckling of a finite delamination embedded in an *infinite* medium. The medium is usually taken to be a layer (being a beam or a plate) attached cohesively or adhesively[2] to another layer. While being a valid treatment on the subject resulting in a variety of useful and practical results, this approach significantly hampers the ability to obtain results for 3-dimensional non-self-similar growth. Further, it circumvents the ability to study the interaction between the "local" and the "global" problem. The local being the delamination and the global being the structure[3] containing the delamination. These deficiencies can be overcome by treating the two problems (i.e., local and global) as one and allowing the distinction to evolve as part of the solution.

To capture the postbuckling behavior, the formulation will include finite (moderately large) rotations in the von Kármán sense. The term buckling will be taken to imply the classical meaning of bifurcation under either an inplane load-controlled or an inplane displacement-controlled environment. These controlled environments will be assumed to be quasi-static uninfluenced by any inertia effects. The entire response of the structure (including growth) will be assumed to be elastic and conservative. All the energy released by any decohesion process will be redistributed back to the structure with no net dissipated energy.

[2]In this context, cohesion implies bonding without an apparent interface, while adhesion implies bonding with an apparent interface.

[3]Throughout this study, the global structure is always a plate.

4.2 Plate Kinematic Relationships

The kinematic formulation follows a Lagrangian description of the problem employing Green's strain tensor. The general expression for total strain tensor is

$$\mathbf{E} = \mathbf{E}^G + \bar{\mathbf{E}} \tag{4.1}$$

where $\mathbf{E}$ is the total strain tensor, $\mathbf{E}^G$ is Green's strain tensor which was introduced by Green and St. Venant, and $\bar{\mathbf{E}}$ is the *imperfection* strain tensor. Using the notation $\hat{u}_{m,n} = \dfrac{\partial \hat{u}_m}{\partial x_n}$ and in terms of the displacement vector $\hat{\mathbf{u}}$ with components $\hat{u}_i$, $i = 1, 2, 3$, $\mathbf{E}^G$ and $\bar{\mathbf{E}}$ can be expressed in component form as follows[4]:

$$E^G_{ij} = \frac{1}{2}\left(\hat{u}_{i,j} + \hat{u}_{j,i} + \hat{u}_{k,i}\hat{u}_{k,j}\right) \tag{4.2}$$

and

$$\bar{E}_{ij} = \frac{1}{2}\left(\bar{\hat{u}}_{k,i}\hat{u}_{k,j} + \bar{\hat{u}}_{k,j}\hat{u}_{k,i}\right) \tag{4.3}$$

where $i, j, k = 1, 2, 3$ and $\bar{\hat{\mathbf{u}}}$ is the displacement's imperfection vector with components $\bar{\hat{u}}_i$. It is understood that Einstein's summation convention is adopted, and it will be throughout this work unless noted otherwise. It is also implied by the above expressions that the rectangular Cartesian coordinate system is employed. Hence, the expression for the ij component of the total strain tensor can be given as:

$$E_{ij} = \frac{1}{2}\left(\hat{u}_{i,j} + \hat{u}_{j,i} + \hat{u}_{k,i}\hat{u}_{k,j} + \bar{\hat{u}}_{k,i}\hat{u}_{k,j} + \bar{\hat{u}}_{k,j}\hat{u}_{k,i}\right) \tag{4.4}$$

[4]Throughout this chapter, a "$\bar{\ }$" implies a dimensional quantity.

At this stage, it is warranted to make some assumptions on the imperfections' fields as well as on strains' order-of-magnitude. Using unabridged notation ($\hat{x}, \hat{y}, \hat{z}$ for x_1, x_2, x_3; $\hat{u}, \hat{v}, \hat{w}$ for $\hat{u}_1, \hat{u}_2, \hat{u}_3$; $\bar{\hat{u}}, \bar{\hat{v}}, \bar{\hat{w}}$ for $\bar{\hat{u}}_1, \bar{\hat{u}}_2, \bar{\hat{u}}_3$) the following assumptions are made:

1. For simplicity, the plate exhibits no inplane imperfection fields, i.e., $\bar{\hat{u}} = \bar{\hat{v}} = 0$.

2. The out-of-plane imperfection field $\bar{\hat{w}}$ is not a function of the thickness coordinate $\hat{z}$, i.e., $\bar{\hat{w}}_{,\hat{z}} = 0$.

3. Of the higher order terms in $\mathbf{E}$, only those contributing to the out-of-plane rotations will be retained.

After employing the above assumptions, the explicit components of $\mathbf{E}$ are given as follows:

$$
\begin{aligned}
E_{\hat{x}\hat{x}} &= \hat{u}_{,\hat{x}} + \frac{1}{2}\hat{w}_{,\hat{x}}^2 + \bar{\hat{w}}_{,\hat{x}}\hat{w}_{,\hat{x}} \\
E_{\hat{y}\hat{y}} &= \hat{v}_{,\hat{y}} + \frac{1}{2}\hat{w}_{,\hat{y}}^2 + \bar{\hat{w}}_{,\hat{y}}\hat{w}_{,\hat{y}} \\
E_{\hat{z}\hat{z}} &= \hat{w}_{,\hat{z}} + \frac{1}{2}\hat{w}_{,\hat{z}}^2 \\
E_{\hat{x}\hat{y}} &= \frac{1}{2}\left(\hat{u}_{,\hat{y}} + \hat{v}_{,\hat{x}} + \hat{w}_{,\hat{x}}\hat{w}_{,\hat{y}} + \bar{\hat{w}}_{,\hat{x}}\hat{w}_{,\hat{y}} + \bar{\hat{w}}_{,\hat{y}}\hat{w}_{,\hat{x}}\right) \\
E_{\hat{x}\hat{z}} &= \frac{1}{2}\left(\hat{u}_{,\hat{z}} + \hat{w}_{,\hat{x}} + \hat{w}_{,\hat{x}}\hat{w}_{,\hat{z}} + \bar{\hat{w}}_{,\hat{x}}\hat{w}_{,\hat{z}}\right) \\
E_{\hat{y}\hat{z}} &= \frac{1}{2}\left(\hat{v}_{,\hat{z}} + \hat{w}_{,\hat{y}} + \hat{w}_{,\hat{y}}\hat{w}_{,\hat{z}} + \bar{\hat{w}}_{,\hat{y}}\hat{w}_{,\hat{z}}\right)
\end{aligned}
\tag{4.5}
$$

Finally, to arrive at the strain-displacement relationships governing the plate's kinematics, and since the structural theories being employed are kinematic theories, assumptions must be made on the *displacement* fields $\hat{u}, \hat{v}$ and $\hat{w}$. Based on the thinness of the plate and to reduce the three-dimensional problem to a two-dimensional

one, the displacement fileds can be expanded as a linear combination of the thickness coordinate $\hat{z}$ and undetermined functions of position $\hat{u}_{ik}(\hat{x},\hat{y})$ in the reference surface $(\hat{z}=0)$:

$$\hat{u}_i \;=\; \sum_{k=0}^{n_i} \hat{u}_{ik}(\hat{x},\hat{y})\;\hat{z}^k, \qquad i=1,2,3 \tag{4.6}$$

where n_i are the number of terms in the expansion. Such an approach is termed the method of power series expansion in $\hat{z}$. In unabridged notation,

$$\begin{aligned}
\hat{u} &= \sum_{k=0}^{n_1} \hat{u}_k(\hat{x},\hat{y})\;\hat{z}^k \\
\hat{v} &= \sum_{k=0}^{n_2} \hat{v}_k(\hat{x},\hat{y})\;\hat{z}^k \\
\hat{w} &= \sum_{k=0}^{n_3} \hat{w}_k(\hat{x},\hat{y})\;\hat{z}^k
\end{aligned} \tag{4.7}$$

where $\hat{u}_k$, $\hat{v}_k$ and $\hat{w}_k$ are spatial functions with proper dimensions. Retaining only the first few terms in the above series has showed a remarkable improvement to the solutions for plate problems where corrections to the classical Kirchhoff-Love plate assumptions are sought after. Such improvements have been demonstrated in the vast literature on thick plate theories with shear deformations [8, 54, 65, 76, 81, 92], to mention a few. Here, we only retain the first and second terms in $\hat{u}$ and $\hat{v}$, and only the first term in $\hat{w}$. These terms constitute what is referred to in the literature as First-Order Shear Deformation Theory (FOSDT). Hence, the resulting displacement fields are:

$$\hat{u} = \hat{u}_0(\hat{x},\hat{y}) \;+\; \hat{u}_1(\hat{x},\hat{y})\;\hat{z}$$

$$\hat{v} = \hat{v}_0(\hat{x}, \hat{y}) \; + \; \hat{v}_1(\hat{x}, \hat{y}) \; \hat{z} \tag{4.8}$$

$$\hat{w} = \hat{w}_0(\hat{x}, \hat{y})$$

where

$\hat{u}_0, \hat{v}_0$ and $\hat{w}_0$ ..... mid-surface (reference surface) displacement fields

$\hat{u}_1$ and $\hat{v}_1$ ..... out-of-plane cross-sectional rotation functions.

The form in (4.8) is due to Reissner [78, 79] who was the first to provide a consistent theory which incorporates the effect of shear deformation. Unlike Reissner's derivation which was stress-based, Mindlin [58] employed kinematic assumptions of the form (4.8) to derive his displacement-based governing equations. Hence, the theory based on the latter is often referred to as the Mindlin plate theory. First-order shear deformation theories are based on linear displacement and/or stress variations through the plate and are extensions of the Reissner-Bollé-Mindlin type theories.

Equations (4.8) can be cast in a more convenient form that is more suited for computational purposes by subtracting from $\hat{u}_1$ and $\hat{v}_1$ the corresponding classical Kirchhoff-Love rotation terms, $\hat{w}_{0,\hat{x}}$ and $\hat{w}_{0,\hat{y}}$. Such a form is as follows[5]:

$$\hat{u} = \hat{u}_0 \; + \; (\hat{u}_1 - \hat{w}_{0,\hat{x}}) \, \hat{z}$$

$$\hat{v} = \hat{v}_0 \; + \; (\hat{v}_1 - \hat{w}_{0,\hat{y}}) \, \hat{z} \tag{4.9}$$

$$\hat{w} = \hat{w}_0$$

where $\hat{u}_0$, $\hat{u}_1$, $\hat{v}_0$, $\hat{v}_1$ and $\hat{w}_0$ are all functions of $\hat{x}$ and $\hat{y}$. By casting the equations into this form the case of the classical Kirchhoff-Love plate theory (no shear deformations)

[5]Although, strictly speaking, different notation for $\hat{u}_1$ and $\hat{v}_1$ is warranted, the meaning and implication of the new form is obvious.

can be recovered just by setting $\hat{u}_1 = \hat{v}_1 = 0$. Note that using the form (4.9) implies that the functions $\hat{u}_1$ and $\hat{v}_1$ are the shear rotations *in addition* to the usual flexural rotations $\hat{w}_{0,\hat{x}}$ and $\hat{w}_{0,\hat{y}}$.

Substituting (4.9) into (4.5) the final strain-displacement relationships can be obtained in terms of the five unknown displacement functions $\hat{u}_0, \hat{u}_1, \hat{v}_0, \hat{v}_1$, and $\hat{w}_0$. Using unabridged notation, the explicit expressions for these strains are as follows:

$$\begin{aligned}
E_{\hat{x}\hat{x}} &= \epsilon_{\hat{x}\hat{x}} + \kappa_{\hat{x}\hat{x}}\,\hat{z} \\
E_{\hat{y}\hat{y}} &= \epsilon_{\hat{y}\hat{y}} + \kappa_{\hat{y}\hat{y}}\,\hat{z} \\
E_{\hat{z}\hat{z}} &= 0 \\
E_{\hat{x}\hat{y}} &= \epsilon_{\hat{x}\hat{y}} + \kappa_{\hat{x}\hat{y}}\,\hat{z} \\
E_{\hat{x}\hat{z}} &= \epsilon_{\hat{x}\hat{z}} \\
E_{\hat{y}\hat{z}} &= \epsilon_{\hat{y}\hat{z}}
\end{aligned} \tag{4.10}$$

where ϵ_{ij} are inplane strains and κ_{ij} are out-of-plane curvatures and are given by the following expressions:

$$\begin{aligned}
\epsilon_{\hat{x}\hat{x}} &= \hat{u}_{0,\hat{x}} + \frac{1}{2}\hat{w}_{0,\hat{x}}^2 + \bar{\hat{w}}_{,\hat{x}}\hat{w}_{0,\hat{x}} \\
\epsilon_{\hat{y}\hat{y}} &= \hat{v}_{0,\hat{y}} + \frac{1}{2}\hat{w}_{0,\hat{y}}^2 + \bar{\hat{w}}_{,\hat{y}}\hat{w}_{0,\hat{y}} \\
\epsilon_{\hat{x}\hat{y}} &= \frac{1}{2}\left(\hat{u}_{0,\hat{y}} + \hat{v}_{0,\hat{x}} + \hat{w}_{0,\hat{x}}\hat{w}_{0,\hat{y}} + \bar{\hat{w}}_{,\hat{x}}\hat{w}_{0,\hat{y}} + \bar{\hat{w}}_{,\hat{y}}\hat{w}_{0,\hat{x}}\right) \\
\epsilon_{\hat{x}\hat{z}} &= \hat{u}_1 \\
\epsilon_{\hat{y}\hat{z}} &= \hat{v}_1
\end{aligned} \tag{4.11}$$

and

$$\kappa_{\hat{x}\hat{x}} = \hat{u}_{1,\hat{x}} - \hat{w}_{0,\hat{x}\hat{x}}$$

$$\kappa_{\hat{y}\hat{y}} = \hat{v}_{1,\hat{y}} - \hat{w}_{0,\hat{y}\hat{y}} \tag{4.12}$$

$$\kappa_{\hat{x}\hat{y}} = \hat{u}_{1,\hat{y}} + \hat{v}_{1,\hat{x}} - 2\hat{w}_{0,\hat{x}\hat{y}}$$

The next step will be to introduce the plate's constitutive relationships relating stresses to strains.

4.3 Plate Constitutive Relationships

The modeled plate will be assumed to be made up of materials exhibiting simple constitutive laws. These laws correspond to material behavior which is isothermal or adiabatic and is in the range of relatively small strain. Corresponding to the total strain tensor **E**, we have Kirchhoff's stress tensor **S** (also referred to sometimes as 2^{nd} Piola-Kirchhoff stress tensor), which can be used in the Lagrangian description. The tensor equation relating them is the generalized Hooke's law which may be written in component form as

$$S_{ij} = L_{ijkl}E_{kl} \tag{4.13}$$

where $i, j, k, l = 1, 2, 3$ and L_{ijkl} is the $ijkl$ component of the elastic modulus fourth-order tensor **L**. Equation (4.13) is the most general linear constitutive relationship[6]. Using contracted notation, (4.13) can be expressed as follows:

$$S_i = C_{ij}E_j \tag{4.14}$$

[6]When thermal effects are included, such a relationship is called the Duhamel-Neumann form of Hooke's Law.

where $i, j = 1, 2, \ldots, 6$ and C_{ij} is the ij component of the elastic modulus in contracted notation. Since the main focus of this study is on the behavior of thin plates, a state of plane stress is assumed to exist. Such a state is accounted for in the C_{ij} values resulting in what is referred to as the plane stress elastic modulus $\bar{C}_{ij}$. Note that, in general, $\bar{C}_{ij} \geq C_{ij}$, i.e., the plane stress condition results in a higher apparent elastic modulus[7].

One thing to note is that the assumption of plane stress is not inconsistent with FOSDT. Considering the terms in (4.8) (or 4.9) as the first terms in a power series expansion in $\hat{z}$, it is seen that the classical theory and the shear deformation theory are of the same order of approximation. The classical theory is merely a special case of the shear deformation theory, wherein the shear modulus in terms associated with the transverse shear deformation is taken to be very large, such that transverse shear deformation can be neglected.

In case of laminates, every lamina (ply) will have different principal directions that do not coincide with the global coordinate directions. In general, a ply is a thin layer with orthotropic properties in two principle directions that are oriented at an angle θ with respect to the global coordinate axes. In order to account for such orientations, the plane-stress elastic modulus tensor $\bar{C}_{ij}$ can be transformed into the global coordinate system resulting in the transformed modulus tensor $\bar{C}^T_{ij}$ through the following operation:

$$\bar{C}^T_{ij} = \mathcal{T}(\bar{C}_{ij}, \theta) \tag{4.15}$$

where $\mathcal{T}$ is a fourth-order tensor-transformation operator. Having defined $\bar{C}^T_{ij}$ it

[7]In the case where any of the Poisson's ratios ν_{ij} is negative, such a generalization may not hold true.

is warranted at this point to introduce the averaged material properties defined in Classical Plate Theory. These averaged properties are:

$$\begin{aligned}
\hat{A}_{ij} &= \int_{-\frac{h}{2}}^{\frac{h}{2}} \bar{C}_{ij}^{T}\, d\hat{z} \\
\hat{B}_{ij} &= \int_{-\frac{h}{2}}^{\frac{h}{2}} \bar{C}_{ij}^{T}\, \hat{z}\, d\hat{z} \\
\hat{D}_{ij} &= \int_{-\frac{h}{2}}^{\frac{h}{2}} \bar{C}_{ij}^{T}\, \hat{z}^2\, d\hat{z}
\end{aligned} \tag{4.16}$$

where $\hat{A}_{ij}$ are the inplane extensional stiffnesses, $\hat{B}_{ij}$ are the extensional-bending coupling stiffnesses and $\hat{D}_{ij}$ are the bending stiffnesses.

A more convenient form of representing the constitutive relationships is via the introduction of plate resultants. Such a form will relate the resultant forces ($\hat{N}_{ij}$) and resultant moments ($\hat{M}_{ij}$), stiffnesses ($\hat{A}_{ij}$, $\hat{B}_{ij}$, $\hat{D}_{ij}$) as well as strains (ϵ_{ij}) and curvatures (κ_{ij}). The resultants $\hat{N}_{ij}$ and $\hat{M}_{ij}$ are defined as follows:

$$\hat{N}_{ij} = \int_{-\frac{h}{2}}^{\frac{h}{2}} S_{ij}\, d\hat{z} \tag{4.17}$$

$$\hat{M}_{ij} = \int_{-\frac{h}{2}}^{\frac{h}{2}} S_{ij}\, \hat{z}\, d\hat{z} \tag{4.18}$$

With proper notation and transformation integrating (4.14) results in the following plate constitutive relationships that are given in matrix form[8]:

$$\hat{\mathbf{N}} = \hat{\mathbf{A}}\, \epsilon + \hat{\mathbf{B}}\, \kappa \tag{4.19}$$

and

$$\hat{\mathbf{M}} = \hat{\mathbf{B}}\, \epsilon + \hat{\mathbf{D}}\, \kappa \tag{4.20}$$

[8]The expansion of this form follows the standard convention found in any book on the subject (e.g., [24]).

4.4 Interphase Kinematic Relationships

The interface will be modeled as an elastic layer with finite thickness. Although the elastic layer is a continuum, computationally it will be modeled as a bed of elastic one-dimensional elements (axial rods). The reason behind using the term "rods" instead of "springs" to describe the modeling stems from the fact that a mathematical spring has no length scale associated with it. Hence, using the terms "thickness" along with "springs" to characterize the layer's finite thickness (Figure 4.1(a)) can add some confusion to the overall mechanical and mathematical discussions to follow.

Each rod can only transfer an axial force which depends on the general kinematic relationships describing the deformation of the rod (Figure 4.1(b)). Such relationships can be derived as follows:

Let

- "O" be a fixed (restrained) reference point in the Eucledian space,
- "A" be the initial position of the rod's unrestrained end,
- "B" be the final position of the rod's unrestrained end,

where the *unrestrained end* means the end that is connected to the plate's lower surface ($\hat{z} = -\frac{h}{2}$). In Figure 4.1(b) L_A is the length of the rod connecting points O and A, L_B is the length of the rod connecting points O and B, $\hat{u}_A$, $\hat{v}_A$ and $\hat{w}_A$ are the coordinates of point A, and $\hat{u}_B$, $\hat{v}_B$ and $\hat{w}_B$ are the coordinates of point B. For any rod, and without loss of generality, the coordinates of point O can be chosen to be the "local origin", hence, point O is always at $(0, 0, 0)$. The lengths of a generic rod is simply

$$L_A = \sqrt{\hat{u}_A^2 + \hat{v}_A^2 + \hat{w}_A^2} \tag{4.21}$$

$$L_B = \sqrt{\hat{u}_B^2 + \hat{v}_B^2 + \hat{w}_B^2} \tag{4.22}$$

Further, the change in length $\hat{\Delta}$, which is a scalar quantity, is simply

$$\hat{\Delta} = L_B - L_A \tag{4.23}$$

It is warranted at this stage to relate the kinematics of the rod to that of the plate. To ensure compatibility between the plate and the elastic layer (rods)[9], the deformation of the rods must match that of the plate's *lower* surface ($\hat{z} = -\frac{h}{2}$) at the particular point of interest (in general, such a point is an integration point). The reasons for specifying the lower surface as opposed to the plate's middle surface are: although the plate is a "thin" structure, it has a finite thickness, and that for small deformation (small rotation) formulation such a distinction (i.e., lower vs. middle surfaces) is transparent, for thick plates undergoing moderately large deformations it is not so. For the latter, the plate's rotations become large enough to contribute significantly to the rod's axial deformation, and hence, force. Such a reasoning is also consistent with the physical situation where the elastic layer is bonded to the lower surface rather than to the middle surface. Figure 4.2 shows clearly that connecting the rod to the middle surface of the plate (Figure 4.2(a)) is significantly different from connecting it to the lower surface (Figure 4.2(b)). For simplicity, let us consider the case where only out-of-plane deformations ($\hat{w}$) are accounted for. In this case, and as can be seen in Figure 4.2(a), the rotation of the cross-section does not contribute to

[9]In regions where the plate and the rods are connected (bonded) such a compatibility is enforced prior to failure (debonding, decohesion), otherwise it is not.

the stretching of the rod and only the (vertical) w-displacement does. The situation in Figure 4.2(b) is physically more accurate where both w-displacement and cross-sectional rotation contribute to the axial stretching of the rod. A schematic showing the general 3-D deformation of a differential-volume plate element as well as the interphase "rod" model that is connected to the plate's lower surface is shown in Figure 4.3.

To relate the notation in Figure 4.1(b) to that of Figure 4.3 the following notation is introduced:

$$\hat{\Delta}_o = L_B$$

$$\bar{\hat{\Delta}} = L_A$$

Combining the above equations with (4.23) results in

$$\hat{\Delta} = \hat{\Delta}_o - \bar{\hat{\Delta}} \tag{4.24}$$

Recalling that the deformation of any material point in/on the plate can be expressed in terms of the displacement fields $\hat{u}$, $\hat{v}$ and $\hat{w}$ as well as the initial imperfection (reference state) fields $\bar{\hat{u}}$, $\bar{\hat{v}}$ and $\bar{\hat{w}}$, the kinematics of a deforming rod can be expressed in terms of these fields as follows:

$$\hat{\Delta}_o = \sqrt{(\hat{u}_- + \bar{\hat{u}}_-)^2 + (\hat{v}_- + \bar{\hat{v}}_-)^2 + (\hat{w}_- + \bar{\hat{w}}_- + \hat{t})^2} \tag{4.25}$$

and

$$\bar{\hat{\Delta}} = \sqrt{(\bar{\hat{u}}_-)^2 + (\bar{\hat{v}}_-)^2 + (\bar{\hat{w}}_- + \hat{t})^2} \tag{4.26}$$

where the subscript "-" denotes that such quantities are evaluated at the plate's lower surface ($\hat{z} = -\frac{h}{2}$) and $\hat{t}$ is the thickness of the elastic layer (original lengths of the rods in the $\hat{z}$-direction). Employing the assumption (stated earlier) that inplane imperfections are not present yields;

$$\hat{\Delta}_o = \sqrt{(\hat{u}_-)^2 + (\hat{v}_-)^2 + (\hat{w}_- + \bar{\hat{w}}_- + \hat{t})^2} \tag{4.27}$$

and

$$\begin{aligned} \bar{\hat{\Delta}} &= \sqrt{(\bar{\hat{w}}_- + \hat{t})^2} \\ &= \bar{\hat{w}}_- + \hat{t} \end{aligned} \tag{4.28}$$

where it is implicit that $|\min \bar{\hat{w}}_-| \leq \hat{t}$, which leads to $\bar{\hat{\Delta}} \geq 0$. But based on physical grounds, $\bar{\hat{\Delta}} > 0$. Expressing $\hat{u}_-$, $\hat{v}_-$, and $\hat{w}_-$ interms of the displacement fields in (4.9) yields;

$$\begin{aligned} \hat{u}_- &= \hat{u}(\hat{z} = -\frac{h}{2}) \\ &= \hat{u}_0 + \frac{h}{2}(\hat{w}_{0,\hat{x}} - \hat{u}_1) \\ \hat{v}_- &= \hat{v}(\hat{z} = -\frac{h}{2}) \\ &= \hat{v}_0 + \frac{h}{2}(\hat{w}_{0,\hat{y}} - \hat{v}_1) \\ \hat{w}_- &= \hat{w}(\hat{z} = -\frac{h}{2}) \\ &= \hat{w}_0 \end{aligned} \tag{4.29}$$

Substituting (4.29) into (4.27) along with using assumption 2 yields;

$$\hat{\Delta}_o = \sqrt{\left(\hat{u}_0 + \frac{h}{2}(\hat{w}_{0,\hat{x}} - \hat{u}_1)\right)^2 + \left(\hat{v}_0 + \frac{h}{2}(\hat{w}_{0,\hat{y}} - \hat{v}_1)\right)^2 + \left(\hat{w}_0 + \bar{\hat{w}} + \hat{t}\right)^2} \tag{4.30}$$

and

$$\bar{\hat{\Delta}} = \bar{\hat{w}} + \hat{t} \tag{4.31}$$

Substituting the above results into (4.24) yields;

$$\hat{\Delta} = \sqrt{\left(\hat{u}_0 + \frac{h}{2}\left(\hat{w}_{0,\hat{x}} - \hat{u}_1\right)\right)^2 + \left(\hat{v}_0 + \frac{h}{2}\left(\hat{w}_{0,\hat{y}} - \hat{v}_1\right)\right)^2 + \left(\hat{w}_0 + \bar{\hat{w}} + \hat{t}\right)^2} - \left(\bar{\hat{w}} + \hat{t}\right) \tag{4.32}$$

The $\hat{\Delta}$ expression in (4.32) is valid for all physically admissible deformations and it describes the deformation of a point common to the plate and the interphase. Further, from physical considerations, the following inequality must always be satisfied:

$$\hat{w}_0 + \bar{\hat{w}} + \hat{t} \geq 0 \tag{4.33}$$

which is equivalent to

$$\hat{w}_0 \geq -\left(\bar{\hat{w}} + \hat{t}\right) \tag{4.34}$$

where the thickness $\hat{t} > 0$. It is very important to point out that $\hat{w}_0 < -\left(\bar{\hat{w}} + \hat{t}\right)$ is not a valid range since it implies that the elastic layer is penetrating into the "rigid" supporting reference surface. Further, the bound (4.34) holds true for all values of $\hat{u}_-$ and $\hat{v}_-$. This can be seen in Figures 4.4-4.6 which show general plots of $\hat{\Delta}$ vs. $\hat{w}_-$ for different values of $\hat{u}_-^2 + \hat{v}_-^2$ and $\bar{\hat{\Delta}}$. When $\hat{u}_-^2 + \hat{v}_-^2 = 0.0$ the relation between $\hat{\Delta}$ and $\hat{w}_-$ is linear for all values of $\bar{\hat{\Delta}}$. For larger values of $\hat{u}_-^2 + \hat{v}_-^2$ such a relationship ceases to be linear especially for $\hat{w}_-$ close to $-\bar{\hat{\Delta}}$. In these figures, the "region of validity" is the region in which such a relationship yields physically admissible values (no interpenetration). In summary, (4.32) is always valid as a general displacement

of a rod attached to the lower surface of a deforming plate as long as $\hat{w}_0$ satisfies the inequality (4.34).

Another point that warrants clarification is the inclusion of the out-of-plane imperfection field $\bar{\hat{w}}$ in the $\hat{\Delta}$ expression. Physically, and generally speaking, the thickness of the layer is $\hat{t}_l = f(\hat{x}, \hat{y})$ where f is a smooth and continuous function, and the subscript l denotes "layer". $f(\hat{x}, \hat{y})$, which is always > 0, can be written as follows:

$$\hat{t}_l = \hat{t} + g(\hat{x}, \hat{y}), \qquad \hat{t}_l > 0 \tag{4.35}$$

where $\hat{t}$ is a constant and $g(\hat{x}, \hat{y})$ is another smooth and continuous function. Hence, one can always choose the elastic layer's thickness variation $g(\hat{x}, \hat{y})$ to be identical to the plate's imperfection field $\bar{\hat{w}}(\hat{x}, \hat{y})$. Such a choice happens to be a very convenient one.

It is important to make a clear distinction between the two physical quantities, namely, the elastic layer's thickness variation $g(\hat{x}, \hat{y})$ and the distribution (if any) of the initially debonded regions. While the former is a continuous analytic function specified a priori for the case being investigated, the latter is discrete and need not be specified (if any) prior to the loading/deformation process. Debonded regions can be accounted for in the interface constitutive relationship(s) to be presented subsequently.

4.5 Nondimesionalization of Variables

It is convenient at this stage to nondimensionalize all the variables involved in the formulation. Let

$$x = \frac{\hat{x}}{b},\ y = \frac{\hat{y}}{b},\ z = \frac{\hat{z}}{h} \tag{4.36}$$

where b is the width (in the y-direction) of the global rectangular plate and h is the plate's (delamination's) thickness. Further, the deformation fields can be nondimensionalized as follows:

$$u_0 = \frac{\hat{u}_0 b}{h^2},\ v_0 = \frac{\hat{v}_0 b}{h^2},\ w_0 = \frac{\hat{w}_0}{h} \tag{4.37}$$

and

$$u_1 = \frac{\hat{u}_1 b}{h},\ v_1 = \frac{\hat{v}_1 b}{h},\ \bar{w} = \frac{\bar{\hat{w}}}{h} \tag{4.38}$$

The plate's constitutive properties can be nondimensionalized as follows:

$$A_{ij} = \frac{\hat{A}_{ij} h^2}{\hat{D}_{11}},\ B_{ij} = \frac{\hat{B}_{ij} h}{\hat{D}_{11}},\ D_{ij} = \frac{\hat{D}_{ij}}{\hat{D}_{11}} \tag{4.39}$$

Before proceeding to the next step it is convenient to define the following geometrical parameters:

$$\xi = \frac{a}{b},\ \zeta = \frac{h}{b} \tag{4.40}$$

where ξ is the aspect ratio of the global rectangular plate containing the delamination and ζ is the thinness parameter which is a measure of the slenderness of the plate.

Having defined the nondimensional constitutive properties the next logical step will be to express the constitutive relationships (equations (4.19) and (4.20)) in their

nondimensional form. In order to do that, strains and curvatures must be expressed nondimensionally in terms of the nondimensional deformation fields. Employing (4.36), (4.37), (4.38) and (4.40) yields;

$$\begin{aligned}
\epsilon_{xx} &= \zeta^2 \left(u_{0,x} + \frac{1}{2} w_{0,x}^2 + \bar{w}_{,x} w_{0,x} \right) \\
\epsilon_{yy} &= \zeta^2 \left(v_{0,y} + \frac{1}{2} w_{0,y}^2 + \bar{w}_{,y} w_{0,y} \right) \\
\epsilon_{xy} &= \frac{1}{2} \zeta^2 \left(u_{0,y} + v_{0,x} + w_{0,x} w_{0,y} + \bar{w}_{,x} w_{0,y} + \bar{w}_{,y} w_{0,x} \right) \\
\epsilon_{xz} &= \zeta u_1 \\
\epsilon_{yz} &= \zeta v_1
\end{aligned} \tag{4.41}$$

and

$$\begin{aligned}
\kappa_{xx}^* &= \frac{1}{h} \kappa_{xx} \\
\kappa_{yy}^* &= \frac{1}{h} \kappa_{yy} \\
\kappa_{xy}^* &= \frac{1}{h} \kappa_{xy}
\end{aligned} \tag{4.42}$$

where

$$\begin{aligned}
\kappa_{xx} &= \zeta^2 \left(u_{1,x} - w_{0,xx} \right) \\
\kappa_{yy} &= \zeta^2 \left(v_{1,y} - w_{0,yy} \right) \\
\kappa_{xy} &= \zeta^2 \left(u_{1,y} + v_{1,x} - 2 w_{0,xy} \right)
\end{aligned} \tag{4.43}$$

The $\frac{1}{h}$ factor in (4.42) is introduced for consistency and clarity. Further, we can define the following nondimensional resultant forces and moments as follows:

$$N_{ij} = \frac{\hat{N}_{ij}h^2}{\hat{D}_{11}},\ M_{ij} = \frac{\hat{M}_{ij}h}{\hat{D}_{11}} \tag{4.44}$$

The above forms for ϵ_{ij} κ_{ij} as well as N_{ij} M_{ij} can be substituted in (4.19) and (4.20) to yield;

$$\mathbf{N} = \mathbf{A}\,\epsilon + \mathbf{B}\,\kappa \tag{4.45}$$

and

$$\mathbf{M} = \mathbf{B}\,\epsilon + \mathbf{D}\,\kappa \tag{4.46}$$

Using the nondimensionalizations presented thus far the generalized displacement quantities $\hat{\Delta}_o$ and $\bar{\hat{\Delta}}$ can be normalized as follows:

$$\Delta_o = \frac{\hat{\Delta}_o}{h},\ \Delta = \frac{\hat{\Delta}}{h},\ \bar{\Delta} = \frac{\bar{\hat{\Delta}}}{h} \tag{4.47}$$

and when expressed in terms of the displacement fields,

$$\Delta_o = \sqrt{\zeta^2\left[\left(u_0 + \frac{1}{2}\left(w_{0,x} - u_1\right)\right)^2 + \left(v_0 + \frac{1}{2}\left(w_{0,y} - v_1\right)\right)^2\right] + \left(w_0 + \bar{w} + t\right)^2} \tag{4.48}$$

$$\bar{\Delta} = \bar{w} + t \tag{4.49}$$

and

$$\Delta = \Delta_o - \bar{\Delta} \tag{4.50}$$

where $t = \dfrac{\hat{t}}{h}$.

Finally, the following nondimensionalizations are introduced:

$$\begin{aligned} \lambda &= \frac{P_x^a b^2}{\pi^2 \hat{D}_{11}} \\ Q &= \frac{q b^4}{h \hat{D}_{11}} \\ \eta_{x0} &= \frac{P_x^0}{P_x^a} \\ \eta_{y0} &= \frac{P_y^0}{P_x^a} \\ \eta_{y1} &= \frac{P_y^b}{P_x^a} \end{aligned} \tag{4.51}$$

where P_x^a, P_x^0, P_y^0 and P_y^b are the applied edge (boundary) distributed loads (See Figure 4.11). Q is the nondimensional transverse load. η_{x0}, η_{y0} and η_{y1} are loading ratios. λ is the applied reference edge load (at $x = \xi$). For displacement-controlled situations the parameter λ is no longer a load parameter. In such situations, λ becomes displacement quantity that is equal to the applied edge (inplane) displacement at $(x = \xi)$ and is normalized similar to u_0.

4.6 Interphase Constitutive Relationships

A general representation of a constitutive relationship that relates a generalized force to a generalized displacement in a nonlinear *elastic* material can be given in the following nondimensional form:

$$F \;=\; \alpha \; \Delta \; \Psi(\Delta) \tag{4.52}$$

where

F ..... nondimensional generalized force

α ..... nondimensional constant (material dependent)

Δ ..... nondimensional generalized displacement

$\Psi(\Delta)$ ..... a nondimensional functional that characterizes the nonlinearity.

For a general nonlinear material Ψ can have different forms depending on the type of nonlinearity of the material being modeled. For this study, the interphase constitutive model will be assumed to exhibit certain characteristics in order to capture some of the main features of the decohesion process of unilaterally constrained plates. Such characteristics are:

- Elastic tension softening
- Elastic compression stiffening
- Softening and stiffening do not influence each other
- Compression stiffness increases to "infinity" simulating the presence of a rigid substrate
- Loss of tensile stiffness does not degrade the compressive stiffness
- Dependence of the force-displacement relationship on the interphase thickness

In addition, the model should depend on the least number of constitutive parameters in its description of the entire behavior. Although the latter in not a requirement, it is a desirable characteristic for any model.

4.6.1 Proposed Constitutive Model

For this study, the relationship between the force (F) and the separation across the interphase layer (Δ) is chosen to have an exponential form. Such a choice is

motivated by the fact that the atomistic calculations reported in the literature that suggest a universal form for the binding energy of metallic and bi-metallic interfaces, which, at least for the case of purely normal separation, can be fit by an exponential expression. This exponential representation for the force-displacement relationship is the basis for the interphase constitutive description used in this study. There is a variety of constitutive models that exhibit all of the above listed characteristics and can be expressed in an exponential form. One such model is the following:

$$\Psi = \frac{1}{\Delta + \bar{\Delta}} e^{-\left(\beta \frac{\Delta}{\bar{\Delta}}\right)} \tag{4.53}$$

Substituting (4.53) into (4.52) yields;

$$F = \alpha \frac{\Delta}{\Delta + \bar{\Delta}} e^{-\left(\beta \frac{\Delta}{\bar{\Delta}}\right)} \tag{4.54}$$

4.6.2 Characteristics of the Proposed Model

The proposed constitutive model exhibits all of the characteristics outlined above. It is history-independent. It has a tension softening as well as a compression stiffening regions, and it depends on the thickness of the interphase layer through $\bar{\Delta}$. Figure 4.7 shows a schematic of two force-displacement relationships, one for a "thin" interphase layer and the other for a thicker one which displays a more "ductile" behavior. Figure 4.8 shows plots of force (F) vs. displacement (Δ) for different values of $\bar{\Delta}$ (recall that $\bar{\Delta}$ includes the original constant thickness of the interphase layer t). Figures 4.7 and 4.8 show identical trends, as expected. Figure 4.9 shows another important property that the model exhibits. The parameter β controls the decay as well as the location of the peak. Increasing β tends to shift the peak of the $F - \Delta$ curve towards the origin. A simple limiting analysis shows that:

$$\lim_{\beta \to \infty} F = \begin{cases} \infty\,, & \Delta < 0 \\ 0\,, & \Delta \geq 0 \end{cases} \tag{4.55}$$

which implies that as $\beta \to \infty$ the interphase constitutive properties approach that of a perfectly rigid and tensionless surface (a unilateral rigid constraint). The peak values for the constitutive relationship (4.54) occur in the tensile region, and are given by the following relationships:

$$\Delta_{peak} = \frac{\bar{\Delta}}{2}(\beta^* - 1) \tag{4.56}$$

and the corresponding force (F_{peak}) is given by:

$$F_{peak} = \alpha \left(\frac{\beta^* - 1}{\beta^* + 1}\right) e^{-\frac{\beta}{2}(\beta^* - 1)} \tag{4.57}$$

where

$$\beta^* = \sqrt{1 + \frac{4}{\beta}} \tag{4.58}$$

In all of the analysis performed, and cases studied, the factor that determines decohesion, i.e., failure of the rod, was displacement based. In other words, the rod fails (becomes tensionless) when the net displacement is greater than or equal a prespecified quantity. The latter criterion can be expressed as follows:

if $\Delta \geq \Gamma \Delta_{peak}$

then rod looses tensile stiffness

where Γ is a multiplier specified a priori which signifies the onset of failure when the displacement exceeds the peak displacement (Δ_{peak}). For all of the analysis performed, Γ was specified to be

$$\Gamma \geq 1.0 \tag{4.59}$$

implying that failure occurs when the displacement reaches or exceeds Δ_{peak}. $\Gamma = 2$ was found to be a reasonable value yielding consistent results (to be presented in Chapter V). Note that failure in this context always refers to the loss of tensile stiffness. The compressive stiffness is never altered nor degraded. This is of course a first order elastic approximation to the behavior of real materials in which plasticity is always involved to some degree, and once present, it influences both tensile and compressive properties.

It should be emphasized that up to this point, all the numerical factors, e.g., α, β and Γ, are based on numerical "suitability" rather than on any experimentally determined properties[10]. The reason for that was given in the introductory chapter where it was mentioned that these types of interphase constitutive models, which are used to model interfaces, have a major drawback that manifests itself in the difficulty of identifying model parameters. Such a difficulty is attributed to the fact that experiments cannot be directly done on the interface. Hence, indirect information must be derived from tests. For these reasons, numerical convergence and stability were the two main criteria in selecting the values for such factors.

[10]A detailed discussion as to how the interphase constitutive model can be related to the interphase measured mechanical properties can be found in the work of Song and Waas [89] and the references listed therein.

4.7 Some Computational Aspects of Decohesion

Figure 4.10 shows a schematic of a typical force-displacement curve along with key points. Point "×" designates a pre-specified failure point (being displacement or force). This failure point can be located anywhere along the curve and need not be on the ascending branch[11]. The entire computational process is divided into steps, and each step is divided into many sub-iterations. At a particular step, and for a particular sub-iteration i the value of Δ (and hence F) varies from one integration point to another. Such a variation is governed by the equilibrium equations governing the behavior of the entire plate-interphase system. At such an integration point (recall that the interphase is composed of a bed of rods, each rod is located at an integration point) the displacement of the interphase rod which is designated by (Δ_i) can change its value depending on the solver's convergence at sub-iteration i. If further sub-iterations are needed to attain convergence then the value of Δ_i will attain a new value Δ_{i+1} (at this particular integration point). Since Δ_{i+1} can be located to the right or to the left of Δ_i on the $F-\Delta$ curve, the following two designations will be given: Δ^f_{i+1} and Δ^b_{i+1} (see Figure 4.10), where "f" for forward and "b" for backward. If $\Delta^f_{i+1} \geq \Delta_{failure}$ ($\Delta_{failure}$ is the point designated by "×", beyond which the local tensile stress vanishes permanently) then decohesion (rod becomes tensionless) takes place at sub-iteration $i+2$. In other words, the rod fails in the next sub-iteration if convergence was not attained in the current sub-iteration (all within the same step). The reason for that is because within a sub-iteration convergence implies satisfaction of the equilibrium equations, and allowing loss of tensile stiffness to occur within an non-converged sub-iteration leads to numerical instability which leads the solver to either diverge or converge to physically inadmissible results (the

[11] Ascending branch is the region on the $F-\Delta$ where the slope is positive.

former is the more common situation). On the other hand, allowing separation to occur at subsequent sub-iterations (e.g., $i+3$ or $i+4$) might lead, in some cases, to convergence without failure within the current step. This implies that the unfailed rod can sustain tensile loads in the subsequent step leading to over stiffening of the entire behavior of the system. The latter situation, although uncommon in most of the cases considered, is worth considering in such numerical simulation since it can control the entire behavior of the system leading to divergence at subsequent steps. The above computational issues are not unique to the proposed model. They arise in many nonlinear analysis where failure or separation is to be predicted using an iterative scheme.

4.8 Virtual Work Formulation

Variational formulation will be adopted for the derivation of the governing differential equations and their corresponding boundary conditions. Some of the most powerful methods suited for such derivation are those based on the Principle of Virtual Work (PVW), which is a principle[12] with a great deal of versatility. In its simplest yet most general form the principle is expressed as follows:

$$\delta W_{external} = \delta W_{internal} \tag{4.60}$$

where $\delta W_{external}$ is the virtual work done by the *external actions* and $\delta W_{internal}$ is the virtual work done by the *internal actions.* Satisfaction of the PVW is both *necessary* and *sufficient* for equilibrium. In what follows we will adopt a formulation in which deformations are the virtual quantities. Such a formulation, as the name

[12]The French mathematician Henri Poincaré once said: "A principle is neither true nor false, it is convenient."

indicates, is sometimes referred to as the Principle of Virtual Displacements. It should be clarified at this point that the terms external and internal refer to the plate-foundation system and not the plate alone. Hence, the foundation's contribution is included in $\delta W_{internal}$ rather than $\delta W_{external}$. In the absence of body forces (forces per unit volume) equation (4.60) can be expressed as

$$\int\int_a t_i \, \delta u_i \, da \; = \; \int\int\int_v \sigma_{ij} \, \delta \varepsilon_{ij} \, dv \tag{4.61}$$

where t_i are the components of the surface force vector per unit deformed area, a is the current deformed surface area of the body, δu_i are the compatible fields of virtual displacements, $\delta \varepsilon_{ij}$ are the corresponding compatible fields of virtual strains, σ_{ij} are the components of the Cauchy (Euler, true) stress tensor, and v is the volume of the body. The variation $\delta \varepsilon_{ij}$ is expressed as follows:

$$\delta \varepsilon_{ij} = \frac{1}{2} (\delta u_{i,j} \; + \; \delta u_{j,i}) \tag{4.62}$$

where differentiation is taken with respect to the current Cartesian coordinate of material points of the body in the deformed configuration. It is possible to express (4.61) with respect to a known reference configuration and such a transformation follows the same steps outlined in [37] resulting in

$$\int\int_A T_i \, \delta U_i \, dA \; = \; \int\int\int_V S_{ij} \, \delta E_{ij} \, dV \tag{4.63}$$

where T_i are the components of the surface force vector acting in the current configuration but measured per unit reference area, A is the surface area measured in the reference state, δU_i are the compatible field of virtual displacements, δE_{ij} are

the corresponding fields of compatible virtual strains (when the reference state is the zero-state, i.e., no initial deformations are present, E_{ij} is referred to as Green's strain tensor), S_{ij} are the components of Kirchhoff stress tensor (also referred to sometimes as 2^{nd} Piola-Kirchhoff stress tensor) acting in the current state but measured with respect to the reference state, and V is the volume of the body in the reference state. One of the main assumptions adopted while studying plates is that strains are small but not deformations, where deformations are taken to imply displacements and rotations. As such, the ratio of the current density to the initial density was taken to be unity implying that the density of the structure remains constant throughout the entire loading (deformation) process.

From (4.4) the variation δE_{ij} can be expressed as follows:

$$\delta E_{ij} = \frac{1}{2}\left(\delta u_{i,j} + \delta u_{j,i} + \delta u_{k,i}u_{k,j} + u_{k,i}\delta u_{k,j} + \bar{u}_{k,i}\delta u_{k,j} + \bar{u}_{k,j}\delta u_{k,i}\right) \quad (4.64)$$

The next step will be to evaluate $\delta W_{external}$ and $\delta W_{internal}$ separately.

4.8.1 Evaluating $\delta W_{external}$

In evaluating $\delta W_{external}$ we will distinguish two controlled environments, namely, load-controlled and displacement-controlled. Both environments are planner (in the $x-y$ plane).

Load-Controlled Environment

Figure 4.11 shows the external loading that the plate under consideration is subjected to. The inplane loads P_x^0, P_x^a, P_y^0 and P_y^b are applied at the boundary edges and at the plate's midplane ($\hat{z}=0$) in the directions shown. The transverse load q is applied at the plate's top surface ($\hat{z}=+\frac{h}{2}$)[13]. But based on the plate's "thinness",

[13]Recall that based on the nondimesionalizations presented, $\hat{z}=+\frac{h}{2} \Leftrightarrow z=+\frac{1}{2}$.

the effect of applying the load as such can be shown to be equal to applying it at the midplane ($\hat{z} = 0$). Using the notation for the displacement fields in (4.9), and using the notation u_i to represent displacement filed in the reference state[14], the expression for $\delta W_{external}$ is

$$\begin{aligned}
\delta W_{external} &= \int\int_A T_i\ \delta\hat{u}_i\ dA \\
&= \int_l T_j\ \delta\hat{u}_j(\hat{x},\hat{y},0) \int_{-\frac{h}{2}}^{\frac{h}{2}} d\hat{z}\ dl + \int_0^b\int_0^a q\ \delta\hat{w}(\hat{x},\hat{y},0)\ d\hat{x}d\hat{y} \\
&= \int_l T_j\ \delta\hat{u}_j(\hat{x},\hat{y},0)\ h\ dl + \int_0^b\int_0^a q\ \delta\hat{w}(\hat{x},\hat{y},0)\ d\hat{x}d\hat{y} \\
&= \int_l P_j^f\ \delta\hat{u}_j(\hat{x},\hat{y},0)\ dl + \int_0^b\int_0^a q\ \delta\hat{w}(\hat{x},\hat{y},0)\ d\hat{x}d\hat{y} \qquad (4.65) \\
&= \int_0^b P_x^a\ \delta\hat{u}(a,\hat{y},0)\ d\hat{y}\ -\ \int_0^b P_x^0\ \delta\hat{u}(0,\hat{y},0)\ d\hat{y}\ + \\
&\quad \int_0^a P_y^b\ \delta\hat{v}(\hat{x},b,0)\ d\hat{x}\ -\ \int_0^a P_y^0\ \delta\hat{v}(\hat{x},0,0)\ d\hat{x}\ + \\
&\quad \int_0^b\int_0^a q\ \delta\hat{w}(\hat{x},\hat{y},0)\ d\hat{x}d\hat{y}
\end{aligned}$$

where $i = 1,2,3$, $j = 1,2$ and $P_j^f = T_j\ h$. q is the out-of-plane (transverse) load. In (4.65), h is the plate's thickness (a constant throughout the formulation), l is some coordinate around the circumference (edges) of the plate, and P_j^f are applied distributed loads at the edges having units of Force/Length, where the superscript f designates the *face* that P acts on. Note that the negative signs in front of P_x^0 and P_y^0 terms are due to the fact that the face-normals point in the negative directions (i.e., on these faces, positive load and positive displacement have opposite directions). It is implicit in the derivation (4.65) that T_j are not functions of $\hat{z}$, i.e., T_j do not generate edge moments. Substituting the displacement fields in (4.9) into (4.65) yields the following final form for $\delta W_{external}$:

[14]While it is customary to use capital letters to refer to the reference state, there should be no confusion in using small notation just to be consistent with the derivations presented thus far.

$$\delta W_{external} = \int_0^b P_x^a \, \delta\hat{u}_0(a,\hat{y}) \, d\hat{y} \; - \; \int_0^b P_x^0 \, \delta\hat{u}_0(0,\hat{y}) \, d\hat{y} \; + \int_0^a P_y^b \, \delta\hat{v}_0(\hat{x},b) \, d\hat{x} \; - \; \int_0^a P_y^0 \, \delta\hat{v}_0(\hat{x},0) \, d\hat{x} \; + \int_0^b \int_0^a q \, \delta\hat{w}_0(\hat{x},\hat{y}) \, d\hat{x} d\hat{y} \tag{4.66}$$

The corresponding nondimensional expression for $\delta W_{external}$ can be given by the aid of equations (4.51). Substituting the quantities defined in (4.51) into (4.66) yields;

$$\delta W_{external} = \int_0^1 \pi^2 \lambda \, \delta u_0(a,y) \, dy \; - \; \int_0^1 \pi^2 \eta_{x0} \lambda \, \delta u_0(0,y) \, dy \; + \int_0^\xi \pi^2 \eta_{y1} \lambda \, \delta v_0(x,b) \, dx \; - \; \int_0^\xi \pi^2 \eta_{y0} \lambda \, \delta v_0(x,0) \, dx \; + \int_0^1 \int_0^\xi Q \, \delta w_0(x,y) \, dx dy \tag{4.67}$$

Note that for tensile load at $x = \xi$, $\lambda > 0$. And that when η_{x0}, η_{y1} and $\eta_{y0} > 0$ it is implied that all inplane loads around the edges have the same sign as λ.

Displacement-Controlled Environment

When the inplane edge displacement is the "loading" parameter the formulation needs to be modified to account for such a change in the controlling parameter. Throughout this work, the term "displacement-control" refers to the inplane edge displacement u_0 at $x = \xi$ ($\hat{x} = a$). All other displacements will be free to attain any finite value. For consistency, the controlling parameter in this case will be the uniform u_0 displacement at $x = \xi$, and it will designated by the same symbol λ. Hence, while **for load-control analysis, λ is the edge load, for displacement-control analysis λ is the edge displacement.**

In Chapter III the method of Galerkin was used which requires the knowledge of some admissible displacement fields in order to perform the analysis. Such admissible

fields are usually given as the sum of functions each being a kinematically admissible one. In Chapter V the analysis will be carried out using Galerkin's method and in order to account for the additional kinematic condition of having a prespecified inplane edge displacement the following form of u_0 is employed:

$$u_0(x,y) = \left(1 - \frac{x}{\xi}\right) \sum_i^M \sum_j^N A_{ij}\Phi_{ij}(x,y) - \lambda \, \frac{x}{\xi} \tag{4.68}$$

The above field can be generalized to be applicable to load-controlled as well as displacement-controlled situations by employing the following form

$$u_0(x,y) = \left(1 - c\frac{x}{\xi}\right) \sum_i^M \sum_j^N A_{ij}\Phi_{ij}(x,y) - c\,\lambda \, \frac{x}{\xi} \tag{4.69}$$

where c is an environment switching parameter that is defined as follows:

$$c = \begin{cases} 0\,, & \textit{for load control} \\ 1\,, & \textit{for displacement control} \end{cases} \tag{4.70}$$

and λ is the value of the nondimensional inplane displacement at the plate's midplane of the $x = \xi$ edge. Although λ is a control parameter in both load-controlled and displacement-controlled situations, it has a totally different physical meaning in both situations. For example, $\lambda = 4.0$ in load-control is not equivalent to $\lambda = 4.0$ in displacement-control. From (4.69) the variation of u_0 can be expressed as follows:

$$\delta u_0(x,y) = \left(1 - c\frac{x}{\xi}\right) \sum_i^M \sum_j^N (\delta A_{ij})\, \Phi_{ij}(x,y) \tag{4.71}$$

It is warranted at this stage to point out that when performing a displacement-controlled analysis, the terms that contain λ in (4.67) should be set = 0. This is

because in a displacement-controlled situation the "external" forces that are doing "external" work are the reaction forces, i.e., the terms that contain $N_{xx}\delta u_0$ and so on (see equation (4.78)).

4.8.2 Evaluating $\delta W_{internal}$

The virtual work done by the internal stresses can be thought of as the sum of the plate's contribution as well as that of the elastic foundation's (interphase). Hence, we can write

$$\delta W_{internal} = \delta W^{p}_{internal} + \delta W^{f}_{internal} \tag{4.72}$$

where the notation is self-explanatory. The expression for $\delta W^{f}_{internal}$ will be dealt with subsequently when considering the elastic foundation's contributions to the governing equations. Obtaining $\delta W^{p}_{internal}$ follows the classical steps widely presented in the solid mechanics literature. For the sake of brevity only the highlights of such steps are shown. The expression for $\delta W^{p}_{internal}$ is

$$\delta W^{p}_{internal} = \int\int\int_{V} S_{ij}\ \delta E_{ij}\ dV \tag{4.73}$$

Utilizing the symmetry of the stress and strain tensors and reverting to the unabridged notation, the expression in (4.73) becomes

$$\begin{aligned}\delta W^{p}_{internal} = \int\int\int_{V} (&S_{xx}\ \delta E_{xx} + S_{yy}\ \delta E_{yy} + S_{zz}\ \delta E_{zz} + \\ &2S_{xy}\ \delta E_{xy} + 2S_{xz}\ \delta E_{xz} + 2S_{yz}\ \delta E_{yz})\ dV\end{aligned} \tag{4.74}$$

Upon substituting the first variations of the strains (ϵ_{ij}) and curvatures (κ_{ij}) into

(4.10) and then in turns into (4.74) and utilizing the definitions of N_{ij} and M_{ij} the following general equation will be arrived at:

$$\delta W^{p}_{internal} = \int_0^1 \int_0^{\xi} (N_{xx}\,\delta\epsilon_{xx} + M_{xx}\,\delta\kappa_{xx} + N_{yy}\,\delta\epsilon_{yy} + M_{yy}\,\delta\kappa_{yy} + 2N_{xy}\,\delta\epsilon_{xy} + 2M_{xy}\,\delta\kappa_{xy} + 2N_{xz}\,\delta\epsilon_{xz} + 2N_{yz}\,\delta\epsilon_{yz})\,dxdy \tag{4.75}$$

where

$$\begin{aligned}
\delta\epsilon_{xx} &= \delta u_{0,x} + w_{0,x}\,\delta w_{0,x} + \bar{w}_{,x}\,\delta w_{0,x} \\
\delta\epsilon_{yy} &= \delta v_{0,y} + w_{0,y}\,\delta w_{0,y} + \bar{w}_{,y}\,\delta w_{0,y} \\
\delta\epsilon_{xy} &= \frac{1}{2}(\delta u_{0,y} + \delta v_{0,x} + w_{0,x}\,\delta w_{0,y} + w_{0,y}\,\delta w_{0,x} + \\
&\qquad \bar{w}_{,x}\,\delta w_{0,y} + \bar{w}_{,y}\,\delta w_{0,x}) \\
\delta\epsilon_{xz} &= \delta u_1 \\
\delta\epsilon_{yz} &= \delta v_1
\end{aligned} \tag{4.76}$$

and

$$\begin{aligned}
\delta\kappa_{xx} &= \delta u_1 - \delta w_{0,xx} \\
\delta\kappa_{yy} &= \delta v_1 - \delta w_{0,yy} \\
\delta\kappa_{xy} &= \delta u_{1,y} + \delta v_{1,x} - 2\delta w_{0,xy}
\end{aligned} \tag{4.77}$$

Note that the $\bar{w}$ field is a prescribed deformation field (imperfection) and is not subject to any variation. Substituting (4.76) and (4.77) into (4.75) and integrating by parts yields the following general result:

$$\delta W^{p}_{internal} = \int_0^1\int_0^\xi (N_{xx,x} + N_{xy,y})\ \delta u_0\ dxdy - \int_0^\xi (N_{xy}\ \delta u_0)_{y=0}^{y=1}\ dx$$
$$- \int_0^1 (N_{xx}\ \delta u_0)_{x=0}^{x=\xi}\ dy \tag{4.78a}$$

$$+ \int_0^1\int_0^\xi (N_{xy,x} + N_{yy,y})\ \delta v_0\ dxdy - \int_0^1 (N_{xy}\ \delta v_0)_{x=0}^{x=\xi}\ dy$$
$$- \int_0^\xi (N_{yy}\ \delta v_0)_{y=0}^{y=1}\ dx \tag{4.78b}$$

$$+ \int_0^1\int_0^\xi \{M_{xx,xx} + 2M_{xy,xy} + M_{yy,yy}$$
$$+ (N_{xx,x} + N_{xy,y})(w_{0,x} + \bar{w}_{,x}) + (N_{xy,x} + N_{yy,y})(w_{0,y} + \bar{w}_{,y})$$
$$+ N_{xx}(w_{0,xx} + \bar{w}_{,xx}) + 2N_{xy}(w_{0,xy} + \bar{w}_{,xy})$$
$$+ N_{yy}(w_{0,yy} + \bar{w}_{,yy})\}\ \delta w_0\ dxdy \tag{4.78c}$$
$$- \int_0^\xi \{[M_{xy,x} + M_{yy,y} + N_{xy}(w_{0,x} + \bar{w}_{,x})$$
$$+ N_{yy}(w_{0,y} + \bar{w}_{,y})]\ \delta w_0 - M_{xy}\ \delta w_{0,x} - M_{yy}\ \delta w_{0,y}\}_{y=0}^{y=1}\ dx$$
$$- \int_0^1 \{[M_{xx,x} + M_{xy,y} + N_{xx}(w_{0,x} + \bar{w}_{,x})$$
$$+ N_{xy}(w_{0,y} + \bar{w}_{,y})]\ \delta w_0 - M_{xx}\ \delta w_{0,x} - M_{xy}\ \delta w_{0,y}\}_{x=0}^{x=\xi}\ dy$$

$$+ \int_0^1\int_0^\xi \left[\zeta^2 (M_{xx,x} + M_{xy,y}) - N_{xz}\right]\ \delta u_1\ dxdy$$
$$- \int_0^\xi \zeta^2 (M_{xy}\delta u_1)_{y=0}^{y=1}\ dx - \int_0^1 \zeta^2 (M_{xx}\delta u_1)_{x=0}^{x=\xi}\ dy \tag{4.78d}$$

$$+ \int_0^1\int_0^\xi \left[\zeta^2 (M_{xy,x} + M_{yy,y}) - N_{yz}\right]\ \delta v_1\ dxdy$$

$$-\int_0^{\xi} \zeta^2 \left(M_{yy}\delta v_1\right)_{y=0}^{y=1}\, dx - \int_0^{1} \zeta^2 \left(M_{xy}\delta v_1\right)_{x=0}^{x=\xi}\, dy \tag{4.78e}$$

The second contribution to the total internal work comes from the internal virtual work of the elastic foundation (interphase) $\delta W^f_{internal}$. To calculate $\delta W^f_{internal}$ we start by the following relationship:

$$\delta W^f_{internal} = \int\int_A F\ \delta\Delta\ dA \tag{4.79}$$

where F is the generalized force, Δ is the generalized displacement and A is the surface area of the plate. Substituting equation (4.52) into (4.79) yields;

$$\delta W^f_{internal} = \int\int_A \alpha\Delta\Psi(\Delta)\ \delta\Delta\ dA \tag{4.80}$$

From equations (4.48), (4.49) and (4.50) one can express $\delta\Delta$ as follows:

$$\delta\Delta = \frac{u}{\Delta_o}\delta u + \frac{v}{\Delta_o}\delta v + \frac{w}{\Delta_o}\delta w \tag{4.81}$$

where

$$u = u_0 + \frac{1}{2}\left(w_{0,x} - u_1\right) \tag{4.82}$$

$$v = v_0 + \frac{1}{2}\left(w_{0,y} - v_1\right) \tag{4.83}$$

$$w = w_0 + \bar{w} + t \tag{4.84}$$

Substituting (4.81) into (4.80) and integrating by parts yields the following:

$$\delta W^f_{internal} = \int_0^1\int_0^{\xi} \left(-\alpha\pi^4\zeta^2\Psi\right)\left[u_0 + \frac{1}{2}\left(w_{0,x} - u_1\right)\right]\left(1 - \frac{\bar{w}+t}{\Delta_o}\right)\ \delta u_0\ dxdy$$

(4.85a)

$$+\int_0^1\int_0^\xi \left(-\alpha\pi^4\zeta^2\Psi\right)\left[v_0+\frac{1}{2}\left(w_{0,y}-v_1\right)\right]\left(1-\frac{\bar{w}+t}{\Delta_o}\right)\,\delta v_0\,dxdy$$

(4.85b)

$$+\int_0^1\int_0^\xi \left[\left(-\alpha\pi^4\Psi\right)\left(w_0+\bar{w}+t\right)\left(1-\frac{\bar{w}+t}{\Delta_o}\right)\right.$$
$$+\alpha\frac{\pi^2}{2}\zeta^2\left(\left[\Psi\left(u_0+\frac{1}{2}\left(w_{0,x}-u_1\right)\right)\left(1-\frac{\bar{w}+t}{\Delta_o}\right)\right]_{,x}\right.$$
$$\left.\left.+\left[\Psi\left(v_0+\frac{1}{2}\left(w_{0,y}-v_1\right)\right)\left(1-\frac{\bar{w}+t}{\Delta_o}\right)\right]_{,y}\right)\right]\delta w_0\,dxdy \qquad (4.85c)$$
$$-\int_0^\xi\left\{\left[\alpha\frac{\pi^4}{2}\zeta^2\Psi\left[v_0+\frac{1}{2}\left(w_{0,y}-v_1\right)\right]\left(1-\frac{\bar{w}+t}{\Delta_o}\right)\right]\,\delta w_0\right\}_{y=0}^{y=1}dx$$
$$-\int_0^1\left\{\left[\alpha\frac{\pi^4}{2}\zeta^2\Psi\left[u_0+\frac{1}{2}\left(w_{0,x}-u_1\right)\right]\left(1-\frac{\bar{w}+t}{\Delta_o}\right)\right]\,\delta w_0\right\}_{x=0}^{x=\xi}dy$$

$$+\int_0^1\int_0^\xi \alpha\frac{\pi^4}{2}\zeta^4\Psi\left[u_0+\frac{1}{2}\left(w_{0,x}-u_1\right)\right]\left(1-\frac{\bar{w}+t}{\Delta_o}\right)\,\delta u_1\,dxdy \qquad (4.85d)$$

$$+\int_0^1\int_0^\xi \alpha\frac{\pi^4}{2}\zeta^4\Psi\left[v_0+\frac{1}{2}\left(w_{0,y}-v_1\right)\right]\left(1-\frac{\bar{w}+t}{\Delta_o}\right)\,\delta v_1\,dxdy \qquad (4.85e)$$

where the multipliers π^2 and π^4 are introduced for convenience and without any loss of generality. The above expression for $\delta W^f_{internal}$ is valid for all Ψ and that $\delta W^f_{internal}$ is identically zero when there are no deformations. The latter can be realized by recalling the definitions of Δ_o, $\bar{\Delta}$ and Δ (equations 4.48, 4.49 and 4.50) and noting that when $u_0 = v_0 = w_0 = u_1 = v_1 = 0$ the value of Δ_o is identical to $\bar{\Delta}$, i.e., when the interphase is not deforming, $\Delta_o = \bar{w} + t$. Hence, no deformation implies

$$\left(1-\frac{\bar{w}+t}{\Delta_o}\right)=0 \qquad (4.86)$$

4.9 The Governing Equations

Having presented the relevant formulation and assumptions in the previous sections, this section will focus on the assembly of the final governing equations. Substituting (4.72) into (4.60) yields;

$$\delta W_{external} = \delta W^{p}_{internal} + \delta W^{f}_{internal} \tag{4.87}$$

where the expression for each of the three contributions is given in equations (4.67), (4.78) and (4.85), respectively. Substituting these three equations into (4.87) yields the variational equation which has the following form:

$$\begin{aligned}
&\int_0^1\int_0^{\xi} DE_1\ \delta u_0 + BC^{x,y}_{u_0} + \\
&\int_0^1\int_0^{\xi} DE_2\ \delta v_0 + BC^{x,y}_{v_0} + \\
&\int_0^1\int_0^{\xi} DE_3\ \delta w_0 + BC^{x,y}_{w_0} + \\
&\int_0^1\int_0^{\xi} DE_4\ \delta u_1 + BC^{x,y}_{u_1} + \\
&\int_0^1\int_0^{\xi} DE_5\ \delta v_1 + BC^{x,y}_{v_1} = 0
\end{aligned} \tag{4.88}$$

where DE implies the Differential Equation and BC the corresponding Boundary Conditions. These differential equations and boundary conditions are not presented here for the sake of brevity. Note that since there are five independent displacement fields there are five differential equations labeled $DE_1 - DE_5$. Using the Extended Galerkin's method the above integral equations were solved employing the same iterative scheme presented in Chapter III namely, the Levenberg-Marquardt algorithm.

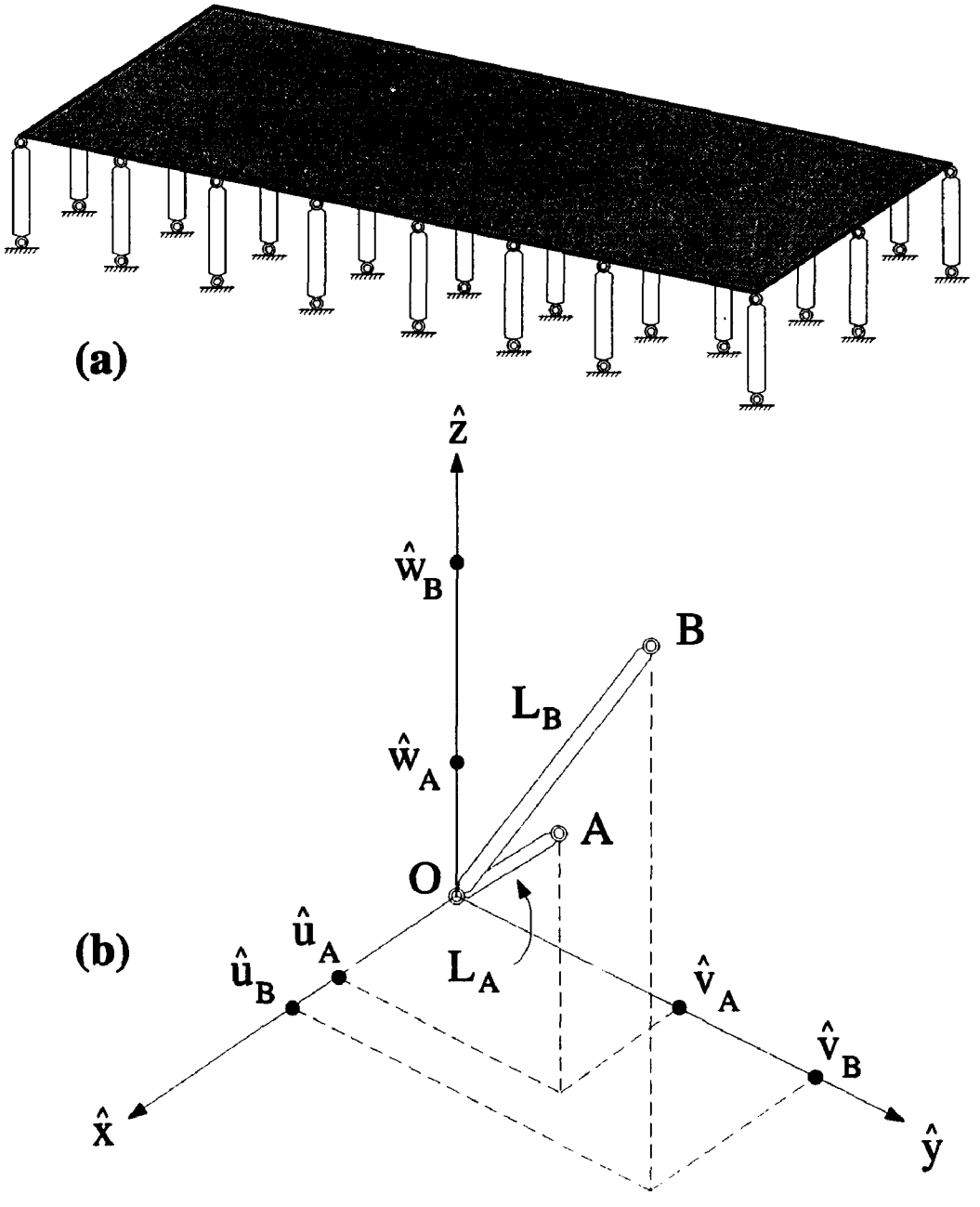

Figure 4.1: (a) A plate attached to a bed of elastic axial rods. The length of the rods is exaggerated for clarity. Theoretically, the number of rods is infinite, but for computational purposes, this number is finite and is equal to the number of integration points. (b) A cartesian description of a rod's kinematics showing all coordinates of points A and B.

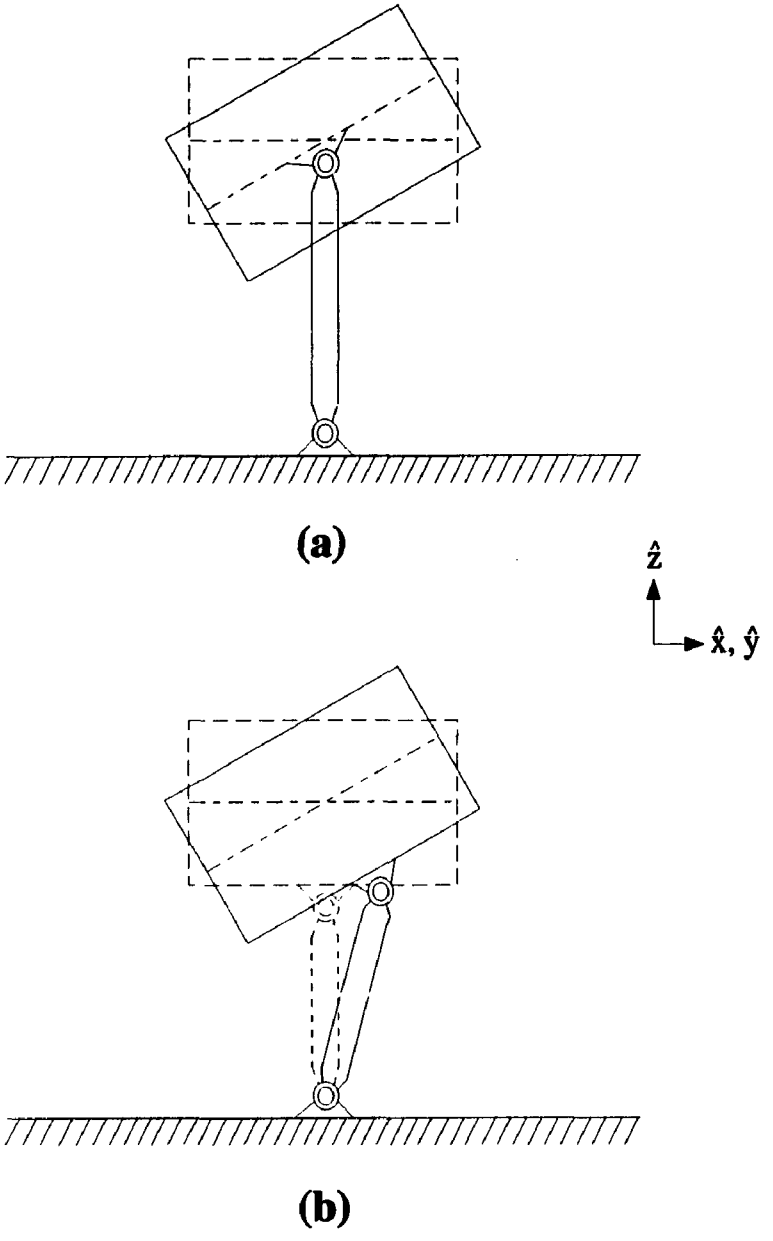

Figure 4.2: A schematic showing the difference between attaching the rod element to the middle surface (a) as opposed to the lower surface (b). (a) Rotation does not cause stretching of the rod, while in (b) rotation does contribute to the rod's stretching.

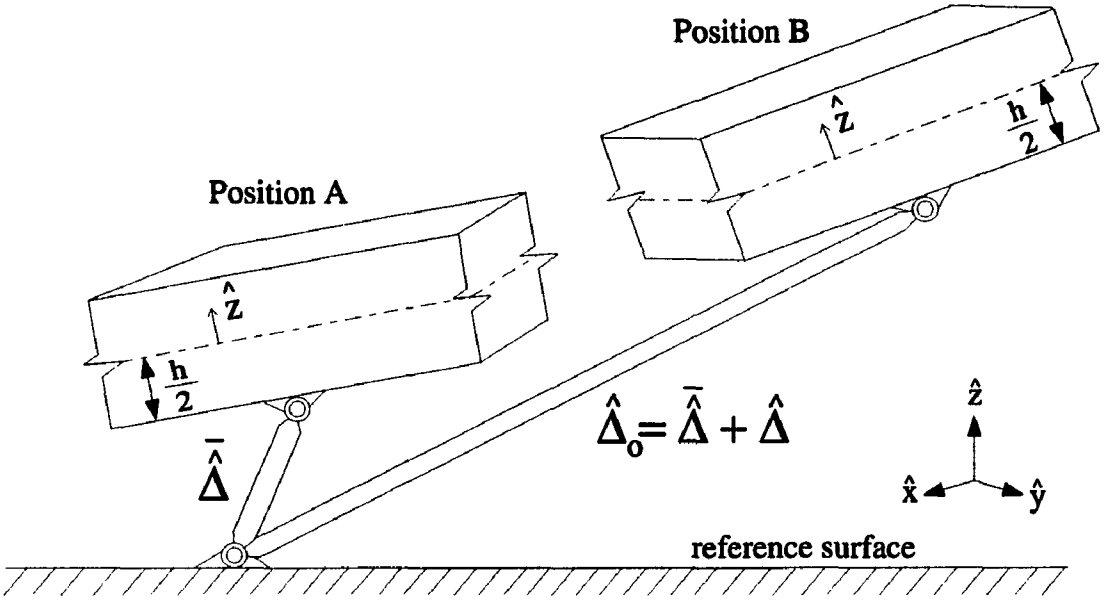

Figure 4.3: A schematic showing the general 3-D deformation of a differential volume plate element as well as the interface "rod" model that connects the plate's lower surface ($\hat{z} = -\frac{h}{2}$) to the reference surface.

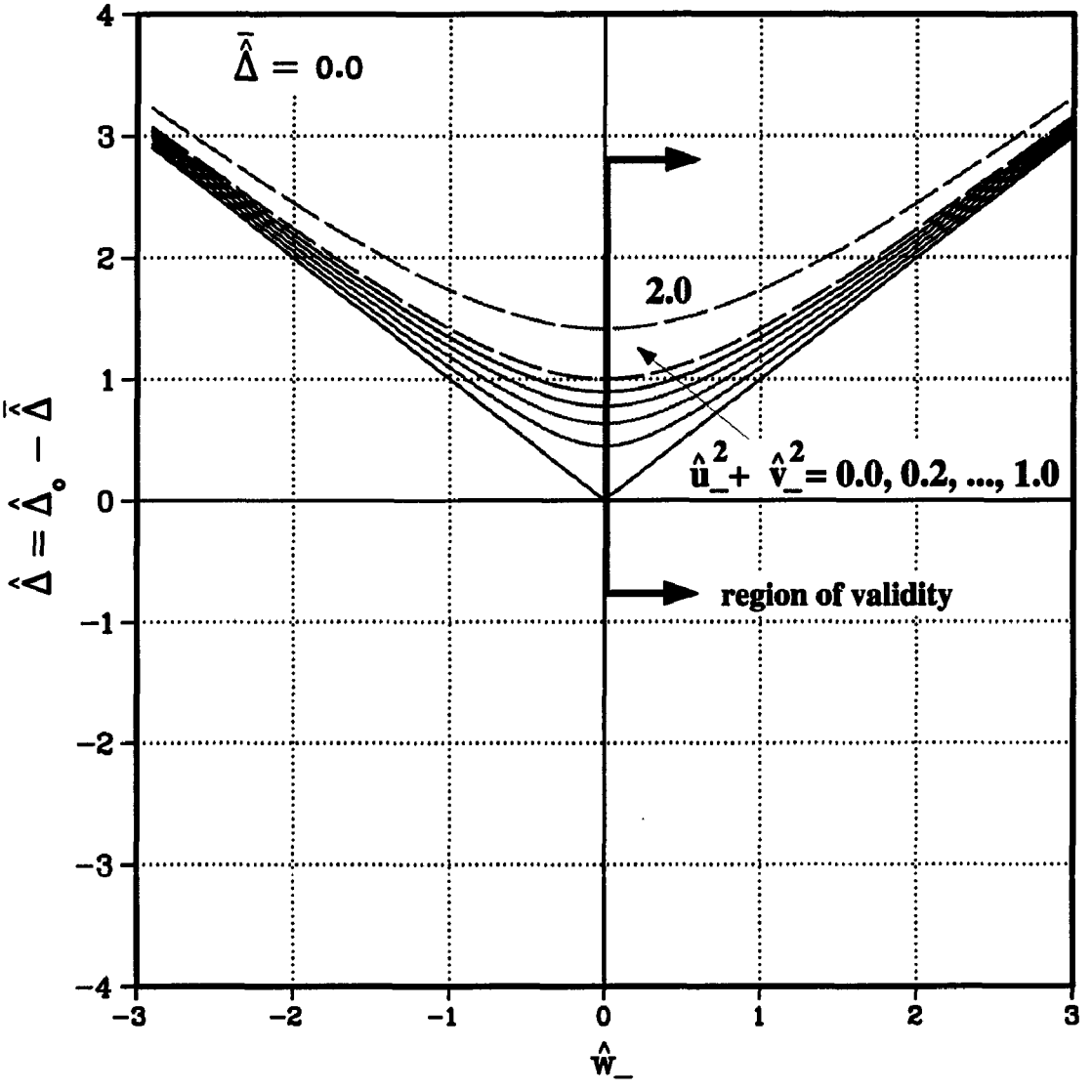

Figure 4.4: General $\hat{\Delta}_o - \bar{\hat{\Delta}}$ vs. $\hat{w}_-$ curves for different values of $\hat{u}_-^2 + \hat{v}_-^2$ and for $\bar{\hat{\Delta}} = 0.0$. The range of validity is for $\hat{w}_- \geq -\bar{\hat{\Delta}}$.

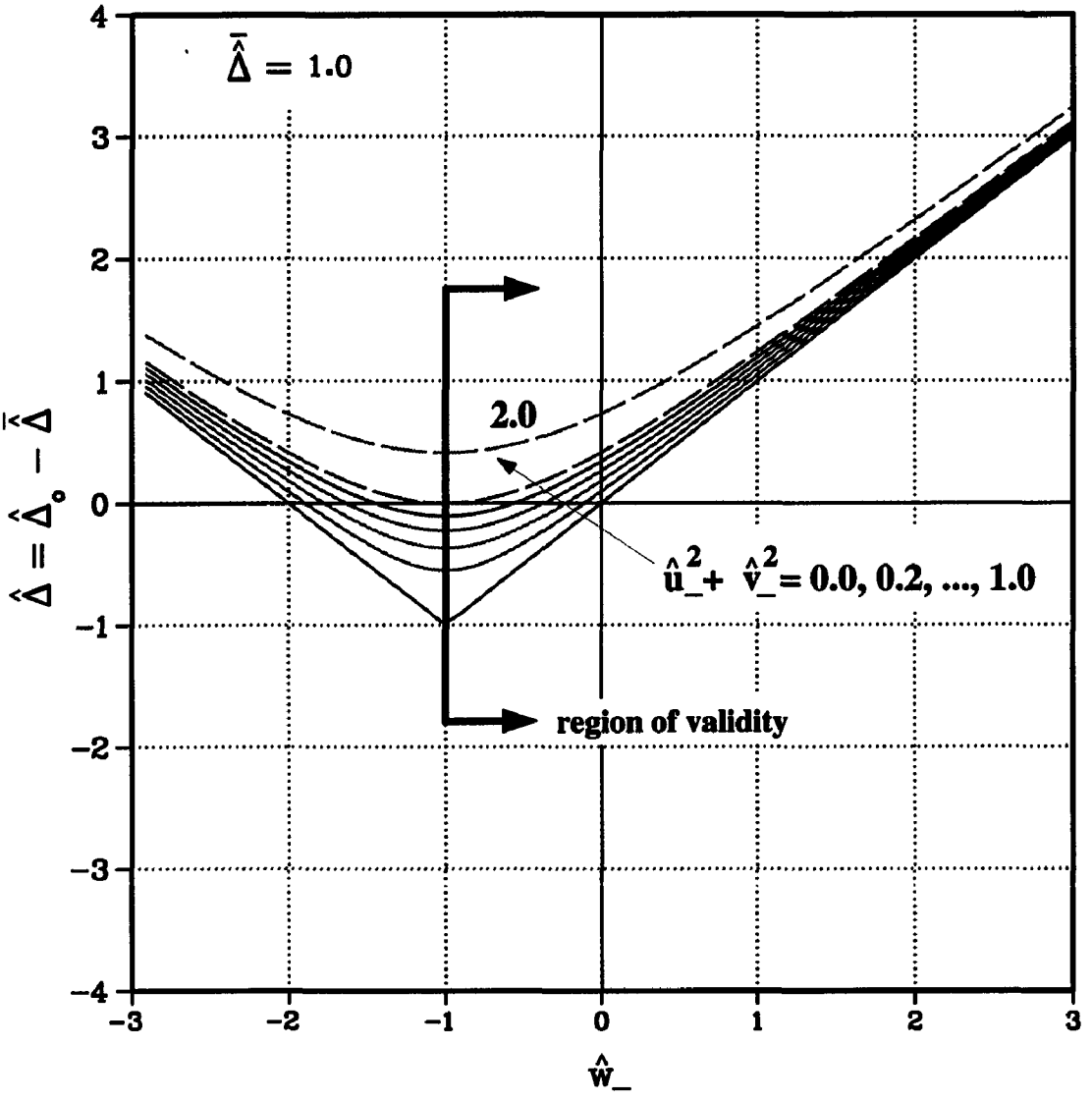

Figure 4.5: General $\hat{\Delta}_o - \bar{\hat{\Delta}}$ vs. $\hat{w}_-$ curves for different values of $\hat{u}_-^2 + \hat{v}_-^2$ and for $\bar{\hat{\Delta}} = 1.0$. The range of validity is for $\hat{w}_- \geq -\bar{\hat{\Delta}}$.

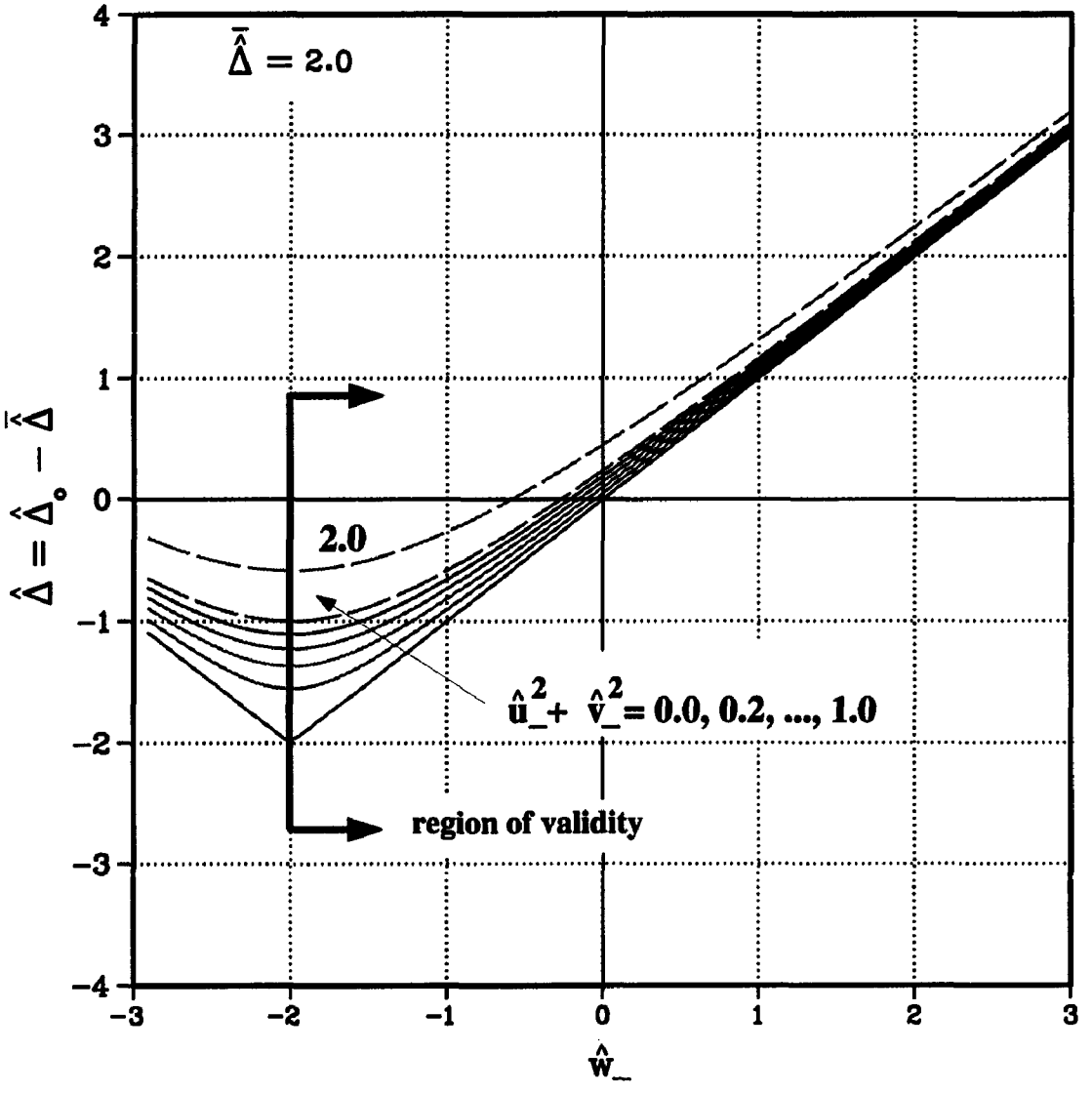

Figure 4.6: General $\hat{\Delta}_o - \bar{\hat{\Delta}}$ vs. $\hat{w}_-$ curves for different values of $\hat{u}_-^2 + \hat{v}_-^2$ and for $\bar{\hat{\Delta}} = 2.0$. The range of validity is for $\hat{w}_- \geq -\bar{\hat{\Delta}}$.

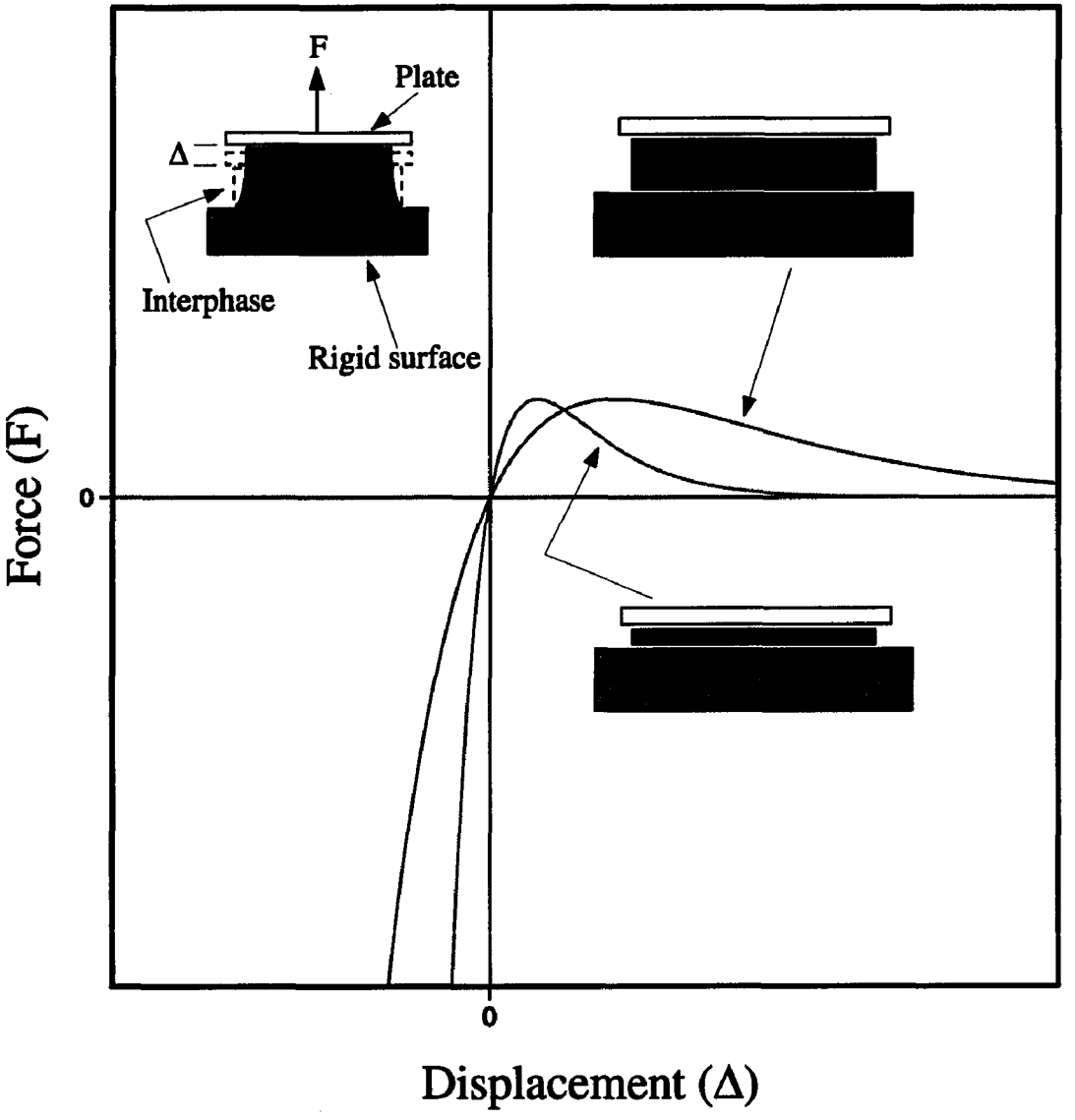

Figure 4.7: General force-displacement relationships for two different interphase thicknesses. In general, the thicker the interphase, the less "brittle" it is. For $\Delta < 0$, the interphase stiffness increases to "infinity" resembling approaching contact between the plate and the supporting rigid surface.

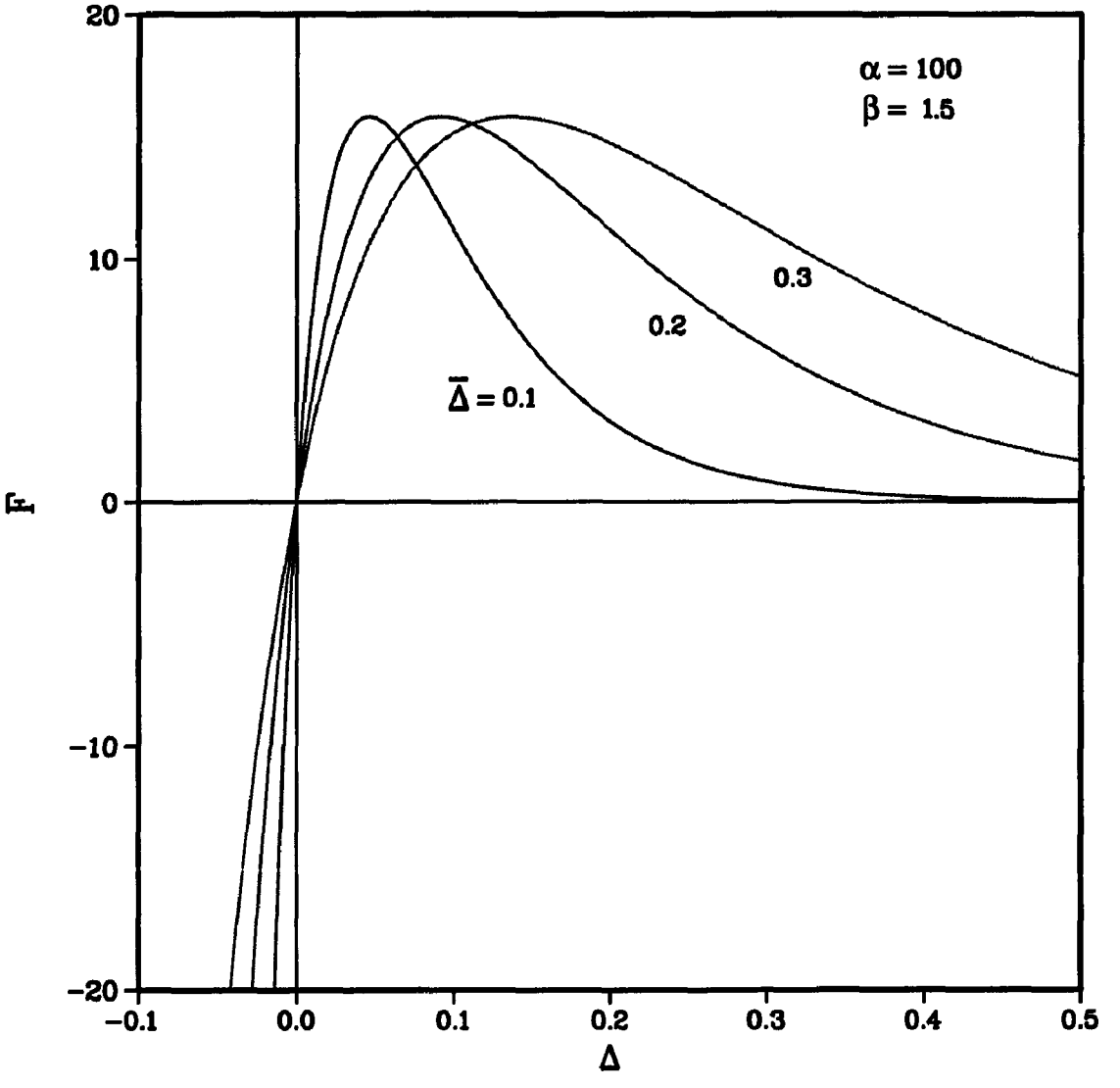

Figure 4.8: Force (F) vs. Displacement (Δ) for different values of the initial length ($\bar{\Delta}$). The curves shown are for $\alpha = 100$ and $\beta = 1.5$.

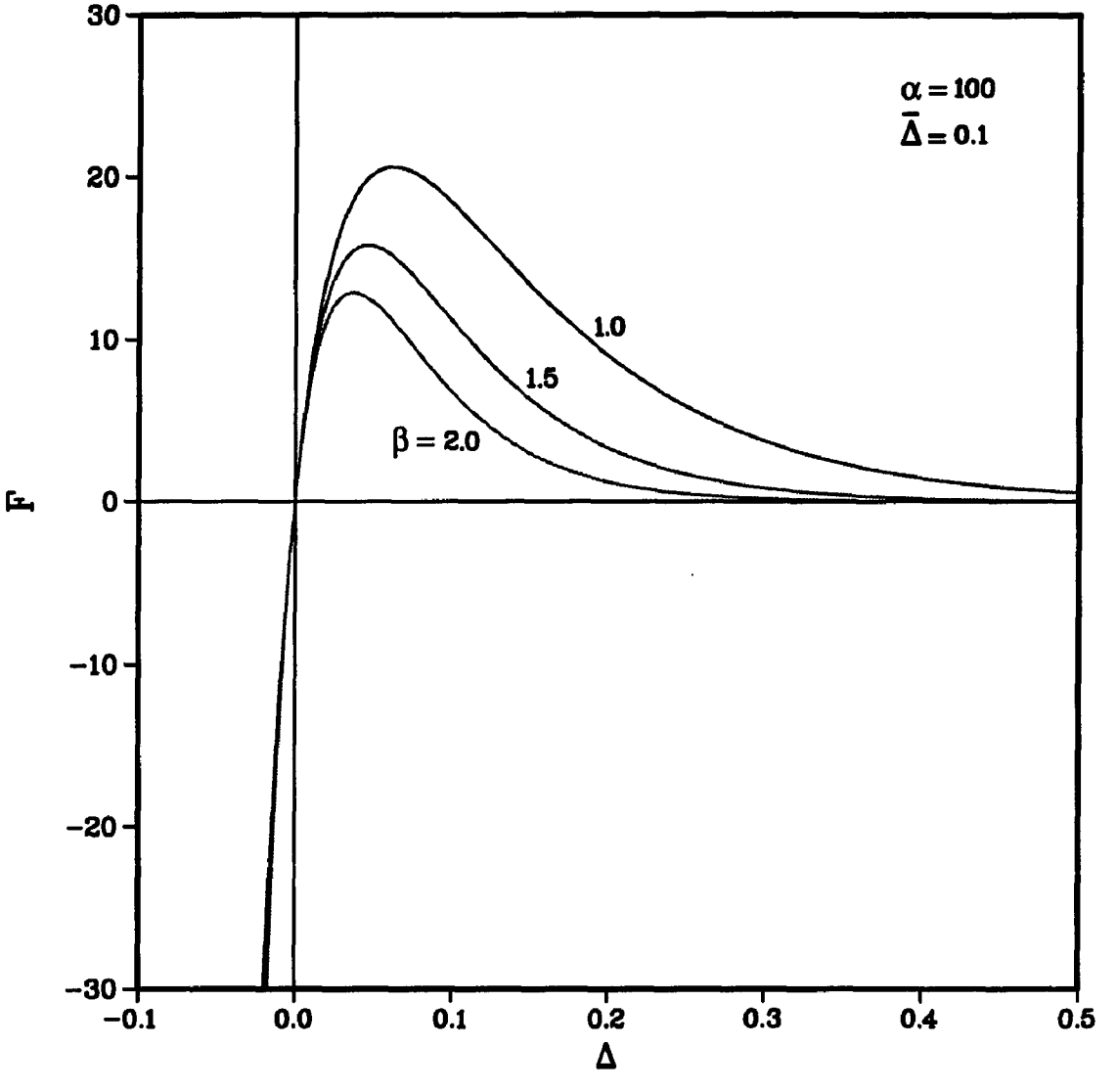

Figure 4.9: Force (F) vs. Displacement (Δ) for different values of β. The curves shown are for $\alpha = 100$ and $\bar{\Delta} = 0.1$.

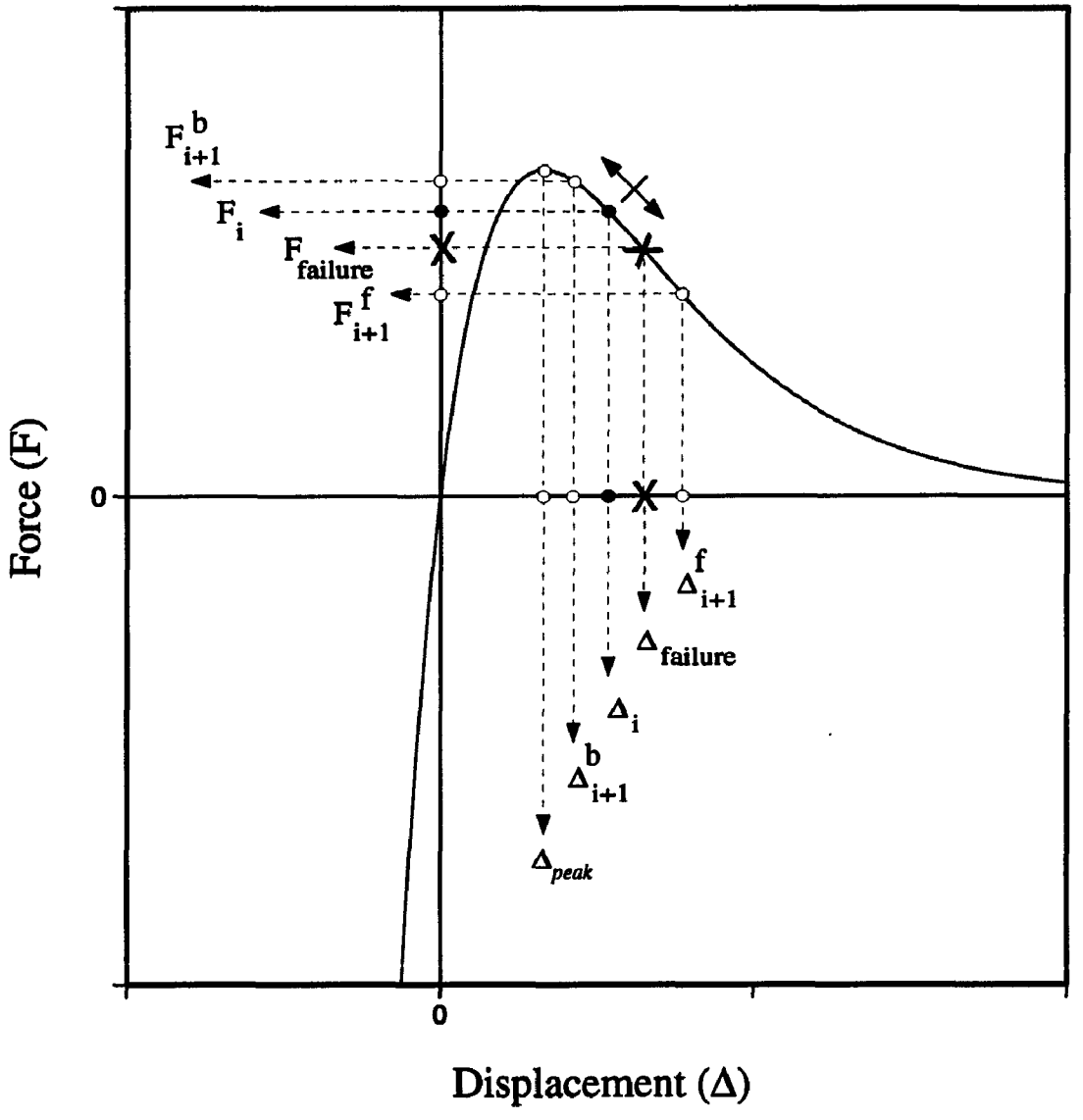

Figure 4.10: A typical force-displacement curve showing that at sub-iteration i, the local constitutive response can proceed (to sub-iteration $i+1$) in either directions ("f" for forward and "b" for backward). The point designated "$\times$" is the pre-specified failure point, beyond which the local tensile stress vanishes permanently. If $\Delta_{i+1}^{f} \geq \Delta_{failure}$ then decohesion (rod becomes tensionless) takes place at sub-iteration $i+2$.

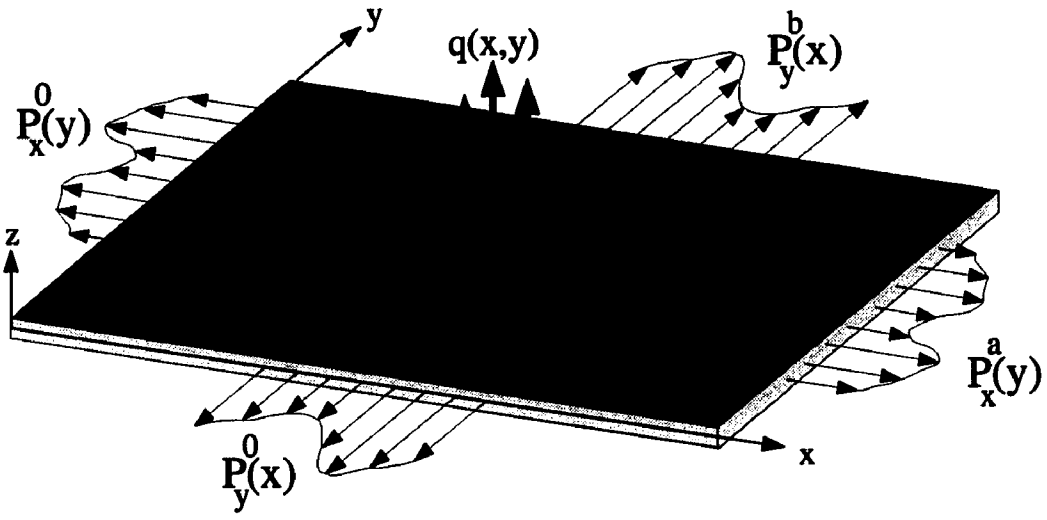

Figure 4.11: Plate under external transverse load q as well as inplane biaxial distributed loads $P_x^0(y)$, $P_x^a(y)$, $P_y^0(x)$ and $P_y^b(x)$.

CHAPTER V

DEMONSTRATIVE CASES

5.1 Introduction

This chapter presents few case studies that demonstrate the simplicity and applicability of the methodology presented in Chapter IV. The choice of these cases was based solely on the fact that they demonstrate the validity of the interphase model.

Although there is a large number of parameters that can be varied, only few were actually varied (i.e., it is not intended for this chapter to present an extensive parametric study). This is mainly due to two reasons: 1) The main intention of the study was to demonstrate that such a model and formulation are viable, and 2) the number of combinations of these parameters needed to carry a comprehensive parametric study is prohibitive and should be the focus of future research. The main distinction between the cases investigated was the type of loading (i.e., load-control vs. displacement-control), plate's aspect ratio (ξ) and the shape and location of the original (initial) delamination. One case study investigated the effect of transverse shear deformations (using first-order shear deformation theory) on the decohesion process.

Further, during the simulation no distinction was made between the phenomena of buckling (and postbuckling) and non-self-similar growth. In other words, the same

equations govern the entire behavior from beginning (starting to load/displace the structure) to end (complete delamination and/or loss of stiffness) without specification to certain regimes of validity.

5.2 Plate's Constitutive Properties

Among the few common parameters that are shared between all cases are the plate's constitutive properties. The plates were modeled as elastic structures exhibiting linear constitutive relationships. These constitutive relationships were given in equations (4.19) and (4.20) along with the definitions of the averaged extensional, coupling and bending stiffnesses given in equations (4.16). These equation were also given in their nondimensional form in equations (4.39), (4.45) and (4.46). Unlike the **B** and **D** matrices the **A** matrix given in (5.1) contains the shear stiffness contribution needed to perform first-order shear deformation analysis. Further, since the plate theory employed in Chapter IV admits no contribution to the internal virtual work by transverse extensional stresses σ_{zz}, all entries in the **A** matrix with at least one index equal to 3 (i.e., A_{i3} or A_{3j}) were not needed for the analysis and hence, they were designated by "––". The nondimensional extensional moduli matrix (**A**) including transverse shear moduli is as follows:

$$\mathbf{A} = \begin{bmatrix} A_{11} & A_{12} & A_{13} & A_{14} & A_{15} & A_{16} \\ & A_{22} & A_{23} & A_{24} & A_{25} & A_{26} \\ & & A_{33} & A_{34} & A_{35} & A_{36} \\ & & & A_{44} & A_{45} & A_{46} \\ & sym. & & & A_{55} & A_{56} \\ & & & & & A_{66} \end{bmatrix}$$

with numerical values given as follows:

$$\mathbf{A} = \begin{bmatrix} 12.00 & 4.00 & -- & 0.00 & 0.00 & 0.00 \\ & 12.00 & -- & 0.00 & 0.00 & 0.00 \\ & & -- & -- & -- & -- \\ & & & 4.50 & 0.00 & 0.00 \\ & sym. & & & 4.50 & 0.00 \\ & & & & & 4.00 \end{bmatrix} \tag{5.1}$$

The constitutive coupling moduli matrix (**B**) is identically equal to zero and is given below. Note that although the constitutive coupling between inplane and out-of-plane actions is not present, the kinematic coupling is present (refer to the strain-displacement relationships given in equation (4.41)). The **B** matrix is

$$\mathbf{B} = \begin{bmatrix} B_{11} & B_{12} & B_{16} \\ & B_{22} & B_{26} \\ sym. & & B_{66} \end{bmatrix}$$

with numerical values given as follows:

$$\mathbf{B} = \begin{bmatrix} 0.00 & 0.00 & 0.00 \\ & 0.00 & 0.00 \\ sym. & & 0.00 \end{bmatrix} \tag{5.2}$$

The nondimensional bending moduli matrix (**D**) is given as

$$\mathbf{D} = \begin{bmatrix} D_{11} & D_{12} & D_{16} \\ & D_{22} & D_{26} \\ sym. & & D_{66} \end{bmatrix}$$

with numerical values given as follows:

$$\mathbf{D} = \begin{bmatrix} 1.00 & 0.33 & 0.00 \\ & 1.00 & 0.00 \\ sym. & & 0.33 \end{bmatrix} \tag{5.3}$$

5.3 Computational Considerations

In this study it was decided to employ the Galerkin's method, and in order to carry out the solution procedure, kinematically admissible global displacement functions were assumed. It is important to note that although the plate is unilaterally constrained, such a constraint does not play any role in choosing these functions and as mentioned earlier (Chapter IV), this constraint condition will be accounted for via the nonlinearity of the interphase model. Further, all the deformation fields will be assumed to be of a separable form where shape functions in x are multiplied by those in y. These functions can be chosen to be the buckling and/or free vibration eigenmodes of beams and/or plates having the same kinematic boundary conditions. For all the cases considered, beam-vibration eigenmodes were employed and can be found in Appendix B. In the forthcoming investigations, all of the deformation functions $u_0(x,y), v_0(x,y)$, etc., were chosen to have the following forms:

$$u_0(x,y) = \left(1 - c\frac{x}{\xi}\right) \sum_{i}^{M^{u_0}} \sum_{j}^{N^{u_0}} A_{ij}^{u_0} \Phi_{ij}^{u_0}(x,y) - \lambda\, c\, \frac{x}{\xi} \tag{5.4}$$

$$v_0(x,y) = \sum_{i=1}^{M^{v_0}} \sum_{j=1}^{N^{v_0}} A_{ij}^{v_0} \Phi_{ij}^{v_0}(x,y) \tag{5.5}$$

$$w_0(x,y) = \sum_{i=1}^{M^{w_0}} \sum_{j=1}^{N^{w_0}} A_{ij}^{w_0} \Phi_{ij}^{w_0}(x,y) \tag{5.6}$$

and when first-order shear deformations are included then

$$u_1(x,y) = \sum_{i=1}^{M^{u_1}} \sum_{j=1}^{N^{u_1}} A_{ij}^{u_1} \Phi_{ij}^{u_1}(x,y) \tag{5.7}$$

$$v_1(x,y) = \sum_{i=1}^{M^{v_1}} \sum_{j=1}^{N^{v_1}} A_{ij}^{v_1} \Phi_{ij}^{v_1}(x,y) \tag{5.8}$$

where A_{ij}^{f} are unknown generalized displacement coefficients for the particular deformation field "f", and $\Phi_{ij}^{f}(x,y)$ are spatial functions that have the following separable form:

$$\Phi_{ij}^{f}(x,y) = \phi_i^f(x)\, \varphi_j^f(y) \tag{5.9}$$

$\phi_i^f(x)$ and $\varphi_j^f(y)$ must satisfy their corresponding plate's kinematic boundary conditions as well as be continuously differentiable up to the highest corresponding derivative in the governing differential equation. The spatial functions used throughout this study are continuously differentiable (see Appendix B). The number of terms carried in the series, i.e., M^f and N^f, is dependent on the field "f" as well as on few parameters such as plate's aspect ratio ξ, delamination size relative to the size of the global plate, degree of accuracy as well as some convergence criteria imposed by the numerical scheme used for solving the governing nonlinear system of equations.

The parameters in (5.4) were presented earlier (Chapter IV). Briefly, this form

is general enough to account for load-control and inplane displacement-control situations. c is an environment switching parameter that is defined as follows (4.70):

$$c = \begin{cases} 0\ , & \textit{for load control} \\ 1\ , & \textit{for displacement control} \end{cases} \tag{5.10}$$

and λ is the value of the nondimensional inplane displacement of the $x = \xi$ edge and at the plate's midplane.

The shear deformation functions u_1 and v_1 were chosen to have the same spatial variations as $w_{0,x}$ and $w_{0,y}$, respectively. This is due to the fact that u_1 and v_1 are actually shear rotations *in addition* to the usual flexural rotations $w_{0,x}$ and $w_{0,y}$ of the classical Kirchhoff-Love plate theory.

By using Galerkin's method the governing equations were reduced to a system of $\sum M^j$ x N^j nonlinear equations. More precisely, the size (S) of the system (i.e., the total number of equations to be solved) is as follows:

$$S = \begin{cases} M^{u_0}N^{u_0} + M^{v_0}N^{v_0} + M^{w_0}N^{w_0}\ , \\ \textit{without shear deformations} \\ \\ M^{u_0}N^{u_0} + M^{v_0}N^{v_0} + M^{w_0}N^{w_0} + M^{u_1}N^{u_1} + M^{v_1}N^{v_1}\ , \\ \textit{with shear deformations} \end{cases} \tag{5.11}$$

The solution of the resulting system of nonlinear equations was carried out iteratively using the Levenberg-Marquardt method as modified by Powell [13].

For all the cases considered an out-of-plane imperfection field was introduced to simplify the solution process. The imperfection field was assumed to exhibit the following form:

$$\bar{w}(x,y) \;=\; 0.001\;\sin^2\left(\pi\frac{x}{\xi}\right)\sin^2(\pi y)\;e^{-10\left(\frac{x}{\xi}-0.5\right)^2}e^{-10(y-0.5)^2} \qquad (5.12)$$

which is a localized imperfection located at the center of the plate with an exponential decay towards the four edges. Further, to reduce boundary effects, at least in the initial decohesion stages, the imperfection field was assumed to have a vanishing slope as well as amplitude at the four edges.

In all of the cases investigated, no transverse load was applied to the plates ($Q = 0$). Table 5.1 lists the values of all the main parameters used for all the cases considered. Table 5.2 lists the boundary conditions imposed on the rectangular plates for all the cases considered. Figure 5.1 shows a typical force vs. displacement ($F-\Delta$) relationship used for this study. The failure in this constitutive model is defined by $\Delta_{failure}$ as marked.

5.4 Case A: A Strip with a Central Delamination (Load-Control)

This case represents a strip (wide column) that is loaded by a uniform edge load (at $x = \xi$). To resist the applied load, the parallel edge ($x = 0$) was restrained from moving in the plane ($u_0 = 0$). Initially, there exists a central square delamination of an area equal to 1.0 (=20% of the total area of the plate). The structure was assumed to be non-shear-deformable.

Figure 5.2 shows a sequence of pictures obtained from the numerical simulation showing the progression of the initially central delamination area at different inplane load level λ. Figure 5.3 shows the deformed shape of the strip at $\lambda = 2.3$. Figure 5.4 shows the postbuckling response curves showing the load λ vs. the transverse deflection w_0 at the three different points A, B and C. Point C is the closest to the loaded

edge. Note that w_0 at points A and C remained almost constant beyond $\lambda \approx 1.9$.

Figure 5.5 shows the average plate axial force $\bar{N}_{xx}$ at the delamination front vs. the applied edge load λ. $\bar{N}_{xx}$ is normalized by π^2 for convenience. Note that up to $\lambda \approx 1.9$ the two quantities were identical, implying that the plate was carrying all the load. Beyond that, the applied load was strongly shared by the interphase layer

5.5 Case B: A Square Plate with a Central Circular Delamination (Uniaxial Load-Control)

This case represents a square plate that is loaded by a uniform edge load (at $x = \xi$). To resist the applied load, the parallel edge ($x = 0$) was restrained from moving in the plane ($u_0 = 0$). Initially, there exists a central circular delamination of an area equal to 0.0314 (=3.14% of the total area of the plate). The structure was assumed to be non-shear-deformable.

Figure 5.6 shows a sequence of pictures obtained from the numerical simulation showing the progression of the initially central delamination area at different inplane load level λ. For $\lambda < 14.9$ no decohesion took place. For $\lambda > 14.9$ the delamination starts to grow in a self-similar manner preserving its overall elliptical shape corresponding to $\lambda = 14.9$. It is important to note that the growth form $\lambda \leq 14.9$ to $\lambda = 14.9$ was non-self-similar since the original shape was circular and at $\lambda = 14.9$ it became elliptical. This is mainly attributed to the fact that the load is uniaxial. For $\lambda \geq 15.4$ boundary effects come into effect altering the shape significantly and forcing the growth towards the four corners. Figure 5.7 shows the delamination progression for $\lambda \geq 15.7$ leading to $\approx 82\%$ total delamination area at $\lambda = 17.9$. Figure 5.8 shows the relationship between the applied load λ and the total delamination area A_d. Such a relationship shows that at the initial stages, the decohesion process is sudden. The

process becomes more gradual as decohesion progresses.

5.6 Case C: A Square Plate with a Central Circular Delamination (Uniaxial Displacement-Control)

This case is identical to the previous case (Case B) except for the control parameter. This case represents a square plate that is loaded by a uniform edge (inplane) displacement (at $x = \xi$). Initially, there exists a central circular delamination of an area equal to 0.0314 (=3.14% of the total area of the plate). The structure was assumed to be non-shear-deformable.

Figures 5.9 and 5.10 show a sequence of pictures obtained from the numerical simulation showing the progression of the initially central and circular delamination area at different inplane displacement level λ. The meaning of the label on top of each picture is as follows: (DC, x, y) $\Leftrightarrow$ (Displacement-Control, λ, number of failed interphase rods). Up to $\lambda = 15.2$ the overall qualitative behavior of the case is very similar to that in Case B[1] where the growth is "almost" self-similar up to $\lambda = 15.2$ beyond which the growth became non-self-similar.

5.7 Case D: A Square Plate with a Central Circular Delamination (Biaxial Load-Control)

This case represents a square plate that is loaded by uniform edge loads (at $x = \xi$ and $y = 1$). Both loads have the same sign and magnitude ($\eta_{y1} = +1.0$). To resist the applied loads, the corresponding parallel edges ($x = 0$ and $y = 0$) were restrained from moving in the plane (@ $x = 0, u_0 = 0$, and @ $y = 0, v_0 = 0$). Initially, there exists a central circular delamination of an area equal to 0.0314 (=3.14% of the total area of the plate). The structure was assumed to be non-shear-deformable.

[1] Recall that λ in this case has a completely different meaning; in Case B, λ was a force quantity, but here it is a displacement quantity.

Figure 5.11 shows a sequence of pictures obtained from the numerical simulation showing the progression of the initially central and circular delamination area at different inplane (biaxial) load levels λ and $\eta_{y1}\lambda$. Up to $\lambda = 8.3$, no decohesion took place, and for $8.4 \leq \lambda \leq 9.2$ the growth was self-similar owing its self-similarity to the symmetry of the applied loads. At $\lambda = 9.3$ a sudden and almost complete delamination took place.

5.8 Case E: A Rectangular Plate ($\xi = 2$) with an Edge Delamination (Uniaxial Load-Control)

This case represents a rectangular ($\xi = 2$) plate that is loaded by a uniform edge load (at $x = \xi$). Initially, there exists an edge rectangular delamination of an area equal to 0.27 (=13.5% of the total area of the plate). The structure was assumed to be non-shear-deformable.

Figure 5.12 shows a sequence of pictures obtained from the numerical simulation showing the progression of the initially edge (rectangular) delamination. The decohesion starts at the inner edge of the delamination with a gradual progression towards the center of the global plate. At $\lambda \approx 11.5$ the delamination size increases by three folds and for $\lambda > 13.5$ a complete delamination was observed.

5.9 Case F: A Square Plate with Two Arbitrary Delaminations (Uniaxial Load-Control)

This case represents a square plate that is loaded by a uniform edge load (at $x = \xi$). Initially, there exists two identical arbitrarily shaped delaminations of a total area equal to 0.13 (=13% of the total area of the plate). The structure was assumed to be non-shear-deformable.

Figure 5.13 shows a sequence of pictures obtained from the numerical simulation

showing the progression of the delaminations towards each other and then joining to form one bigger delamination. Such a case demonstrates the viability of the proposed modeling and formulation.

5.10 Case G: A Square Plate with Two Arbitrary Delaminations (Uniaxial Displacement-Control)

This case represents a square plate that is loaded by a uniform edge displacement (at $x = \xi$). This case is identical to Case F except for the control parameter.

Similar to the results obtained in Case F, Figures 5.14 and 5.15 shows a sequence of pictures that shows the progression of the delaminations towards each other and then joining to form one bigger delamination.

5.11 Case H: A Rectangular ($\xi = 5$) Plate with an Edge Delamination (Uniaxial Load-Control)

This case represents a rectangular ($\xi = 5$) plate that is loaded by a uniform edge load (at $x = \xi$). Initially, there exists a rectangular edge delamination of an area equal to 0.45 (=9% of the total area of the plate). The structure was assumed to be non-shear-deformable.

Figure 5.16 shows a sequence of pictures obtained from the numerical simulation showing the progression of the initially edge (rectangular) delamination. The decohesion starts at the inner edge of the delamination (towards the global plate's center) as well as along the free edge of the global plate (Table 5.2). These delamination patterns can be better understood by referring to Figures 5.17 and 5.18 which show the distribution of forces in the interphase rods. Unilateral contact plays a significant role in this case. Due to the fact that the edge at $y = 1$ ($\hat{y} = b$) edge is free, the deformation near that edge is periodic implying that at certain regions the plate is

compressing the interphase, i.e., contact is present.

5.12 Case I: A Square Thick Plate with Central Circular Delamination (Uniaxial Load-Control)

This case represents a square plate that is loaded by a uniform edge load (at $x = \xi$). Initially, there exists a central circular delamination of an area equal to 0.0314 (=3.14% of the total area of the plate). The structure was assumed to be shear-deformable. This case is identical to Case B except for allowing for shear deformations. Figure 5.19 shows a sequence of pictures obtained from the numerical simulation showing the progression of the initially central delamination area at different inplane load level λ. Comparing the delamination patterns for this case to those of Case B (Figures 5.6 and 5.7) one can observe that in this case the decohesion starts from the edge that is parallel to the loading direction and progresses towards the central (initial) delamination. Further, being a more compliant system, the onset of delamination in this case occurs at $\lambda = 4.0$ as opposed to $\lambda = 14.9$ for Case B.

One common feature that can be observed in all of the presented results is the creation of "new" and discontinuous delaminations away from the main delamination. In other words, not only the initial delaminations increased in size but other separate delaminations were created. It can be argued that the reasons for the creation of these separate delaminations can be attributed to: 1) numerical accuracies and tolerances that control the solver's convergence criteria, and 2) the number as well as the accuracy of the shape functions used to fully describe the plate's deformations. The constitutive parameters for the "interphase rod" and the family of shape functions can be adjusted such that spontaneous creation of new delamination does not occur.

However, this was not done selectively in order to compare results between different cases.

	Cases								
Parameter	A	B	C	D	E	F	G	H	I
Control	Load	Load	Displ.	Load	Load	Load	Displ.	Load	Load
ξ	5.0	1.0	1.0	1.0	2.0	1.0	1.0	5.0	1.0
ζ	0.001	0.001	0.001	0.001	0.001	0.001	0.001	0.001	0.1
η_{x0}	0.0	0.0	0.0	0.0	0.0	0.0	0.0	0.0	0.0
η_{y0}	0.0	0.0	0.0	0.0	0.0	0.0	0.0	0.0	0.0
η_{y1}	0.0	0.0	0.0	1.0	0.0	0.0	0.0	0.0	0.0
α	1000.0	100.0	100.0	100.0	100.0	100.0	100.0	100.0	100.0
β	10.0	10.0	10.0	10.0	10.0	10.0	10.0	10.0	10.0
t	0.1	0.1	0.1	0.1	0.1	0.1	0.1	0.1	0.1
A_{id}	1.0	0.0314	0.0314	0.0314	0.27	0.13	0.13	0.45	0.0314
FOSDT	No	No	No	No	No	No	No	No	Yes

Table 5.1: Parameters used for all the cases considered. Note that cases B and I differ only in shear deformation. A_{id} is the area of the initial delamination.

B. C. @	u_0	v_0	w_0	$w_{0,x}$	$w_{0,y}$	u_1	v_1
	Case A						
$x = 0$	c[a]	f	c	c			
$x = \xi$	f[b]	f	c	c			
$y = 0$	f	c	f		f		
$y = 1$	f	f	f		f		
	Cases B, C, D, F, & G						
$x = 0$	c	f	c	f			
$x = \xi$	f	f	c	f			
$y = 0$	f	c	c		f		
$y = 1$	f	f	c		f		
	Case E						
$x = 0$	c	f	c	c			
$x = \xi$	f	f	c	c			
$y = 0$	f	c	c		f		
$y = 1$	f	f	f		f		
	Case H						
$x = 0$	c	f	c	f			
$x = \xi$	f	f	c	f			
$y = 0$	f	c	c		f		
$y = 1$	f	f	f		f		
	Case I						
$x = 0$	c	f	c	f		f	
$x = \xi$	f	f	c	f		f	
$y = 0$	f	c	c		f		f
$y = 1$	f	f	c		f		f

[a] c = constrained
[b] f = free

Table 5.2: Boundary conditions imposed on the rectangular plates for all the cases considered. Note that an empty entry implies that the corresponding quantity is not applicable.

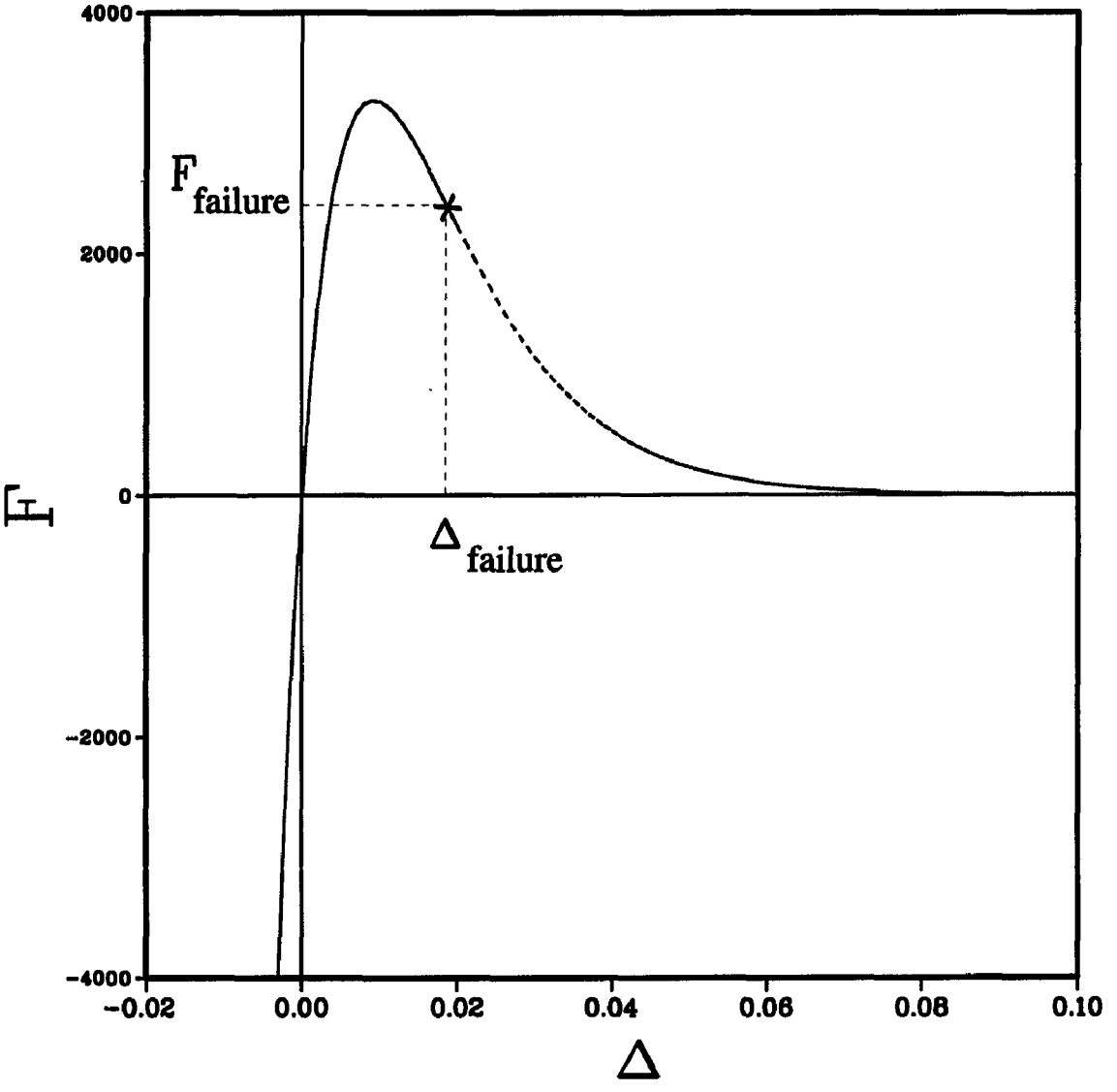

Figure 5.1: A typical force vs. displacement ($F-\Delta$) relationship used for this study. The failure in this constitutive model is defined by $\Delta_{failure}$ as marked.

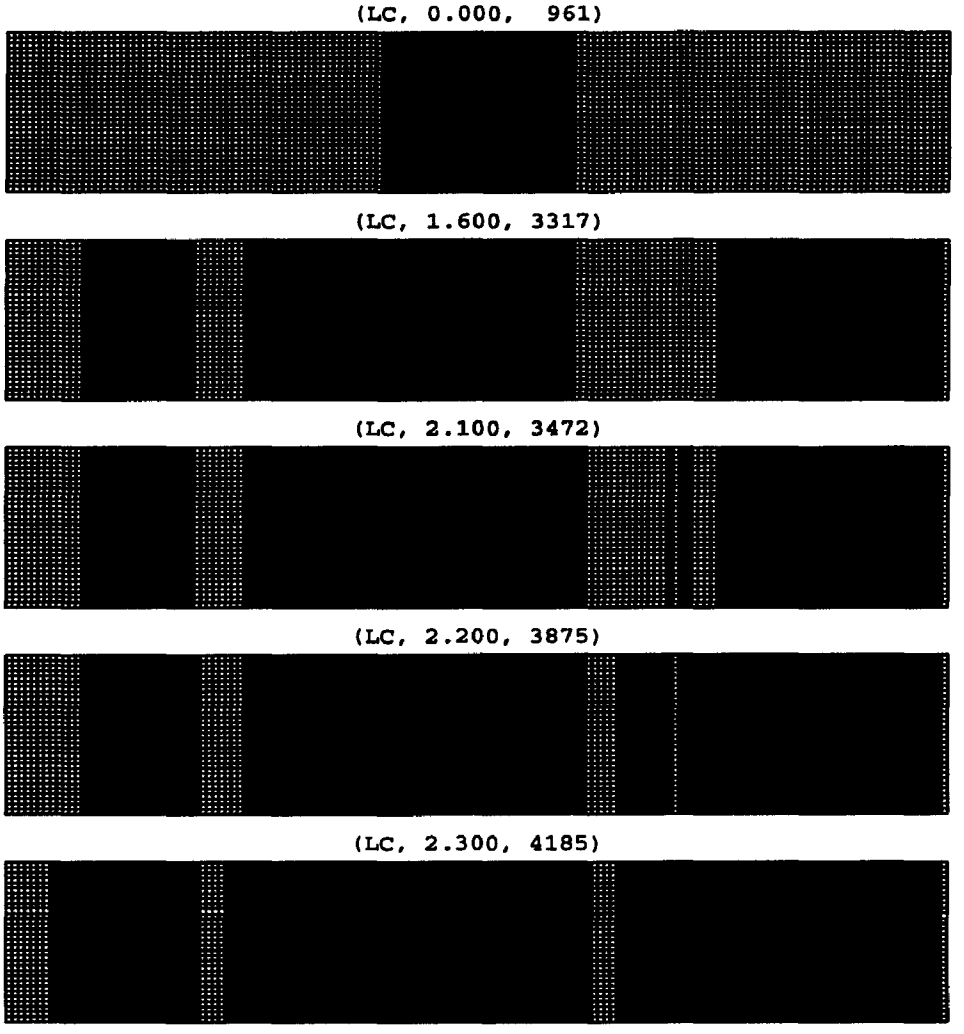

Figure 5.2: Case A: Sequence of pictures obtained from the numerical simulation showing the progression of the initially central and square delamination at different inplane load level λ. The meaning of the label on top of each picture is as follows: (LC, x, y) $\Leftrightarrow$ (Load-Control, λ, number of failed rods).

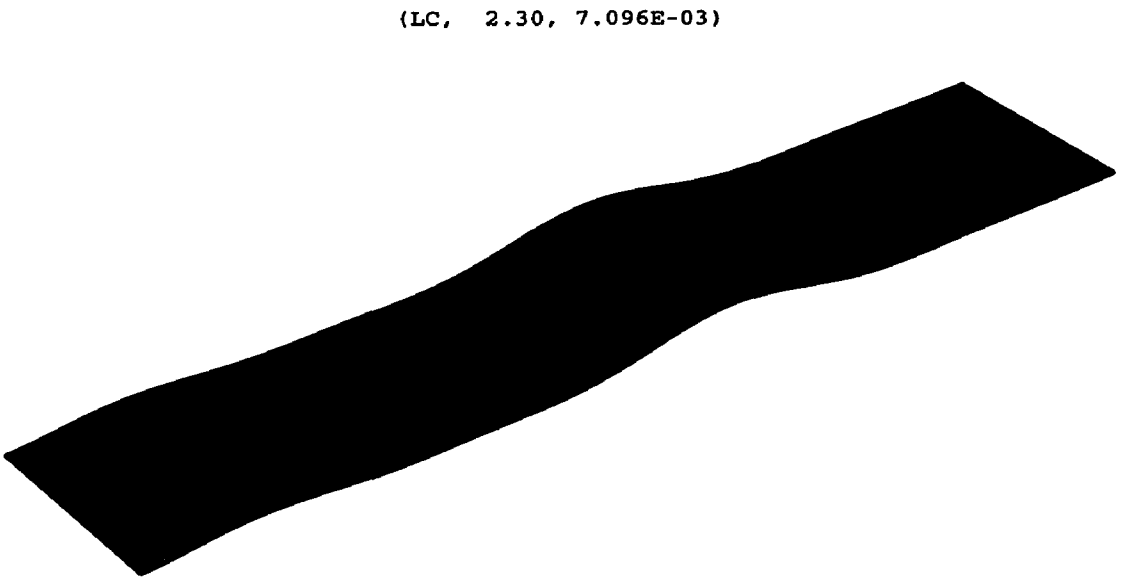

Figure 5.3: Case A: The deformed shape obtained from the numerical simulation shows the areas of greatest deformations at $\lambda = 2.3$. The meaning of the label on top of the picture is as follows: (LC, x, y) $\Leftrightarrow$ (Load-Control, λ, max. deflection (w_0^{max})).

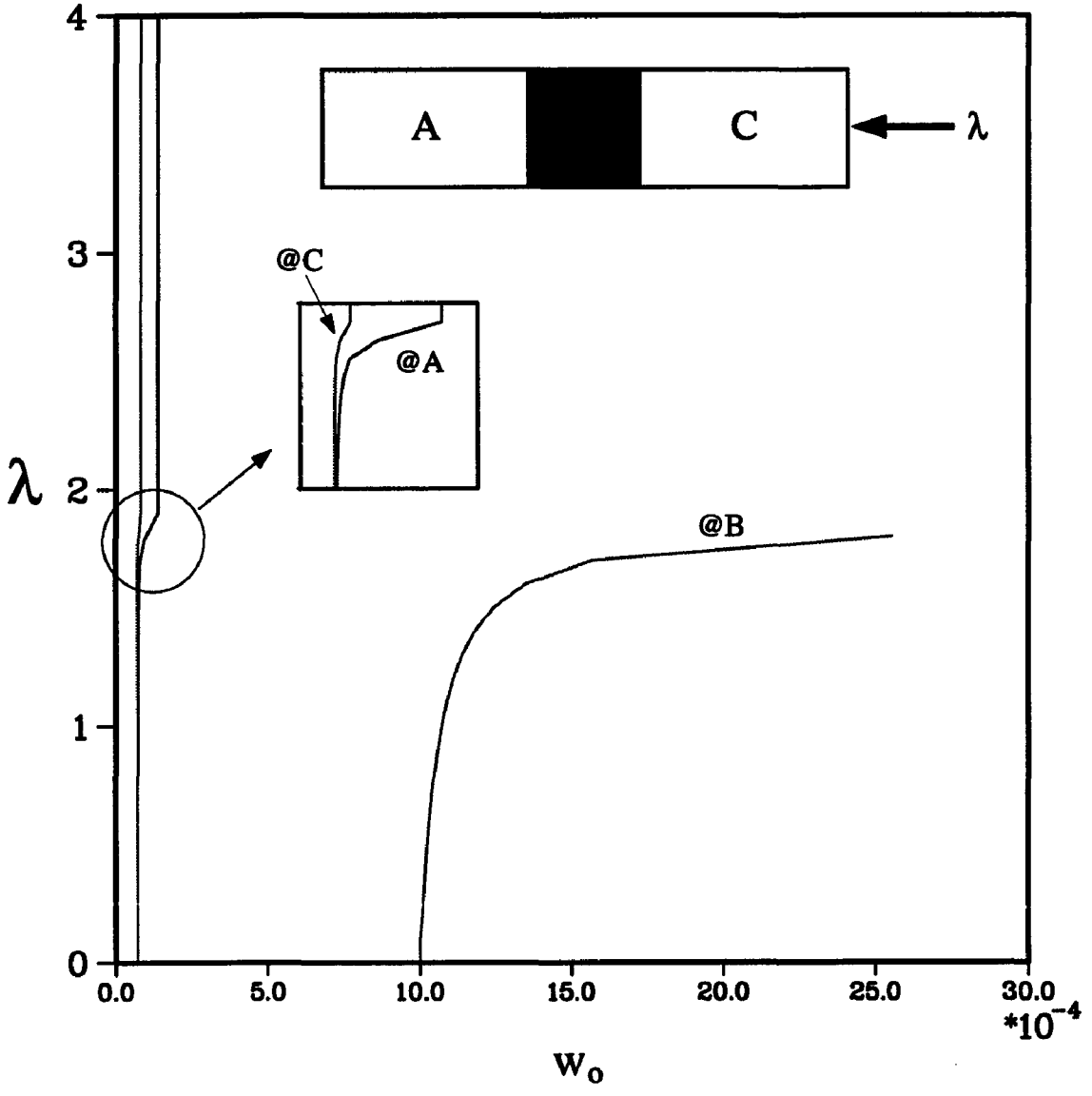

Figure 5.4: Case A: Postbuckling response curves showing the load λ vs. the transverse deflection w_0 at the three different points A, B and C. Point C is the closest to the loaded edge. Note that w_0 at points A and C remained almost constant beyond $\lambda \approx 1.9$.

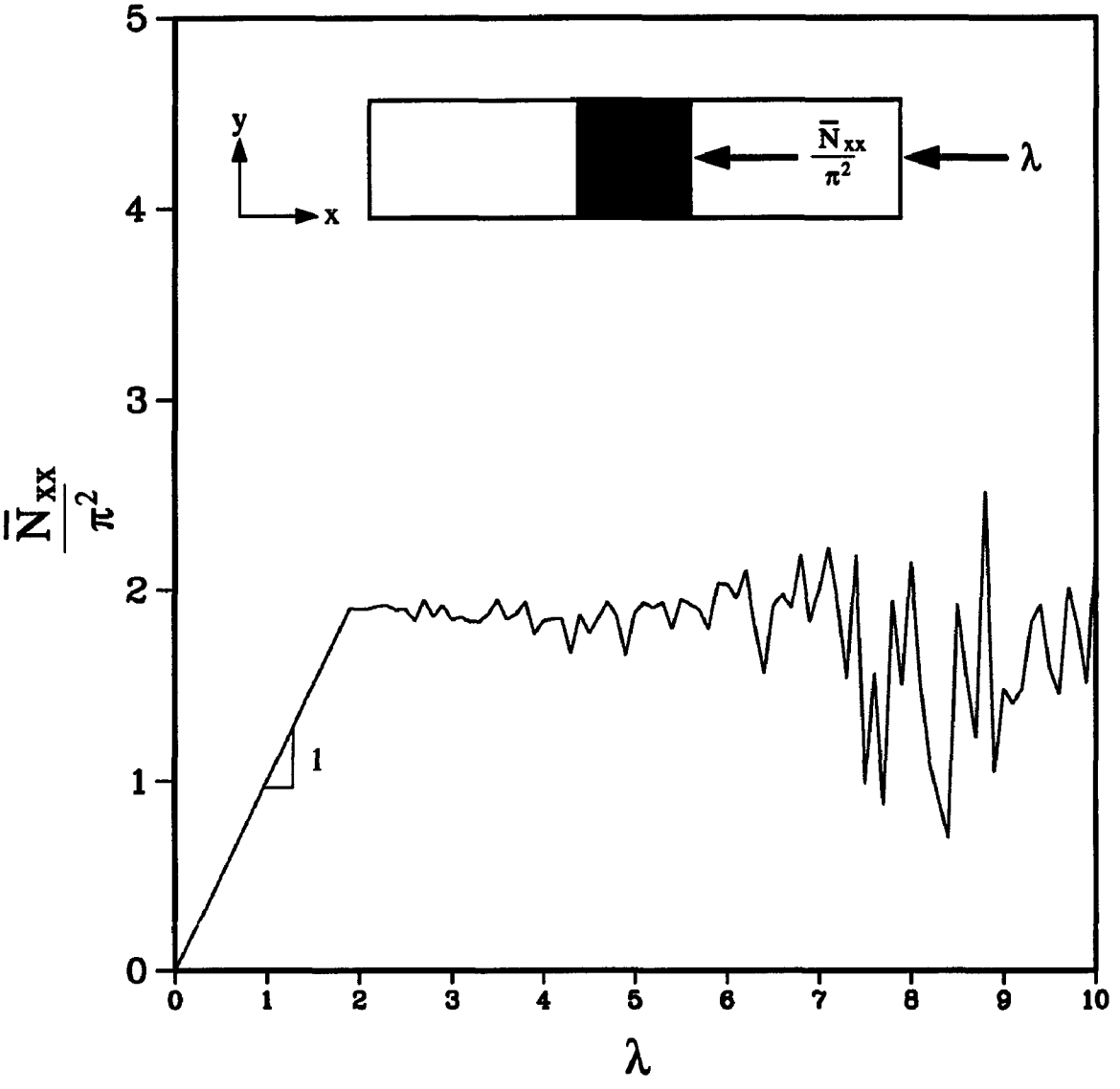

Figure 5.5: Case A: Average plate axial force $\bar{N}_{xx}$ at the delamination front vs. the applied edge load λ. $\bar{N}_{xx}$ is normalized by π^2 for convenience. Note that up to $\lambda \approx 1.9$ the two quantities were identical, implying that the plate was carrying all the load. Beyond that, the applied load was strongly shared by the interphase layer.

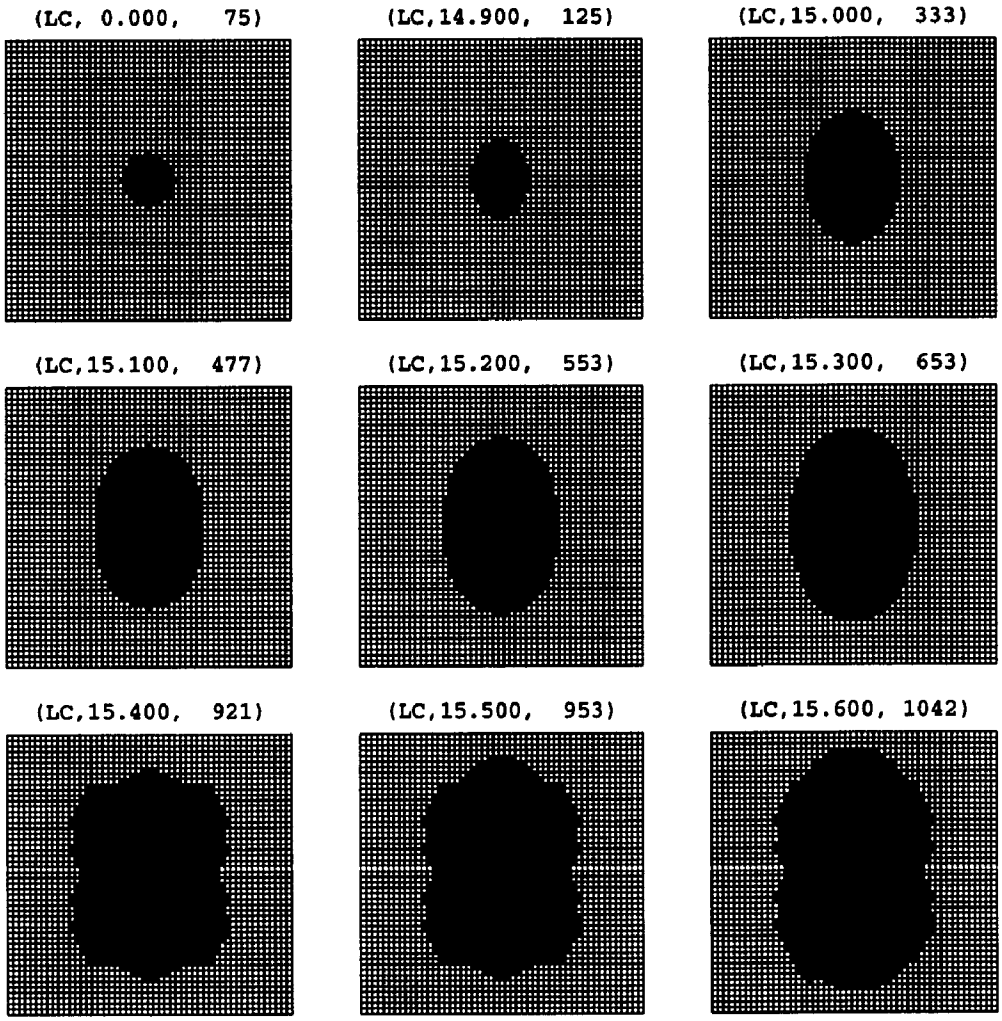

Figure 5.6: Case B: Sequence of pictures obtained from the numerical simulation showing the progression of an initially central and circular delamination at different inplane load level λ.

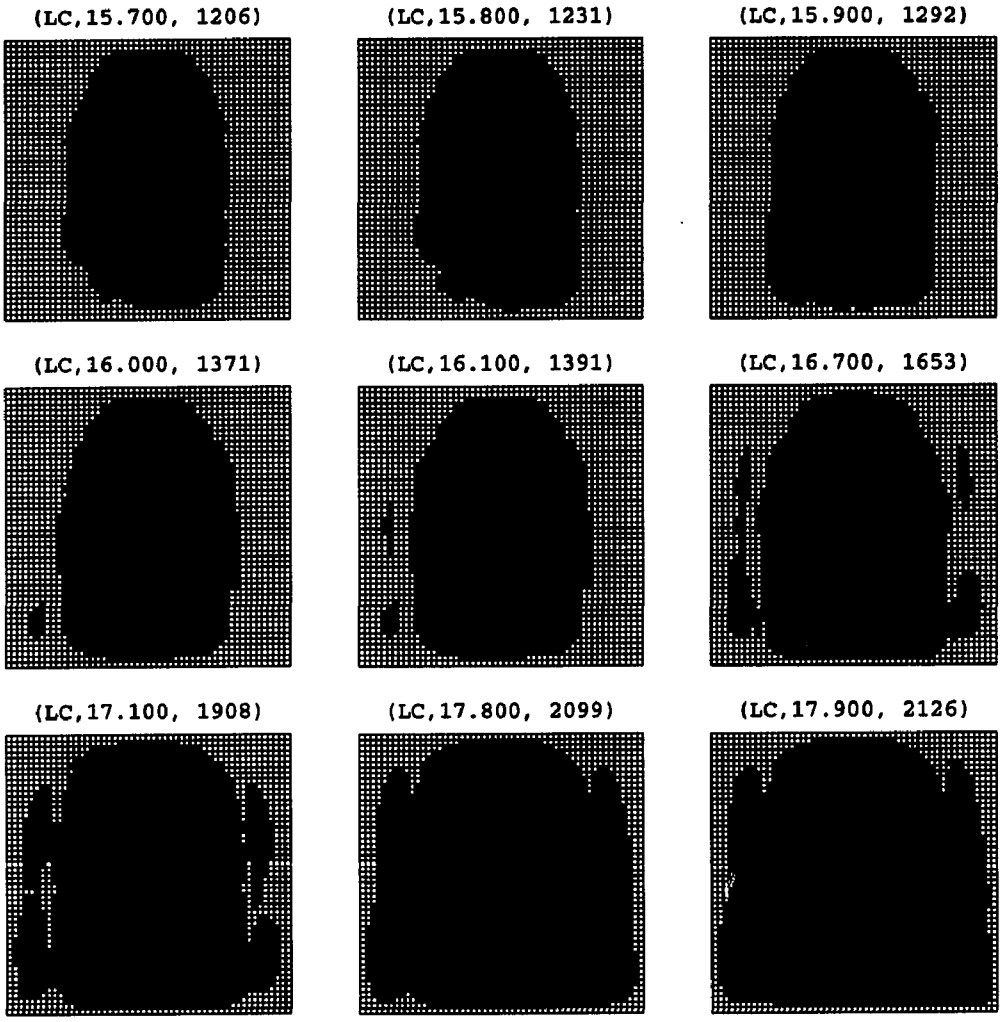

Figure 5.7: Case B: Sequence of pictures (cont'd) showing the progression of the delamination for $\lambda \geq 15.7$ leading to $\approx 82\%$ total delamination area at $\lambda = 17.9$.

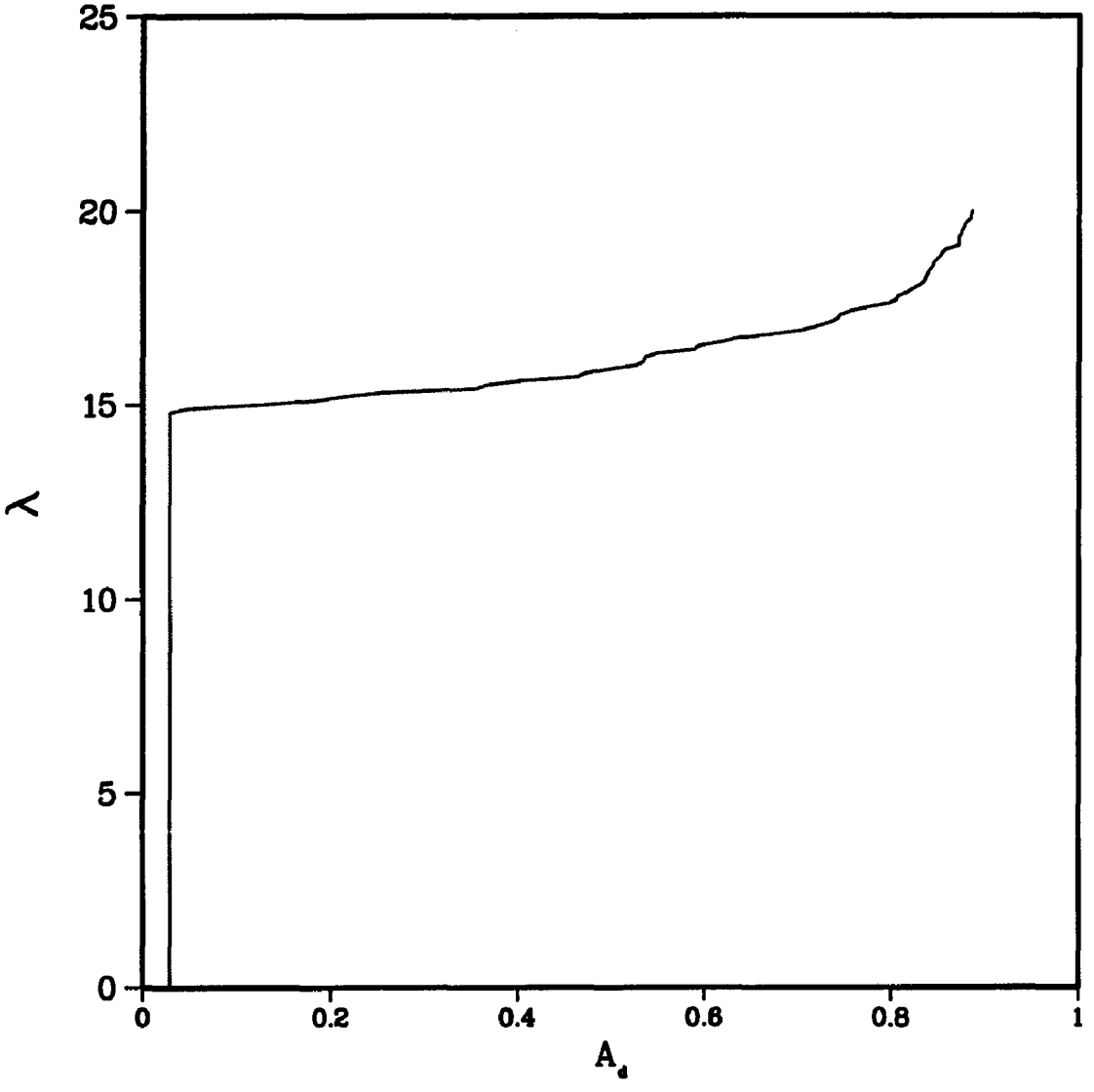

Figure 5.8: Case B: λ vs. delamination area (A_d).

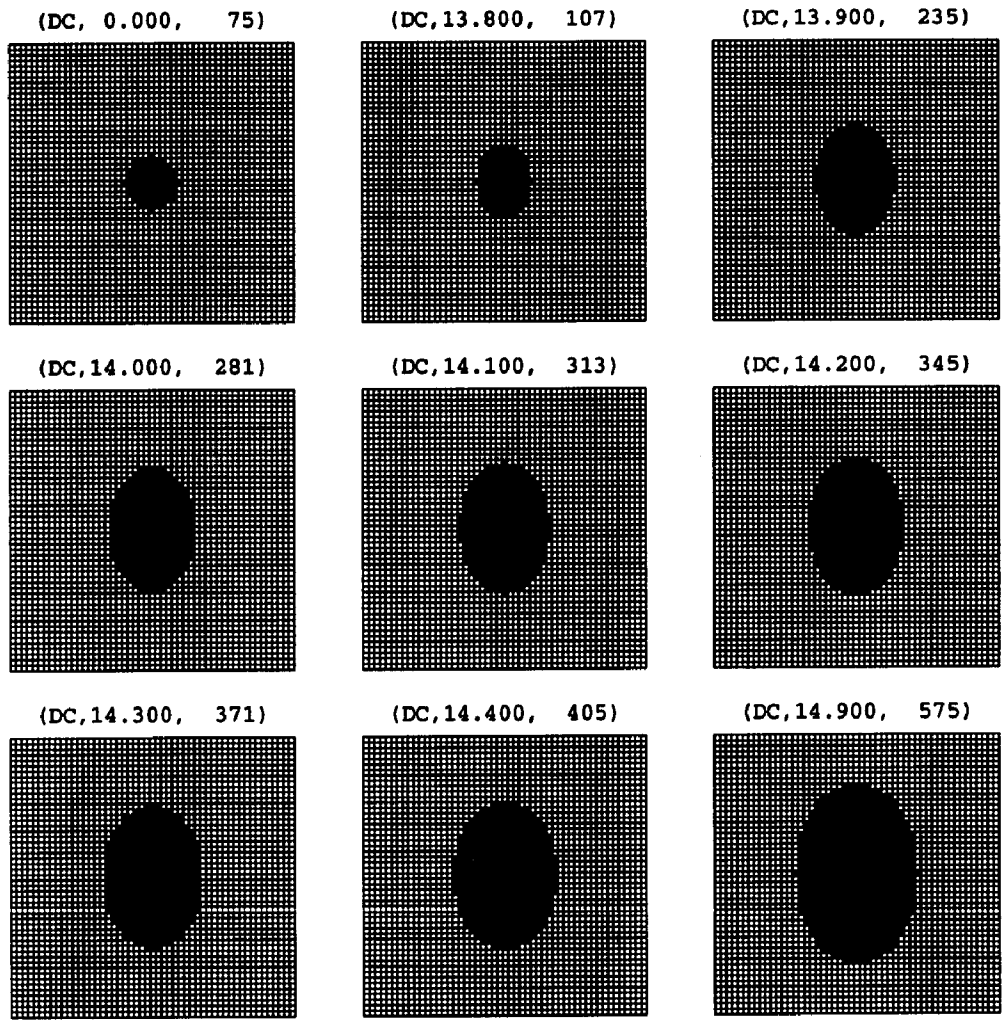

Figure 5.9: Case C: Sequence of pictures obtained from the numerical simulation showing the progression of an initially central and circular delamination at different inplane load level λ. The meaning of the label on top of each picture is as follows: (DC, x, y) $\Leftrightarrow$ (Displacement-Control, λ, number of failed rods).

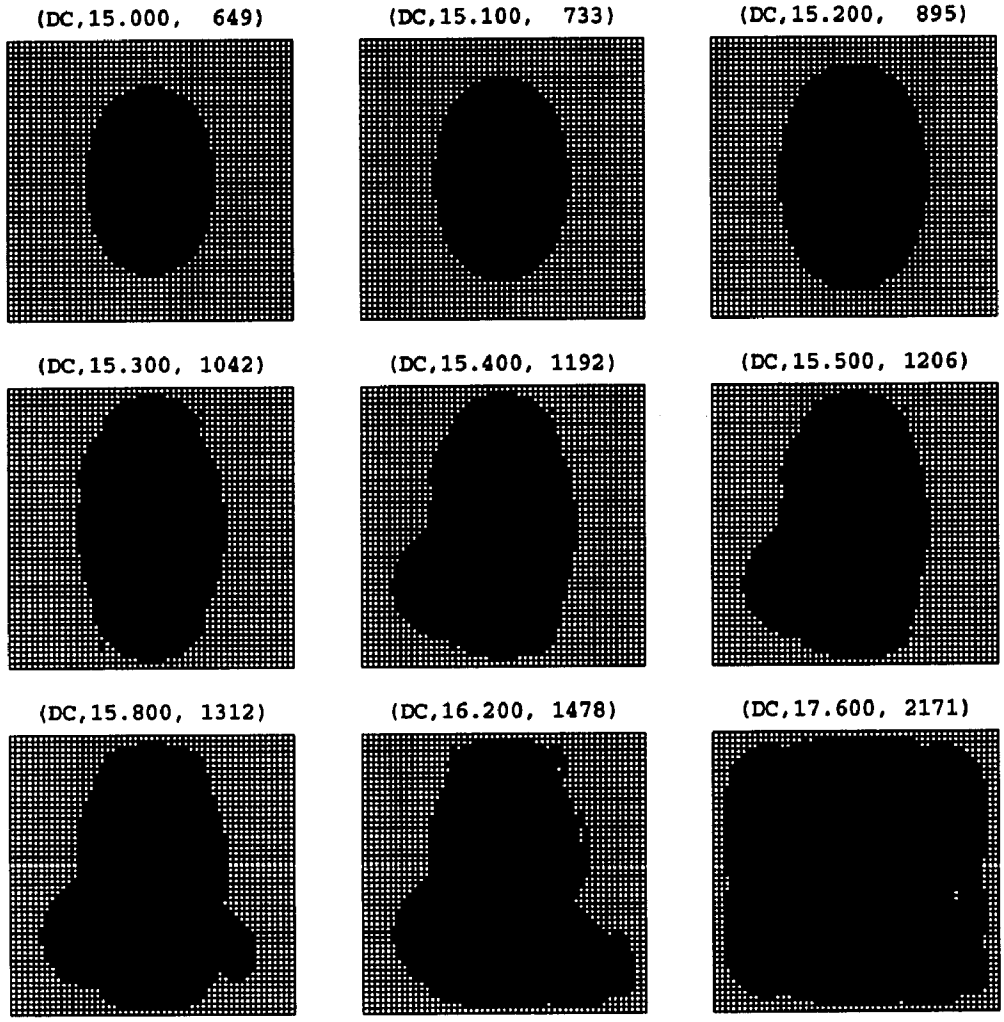

Figure 5.10: Case C: Sequence of pictures (cont'd) showing the progression of the delamination for $\lambda \geq 15.0$ leading to $\approx 83\%$ total delamination area at $\lambda = 17.6$.

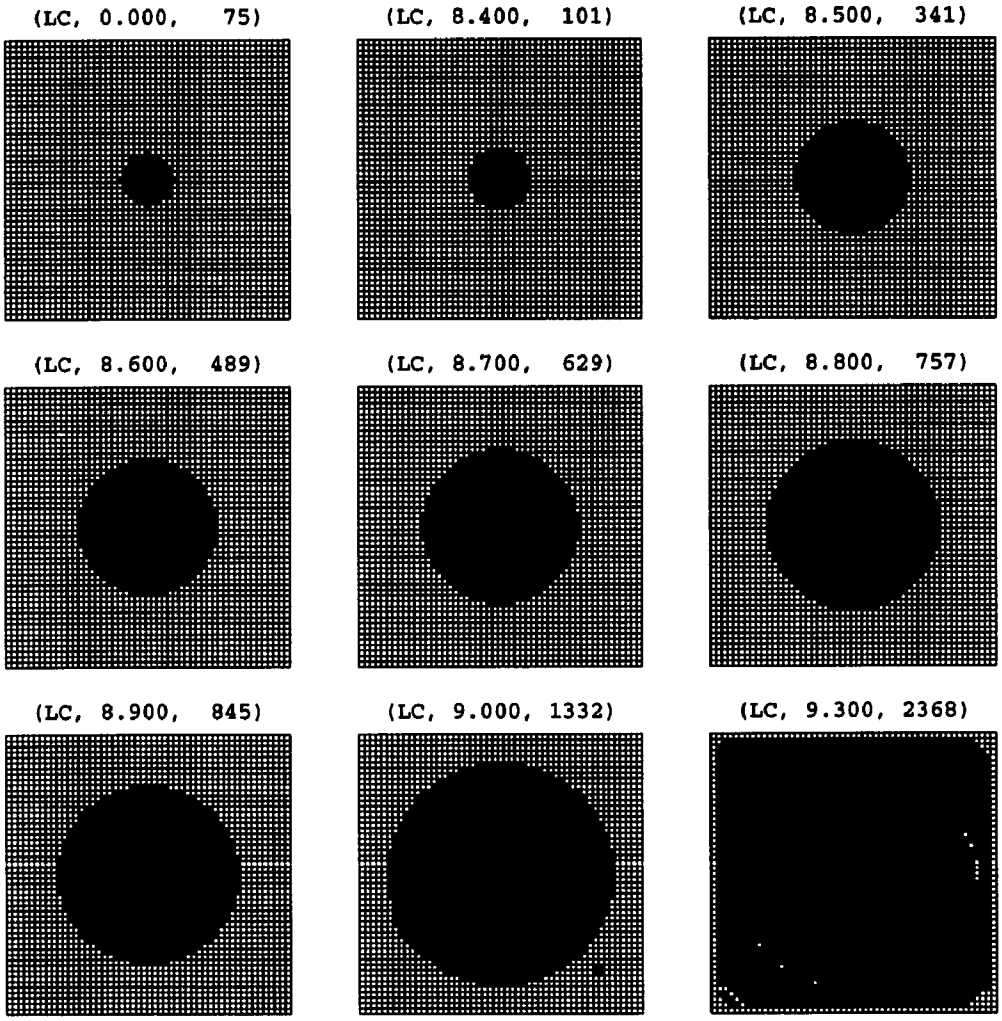

Figure 5.11: Case D: Sequence of pictures obtained from the numerical simulation showing the progression of an initially central and circular delamination at different inplane load level λ.

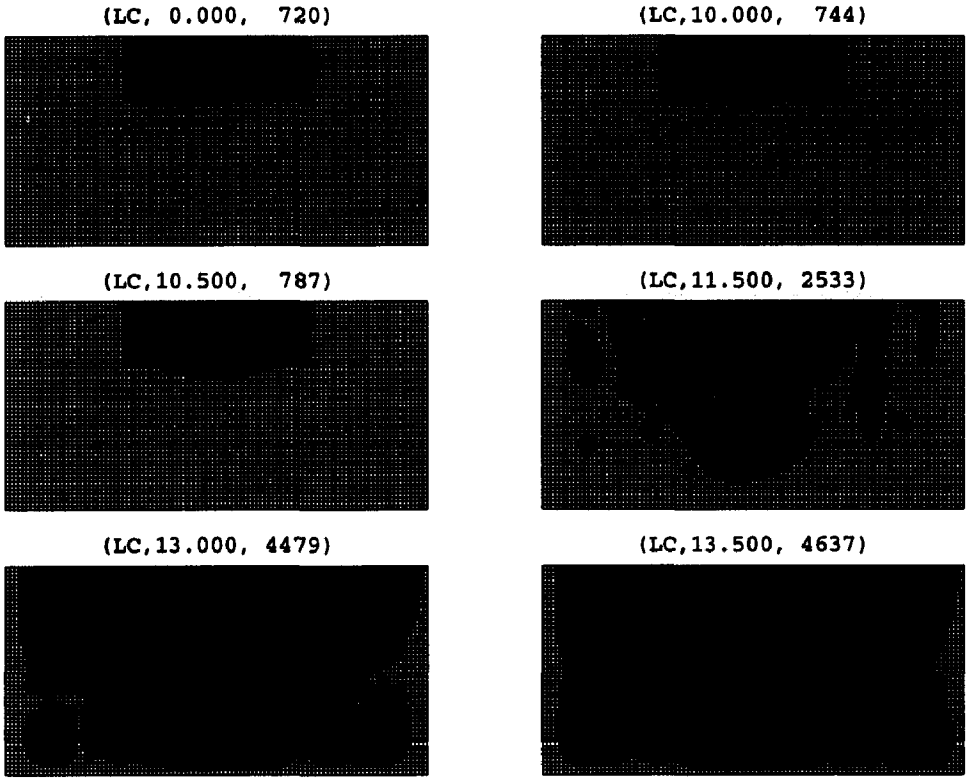

Figure 5.12: Case E: Sequence of pictures obtained from the numerical simulation showing the progression of an edge (rectangular) delamination at different inplane load level λ.

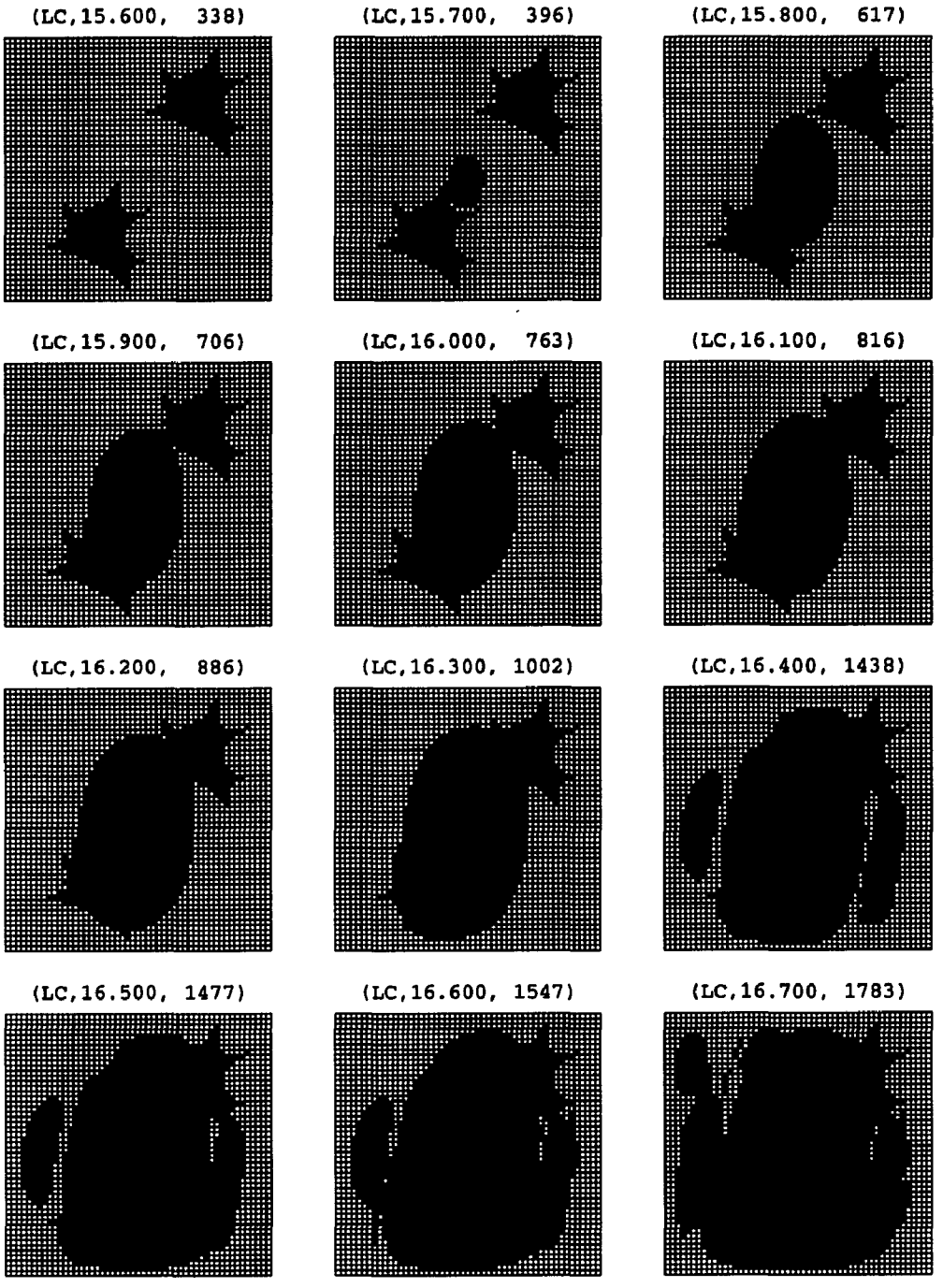

Figure 5.13: Case F: Sequence of pictures obtained from the numerical simulation showing the progression of two arbitrary shaped delaminations at different inplane load level λ.

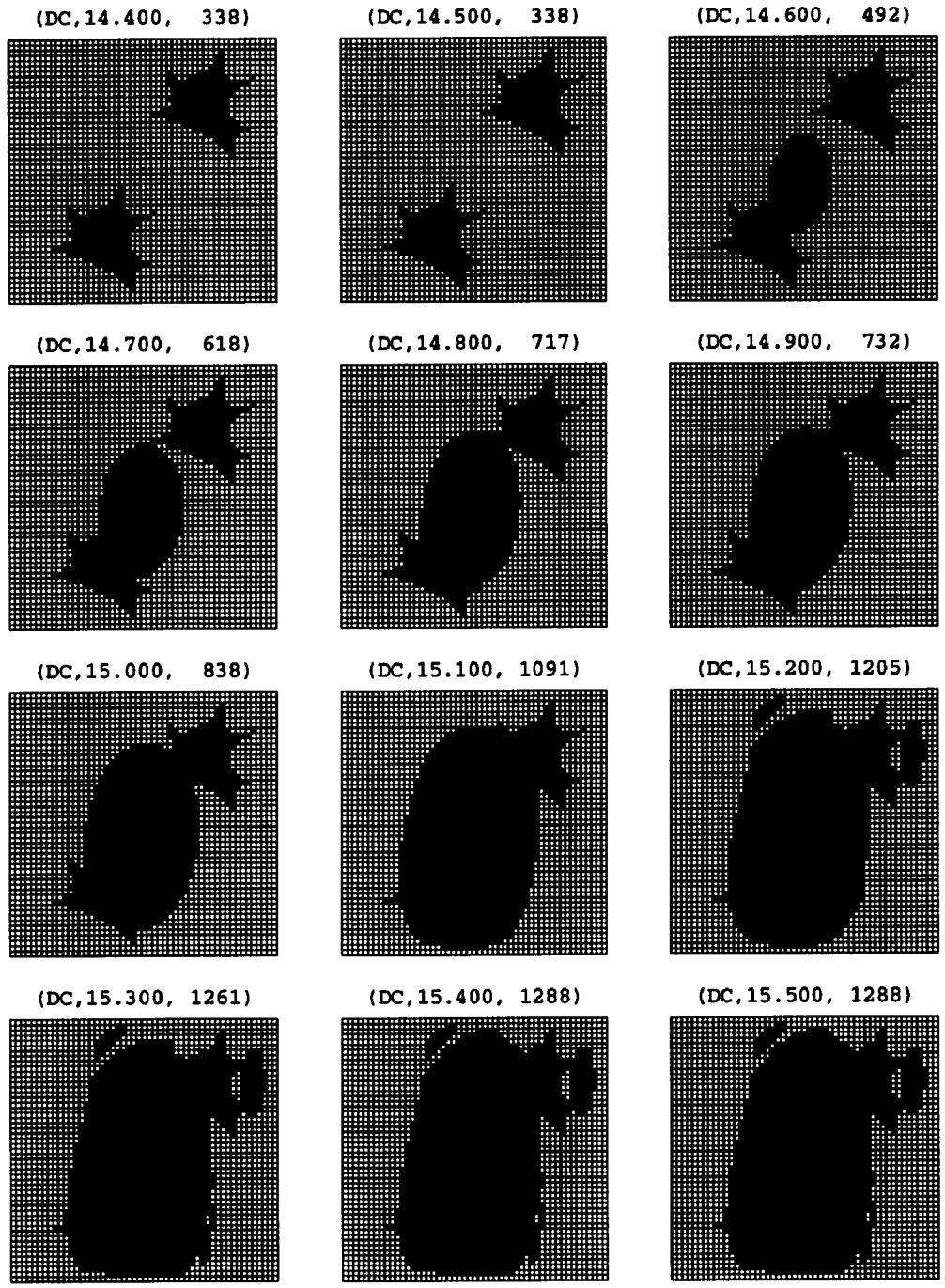

Figure 5.14: Case G: Sequence of pictures obtained from the numerical simulation showing the progression of two arbitrary shaped delaminations at different inplane displacement level λ.

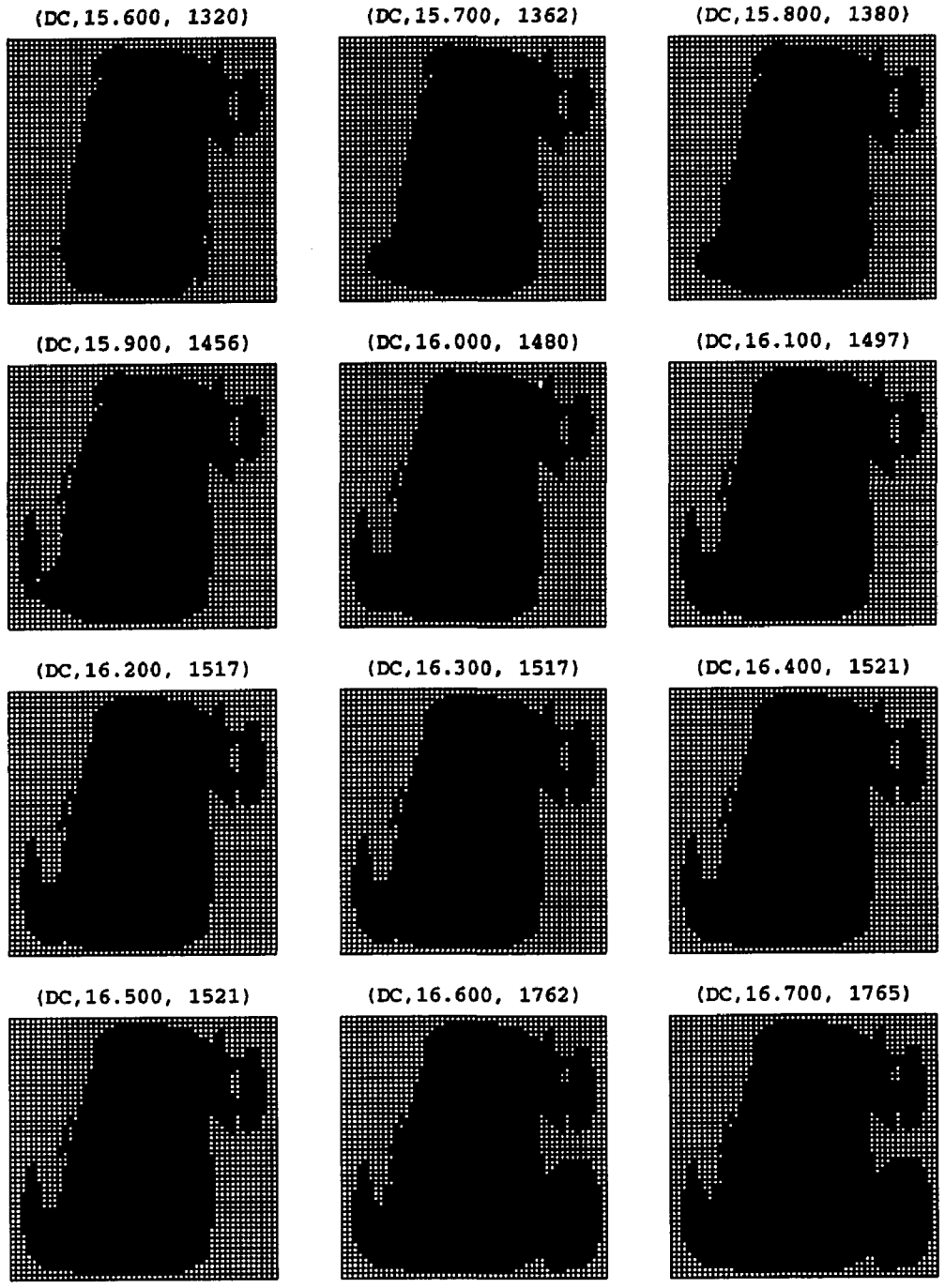

Figure 5.15: Case G: Sequence of pictures (cont'd) showing the progression of the two arbitrary shaped delamination areas.

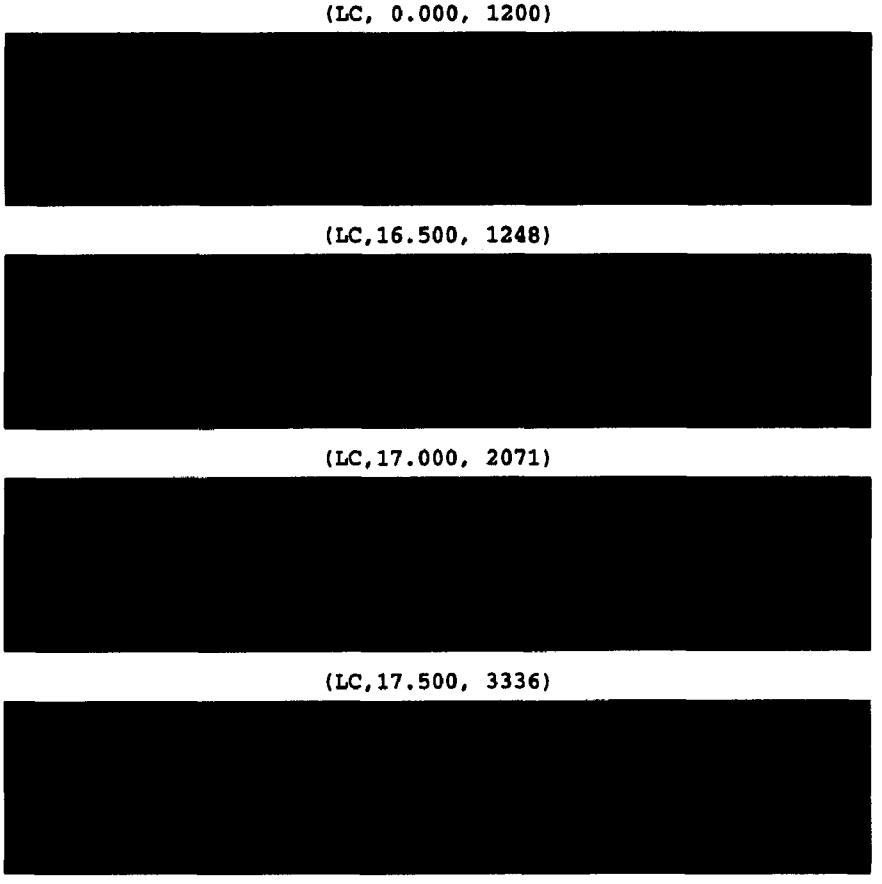

Figure 5.16: Case H: Sequence of pictures obtained from the numerical simulation showing the progression of an edge (rectangular) delamination at different inplane load level λ.

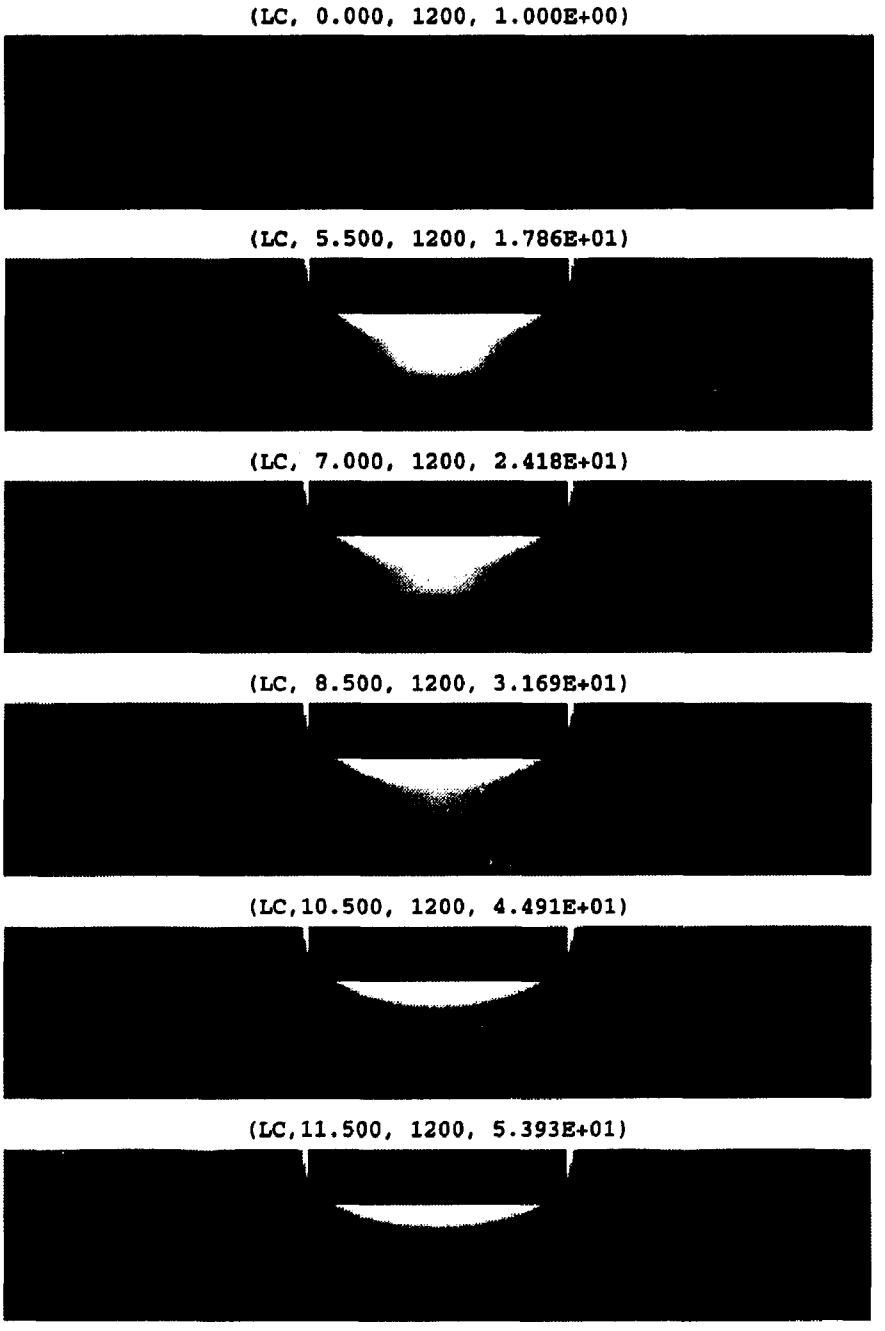

Figure 5.17: Case H: Sequence of pictures obtained from the numerical simulation showing the distribution of forces in the interphase elements (rods) at different inplane load level λ. The meaning of the label on top of the picture is as follows: (LC, x, y, z) $\Leftrightarrow$ (Load-Control, λ, number of failed rods, max. force).

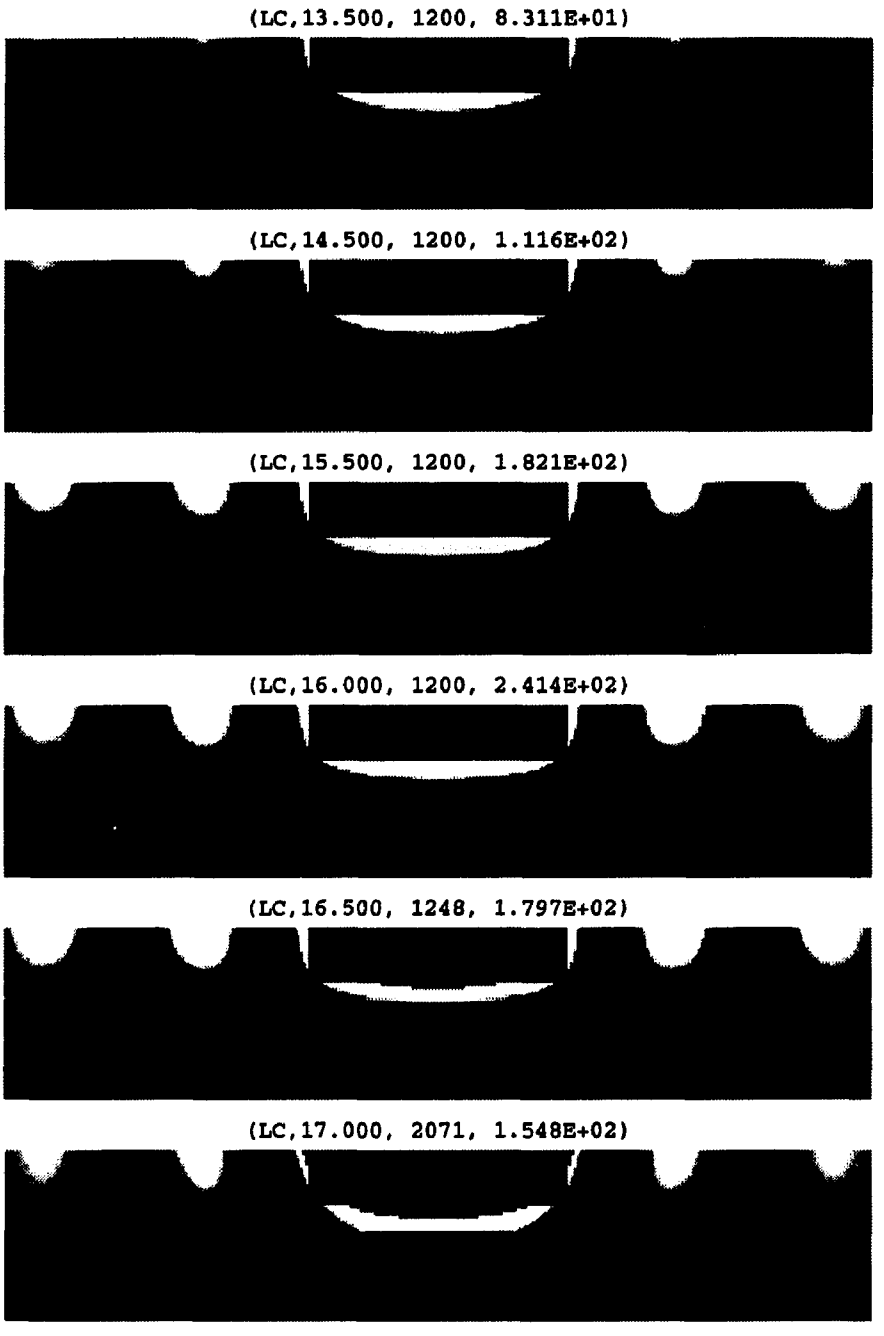

Figure 5.18: Case H: Sequence of pictures (cont'd) showing the distribution of forces in the interphase elements (rods).

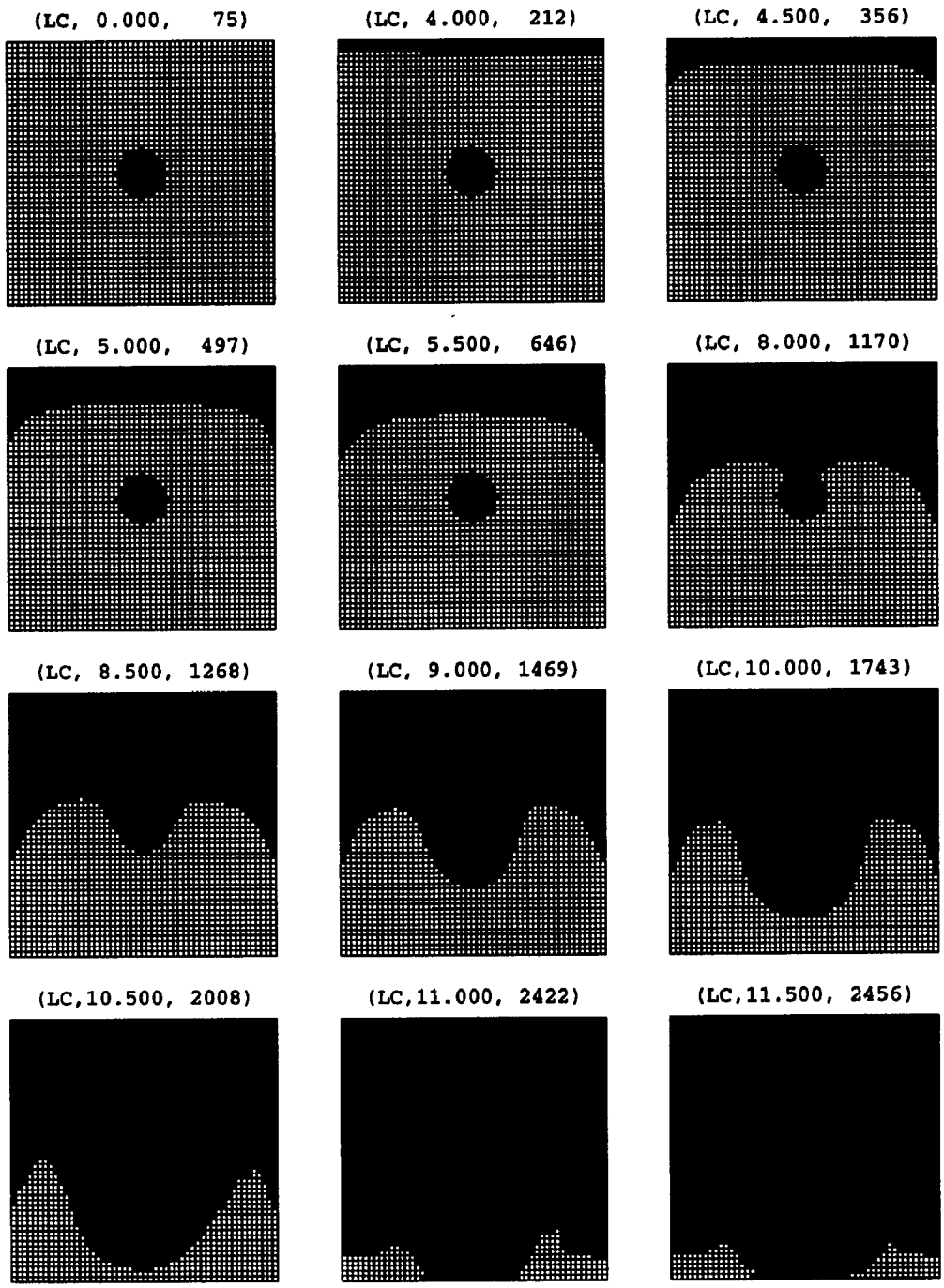

Figure 5.19: Case I: Sequence of pictures obtained from the numerical simulation showing the progression of an initially central and circular delamination area at different inplane load level λ.

CHAPTER VI

SUMMARY AND CONCLUSIONS

This chapter presents a brief summary along with the main conclusions of this study. To keep this chapter short, all issues pertaining to a particular subject were discussed and explained in detail in the corresponding chapters presented earlier.

This dissertation presented a study on the subject of buckling, postbuckling and non-self-similar decohesion of unilaterally constrained delaminations in composites. This subject involves many important issues that arise in a variety of different fields in mechanics. These issues have been the subject of intense studies and investigations for the past 15-20 years and no study thus far has "closed the chapter" on any of these issues. The present thesis attempted to treat these issues as one. Such an attempt was the main contribution of this dissertation. These issues are:

1. *How does one determine the delamination behavior when contact is involved? In other words, how would the presence of a unilateral constraint influence the buckling and postbuckling behavior, growth criteria, and the shape of the delamination front?*

2. *How does one determine the decohesion and growth criteria? In other words, at what point in the loading (deformation) history would the delamination front move?*

3. *How does one determine the delamination front contour? In other words, after the decohesion criteria have been met, what would the new delamination zone look like?*

6.1 Buckling of Unilaterally Constrained Plates

The unilateral constraint issue as related to the buckling of rectangular plates was investigated in two different contexts. First, buckling of unilaterally constrained infinite plates was considered in Chapter II. Different boundary conditions and material properties (isotropic and specially orthotropic) were considered and, assuming a periodic response, the governing equations were solved exactly and approximately depending on the boundary conditions along the infinite direction. This chapter focused on finding the buckling loads when the buckling mode is constrained to be of one sign. The condition of contact at buckling which renders the problem to be of the nonlinear eigenvalue type was bypassed by modeling the system as a plate resting on a tensionless elastic foundation. By formulating the problem as having two distinct regions, a contacted and an uncontacted regions, resulted in a problem of the linear eigenvalue type. Due to the constraint on the deformation being one-sided, an increase in the buckling load of (i) $22-33\%$ for the case of simple supports and (ii) $24-36\%$ for the case of clamped-free supports, over the unconstrained situation, was obtained for such cases.

The second context in which the buckling of unilaterally constrained rectangular plates was investigated pertains to finite plates. This was investigated in Chapter III where the problem, which is in a rectangular domain, was formulated and solved for different boundary conditions and material properties. The governing equations were solved approximately for a wide variety of parameters and general, useful and

practical results were obtained. As a check on the validity of such results, the buckling loads for infinite plates obtained in Chapter II were obtained again as the limiting cases when the aspect ratio of the finite plates was taken to be large. The results of this chapter demonstrated that using nonlinear elastic foundation models to model unilateral constraints is viable.

Experimental investigation has further revealed that the buckling mode of the delamination (plate) may involve regions or points of contact with the undelaminated portion of the substrate. The effect of this physical constraint was shown to cause the response of the plate to occur in a progressive fashion. The shadow Moiré technique that was employed was able to clearly show that the mode shape for relatively long plates (aspect ratio = 5) was periodic and contained points and/or regions of contact. The results obtained from the theoretical investigation were found to bound the experimental values. It is clear that the stiffness of a postbuckled delaminated plate is highly influenced by whether the buckled portion involves points (or regions) of contact or not. Thus, in analytical model development, the possibility of the delaminated portion contacting the plate cannot be excluded. Instead, the corresponding buckling problem must be addressed within this wider setting that incorporates the possibility of contact. The resulting boundary value problem solution should then deliver the result whether contact occurs or not.

6.2 Decohesion of Delaminations

The main contribution of this work resides in modeling decohesion of delaminations. Chapter IV presented a simplified treatment on the subject where the three aspects, namely, unilaterally constrained buckling, postbuckling and non-self-similar growth are accounted for simultaneously. Replacing the interface by a nonlinear elas-

tic interphase only the mechanical properties (stiffness, thickness, etc.) was required to fully characterize the decohesion process without resorting to any fracture mechanics concepts. Such a modeling technique was employed to overcome the limitations of fracture mechanics approaches in predicting general delamination growth. Using virtual work formulation, the plate-interphase-substrate system was modeled as one, resulting in a system of integral equations that was solved using an approximate method.

Further, during the formulation no distinction was made between the phenomena of buckling (and postbuckling) and non-self-similar growth. In other words, the same equations govern the entire behavior from beginning (starting to load/displace the structure) to end (complete delamination and/or loss of stiffness) without specification to certain regimes of validity. The entire decohesion process was assumed to be conservative.

The cases presented in Chapter V are few and their choice was based solely on the fact that they demonstrate the validity, applicability and generality of the interphase model as well as the modeling presented in Chapter IV. Although there is a large number of parameters that can be varied, only few were actually varied. This is mainly due to two reasons: 1) The main intention of the study was to demonstrate that such a model and formulation are viable, and 2) the number of combinations of these parameters needed to carry a comprehensive parametric study is prohibitive. The main distinction between the cases investigated was the type of loading (i.e., load control vs. displacement control), plate's aspect ratio and the shape and location of the original delamination. One case study investigated the effect of transverse shear deformations on the decohesion process.

The results of the case studies demonstrated the generality and simplicity of the

model as well as the formulation. One important thing to note is that these results are in *qualitative* not *quantitative* agreement with commonly observed experimental results as well as engineering intuition. That is because only a limited amount of quantitative results exist in the available literature.

6.3 Main Conclusions

To summarize, the main conclusions are:

- Using nonlinear elastic foundation models to characterize unilateral constraints is viable.
- For unilaterally constrained infinite plates, the increase in the buckling loads varied between 22-36%, for the cases studied. For the isotropic simply-supported plate, the increase was 33%.
- For unilaterally constrained finite plates, the increase depends on the aspect ratio (ξ) up to ξ^* beyond which the buckling load reaches a constant.
- ξ^* depends on the overall stiffness of the plate. Stiffer plates have smaller ξ^*.
- Using interphase models to analyze delamination decohesion and growth proved to be viable.
- The cases investigated demonstrated that delamination growth can take place prior to buckling.
- Non-self-similar delamination growth patterns were simulated without resorting to fracture mechanics concepts.
- The results obtained are highly dependent on the interphase's constitutive properties indicating that realistic and actual interphase constitutive models

need to be implemented.

- Unilateral contact can occur at buckling or in the postbuckling regime, as well as prior to delamination growth or after delamination growth.

6.4 Recommendations

This study has revealed that much work needs to be done in order to accurately and correctly model the decohesion process in real materials, especially composites. Although there are few issues that were beyond the scope of this work, they are nevertheless very important to address. Hence, it is recommended that the following be considered in future studies:

- Decohesion due to shear failure, where additional shear failure criteria are incorporated into the interphase constitutive law.

- Influence of certain parameters on the buckling and decohesion processes. Parameters like, interphase layer thickness and strength, and initial delamination size and location, to mention a few.

- First-order and higher-order shear deformation effects on delamination decohesion and growth.

- Buckling and postbuckling stability analysis of local delaminations and of the global finite medium containing such delaminations.

- Interaction between the local and the global problem. The local being the delamination, and the global being the medium containing the delamination.

- Experimental characterization of interphases, and experimental validation of numerical simulations. Some preliminary work related to this issue can be

found in the work of Song [88], Song and Waas [89] as well as the references listed therein.

APPENDICES

APPENDIX A

LIMITING VALUES FOR THE BUCKLING LOAD AND WAVE LENGTH: RIGIDLY CONSTRAINED INFINITE PLATES ($\alpha = \infty$)

The two general equations that were derived earlier relating the three unknowns λ, c and Ω are shown again,

$$(1-c)\frac{\Omega}{b} = \frac{1}{\varrho_1}\arctan\left(\frac{\frac{T_3}{2\rho_1}\sinh(2\rho_1\frac{c\Omega}{b}) + \frac{T_4}{2\rho_2}\sin(2\rho_2\frac{c\Omega}{b})}{\varrho_1\left[\cosh(2\rho_1\frac{c\Omega}{b}) + \cos(2\rho_2\frac{c\Omega}{b})\right]}\right) \tag{A.1}$$

and

$$\left(\frac{\frac{T_1}{2\rho_1}\sinh(2\rho_1\frac{c\Omega}{b}) + \frac{T_2}{2\rho_2}\sin(2\rho_2\frac{c\Omega}{b})}{\varrho_2\left[\cosh(2\rho_1\frac{c\Omega}{b}) + \cos(2\rho_2\frac{c\Omega}{b})\right]}\right) =$$

$$\tan\left\{\frac{\varrho_2}{\varrho_1}\left[\arctan\left(\frac{\frac{T_3}{2\rho_1}\sinh(2\rho_1\frac{c\Omega}{b}) + \frac{T_4}{2\rho_2}\sin(2\rho_2\frac{c\Omega}{b})}{\varrho_1\left[\cosh(2\rho_1\frac{c\Omega}{b}) + \cos(2\rho_2\frac{c\Omega}{b})\right]}\right)\right]\right\} \tag{A.2}$$

Here, we show how to extract a simpler solution from these two equations for the special case of a plate resting on a rigid foundation by taking the limit as $\alpha \to \infty$. The limiting process will be carried out in several steps rather than in one step. Although the final result is the same, this way facilitates better understanding of the operations envolved. For convenience, let us define the following:

$$\epsilon = \frac{c\Omega}{b}$$

$$L_1 = \left(\frac{\frac{T_1}{2\rho_1}\sinh(2\rho_1\frac{c\Omega}{b}) + \frac{T_2}{2\rho_2}\sin(2\rho_2\frac{c\Omega}{b})}{\varrho_2\left[\cosh(2\rho_1\frac{c\Omega}{b}) + \cos(2\rho_2\frac{c\Omega}{b})\right]} \right)$$

$$L_2 = \tan\left\{ \frac{\varrho_2}{\varrho_1}\left[\arctan\left(\frac{\frac{T_3}{2\rho_1}\sinh(2\rho_1\frac{c\Omega}{b}) + \frac{T_4}{2\rho_2}\sin(2\rho_2\frac{c\Omega}{b})}{\varrho_1\left[\cosh(2\rho_1\frac{c\Omega}{b}) + \cos(2\rho_2\frac{c\Omega}{b})\right]} \right) \right] \right\}$$

and rewrite the second general equation as follows:

$$L_1 = L_2 \tag{A.3}$$

Recall that

$$\rho_1 = \left(\frac{\pi}{2}\right)\sqrt{2\left(\sqrt{\alpha + \mu D_{22}}\right) - (\lambda - 2\eta D_s)} \tag{A.4}$$

$$\rho_2 = \left(\frac{\pi}{2}\right)\sqrt{2\left(\sqrt{\alpha + \mu D_{22}}\right) + (\lambda - 2\eta D_s)} \tag{A.5}$$

$$\varrho_1 = \left(\frac{\pi}{2}\right)\sqrt{2(\lambda - 2\eta D_s) - \sqrt{4(\lambda - 2\eta D_s)^2 - 16\mu D_{22}}} \tag{A.6}$$

$$\varrho_2 = \left(\frac{\pi}{2}\right)\sqrt{2(\lambda - 2\eta D_s) + \sqrt{4(\lambda - 2\eta D_s)^2 - 16\mu D_{22}}} \tag{A.7}$$

The limiting process starts by calculating the relation between the roots ρ_1, ρ_2 and α as α becomes large. ρ_1 and ρ_2 can be written as follows:

$$\rho_{1,2} = \left(\frac{\pi}{2}\right)\sqrt{2\sqrt{\alpha}\left(\sqrt{1+\mu\frac{D_{22}}{\sqrt{\alpha}}}\right) \mp \sqrt{\alpha}\left(\frac{\lambda}{\sqrt{\alpha}} - 2\eta\frac{D_s}{\sqrt{\alpha}}\right)}$$
$$= \left(\frac{\pi}{2}\right)\sqrt{2}\left(\alpha^{\frac{1}{4}}\right)\sqrt{\sqrt{1+\mu\frac{D_{22}}{\sqrt{\alpha}}} \mp \left(\frac{\lambda}{2\sqrt{\alpha}} - \eta\frac{D_s}{\sqrt{\alpha}}\right)}$$

For large α,

$$\rho_{1,2} \rightarrow \left(\frac{\pi}{2}\right)\sqrt{2}\left(\alpha^{\frac{1}{4}}\right)$$

which implies that the two roots, ρ_1 and ρ_2 approach each other. Let

$$\rho = \left(\frac{\pi}{2}\right)\sqrt{2}\left(\alpha^{\frac{1}{4}}\right)$$

and rewriting L_1 and L_2 yields;

$$L_1 = \left\{\frac{\frac{T_1}{2\rho}\sinh(2\rho\epsilon) + \frac{T_2}{2\rho}\sin(2\rho\epsilon)}{\varrho_2\left[\cosh(2\rho\epsilon) + \cos(2\rho\epsilon)\right]}\right\}$$

$$L_2 = \tan\left\{\frac{\varrho_2}{\varrho_1}\left[\arctan\left(\frac{\frac{T_3}{2\rho}\sinh(2\rho\epsilon) + \frac{T_4}{2\rho}\sin(2\rho\epsilon)}{\varrho_1\left[\cosh(2\rho\epsilon) + \cos(2\rho\epsilon)\right]}\right)\right]\right\}$$

where for large α

$$T_1 \rightarrow \varrho_1^2 + 2\rho^2$$

$$T_2 \rightarrow \varrho_1^2 - 2\rho^2$$

$$T_3 \rightarrow \varrho_2^2 + 2\rho^2$$

$$T_4 \rightarrow \varrho_2^2 - 2\rho^2$$

Dividing both sides by 2ρ yields;

$$\begin{aligned}
\frac{T_1}{2\rho} &\to \frac{\varrho_1^2}{2\rho} + \rho \\
\frac{T_2}{2\rho} &\to \frac{\varrho_1^2}{2\rho} - \rho \\
\frac{T_3}{2\rho} &\to \frac{\varrho_2^2}{2\rho} + \rho \\
\frac{T_4}{2\rho} &\to \frac{\varrho_2^2}{2\rho} - \rho
\end{aligned}$$

Substituting the above expressions into L_1 and dividing by $\cosh(2\rho\epsilon)$ yields;

$$L_1 = \frac{\left(\frac{\varrho_1^2}{2\rho} + \rho\right)\tanh(2\rho\epsilon) + \left(\frac{\varrho_1^2}{2\rho} - \rho\right)\frac{\sin(2\rho\epsilon)}{\cosh(2\rho\epsilon)}}{\varrho_2\left[1 + \frac{\cos(2\rho\epsilon)}{\cosh(2\rho\epsilon)}\right]} \tag{A.8}$$

and for large values of α, L_1 approaches the following limit:

$$L_1 \to \frac{\rho}{\varrho_2}$$

where we have used the facts that (recall that ϱ_1 and ϱ_2 are independent of α)

$$\begin{aligned}
\lim_{\alpha\to\infty} \frac{\rho\sin(2\rho\epsilon)}{\cosh(2\rho\epsilon)} &= 0 \\
\lim_{\alpha\to\infty} \frac{\cos(2\rho\epsilon)}{\cosh(2\rho\epsilon)} &= 0 \\
\lim_{\alpha\to\infty} \tanh(2\rho\epsilon) &= 1
\end{aligned}$$

and

$$\lim_{\alpha\to\infty} \frac{\varrho_1^2}{2\rho} = 0$$

Performing similar steps on L_2 one arrives at the following limit:

$$L_2 \rightarrow \tan\left[\frac{\varrho_2}{\varrho_1}\arctan\left(\frac{\rho}{\varrho_1}\right)\right]$$

The above result can be further simplified by realizing the fact that for large α

$$\arctan\left(\frac{\rho}{\varrho_1}\right) = \arctan\left(\frac{\left(\frac{\pi}{2}\right)\sqrt{2}\left(\alpha^{\frac{1}{4}}\right)}{\varrho_1}\right) \rightarrow \pm(2n-1)\frac{\pi}{2}, \qquad n = 1,2,3,\ldots$$

hence,

$$L_2 \rightarrow \tan\left[\pm\frac{\varrho_2}{\varrho_1}(2n-1)\frac{\pi}{2}\right]$$

Substituting the above two limits of L_1 and L_2 into (A.3) yields;

$$\frac{\rho}{\varrho_2} = \tan\left[\pm\frac{\varrho_2}{\varrho_1}(2n-1)\frac{\pi}{2}\right] \tag{A.9}$$

As α is increased further (i.e., ρ is increased) the above equation can be futher simplified by using the fact that

$$\tan(\theta) = \infty \;\Rightarrow\; \theta = \pm(2j-1)\frac{\pi}{2}, \qquad j = 1,2,3,\ldots$$

which yields the following result:

$$\pm\frac{\varrho_2}{\varrho_1}(2n-1)\frac{\pi}{2} = \pm(2m-1)\frac{\pi}{2}, \qquad m = 1,2,3,\ldots$$

$$\Rightarrow \frac{\varrho_2}{\varrho_1} = \pm\frac{2m-1}{2n-1} \tag{A.10}$$

Substituting (A.6) and (A.7) into (A.10) yields;

$$\frac{\left(\frac{\pi}{2}\right)\sqrt{2\left(\lambda_{cr}-2\eta D_s\right)+\sqrt{4\left(\lambda_{cr}-2\eta D_s\right)^2-16\mu D_{22}}}}{\left(\frac{\pi}{2}\right)\sqrt{2\left(\lambda_{cr}-2\eta D_s\right)-\sqrt{4\left(\lambda_{cr}-2\eta D_s\right)^2-16\mu D_{22}}}}=\pm\frac{2m-1}{2n-1} \qquad \text{(A.11)}$$

The goal behind all of the above is to arrive at a closed-form relationship that relates the buckling load coefficient λ_{cr} to the plate's parameters. This relationship should have a form that is comparable to the previously presented upper bound[1] on λ (2.70). Such a sought-after form is

$$\lambda_{cr}=2\left(\vartheta_1\eta D_s+\sqrt{\vartheta_2+\vartheta_3\mu D_{22}}\right)$$

where ϑ_1, ϑ_2 and ϑ_3 are coefficients that need to be determined. To extract these coefficients from (A.11) one needs to solve for λ_{cr} first. Multiplying and dividing (A.11) by $\sqrt{2\left(\lambda_{cr}-2\eta D_s\right)}$ yields;

$$\sqrt{\frac{1+\sqrt{1-\frac{4\mu D_{22}}{\left(\lambda_{cr}-2\eta D_s\right)^2}}}{1-\sqrt{1-\frac{4\mu D_{22}}{\left(\lambda_{cr}-2\eta D_s\right)^2}}}}=\pm\frac{2m-1}{2n-1}$$

Upon solving for λ_{cr} one arrives at the following result:

$$\lambda_{cr}=2\left(\eta D_s+\sqrt{\vartheta\mu D_{22}}\right) \qquad \text{(A.12)}$$

where

[1]The form of the upper bound is used due to its more general nature. Recall that the lower bound's form is a special case of the upper's.

$$\vartheta_1 = 1$$

$$\vartheta_2 = 0$$

$$\vartheta_3 = \vartheta$$

and

$$\vartheta = \frac{1}{1 - \left[\frac{1 - \left(\frac{2m-1}{2n-1}\right)^2}{1 + \left(\frac{2m-1}{2n-1}\right)^2}\right]^2} \tag{A.13}$$

The quantity $(1-c)\frac{\Omega}{b}$, which is a measure of the buckling wave length, can be solved for using a similar limiting process. Hence, for the case of a plate resting (unattached) to a rigid surface the buckling half-wave length is simply given by

$$(1-c)\frac{\Omega}{b} = \frac{\pi}{2}\frac{(2n-1)}{\varrho_1} \tag{A.14}$$

Substituting for ϱ_1 from (A.6) results in the following relationship:

$$(1-c)\frac{\Omega}{b} = \frac{1}{2}\frac{(2n-1)}{\sqrt{\sqrt{\vartheta} - \sqrt{\vartheta - 1}}}(\mu D_{22})^{-\frac{1}{4}} \tag{A.15}$$

which is independent of D_s. It is important to point out that the value of $c\frac{\Omega}{b}$approaches 0[2] as α approaches ∞. Recalling the definition of $c\frac{\Omega}{b}$ [3], one finds that this is consistant with the physical situation where no penetration into the foundation is possible when the foundation is infinitely rigid.

[2]Note that $c\frac{\Omega}{b} = 0$ implies $c = 0$ not $\Omega = 0$.

[3]$c\frac{\Omega}{b}$ was defined to be half the length of the contact region.

APPENDIX B

ADMISSIBLE ONE-DIMENSIONAL STRUCTURAL DEFORMATION FUNCTIONS

Using approximate methods like the Rayleigh-Ritz or Galerkin's for solving boundary value problems requires, by definition, knowledge of the existing boundary conditions. Further, using Galerkin's method requires knowledge of the order of the differential equation governing the behavior of the system. In order to implement these methods into a numerical solver it is necessary to assume some kinematically admissible functions. In addition to the admissibility requirement, another requirement, that is also necessary when using Galerkin's method, is that the function(s) assumed must be at least differentiable to the same degree as the governing differential equation(s).

It is well established that in order to solve plate problems one can make use of the kinematically admissible fucntions derived from beam analysis (e.g., beam eigenmodes). To obtain such beam functions one typically solves the corresponding beam vibration (or buckling) problem.

In this appendix we outline the results obtained from the free-vibration analysis of beams. Two types of vibrations will be considered, axial and transverse, along with the most common types of classical boundary conditions.

Axial Deformation Functions

The differential equation governing the axial free vibration of a uniform rod is

$$E\frac{\partial^2 u}{\partial x^2} - \rho\frac{\partial^2 u}{\partial t^2} = 0 \tag{B.1}$$

where E is Young's Modulus, u is the axial deformation, ρ is the mass density (per unit volume), t is time and x is the spatial coordiante. For a rod that is constrained at one end ($x = 0$) and free at the other ($x = l$) the solution of (B.1) yields the following characteristic equation:

$$\cos\left(\omega l\sqrt{\frac{E}{\rho}}\right) = 0 \tag{B.2}$$

where l is the length of the rod and ω is the natural frequency of the system. Solving (B.2) for the natural frequencies yields:

$$\omega_j = (2j-1)\frac{\pi}{2l}\sqrt{\frac{E}{\rho}}, \qquad j = 1, 2, 3, \ldots \tag{B.3}$$

Having obtained the natural frequencies of the system one can write down the expression for the function describing the axial deformation of a constrained-free rod as

$$u(x,t) = A\phi_j(x)e^{i\omega_j t} \tag{B.4}$$

where A is the amplitude, $i = \sqrt{-1}$ and

$$\phi_j(x) = \sin\left[(2j-1)\frac{\pi}{2}\frac{x}{l}\right] \tag{B.5}$$

are the spatial functions. For the plate problems investigated it was observed that the first term (i.e., $\phi_1 = \sin\left(\frac{\pi}{2}\frac{x}{l}\right)$) gives poor results. Hence, it was decided to replace the first term ONLY by the corresponding static deformation function, which can be obtained by setting $\rho = 0$ in the original governing differential equation (B.1). Such a function is given below,

$$\phi(x) = \frac{x}{l} \tag{B.6}$$

Other admissible functions that were also used to describe the axial deformation are the simple-free beam transverse vibration modes [98] (to be presented later). Such functions are

$$\phi_j(x) = a\ \left[\sin\left(r_j\frac{x}{l}\right) + \sinh\left(r_j\frac{x}{l}\right)\right] + \sin\left(r_j\frac{x}{l}\right) - \sinh\left(r_j\frac{x}{l}\right) \tag{B.7}$$

where

$$a = \frac{\sin(r_j) + \sinh(r_j)}{\sinh(r_j) - \sin(r_j)} \tag{B.8}$$

and the eigenvalues r_j are

$$r_1 = 0.00000000000000$$

$$r_2 = 3.92660231204791$$

$$r_3 = 7.06858274562873$$

$$r_4 = 10.21017612281302$$

$$r_5 = 13.35176877775409$$

$$r_6 = 16.49336143134641$$

$$r_7 = 19.63495408493620$$

$$\vdots$$

$$r_j = (4j+1)\frac{\pi}{4}$$

Note that for small values of j ($j < 10$) the last general expression is not valid and the above numerical values must be used. It is very important to point out that the value of ϕ_j, especially at the boundaries, is highly dependent on the accuracy of the r_j values. It is customary to list only the first few values of r_j with few decimals (usually < 5 decimals) [98], but as this study revealed[1], the decimal accuracy needed to obtain valid results cannot be overemphasized. The above partial list of numerical values for r_j shows a 14-digit accuracy. For higher values of j (i.e., $j > 7$) the accuracy needed exceeded that of the machine's precision[2], hence, such values cannot be used with confidence. It is recommended that higher modes should only be used when they are essential to the analysis and should be avoided otherwise.

Transverse Deformation Functions

The differential equation governing the transverse free vibration of a uniform beam is

$$EI\frac{\partial^4 w}{\partial x^4} + m\frac{\partial^2 w}{\partial t^2} = 0 \tag{B.9}$$

where E is Young's Modulus, I is the cross-sectional moment of interia, w is the transverse deformation of the beam's center line, m is the mass density (per unit

[1]The author is not aware of any literature that emphasized the importance of the decimal accuracy needed when using such functions.

[2]The calculatios were performed on an Hewlett Packard (HP) Workstation, 9000 Series, Model 715/50 with a 50MHz PA-RISC 7100 Processor using a FORTRAN program with Double Precision accuracy.

length), t is time and x is the spatial coordinate. The general solution of (B.9) can be given in the following form:

$$w(x,t) = A\phi_j(x)e^{i\omega_j t}, \qquad j = 1,2,3,\ldots \tag{B.10}$$

where ω_j are the natural frequencies (eigenvalues). The eigenvalues and the corresponding eigenmodes of (B.9) are given below for different homogeneous boundary conditions. For each case the characteristic (frequency) equation will be presented, followed by the eigenmodes along with the corresponding eigenvalues. The following boundary conditions are considered:

Free-Free

Characteristic equation:

$$\cos(r)\ \cosh(r) = 1$$

Eigenmodes:

$$\phi_j(x) = a\ \left[\sin\left(r_j\frac{x}{l}\right) + \sinh\left(r_j\frac{x}{l}\right)\right] + \cos\left(r_j\frac{x}{l}\right) + \cosh\left(r_j\frac{x}{l}\right)$$

$$a = \frac{\cos(r_j) - \cosh(r_j)}{\sinh(r_j) - \sin(r_j)}$$

Eigenvalues:

$$r_1 = 0.00000000000000$$

$$r_2 = 0.00000000000000$$

$$r_3 = 4.73004074500006$$

$$r_4 = 7.85320462409601$$

$$r_5 = 10.99560783800137$$

$$r_6 = 14.13716549125746$$

$$r_7 = 17.27875965739947$$

$$\vdots$$

$$r_j = (2j+1)\frac{\pi}{2}$$

The first two modes correspond to rigid body motion. The first is a rigid body translation for which ϕ_1 can be given as follows:

$$\phi_1 = 1.0$$

The second is a rigid body rotation that can be expressed with respect to the point $x = 0$ or the center of mass at $x = \frac{l}{2}$. With respect to the latter, ϕ_2 can be given as follows:

$$\phi_2 = \left(1 - 2\frac{x}{l}\right)$$

Simple-Free

Characteristic equation:

$$\tan(r) = \tanh(r)$$

Eigenmodes:

$$\phi_j(x) = a\ \left[\sin\left(r_j\frac{x}{l}\right) + \sinh\left(r_j\frac{x}{l}\right)\right] + \sin\left(r_j\frac{x}{l}\right) - \sinh\left(r_j\frac{x}{l}\right)$$

$$a = \frac{\sin(r_j) + \sinh(r_j)}{\sinh(r_j) - \sin(r_j)}$$

Eigenvalues:

$$r_1 = 0.00000000000000$$

$$r_2 = 3.92660231204791$$

$$r_3 = 7.06858274562873$$

$$r_4 = 10.21017612281302$$

$$r_5 = 13.35176877775409$$

$$r_6 = 16.49336143134641$$

$$r_7 = 19.63495408493620$$

$$\vdots$$

$$r_j = (4j+1)\frac{\pi}{4}$$

The first mode corresponds to a rigid body motion. In this case this motion is a rigid body rotation that can be given as follows:

$$\phi_1 = \frac{x}{l}$$

Simple-Simple

Characteristic equation:

$$\sin(r) = 0$$

Eigenmodes:

$$\phi_j(x) = \sin\left(r_j \frac{x}{l}\right)$$

Eigenvalues:

$$r_j = j\pi$$

Clamped-Free

Characteristic equation:

$$\cos(r)\ \cosh(r) = -1$$

Eigenmodes:

$$\phi_j(x) = a\ \left[\cos\left(r_j\frac{x}{l}\right) - \cosh\left(r_j\frac{x}{l}\right)\right] + \sin\left(r_j\frac{x}{l}\right) - \sinh\left(r_j\frac{x}{l}\right)$$

$$a = \frac{-\sin(r_j) - \sinh(r_j)}{\cosh(r_j) + \cos(r_j)}$$

Eigenvalues:

$$r_1 = 1.87510406871196$$

$$r_2 = 4.69409113297417$$

$$r_3 = 7.85475743823761$$

$$r_4 = 10.99554073487547$$

$$r_5 = 14.13716839104647$$

$$r_6 = 17.27875953208823$$

$$r_7 = 20.42035225104124$$

$$\vdots$$

$$r_j = (2j-1)\frac{\pi}{2}$$

Clamped-Simple

Characteristic equation:

$$\tan(r) = \tanh(r)$$

Eigenmodes:

$$\phi_j(x) = a\ \left[\cos\left(r_j\frac{x}{l}\right) - \cosh\left(r_j\frac{x}{l}\right)\right] + \sin\left(r_j\frac{x}{l}\right) - \sinh\left(r_j\frac{x}{l}\right)$$

$$a = \frac{\sin(r_j) - \sinh(r_j)}{\cosh(r_j) - \cos(r_j)}$$

Eigenvalues:

$$r_1 = 3.92660231204791$$

$$r_2 = 7.06858274562873$$

$$r_3 = 10.21017612281302$$

$$r_4 = 13.35176877775409$$

$$r_5 = 16.49336143134641$$

$$r_6 = 19.63495408493620$$

$$r_7 = 22.77654673852600$$

$$\vdots$$

$$r_j = (4j+1)\frac{\pi}{4}$$

Clamped-Clamped

Characteristic equation:

$$\cos(r)\ \cosh(r) = 1$$

Eigenmodes:

$$\phi_j(x) = a\ \left[\cos\left(r_j\frac{x}{l}\right) - \cosh\left(r_j\frac{x}{l}\right)\right] + \sin\left(r_j\frac{x}{l}\right) - \sinh\left(r_j\frac{x}{l}\right)$$

$$a = \frac{\cos(r_j) - \cosh(r_j)}{\sin(r_j) + \sinh(r_j)}$$

Eigenvalues:

$$r_1 = 4.73004074500006$$

$$r_2 = 7.85320462409601$$

$$r_3 = 10.99560783800137$$

$$r_4 = 14.13716549125746$$

$$r_5 = 17.27875965739947$$

$$r_6 = 20.42035224562606$$

$$r_7 = 23.56194490204045$$

$$\vdots$$

$$r_j = (2j+1)\frac{\pi}{2}$$

BIBLIOGRAPHY

BIBLIOGRAPHY

[1] Allan, T., (1968), "One-Way Buckling of a Compressed Strip Under Lateral Loading," *Journal of Mechanical Engineering Science*, Vol. 10, No. 2, pp. 173-181.

[2] Ames, W. F., (1965), **Nonlinear Partial Differential Equations in Engineering**, Academic Press, pp. 243-262.

[3] Ames, W. F., (1972), **Nonlinear Partial Differential Equations in Engineering**, Vol. II, Academic Press, pp. 178-180.

[4] Anderson, W. F., (1972), "Buckling of a Strip on a Rigid Half-Space with a Transverse Pressure: Wrinkling of Non-Bonded Cladding," *Proceedings of the First International Conference on "Structural Mechanics in Reactor Technology,"* Vol. 2, Part C, pp. 123-144, Berlin, Germany.

[5] Barbero, E. J., and Reddy, J. N., (1991), "Modeling of Delamination in Composite Laminates Using a Layer-Wise Plate Theory," *International Journal of Solids and Structures*, Vol. 28, No. 3, pp. 373-388.

[6] Benson, R., (1991), "Plate Tenting with a One-Sided Constraint," *Journal of Applied Mechanics*, Vol. 58, pp. 484-492.

[7] Berger, H. M., (1955), "A New Approach to the Analysis of Large Deflections of Plates," *Journal of Applied Mechanics*, American Society of Mechanical Engineers (ASME) Trans., Vol. 22, December, pp. 465-472.

[8] Bhimaraddi, A., (1992), "Buckling and Post-Buckling Behavior of Laminated Plates Using The Generalized Nonlinear Formulation," *International Journal of Mechanical Sciences*, Vol. 34, No. 9, pp. 703-715.

[9] Bottega, W. J., (1983), "A Growth Law for Propagation of Arbitrary Shaped Delaminations in Layered Plates," *International Journal of Solids and Structures*, Vol. 19, No. 11, pp. 1009-1017.

[10] Bottega, W. J., and Maewal, A., (1983), "Delamination Buckling and Growth in Laminates," *Journal of Applied Mechanics*, Vol. 50, American Society of Mechanical Engineers (ASME) Trans., pp. 184-189.

[11] Bottega, W. J., and Maewal, A., (1983), "Dynamics of Delamination Buckling," *International Journal of Non-Linear Mechanics*, Vol. 18, No. 6, pp. 449-463.

[12] Broek, David, (1986), **Elementary Engineering Fracture Mechanics**, 4^{th} revised edition, Kluwer Academic Publishers.

[13] Broyden, C. G., (1970), "Recent Developments in Solving Nonlinear Algebraic Systems," in **Numerical Methods for Nonlinear Algebraic Equations**, edited by P. Rabinowitz, Chapter 4, Gordon and Breach, New York.

[14] Brunelle, E. J., and Oyibo, G. A., (1983), "Generic Buckling Curves for Specially Orthotropic Rectangular Plates," *American Institute of Aeronautics and Astronautics (AIAA) Journal*, August, pp. 1150-1156.

[15] Bruno, D., and Grimaldi, A., (1990), "Delamination Failure of Layered Composite Plates Loaded in Compression," *International Journal of Solids and Structures*, Vol. 26, No. 3, pp. 313-330.

[16] Burgess, I. W. (1971), "On the equilibrium and stability of discrete one-way structural systems," *International Journal of Solids and Structures*, Vol. 7, pp. 667-683.

[17] Burgess, I. W. (1971), "The buckling of a radially constrained imperfect circular ring," *International Journal of Mechanical Sciences*, Vol. 13, pp. 741-753.

[18] Celep, Z., (1988), "Rectangular Plates Resting on Tensionless Elastic Foundation," *Journal of Engineering Mechanics Division*, Proceedings of the American Society of Civil Engineers (ASCE), Vol. 114, No. 12, pp. 2083-2092.

[19] Chai, Herzl, (1990), "Three-Dimensional Fracture Analysis of Thin-Film Debonding," *International Journal of Fracture*, Vol. 46, pp. 237-256.

[20] Chai, H., (1990), "Buckling and Post-Buckling Behavior of Elliptical Plates: Part I - Analysis," *Journal of Applied Mechanics*, Vol. 57, pp. 981-988.

[21] Chai, H., (1990), "Buckling and Post-Buckling Behavior of Elliptical Plates: Part II - Results," *Journal of Applied Mechanics*, Vol. 57, pp. 989-994.

[22] Chai, H., Babcock, C., and Knauss, W. G., (1981), "One Dimensional Modeling of Failure in Laminated Plates by Delamination Buckling," *International Journal of Solids and Structures*, Vol. 17, No. 11, pp. 1069-1083.

[23] Chai, H., and Babcock, C., (1985), "Two Dimensional Modeling of Compressive Failure in Delaminated Laminates," *Journal of Composite Materials*, Vol. 19, pp. 67-98.

[24] Chia, C-Y., (1980), **Nonlinear Analysis of Plates**, McGraw-Hill Book Co., pp. 54-107.

[25] Civelek, M. B., and Erdogan, F., (1976), "Interface Separation in a Frictionless Contact Problem for an Elastic Layer," *Journal of Applied Mechanics*, American Society of Mechanical Engineers (ASME) Trans., March, pp. 175-177.

[26] Comiez, J. M., Waas, A. M., and Shahwan, K. W., (1995), "Delamination Buckling; Experiment and Analysis," *International Journal of Solids and Structures*, Vol 32, No. 6/7, pp. 767-782.

[27] Corigliano, Alberto, (1993), "Formulation, Identification and Use of Interface Models in the Numerical Analysis of Composite Delamination," *International Journal of Solids and Structures*, Vol. 30, No. 20, pp. 2779-2811.

[28] Crossman, F. W., and Wang, A. S. D., (1982), *ASTM STP 775*, by American Society of Testing and Materials (ASTM), p. 118.

[29] Do, C., (1976), "The Buckling of a Thin Elastic Plate Subjected to Unilateral Conditions," in *Applications of Methods of Functional Analysis to Problems of Mechanics*, Lecture Notes in Mathematics, edited by P. Germain, and B. Naijroles, Vol. 503, Springer, Berlin.

[30] Do, C., (1977), "Bifurcation Theory for Elastic Plates Subjected to Unilateral Conditions," *Journal of Mathematical Analysis and Applications*, Vol. 60, pp. 435-448.

[31] Donaldson, S. L., (1985), "Fracture Toughness Testing of Graphite/Epoxy and Graphite/PEEK Composites," *Composites*, Vol. 16, No. 2, pp. 103-112.

[32] Dorey, G., (1982), *AGARD-LS 124*, pp. 6.11-6.11.

[33] Evans, A. G. and Hutchinson, J. W., (1984), "On the Mechanics of Delamination and Spalling in Compressed Films," *International Journal of Solids and Structures*, Vol. 20, No. 5, pp. 455-466.

[34] Farshad, M., and Shahinpoor, M., (1972), "Beams on Bilinear Elastic Foundations," *International Journal of Mechanical Sciences*, Vol. 14, pp. 441-445.

[35] Fichera, G., (1972), "Boundary Value Problems of Elasticity with Unilateral Constraints," in **HandBuch Der Physik (Encyclopedia Of Physics)**, Vol. VIa/2, Mechanics of Solids II, Truesdell, C. (editor), Springer-Verlag, pp. 391-424.

[36] Fu, L., and Waas, A. M., (1992), "Buckling of Polar and Rectilinearly Orthotropic Annuli under Uniform Internal or External Pressure Loading," *Composite Structures*, Vol. 22, pp. 47-57.

[37] Fung, Y. C., (1965), **Foundations of Solid Mechanics**, Prentice-Hall, Inc.

[38] Garg, Amar, C., (1988), "Delamination-A Damage Mode in Composite Structures," *Engineering Fracture Mechanics*, Vol. 29, No. 5, pp. 557-584.

[39] Gerard, G., (1962), **Introduction to Structural Stability Theory**, McGraw-Hill Book Company, Inc., pp. 57-60.

[40] Gerard, G., and Becker, H., (1957), **Handbook of Structural Stability**. I: Buckling of Flat Plates, NACA TN 3781.

[41] Gladwell, G. M. L., (1976), "On Some Unbonded Contact Problems in Plane Elasticity Theory," *Journal of Applied Mechanics*, American Society of Mechanical Engineers (ASME) Trans., June, pp. 263-267.

[42] Hahn, H. T., (1983), "A Mixed Mode Fracture Criterion For Composite Materials," *Composites Technology Review*, Vol. 5, No. 1, pp. 26-29.

[43] Hobbs, R. E., (1990), "Axisymmetric Upheaval Buckling of a Heavy Sheet," *Journal of Applied Mechanics*, Vol. 57, pp. 472-474.

[44] Hobbs, R. E., (1985), Discussion of: "Buckling and Postbuckling of the Lying Sheet (by C. Y. Wang)," *International Journal of Solids and Structures*, Vol. 21, No. 4, pp. 423-424. Author's reply to R. E. Hobbs, (1985), Vol. 21, No. 4, p. 425.

[45] Hutchinson, J. W., and Suo, Z., (1992), "Mixed Mode Cracking in Layered Materials," in **Advances in Applied Mechanics**, Vol. 29, edited by J. W. Hutchinson and T. Y. Wu, pp. 63-191, Academic Press, Inc.

[46] James, A. M., and Williams, E., (1986), *Lockheed Horizon.*

[47] Jensen, Henrik M., and Thouless, M. D., (1993), "Buckling Instability of Straight Edge Cracks," The Danish Center for Applied Mathematics and Mechanics, Report No. 473, November.

[48] Kachanov, L. M., (1988), **Delamination Buckling of Composite Materials**, Kluwer Academic Publishers.

[49] Kamiya, N., (1977), "Circular Plates Resting On Bimodulus and No-Tension Foundations," *Journal of the Engineering Mechanics Division*, Proceedings of the American Society of Civil Engineers (ASCE), Vol. 103, No. EM6, December, pp. 1161-1164.

[50] Kardomateas, G., (1993), "The Initial Post-buckling and Growth Behavior of Internal Delaminations in Composites," *Journal of Applied Mechanics*, American Society of Mechanical Engineers (ASME) Trans., December, Vol 60, pp. 903-910.

[51] Kooi, B. W., (1985), "A Unilateral Contact Problem with the Heavy Elastica Solved by Use of Finite Elements," *Computers & Structures*, Vol. 21, No. 1/2, pp. 95-103.

[52] Kubrusly, R. S., and Oden, J. T., (1981), "Nonlinear Eigenvalue Problems Characterized by Variational Inequalities with Applications to the Postbuckling of Unilaterally-Supported Plates," *Nonlinear Analysis, Theory, Methods, & Applications*, Vol. 5, No. 12, pp. 1265-1284.

[53] Leipholz, H. H. E., (1983), "On Direct Methods in the Calculus of Variations," *Computer Methods in Applied Mechanics and Engineering*, Vol. 37, pp. 57-78.

[54] Lo, K. H., Christensen, R. M., and Wu, E. M., (1977), "A High-Order Theory of Plate Deformation Part 1: Homogeneous Plates," *Journal of Applied Mechanics*, December, pp. 663-668.

[55] Lo, K. H., Christensen, R. M., and Wu, E. M., (1977), "A High-Order Theory of Plate Deformation Part 2: Laminated Plates," *Journal of Applied Mechanics*, December, pp. 669-676.

[56] Madenci, Erdogan, (1991), "Delamination Growth and Buckling in an Orthotropic Strip," *International Journal of Solids and Structures*, Vol. 27, No. 14, pp. 1773-1788.

[57] Majumdar, S., (1971), "Buckling of a Thin Annular Plate under Uniform Compression," *American Institute of Aeronautics and Astronautics (AIAA) Journal*, September, pp. 1701-1707.

[58] Mindlin, R. D., (1951), "Influence of Rotatory Inertia and Shear on Flexural Motions of Isotropic, Elastic Plates," *Journal of Applied Mechanics*, Vol. 18, No. 1, American Society of Mechanical Engineers (ASME) Trans., Vol. 73, March, pp. 31-38.

[59] Nairn, J. A., and Hu, S., (1992), "The Initiation and Growth of Delaminations Induced by Matrix Microcracks in Laminated Composites," *International Journal of Fracture*, Vol. 57, pp. 1-24.

[60] Naumann, J., (1975), "On Some Unilateral Boundary Value Problems for the von Kármán Equations, Part I: The Coercive Case," *Aplikace Matematiky*, Vol. 20, pp. 96-125.

[61] Naumann, J., (1977), "On Some Unilateral Boundary Value Problems in Nonlinear Plate Theory," *Beiträge zur Analysis*, Vol. 10, pp. 119-134.

[62] Needleman, A., (1990), "An Analysis of Tensile Decohesion Along an Interface," *Journal of The Mechanics and Physics of Solids*, Vol. 38, No. 3, pp. 289-324.

[63] Needleman, A., (1994), "Computational Modeling of Material Failure," part of **Mechanics USA 1994**, edited by A. S. Kobayashi, *Applied Mechanics Reviews*, Vol. 47, No. 6, part 2, June, pp. S34-S42.

[64] Nilsson, K.-F., Thesken, J. C., Sindelar, P., Giannakopoulos, A. E., and Storåkers, B., (1993), "A Theoretical and Experimental Investigation of Buckling Induced Delamination Growth," *Journal of The Mechanics and Physics of Solids*, Vol. 41, No. 4., pp. 749-782.

[65] Noor, A. K., and Burton, W. S., (1989), "Assessment of Shear Deformation Theories for Multilayered Composite Plates," *Applied Mechanics Reviews*, Vol. 42, No. 1, January, pp. 1-13.

[66] O'Brien, T. K., (1982), *ASTM STP 775*, by American Society of Testing and Materials (ASTM), pp. 140-167.

[67] O'Brien, T. K., (1984), *NASA-TM 85768.*

[68] Oden, J. T., (1972), **Finite Elements of Nonlinear Continua**, McGraw-Hill Book Co., pp. 262-297.

[69] Ohtake, K., Oden, J. T., and Kikuchi, N., (1980), "Analysis of Certain Unilateral Problems in von Kármán Plate Theory by a Penalty Method, Part 1: A Variational Principle with Penalty," *Computer Methods in Applied Mechanics and Engineering*, Vol. 24, pp. 187-213.

[70] Ohtake, K., Oden, J. T., and Kikuchi, N., (1980), "Analysis of Certain Unilateral Problems in von Kármán Plate Theory by a Penalty Method, Part 2: Approximation and Numerical Analysis," *Computer Methods in Applied Mechanics and Engineering*, Vol. 24, pp. 317-337.

[71] Ortiz, Michael, and Gioia, Gustavo, (1994), "The Morphology and Folding Patterns of Buckling-Driven Thin-Film Blisters," *Journal of The Mechanics and Physics of Solids*, Vol. 42, No. 3, pp. 531-559.

[72] Pavier, M. J., and Chester, T. W., (1990), "Compression Failure of Carbon Fiber-Reinforced Coupons Containing Central Delaminations," *Composites*, Vol. 21, pp. 23-31.

[73] Plaut, R. H., and Mróz, Z., (1992), "Uni-Directional Buckling of a Pinned Elastica with External Pressure," *International Journal of Solids and Structures*, Vol. 29, No. 16, pp. 2091-2100.

[74] Powell, M. J. D., (1970), "A Hybrid Method for Nonlinear Equations," in **Numerical Methods for Nonlinear Algebraic Equations**, edited by P. Rabinowitz, Chapter 6, Gordon and Breach, New York.

[75] Reddy, J. N., (1986), **Applied Functional Analysis and Variational Methods in Engineering**, McGraw-Hill Book Co., pp. 287-297.

[76] Reddy, J. N., (1989), "On the Generalization of Displacement-Based Laminate Theories," *Applied Mechanics Reviews*, Vol. 42, No. 11, Part 2, November, pp. S213-S222.

[77] Reifsnider, K. L., Henneke, E. G., Stinchcomb, W. W., and Duke, J. L., (1982), Proceedings of the International Union of Theoretical and Applied Mechanics, Blacksburg, Virginia. Pergamon Press, New York, pp. 339-390.

[78] Reissner, E., (1944), "On The Theory of Bending of Elastic Plates," *Journal of Mathematics and Physics*, Vol. 23, pp. 184-191.

[79] Reissner, E., (1945), "The Effects of Transverse Shear Deformations on the Bending of Elastic Plates," *Journal of Applied Mechanics*, Vol. 12, No. 2, American Society of Mechanical Engineers (ASME) Trans., Vol. 67, June, pp. 69-77.

[80] Reissner, E., (1969), "A Note on Imperfection Sensitivity of Thin Plates on a Non-linear Elastic Foundation," in **Instability of Continuous Systems**, edited by H. Leipholz, part of the International Union of Theoretical and Applied Mechanics Symposium, September 8-12, Herrenalb, Germany.

[81] Reissner, E., (1975), "On Transverse Bending of Plates, Including the Effect of Transverse Shear Deformation," *International Journal of Solids and Structures*, Vol. 11, pp. 569-573.

[82] Rhodes M. D., and Williams, J. G., (1984), *NASA-TM 85748.*

[83] Roorda, J., (1988), "Buckles, Bulges and Blow-ups," **Applied Solid Mechanics-2**, edited by A. S. Tooth and J. Spence, pp. 347-380, Elsevier, London.

[84] Sallam, S., and Simitses, G. J., (1985), "Delamination Buckling and Growth of Flat, Cross-Ply Laminates," *Composite Structures*, Vol. 4, pp. 361-381.

[85] Seide, P., (1958), "Compressive Buckling of a Long Simply Supported Plate on an Elastic Foundation," *Journal of Aeronautical Sciences*, June, pp. 382-392.

[86] Shahwan, K. W., and Waas, A. M., (1991) "Elastic Buckling of Infinitely Long Specially Orthotropic Plates on Tensionless Foundations," *Journal of Engineering Materials and Technology*, American Society of Mechanical Engineers (ASME) Trans., Vol. 113, pp. 396-403. Errata in Vol. 114, pp. 124-125.

[87] Shahwan, K. W., and Waas, A. M., (1994), "A Mechanical Model for the Buckling of Unilaterally Constrained Rectangular Plates," *International Journal of Solids and Structures*, Vol. 31, No. 1, pp. 75-87.

[88] Song, S. J., (1994), "A New Approach to Fracture of Layered Fibrous Composites: Experiments and Analysis," PhD Dissertation, Department of Aerospace Engineering, The University of Michigan, Ann Arbor, MI.

[89] Song, S. J., and Waas, A. M., (1995), "Mixed-Mode Failure in Laminated Composites using an Energy Approach," *American Institute of Aeronautics and Astronautics (AIAA) Journal*, to appear in March issue.

[90] Soong, T. C., and Choi, I., (1986), "An Elastica that Involves Continuous and Multiple Discrete Contacts with a Boundary," *International Journal of Mechanical Sciences*, Vol. 28, No. 1, pp. 1-10.

[91] Stein, E., and Wriggers, P., (1984), "Stability of Rods with Unilateral Constraints, a Finite Element Solution," *Computers and Structures*, Vol. 19, No. 1-2, pp. 205-211.

[92] Stein, M., (1986), "Nonlinear Theory for Plates and Shells Including the Effects of Transverse Shearing," *American Institute of Aeronautics and Astronautics (AIAA) Journal*, Vol. 24, No. 9, September, pp. 1537-1544.

[93] Storåkers, Bertil, and Andersson, Börje, (1988), "Nonlinear Plate Theory Applied to Delaminations in Composites," *Journal of The Mechanics and Physics of Solids*, Vol. 36, No. 6, pp. 689-718.

[94] Storåkers, Bertil, and Nilsson, Karl-Fredrik, (1993), "Imperfection Sensitivity at Delamination Buckling and Growth," *International Journal of Solids and Structures*, Vol. 30, No. 8, pp. 1057-1074.

[95] Stringfellow, R. G., and Freund, L. B., (1993), "The Effect of Interfacial Friction on the Buckle-Driven Spontaneous Delamination of a Compressed Thin Film," *International Journal of Solids and Structures*, Vol. 30, No. 10, pp. 1379-1395.

[96] Suemasu, H., Gozu, K. and Hayashi, K., (1995), "Compressive Buckling of Rectangular Plates with a Free-Edge Delamination," *American Institute of Aeronautics and Astronautics (AIAA) Journal*, Vol. 33, No. 2, February, pp. 312-319.

[97] Thouless, M. D., Hutchinson, J. W., and Liniger, E. G., (1992), "Plane-Strain, Buckling-Driven Delaminations of Thin Films: Model Experiments and Mode-II Fracture," *Acta Metall. Mater.*, Vol. 40, No. 10, pp. 2639-2649.

[98] Timoshenko, S. P., (1955), **Vibration Problems in Engineering**, in collaboration with D. H. Young, 3^{rd} edition, pp. 331-341.

[99] Timoshenko, S. P., (1961), **Theory of Elastic Stability**, in collaboration with J. M. Gere, 2^{nd} edition, (1988 print), McGraw-Hill Book Co., pp. 351-360.

[100] Tsai, N., and Westmann, R., (1967), "Beams on Tensionless Foundation," *Journal of the Engineering Mechanics Division*, Proceedings of the American Society of Civil Engineers (ASCE), Vol. 93, No. EM5, pp. 1-12.

[101] Villaggio, P., (1979), "Buckling Under Unilateral Constraints," *International Journal of Solids and Structures*, Vol. 15, pp. 193-201.

[102] Waas, A. M., (1992), "Effect of an Interphase on Compressive Strength of Unidirectional Composites," *Journal of Applied Mechanics*, American Society of Mechanical Engineers (ASME) Trans., June, Vol. 59, pp. S183-S188.

[103] Waas, A. M., Babcock, C. D., and Knauss, W. G., (1990), "An Experimental Study of Compression Failure of Fibrous Laminated Composites in the Presence of Stress Gradients," *International Journal of Solids and Structures*, Vol. 26, No. 9-10, pp. 1071-1098.

[104] Wang, C. Y., (1984), "On Symmetric Buckling of a Finite Flat-Lying Heavy Sheet," *Journal of Applied Mechanics*, Vol. 51, pp. 278-282.

[105] Wang, C. Y., (1984), "Buckling and Postbuckling of the Lying Sheet," *International Journal of Solids and Structures*, Vol. 20, No. 4, pp. 351-358.

[106] Wang, S. S., (1981), *NASA-CR 165439.*

[107] Weitsman, Y., (1969), "On the Unbonded Contact Between Plates and an Elastic Half Space," *Journal of Applied Mechanics*, Vol. 36, No. 2, American Society of Mechanical Engineers (ASME) Trans., Vol. 91, Series E, June, pp. 198-202.

[108] Weitsman, Y., (1970), "On Foundations That React in Compression Only," *Journal of Applied Mechanics*, American Society of Mechanical Engineers (ASME) Trans., December, pp. 1019-1030.

[109] Weitsman, Y., (1972), "A Tensionless Contact Between a Beam and an Elastic Half-Space," *International Journal of Engineering Science*, Vol. 10, pp. 73-81.

[110] Wilkins, D. J., Eisenmann, J. R., Camin, R. A., Margolis, W. S., and Benson, R. A., (1982), *ASTM STP 775*, by American Society of Testing and Materials (ASTM), pp. 168-183.

[111] Williams, J. G., (1984), **Fracture Mechanics of Polymers**, Ellis Horwood Limited.

[112] Yin, Wan-Lee, (1985), "Axisymmetric Buckling and Growth of a Circular Delamination in a Compressed Laminate," *International Journal of Solids and Structures*, Vol. 21, No. 5, pp. 503-514.

[113] Yin, W.-L., and Jane, K. C., (1992), "Refined Buckling and Postbuckling Analysis of Two-Dimensional Delaminations, Part I-Analysis and Validations," *International Journal of Solids and Structures*, Vol. 29, No. 5, pp. 591-610.

[114] Yin, W.-L., and Jane, K. C., (1992), "Refined Buckling and Postbuckling Analysis of Two-Dimensional Delaminations, Part II-Results for Anisotropic Laminates and Conclusion," *International Journal of Solids and Structures*, Vol. 29, No. 5, pp. 611-639.

[115] Yun, H. D., and Kyriakides, S., (1983), "Localized Buckling of a Heavy Beam on a Contacting Surface: A Model for Beam Mode Buckling of Buried Pipelines," Engineering Mechanics Research Laboratory, EMRL report No. 83/5, Department of Aerospace Engineering and Engineering Mechanics, The University of Texas, Austin, Texas.